IJSET JOURNAL
Advancing Technology & Research

ISSN (O): 2348-4098
ISSN (P): 2395-4752

International Journal of Science, Engineering and Technology

Volume 3 Issue 3 : 2015
Volume 3 Issue 4 : 2015

Published by :
IJSET Journal Publication
E-mail : editor@ijset.in

www.ijset.in

International Journal of Science, Engineering and Technology

ISSN (Online): 2348-4098

ISSN (Print): 2395-4752

Print Version

Volume 3 Issue 3: 2015

Volume 3 Issue 4: 2015

Published By:

IJSET JOURNAL PUBLICATION

Website: www.ijset.in | Email: editor@ijset.in

COPYRIGHT

DISCLAIMER

CONTACT INFORMATION

Dr. Kavita Sharma

Editor-in-Chief

E-mail: editor@ijset.in

Website: http://www.ijset.in

EDITORIAL BOARD

TABLE OF CONTENTS

S. No.	Manuscript Title and Author(s)	Page No.
1.	**Community Analysis of Collembola In A Natural Forest and Jhumland Ecosystem of Mokokchung, Nagaland** *Kruolalie Tsurho, Bendang Ao, Vetselo Duolo*	1- 6
2.	**Chaetomorpha Linum Extract As A Green Inhibitor For Corrosion Of Brass In 0.1 N Phosphoric Acid Solution** *Selva Kumar R., Chandrasekaran V*	7- 16
3.	**Multi-Walled Carbon Nanotube (Mwcnt) Based Composite Material: A Review** *Abdul Rahman Sanad, M.N.M.Ansari, Jamal O.Sameer, Abdulbasit Abdullah, Bassam Alaseel*	17- 26
4.	**A Methodology Of Optimal Sizing For Wind Solar Hybrid System** *Avinash Nath Tiwari, Navnit Dubey*	27- 31
5.	**Fishing Trails With Modified Two–Seam Overhang Trawl- Intraspecific Selectivity Studies** *N.A.Talwar, B.Hanumanthappa, M.T.Laxmipathi*	32- 38
6.	**Experimental Study Of Local Scour Around Circular Compound Bridge Pier** *Prof. P.T. Nimbalkar, S.S. Thorat*	39- 42
7.	**Design And Development Of Verification Environment To Verify Spi Master Core Using Uvm** *Rajesh C, Shivananda, Mrs. Shanthi V A*	43- 45
8.	**Estimation Of Domestic, Crop Water Requirements And Estimation Of Groundwater, Surface Water Resources Of Renia City - Iraq** *Ahmed Talib Abduljaleel Al-Alikhan, Prof. P.T.Nimbalkar*	46- 48
9.	**Effect Of Filler Concentration On Properties Of Graphite Composite Bipolar Plate** *Mohammed A. M., El-Nafaty U. A., Bugaje I., M. Mukthar B.*	49- 61
10.	**Seismic Performance Evaluation Of Rc Buildings With Vertical Irregularities Subjected To Biaxial Excitation** *Dr.Mohd.Hamraj, Mohammed Moiz Khan*	62- 69

11. **Study Of The Iodination Of Indole-3-Butyric Acid By Aqueous Iodine Using Hydrodynamic Voltammetry** 70- 73

Rajendra P.Yadav, Bharat B. Bahule, Vitthal T. Borkar, Vijay T. Dangat, Kanchan G. Shinde

12. **De-Embedding Of Test Fixture: A Necessary Step In Post Silicon Validation For Accurate Characterization Of High Speed Devices** 74- 77

Surendra Kumar Dadore, Lalita Gupta, Siyaram Sahu

13. **Implementation Of Doubly-Fed Wind Turbine Along With Pid Controller To Maintain The Desired Output Levels And Control The Pitch According To Wind Direction** 78- 83

Ajay Shukla, Anil Gupta

14. **Diversity, Prevalence And Role Of Superoxide Dismutase In Cyanobacteria** 84- 91

Kanu Priya, Namita Singh, Inderjeet Singh

15. **Synthesis, Characterization And Antimicrobial Efficacy Of Cyanobacterial (Polymer) Silver Nano Particle Conjugates** 92- 99

Ritika Chanan, Minakshi Lalit, Naveen, Namita Singh

COMMUNITY ANALYSIS OF COLLEMBOLA IN A NATURAL FOREST AND JHUMLAND ECOSYSTEM OF MOKOKCHUNG, NAGALAND

[1]KRUOLALIE TSURHO, [2]BENDANG AO, [3]VETSELO DUOLO

[1]Assistant Professor, Department of Zoology, Fazl Ali College, Mokokchung, Nagaland. India, Email: krultsurho@gmail.com

[2]Assistant Professor, Department of Zoology, Nagaland University, Lumami, Zunheboto, Nagaland, India, Email: nbwalling@rediffmail.com

[3]Assistant Professor, Department of Zoology, Kohima Science College, Jotsoma, Kohima. Nagaland, India.

ABSTRACT

The present study was carried out in two adjacent areas of a natural forest and jhumland ecosystems in Mopungchuket village and Chuchuyimpang village respectively, under Mokokchung district, Nagaland, which lies at 26^{o} 11' 36'' North latitude and in between 94^{o} 17' 44'' to 94^{o} 45' 42'' (E) longitude. The study was conducted during January 2009 to December 2011. The vertical distribution and abundance of total Collembola were found to be more in a natural forest ecosystem (324.69 x 10^{2} m^{-2}) than jhum land ecosystem (222.42 x 10^{2} m^{-2}) and showed a significant decrease from upper layer to deeper layers from 0 cm to 30 cm depth. In a natural forest ecosystem, the Collembola recorded higher population during rainy season (143.29 x 10^{2} m^{-2}), followed by summer (108.06 x 10^{2} m^{-2}) and winter season (73.34 x 10^{2} m^{-2}) than jhum land ecosystem respectively. The physico-chemical factors, except soil potassium exhibited significant correlation. The community analysis was carried out for Collembola being one of the major groups of soil microarthropods as their contributions are maximum in term of species, abundance and distribution.

Key words: *Community analysis, Collembola, microarthropods, natural forest and jhum land.*

1. INTRODUCTION

Collembolans are wingless insects or apterygotes, which can be placed under three sub-groups *viz*. *Entomorbryomorpha*, *Poduromorpha* and *Symphypleona*. They are largely detritus or fungal feeders - most of them feeding on decaying vegetation, bacteria, fungi, algae, pollen and other forms of organic material and have well developed mouthparts capable of fragmenting plant material (Seastedt, 1984). These microarthropods play an important role in nurturing or maintaining the sustainability of an ecosystem through decomposition of organic matter (Christensen & Bellinger, 1980) and mineralization of leaf litter thus enriching the soil fertility. They also maintain soil physical structure, nutrient cycling, energy flow and enhance primary productivity (Badejo and Staalen, 1993; Hofer *et al*., 2001; Yang and Chen, 2009). Thus Hagvar (1984) considers them good indicators of soil quality particularly because of their relationship with minerals/chemicals like Na, K and N of soil.

In India, studies on different aspects of soil microarthropods have been conducted by Harza and Choudhuri (1983), Hattar and Alfred (1986) and Alfred *et. al.* (1991) *etc*. In North Eastern India, some prominent works have been conducted by Vatauliya & Alfred (1980), Darlong & Alfred (1982), Paul & Alfred (1986), Sarkar (1991), Singh *et. al*. (1998), Chitrapati *et. al*. (2002) *etc*. In case of Nagaland, works on microarthopods are scarce, except for some works by Alemla (1987), Duolo and Kakati (2009), Kruolalie and Bendang (2014) *etc*.

In Nagaland, jhum cultivation accounts for about 73% of the net cropped area, while wet terrace rice cultivation (WTRC) accounts for about 27%. Jhum cultivation essentially entails the process of "slash and burn" and this would naturally disturb the ecological balance because of destruction of flora and fauna. Therefore, it is important to understand the effects of deforestation and the practice of jhumming on soil microarthropod populations. In this connection, it is worthwhile to note that Duolo and Kakati (2009) recorded a higher population of microarthropods in natural forest as compared to a degraded forest.

The present study was taken up to study the effects of deforestation, the effects of climatic and edaphic factors on Collembolan abundance, distribution and diversity in a natural forest and jhum land ecosystem in Mokokchung district of Nagaland.

2. MATERIALS AND METHODS

2.1 STUDY SITES

The present study was carried out in two adjacent areas of natural forest and jhum land ecosystems in Mopongchuket village and Chuchuyimpang village under Mokokchung district, Nagaland which lies at 26°11'36'' North latitude and in between 94°17'44'' to 94°45'42'' (E) longitude. The forest site comprised of rich

vegetation which had not been disturbed for more than twenty years while the jhum land had almost no vegetation due to frequent human activities and interference.

The natural forest comprised of rich vegetation with a distinct vertical stratification. The canopy layer has an average height of 20 metres or more, comprising of Albizia procera, Schima wallichii, Alnus nepalensis, Castinopsis indica, Lithocarpus elegans, Michellia champaca and Persia villosa. Emergent trees that overshoot the canopy layers were not present. The smaller trees mostly belong to the families of Lauraceae, Euphobiaceae, Araliaceae, Ficaseae and Rubiaceae. The average height of these members is found to be 5 to 15 mts. The ground flora is rich and epiphytes, climbers and lianas were also found to be growing abundantly. The jhum land, on the other hand was not as well stratified as the natural forest. The tree species present are the species that were left uncut while clearing the forest, and the stumps that survived the jhum cultivation. Quercus serrata, Erythrina striata, Albizia procera, Schima walichii were the dominant species present in the jhum areas.

2.2 CLIMATE

The climate of the area is monsoonal, with warm moist summers and cool dry winters. The meteorological data based on three years (2009-2011) as shown in tabular as well as graphical forms (tables 1-3 and figures 1-3) reveals that June to October constitutes wet months and November to May the dry months. The dry period can be further divided into summer (March to May) and cool dry season (November to February). Thus there is distinct summer (March to May), rainy (June to October) and winter (November to February) seasons. March constitutes the transitional month between winter and summer whereas October is the transitional month between rainy and winter season.

The maximum and minimum air temperature was 21.4°C (August) and 6.3°C (January) respectively in 2010 (Average: Max = 21.4 °C Min = 8.1 °C). The maximum and minimum relative humidity was 85% (August) in 2009 and 35.55 (December) in 2011 respectively (Average: Max = 83.3% Min = 54.5%). The maximum and minimum total rainfall was 972.5 cms (July) in 2011 and the minimum was 3.7 cms (March) in 2009 (Average: Max = 572.5 cm Min = 11.3 cm, total average rainfall = 1859.93 cms).

2.3 SAMPLING AND EXTRACTION

In both the forest and jhumland ecosystems, the sampling collection sites were divided according to elevation because of the terrain *viz*. upper elevation site, middle elevation site and lower elevation site. In each elevation site, three different plots having a size of 10m x 10m each spaced 25-30 meters apart were selected from where soil samples were collected. Soil samples were taken at one month intervals in the middle week of each month between 10:00 and 11:00 AM. The soil samples were collected with the help of iron cylindrical core with sampler size of 3.925 cm, which are 10cm in depth and 5cm in diameter. Three replicates were collected from each area or collection site.The samples were immediately bound in polytene bags, labelled and brought to the laboratory for analysis within an average of one hour after the field collection. In each study site a total of 1944 soil samples were collected during the whole study period.

The samples were then divided into sections and placed in a Tullgren funnel as described by Crossley and Blair (1991). The soil microarthropods were extracted into collecting vials containing 70% alcohol. After extraction, the vials and the contents were transferred into a petridish - the vials being washed several times with 70% alcohol. The extracted soil microarthropods were preserved in 70% alcohol to which few drops of glycerine were added to prevent desiccation. Identification and counting was done under a binocular microscope, and density calculated.

2.4 SOIL ANALYSIS

Physico-chemical factors of the soil like temperature, moisture, pH, organic carbon, total nitrogen, available phosphorus, and potassium were analyzed during each sampling period in order to study the impact of these factors in the population changes of soil microarthropods. The methodologies utilized for each are as follows: Soil temperature (soil thermometer), Soil moisture content (gravimetric method according to Misra, 1968 and Wilde et al., 1985), Soil pH (portable glass electrode pH meter (according to Jackson, 1958), Soil organic carbon (oxidation calorimetric method i.e., modified Walkey and Black method according to Anderson and Ingram, 1993), Soil total nitrogen (acid digestion Kjeldahl procedures according to Anderson and Ingram, 1993), Phosphorus (ammonium molybdate stannous chloride method according to Sparling et al., 1985), Potassium (flame photometer according to Steward, 1971).

2.5 COMMUNITY ANALYSIS

In community analysis, species diversity and community similarity were analyzed for Collembola using the following formulae:

(i) Species diversity (number of species) or species richness was calculated after Margalef (1968).

$$Da = (S - 1)/\log N$$

Where,

Da = Margalefs Index

S = No. of Species

N = Total No. of Individuals.

(ii) Measure of species diversity based on information theory or related to the concept of uncertainty was calculated after Shannon and Wiener (1949),

Where,

$$H' = -\sum_{i=1}^{s} Pi \log pi$$

H' = Measure of Shannon - Wiener Diversity

S = Total No. of Species in a sample

Pi = Proportion of the total number of individuals occurring in species i.

(iii) The maximum possible diversity of H' or H max' was calculated using the following formula:

$H\ max' = Log_2 S$

Where, S = Number of species or category

3. RESULT AND DISCUSSION

Community analysis of Collembola populations in both forest and jhumland ecosystems showed maximum abundance, and species diversity in rainy season and slowly decreased in summer and winter seasons. Seasonal differences in the abundance of soil arthropods have been demonstrated by various workers (Salt, 1952; Davis, 1963; Block, 1966; Nijima, 1971; Usher, 1975). These workers reported that microarthropods undergo enormous fluctuations in numbers, these being susceptible to small changes factor influencing population size. Wallwork (1970), Fujikawa (1970) and Anderson (1988) suggest that the temporal pattern is related to transition from one season to another which is mostly due to shift in soil moisture and temperature.

The Data analysis of Collembola (Table no. 1 & 2) using Margalefs index (Da) and Shannon-Wiener diversity index (H') show more diversity in forest than the jhum land ecosystem. In forest ecosystem, maximum value of diversity (Da = 8.246, H' = 3.775) was shown during summer season and minimum during winter season. While in jhumland ecosystem, maximum value of diversity (Da =7.433, H' = 3.875) were recorded in summer season. Hmax' of Collembola (Table no. 1 & 2) was found to be higher in forest ecosystem as compared with jhumland ecosystem. In forest ecosystem, Hmax' value was highest in rainy season (4.000) and lowest in winter seasons (2.587) respectively. While in jhumland ecosystem, Hmax' value was highest in summer season (3.751) and lowest in winter (2.773) respectively. The higher diversity indices in both the study sites have been recorded higher during summer and rainy season in all depths i.e., at 0-10 cm, 10-20cm and 20-30cm. While lesser diversity indices have been recorded during winter season in all the soil layers of the two study sites. The Hmax' i,e the maximum diversity was also recorded with higher value in summer and rainy season than winter season in all layers.

A total of fifteen (15) Collembola species were identified from the two study sites (Table no. 3 & 4). The result from the two study sites showed variation in its community structure. Overall the number of individuals, species and the value of diversity were found to be higher and more consistent in the forest ecosystem than that of jhumland ecosystem. It was also seen that some of the species of Collembola that were found in a natural forest ecosystem were totally absent in jhumland which brings about a decrease or disappearance of the least abundant species, while the most abundant species persist (Gurrea *et al.,* 2000).

In the natural forest ecosystem, the concentration of Collembola was higher which is due to canopy and vegetative cover, accumulation of litter and optimum physico-chemical factors favouring these microarthropods, but in the jhumland ecosystem showed negative impact due to disturbance in the type of vegetative cover, lack of canopy, physico-chemical properties of soil and depth of litter etc. (Price, 1973; Seastedt, 1984; Badejo and Staalen, 1993; Wardle and Giller, 1996).

REFERENCES

1. Anderson, J.M., 1988. Spatiotemporal effects of invertebrates on soil processes. Biol. Fertil. Soils. 6, 216-227.

2. Anderson, J. H. and Ingram, J. S. (1993). Tropical soil biology and fertility. A handbook of method. UK. C.A.B. Int.

3. Alfred, J. R. B., Darlong V.T., Hattar, S. J. S and Paul, D. (1991). Microarthropods and their conservation in some North East Indian soil, In "Advances in management and conservation of soil fauna" (Eds, G.K. Vecresh, D. Rajagopal and C.A. virak Tamath) Bangalore.

4. Ao, M, Alemla. (1987). Ecological investigation on the soil arthropods communities with particular reference to insects of two 'Jhum' agro-ecosystems of Nagaland, North- Eastern India. Ph. D. thesis, North Eastern Hill University, Shillong.

5. Badejo, M. A. and Van Straalen, N. M. (1993). Seasonal abundance of Springtails in two contrasting Environments. *Biotropica*. 25: 222-228.

6. Bhandari, S. C. and Somani, L. L. (1994). In "*Ecology and Biology of soil organisms*", Agrotech publishing Academy, Udaipur.

7. Block, W. C. (1966). Seasonal fluctuations and distribution of mite populations in moorland soil with a note on biomass. *J. Anim. Ecol*. 35: 487-503.

8. Crossley, D. A., Blair, J. M. (1991). A high-efficiency, low-technology Tullgren-type extractor for soil microarthropods. *Agric. Ecosyst. Environ*. 34, 187–192.

9. *Davis, B. N. K. (1963). A study of microarthropod communities in mineral soils near Corby Northants. J. Animal Ecol. 32: 49-71.*

10. Fujikawa, T. (1970). Distribution of soil animals in three forests of Northern Hokkaido I I Horizontal

and vertical distribution of Oribatid mites (Acarina: Cryptostigmata). *App. Ent. Zool*. 5(40): 208-212.

11. Gurrea, P., Ferrin, J. M.,Martin, J., Perez, F., Ruiz, M. and Simon, J. C. (2000). Loss of biodiversity due to reforestation in central Spain (Lepidoptera Papilionoidea; Coleoptera Curculionidae; Collembola). *Belgian Journal of Entomology*. 2: 149-170.

12. Hofer H, Hanagarth W, Garcia M, Martius C, Franklin, Rombke J and Beck L (2001). Structure and function of soil fauna communities in Amazonian anthropogenic and natural ecosystems. European journal of soil Biology 37. 229 –235.

13. Jackson, M. L. (1958). Soil chemical analysis. *Prentice Hall Inc, New Jersey, USA*.

14. Kruolalie Tsurho and Bendang Ao (2014). Vertical distribution and abundance of Collembola in a natural forest and jhum land ecosystem of Mokokchung, Nagaland. IJSET 2 (6): 1-17.

15. Margalef, R. (1968). Perspectives in ecological theory. *University of Chicago Press, Chicago*.

16. Misra, R. (1968). Ecology work book. *Oxford and IBH Pub. Co. Calcutta, India.*

17. Nijima, K. (1971). Seasonal changes in Collembolan population in a warm temperate forest of Japan. *Pedobiologia*. 1 1 : 1 1 -26.

18. Price, D. W. (1973). Abundance and vertical distribution of microarthropods in the surface layers of a California pine forest soil. *Hilgardia*. 42: 121-174.

19. Seastedt, T. R. (1984). The role of microarthropods in decomposition and mineralization processes. *Ann. Rev. Entom*. 29: 25-46.

20. Shannon, C. E. and Wiener, W. (1949). The mathematical theory of communication. *Urbana III; Univ. Illionis Press*. pp. 117.

21. Sorensen, T. (1948). A method of establishing group of equal amplitude in plant sociology based on the similarity of species content and its application to analysis of the vegetation Danish commons. *Biol. Skr*. 5: 1-34.

22. Sparling, G. P. and Shale, K. N. *(*1985). Quantifying the contribution from the soil microbial biomass to the extractable levels of fresh and air dried soils. Aust. J. of soil Res. 23: 613-621.

23. Steward, E. A. (1971). Chemical analysis of ecological materials. Blackwell Scientific Publication, Oxford.

24. Usher, M. B. (1975). Some properties of the aggregations of soil arthropods, Cryptostigmata. *Pedobiologia*. 15: 355-363.

25. Wardle, D. A. & Giller, K. E. (1996). The quest for a contemporary ecological dimension to soil biology. Discussion. *Soil Biology and Biochemistry*. 28:1549-1554.

26. Wilde, S. A., Corey, R. B., Iyer, J. G. and Viogt, G. K. (1985). Soil and plant analysis for tree culture. *Oxford and IBH Pub. Co.*

27. Yang X and Chen J (2009). Plant litter quality influences the contribution of soil fauna to litter decomposition in humid tropical forests, southwestern China. Soil Biology and Chemistry 41: 910-918.

Table 1: Species diversity of the total indentified Collembola in different soil depth in forest ecosystem.

Area	***Soil layers***	***Season***	***Data analysis***		
			Margalef's Index (Da)	**Diversity(H')**	**Hmax'**
Forest ecosystem	*0-10 cm*	*Summer*	8.246	3.775	3.344
	0-10 cm	*Rainy*	7.552	3.221	3.558
	0-10 cm	*Winter*	6.533	2.885	2.735
	10-20 cm	*Summer*	7.991	3.595	3.441
	10-20 cm	*Rainy*	7.323	3.353	3.237
	10-20 cm	*Winter*	5.626	2.336	2.587
	20-30 cm	*Summer*	6.557	3.325	3.444
	20-30 cm	*Rainy*	7.224	3.651	4.000
	20-30 cm	*Winter*	4.616	3.215	3.101

Table 2: Species diversity of the total identified Collembola in different seasons at different soil depth in Jhumland ecosysystem.

Area	***Soil layers***	***Season***	***Data analysis***		
			Margalef's Index (Da)	**Diversity(H')**	**Hmax'**
Jhumland ecosystem	*0-10 cm*	*Summer*	7.443	3.875	3.751
	0-10 cm	*Rainy*	7.112	3.550	3.661
	0-10 cm	*Winter*	5.636	3.664	3.223
	10-20 cm	*Summer*	7.113	3.993	3.622
	10-20 cm	*Rainy*	6.995	3.000	3.229
	10-20 cm	*Winter*	5.312	2.887	2.773
	20-30 cm	*Summer*	6.335	3.559	3.559
	20-30 cm	*Rainy*	6.223	3.441	3.636
	20-30 cm	*Winter*	5.000	3.111	3.005

Table 3 : Distribution of Collembola species in different seasons of forest ecosystem

Sl.No	Species	**Summer**	**Rainy season**	**Winter**
1	*Cyphoderus albinos*	+++	++	-
2	*Entomobrya triangularis*	++	-	-
3	*Entomobrya clitellaria*	+++	++	-
4	*Isotomodes productus*	++	+++	-

5	*Isotomurus unifasciatus*	-	+++	+
6	*Lepidocyrtus kauriensis*	++	++	++
7	*Lepidocyrtus curvicollis*	++	+++	-
8	*Lepidocyrtus rataensis*	++	+++	-
9	*Odontella minutudentata*	-	+++	++
10	*Proisotoma subminuta*	++	+++	-
11	*Pseudofolsomia sp*	-	+++	-
12	*Pseudosinella orba*	++	+++	-
13	*Pachytullbergia scabra*	++	++	+++
14	*Scutisotoma millimetrica*	++	-	-
15	*Weberacantha*	-	++	+++

Table 4 : Distribution of Collembola species in different seasons of Jhumland ecosystem.

Sl.No	Species	**Summer**	**Rainy season**	**Winter**
1	*Entomobrya clitellaria*	-	++	-
2	*Isotomodes productus*	+++	+++	-
3	*Isotomeilla minor*	-	+++	-
4	*Pseudofolsomia sp.*	-	++	-
5	*Proisotoma subminuta*	+++	-	-
6	*Lepidocyrtus kauriensis*	++	++	-
7	*Lepidocyrtus rataensis*	++	+++	++
8	*Pseudosinella orba*	-	++	-
9	*Pachytullbergia scabra*	++	+++	-
10	*Bourletiella arvalis*	-	-	++
11	*Dicyrtoma melitensis*	++	++	-
12	*Deuterosminthurus pallipes*	-	+++	-
13	*Weberacantha*	+++	++	-
14	*Scutisotoma millimetrica*	++	-	-
15	*Entomobrya triangularis*	++	-	-

+++ = High

++ = Moderate

+ = Low

- = Absent

CHAETOMORPHA LINUM EXTRACT AS A GREEN INHIBITOR FOR CORROSION OF BRASS IN 0.1 N PHOSPHORIC ACID SOLUTION

SELVA KUMAR R.[12*] AND CHANDRASEKARAN V.[3]

[1]Research Scholar (PT), Department of Chemistry, Bharathiar University, Coimbatore-641 046, Tamil Nadu, India, rselvakumar86@yahoo.com

[2]Lecturer, Department of Chemistry, Sree Krishna Polytechnic College, Nagercoil-629 003, Tamil Nadu, India.

[3]Assistant Professor, Department of Chemistry, Govt. Arts College (Autonomous), Salem – 636 007, Tamil Nadu, India, chandru_v_m@yahoo.co.in

ABSTRACT

*The effect of marine algae Chaetomorpha linum extract on corrosion inhibition of brass in phosphoric acid was investigated by weight-loss method, potentiodynamic polarization and e*lectrochemical impedance spectroscopy studies. *The inhibition efficiency is found to increase with increasing concentration of extract and decreases with rise in temperature. The inhibitive effect could be attributed to the phytochemical constituents present in the inhibitor containing N, S, O atoms. The activation energy, thermodynamic parameters (free energy, enthalpy and entropy change) and kinetic parameters (rate constant and half-life) for inhibition process were calculated. These thermodynamic and kinetic parameters indicate a strong interaction between the inhibitor and the brass surface. The inhibition is assumed to occur via adsorption of inhibitor molecules on the brass surface, which obeys Temkin adsorption isotherm. The adsorption of inhibitor on the brass surface is exothermic, physical, and spontaneous, follows first order kinetics. The polarization measurements showed that the inhibitor behaves as a mixed type inhibitor and the higher inhibition surface coverage on the brass was predicted. Inhibition efficiency values were found to show good trend with weight-loss method, potentiodynamic polarization and electrochemical impedance spectroscopy studies. Surface analytical techniques (FT-IR and SEM) were carried out to ascertain the inhibitive nature of the algal extract on the brass surface.*

Index Terms: Brass, Phosphoric acid, *Chaetomorpha linum,* Inhibition, Polarization, and Isotherm.

1. INTRODUCTION

Phosphoric acid (H_3PO_4) is a major chemical product, which has many important uses especially in the production of fertilizers. Most of the acid is produced from phosphate rock by wet process. Brass and stainless steel are frequently used in many parts of the wet process and a considerable quantity of data has been published about the resistance of these materials to corrosion by acid solutions [1,2]. Most of the previous studies were focused on the inhibition of metals in HCl or H3PO4 solutions using organic compounds containing N, S, O atoms as corrosion inhibitors [3-5]. A lot of research has been done with naturally occurring substances since they are known to be eco-friendly and with little or no side effect on the humans. Among the naturally occurring substances reported in the corrosion study of metals like brass, aluminium, tin and mild steel, there leave extracts, gums and exudates, dyes, oils from plant materials, plant seeds and fruits, and anti-bacterial drugs. Plant extracts like the extract of cocos nucifera-coconut palm-petiole [6]; *Musa Paradisiaca* [7]; *Mentha Pulegium* [8]; *Treculia Africana* leaves [9] and *Lupinus varius* leaves [10] have been studied and established their corrosion inhibition effects. They were all found to be good corrosion inhibitors with no effect on the environment.

In the present study, the effect of addition of marine algae *Chaetomorpha linum* extract on corrosion inhibition of brass in 0.1 N phosphoric acid solutions at different temperatures and various time intervals have been investigated by weight-loss method, potentiodynamic polarization and electrochemical impedance spectroscopy studies. The weight loss measurements aimed to predict the inhibition efficiency on brass corrosion and the adsorption isotherm, thermodynamic and kinetic feasibility of inhibition via surface coverage on brass by adsorbed Chaetomorpha linum extract. The inhibition type and inhibition efficiency were determined from the polarization measurements and impedance spectroscopy studies. Surface analytical techniques (FT-IR and SEM) were carried out to ascertain the inhibitive nature of the algal extract on the brass surface.

2. METERIAL AND METHODS

2.1 MATERIALS

The chemical composition (weight percent) of the brass used in the present study was 71.5 % Cu, 28.38 % Zn, 0.07 % Pb, and 0.05 % Fe. The geometry of the specimens for weight-loss experiments was as follows: The brass specimens were polished mechanically with different grades of emery papers (1/0 to 4/0) and were thoroughly washed with double distilled water then degreased in acetone and dried. The solutions were prepared from analar grade chemicals using double distilled water. Phosphoric acid solution (H3PO4) was used as a

corrosion medium. The inhibitor *Chaetomorpha linum* extract (CLE) was extracted with ethanol using soxhelt extractor from marine algae *Chaetomorpha linum*.

2.2 WEIGH-LOSS MEASUREMENT

Measurements of weight changes were performed with rectangular brass specimens (length: 5 cm, width: 1 cm, and thickness: 0.3 cm). The specimens with same dimensions were immersed in 100 ml of 0.1 N H_3PO_4 solutions with and without different concentrations (0.0001 % to 0.0005 %) of CLE and allowed stand for 3 h and 6 h at various temperatures were as follows: 300 K, 318 K, 328 K, and 338 K. At 300 K the specimens were immersed for immersion time of 24, 48, 72, and 96 h. Then, the specimens were rinsed with distilled water and adherent corrosion products for 20 s. then the specimens were rinsed with water, cleaned with acetone and dried. The percentage of inhibition efficiency (IE) over the exposure period was calculated using the following equation (1) [11]:

$$\text{Inhibition efficiency (\%)} = \frac{Wo - Wi}{Wo} \times 100 \qquad (1)$$

where W_o and W_i are the rate of corrosion for brass with and without inhibitor, respectively.

2.3 POTENTIODYNAMIC POLARIZATION STUDIES

The potentiodynamic polarization studies were carried out with brass strips having an exposed area of 1 cm^2. The cell assembly consisted of brass as working electrode, a platinum foil as counter electrode and a saturated calomel electrode as a reference electrode. Polarization studies were carried out using a potentiostat/galvanostat (Model BAS-100 A). The working electrode was immersed in a 0.1 N H3PO4 and allowed to stabilize for 30 min. Each electrode was immersed in a 0.1 N H3PO4 in the presence and absence of different concentrations of inhibitor to which a current of 1.5 mA/cm^2 was applied for 20 minutes to reduce oxides. The cathodic and anodic polarization curves for brass specimen in the test solution with and without various concentrations of the inhibitor were recorded by scanning the potential range $\pm$200 from the corrosion potential at a sweep rate of 1 mV/s. The inhibition efficiencies were determined from corrosion currents using the Tafel extrapolation method. The corrosion inhibition efficiency (IE) was calculated from the following equation (2):

$$\text{IE (\%)} = \frac{i_{corr} - i_{corr\,(i)}}{i_{corr}} X\,100 \qquad (2)$$

Where i_{corr} and $i_{corr(i)}$ are the corrosion current density values without and with inhibitor, respectively.

2.4 ELECTROCHEMICAL IMPEDANCE SPECTROSCOPY STUDIES

A well polished brass electrode was introduced into 100 ml of test solution and allowed to attain a steady potential value. AC signal of amplitude of 10mV was applied and the frequency was varied from 10 MHz to 10 KHz using Solartron electrochemical measurement unit (1280B). The real and imaginary parts of the impedance were plotted in Nyquist plots as shown in Figure 5. From the Nyquist plot, the charge transfer resistance (R_{ct}) and double layer capacitance (C_{dl}) values were calculated.

The charge transfer resistance values were obtained from the plots of Z' vs Z". The values of (R_s + R_{ct}) correspond to the point where the plots cuts Z' axis at low frequency and R_s corresponds to the point where the plot cuts Z' axis at high frequency. The difference between R_{ct} and R_s values give the charge transfer resistance (R_{ct}) values. The C_{dl} values were obtained from the following equation (3):

$$C_{dl} = \frac{1}{2\pi f_{max} \times R_{ct}} \qquad (3)$$

where C_{dl} is double layer capacitance, R_{ct} is charge transfer resistance and f_{max} is frequency at Z" value maximum.

The inhibition efficiencies were calculated from R_{ct} values using the following equation (4):

$$IE\% = \frac{R_{ct(i)} - R_{ct}}{R_{ct(i)}} \times 100 \qquad (4)$$

where R_{ct} and $R_{ct(i)}$ are the charge transfer resistance in the absence and presence of inhibitor respectively.

2.5 SURFACE STUDY

The brass specimen was immersed in 0.1 N H3PO4 in the presence of inhibitor for 6 h at 300 K. After 6 h the specimen was taken out and dried. The nature of the film formed on the brass surface was analyzed by FT-IR Perkin Elmer-1600 spectrometer. SEM images were recorded with a Hitachi 3000 H Microscope from the dried film formed on the surface of the brass specimens taken from 0.1 N H3PO4 in the presence and absence of inhibitor immersed for 6 h at 300 K.

3. RESULTS AND DISCUSSION

3.1 WEIGH-LOSS METHOD

Table-1 shows the inhibition efficiency values of brass by weight-loss measurements at different inhibitor concentrations in 0.1 N H3PO4 for different immersion times and temperatures. It has been observed that the inhibition efficiency increases with increase in concentration of inhibitor and decreases with increase in temperature and immersion time. The maximum IE (78.95 %) of inhibitor was achieved at 0.0005 % of inhibitor at 300 K for 3 h.

Table -1: Calculated inhibition efficiency (IE) and surface coverage (SC) values for CLE on brass corrosion in 0.1 N H_3PO_4 for different immersion temperatures and times

Conc. of inhibitor (%)	For 3 h		For 6 h		At 300 K	
	SC (θ)	IE (%)	SC (θ)	IE (%)	SC (θ)	IE (%)
	300 K				24 h	
0.0000	0	0	0	0	0	0
0.0001	0.4211	42.11	0.2692	26.92	0.2857	28.57
0.0002	0.4737	47.37	0.3462	34.62	0.3117	31.17
0.0003	0.6316	63.16	0.3846	38.46	0.3507	35.07
0.0004	0.6842	68.42	0.5000	50.00	0.4026	40.26
0.0005	0.7895	78.95	0.6539	65.39	0.4675	46.75
	318 K				48 h	
Blank	0	0	0	0	0	0
0.0001	0.3333	33.33	0.2121	21.21	0.2191	21.91
0.0002	0.4286	42.86	0.3030	30.30	0.2303	23.03
0.0003	0.5238	52.38	0.3636	36.36	0.2528	25.28
0.0004	0.5714	57.14	0.4546	45.46	0.3034	30.34
0.0005	0.6667	66.67	0.6061	60.61	0.3820	38.20
	328 K				72 h	
Blank	0	0	0	0	0	0
0.0001	0.2500	25.00	0.1786	17.86	0.1857	18.57
0.0002	0.3750	37.50	0.2321	23.21	0.2236	22.36
0.0003	0.4167	41.67	0.2679	26.79	0.2405	24.05
0.0004	0.5000	50.00	0.3036	30.36	0.2700	27.00
0.0005	0.5833	58.33	0.4107	41.07	0.3291	32.91
	338 K				96 h	
Blank	0	0	0	0	0	0
0.0001	0.1765	17.65	0.1642	16.42	0.1398	13.98
0.0002	0.2647	26.47	0.1791	17.91	0.1550	15.50
0.0003	0.3823	38.23	0.2239	22.39	0.1672	16.72
0.0004	0.4706	47.06	0.2836	28.36	0.2006	20.06
0.0005	0.5882	58.82	0.3881	38.81	0.2584	25.84

3.2 THERMODYNAMIC AND KINETIC ANALYSIS

The adsorption of the organic compounds can be described by two main types of interactions: physical adsorption and chemisorptions. They are influenced by the nature of the charge of the metal, the chemical structure of the inhibitor, pH, the type of the electrolyte and temperature [6].

3.2.1 ACTIVATION ENERGY

In order to elucidate the inhibitive properties of the inhibitor and the temperature dependence on the corrosion rates, the energy of activation for the corrosion process in the absence and presence of the inhibitor was evaluated from the following Arrhenius equation (4) and the values obtained are presented in Table-2:

$$\log \frac{p_2}{p_1} = \frac{Ea}{2.303 \times R}\left[\frac{1}{T_1} - \frac{1}{T_2}\right] \quad (5)$$

where p_1 and p_2 are rate of corrosion at temperatures T_1 and T_2 respectively.

Arrhenius plot for the corrosion rate of brass in the presence CLE for 3 h and 6 h are given in Figure 1: (a)-(b). Straight lines were obtained from the plot of Log P versus 1/T with slope equal to - E_a / 2.303 R. Note first that the E_a values are low, indicating fast corrosion of brass in both the solutions [13]. The values of E_a calculated from the slopes of Arrhenius plot and by using equation (4) are approximately almost similar.

The estimated values of E_a for brass corrosion in the presence of CLE are listed in the Table -2. The values of E_a > 80 KJ/mol indicate chemical adsorption where as E_a < 80 KJ/mol infer physical adsorption. The E_a values indicate that the process is activation controlled. In the present study, the E_a values support the fact that the inhibitors are physically adsorbed on brass surface. The estimated E_a in the presence of inhibitor infer that the interaction between the metal surface and the inhibitor was found to be strong enough to reduce corrosion [13]. The E_a values increases in the presence of CLE is often interpreted as physical adsorption with the formation of an adsorptive film with an electrostatic character [12]. In addition, the E_a values increases in the same order as the inhibition efficiency. This indicates that the energy barrier for the corrosion reaction increases in the presence of inhibitor in the acid solutions, the corrosion reaction will be further pushed to surface sites that are characterized by higher values of E_a indicating that corrosion occurs at the uncovered part of the surface [15].

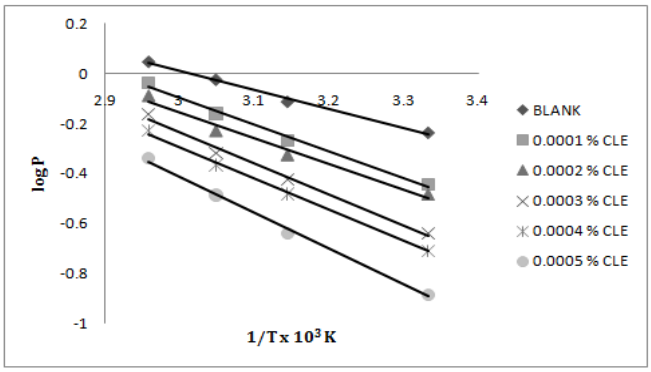

(a)

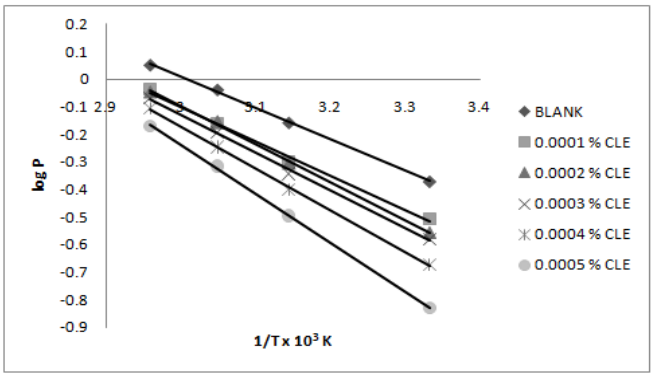

(b)

Figure 1: Arrhenius plot for 0.1 N H_3PO_4 with different concentrations of CLE for different times

3.2.2 FREE ENERGY OF ADSORPTION

The free energy of adsorption ΔG_{ads} were obtained from the following equations and the values obtained are presented in Table-2:

$$\Delta G_{ads} = - RT \ln (55.5K) \quad (6)$$

where K is given by

$$K = \frac{\theta}{C\,(1 - \theta)} \quad (7)$$

where θ is surface coverage on the metal surface, C is the concentration of inhibitor in mol/l and K is equilibrium constant.

Results obtained indicate that the values of ΔG_{ads} are negative in all cases, indicating that the CLE extract is strongly adsorbed on the brass surface [14]. The value of ΔG_{ads} indicates that the inhibitor functions by physically adsorbing on the surface of the brass. Generally values of ΔG_{ads} upto the -29.47 $KJmol^{-1}$ are consistent with electrostatic interaction between charged molecules and a charged metal, while those more negative than the -40 $KJmol^{-1}$ involve charge sharing or transfer from the inhibitor molecules to the metal surface to form a co-ordinate type of bond [15]. Physical adsorption is a result of electrostatic attraction between charged metal surface and charged species in the bulk of the solution. Adsorption of negatively charged species can also protect the positively charged metal surface acting with a

negatively charged intermediate such as acid anions adsorbed on the metal surface [6].

Table -2: Calculated activation energy (E_a), free energy of adsorption (ΔG_{ads}), enthalpy change (ΔH), entropy change (ΔS) values for CLE on brass corrosion in 0.1 N H_3PO_4 at 300 K

Conc. of inhibitor (%)	E_a from equation (kJ/mol)	E_a from Arrhenius Plot (kJ/mol)	ΔG_{ads} (kJ/mol)	ΔH (kJ/mol)	ΔS (mol/kJ)
For 3 Hours					
Blank	12.91	12.98	0	0	0
0.0001	20.73	19.15	-29.47	-24.75	0.0157
0.0002	20.33	21.28	-27.80	-24.73	0.0102
0.0003	24.37	22.68	-26.61	-24.72	0.0063
0.0004	24.38	23.94	-25.71	-24.70	0.0034
0.0005	27.79	27.36	-24.50	-24.67	0.0006
For 6 Hours					
Blank	21.00	16.76	0	0	0
0.0001	23.99	23.94	-28.94	-24.70	0.0141
0.0002	26.05	25.53	-27.56	-24.69	0.0096
0.0003	26.15	29.93	-26.66	-24.64	0.0067
0.0004	28.98	28.16	-26.08	-24.66	0.0047
0.0005	33.65	31.92	-25.27	-24.62	0.0022

3.2.3 ENTROPY AND ENTHALPY

Kinetic parameters such as enthalpy (ΔH) and entropy (ΔS) of activation of corrosion process is calculated from the following thermodynamic basic equations and the values obtained are presented in Table-2:

$$\Delta H = E_a - RT \quad (8)$$

$$\Delta G_{ads} = \Delta H - T\Delta S \quad (9)$$

Enthalpy of activation of absolute values lower than the -24.75 $KJmol^{-1}$ indicates physical adsorption, and the values approaching 100 $KJmol^{-1}$ indicate chemical adsorption. In this study, the values of ΔH are lower than the -24.75 $KJmol^{-1}$ confirming physical adsorption on the acid solutions [10]. The negative values of ΔH also show that the adsorption of inhibitor is an exothermic process [14].

The ΔS values are positive for the acidic bath. This implies that the activation complex is the rate determining step representing association rather than dissociation, indicating that a decrease in disorder takes place on going from reactant to the activated complex [10].

3.2.4 RATE CONSTANT AND HALF LIFE

Figure 2: show the plots of log W_f (final weight loss) obtained in weight-loss studies *vs.* time in days for the brass dissolution. From the plots, the values of rate constant and half-life were evaluated using the following equations [16,17] and the values obtained are presented in Table-3:

$$\text{Rate constant (k)} = 2.303 \times \text{slope } (sec^{-1}) \quad (10)$$

$$\text{Half - life period } t_{1/2} = \frac{0.693}{k} (sec) \quad (11)$$

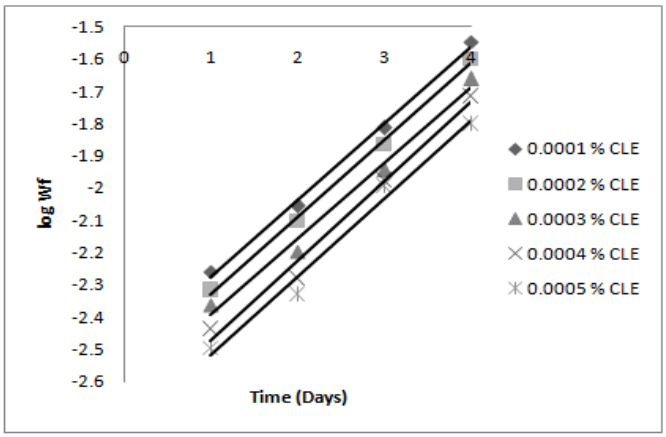

Figure 2: Plot of log W_f *vs.* time (days) for 0.1 N H_3PO_4 with different concentrations of CLE

In this study, linear plots were obtained, which indicates first order kinetics [9]. In this study the rate constant values were decreased where as the half-life values were increased with increasing concentration of CLE.

Table -3: Calculated rate constant (k) and half-life period ($t_{1/2}$) values for CLE on brass corrosion in 0.1 N H_3PO_4 at 300 K

Conc. of inhibitor (%)	Rate constant (sec^{-1})	Half-life Period (sec)
0.0001	0.5117	1.3542
0.0002	0.5117	1.3542
0.0003	0.5117	1.3542
0.0004	0.5315	1.3038
0.0005	0.5758	1.2037

3.2.5 ADSORPTION ISOTHERMS

The values of surface coverage Θ for different concentrations of the CLE at 300 K have been used to identify the best isotherm to determine the adsorption process. The adsorption of organic adsorbate on the surface of copper is regarded as substitutional process between the organic compound in the aqueous phase org_{aq} and the water molecules adsorbed on the copper surface $(H_2O)_{ads}$ [18].

$$Org_{(aq)} + x\,(H_2O)_{(ads)} \rightarrow Org_{(ads)} + x\,H_2O_{(aq)}$$

where x is the size ratio, that is the number of water molecules displaced by one molecule of organic inhibitor. Attempts were made to fit Θ values of various isotherms, including Langmuir, Freundlich, Temkin and Frumkin isotherms. By far the results were best fitted by Temkin adsorption isotherm. The Temkin adsorption isotherm is given by the following equation.

$$\ln kC = a\theta$$

where k is the equilibrium constant of the adsorption reaction, C is the inhibitor concentration in the bulk of the solution and a is the molecule interaction parameters depending upon molecular interactions in the adsorption layer and the degree of heterogeneity of the metal surface. The plot of Θ against log C for all additives gives straight lines, as shown in Figure 3: (a)-(b). This indicates that these compounds are adsorbed on the surface of brass according to Temkin adsorption isotherm [19,20].

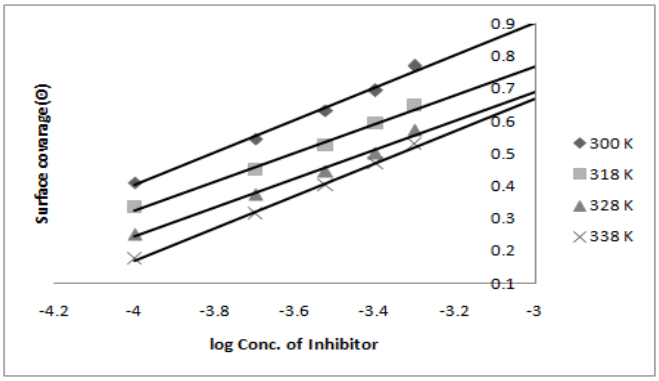

(a)

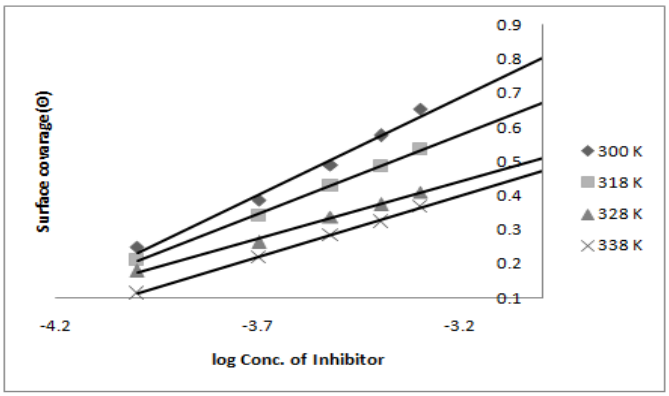

(b)

Figure 3: Temkin's adsorption isotherm plot for 0.1 N H_3PO_4 with different concentration of CLE for different times

3.3 POTENTIOSTATIC POLARIZATION STUDIES

Polarization measurement is an important research tool in the investigation of a variety of electrochemical phenomena. Such measurements permit studies of the reaction mechanism and the kinetics of corrosion phenomena on the metal deposition. Figure 4: shows the cathodic and anodic polarization curves of brass in 0.1 N H3PO4 with and without addition different concentrations of CLE. Table-4 gives the values of associated electrochemical parameters. The i_{corr} values decreased with increasing concentration of inhibitor. The values of anodic Tafel slope (b_a) and cathodic Tafel slope (b_c) of CLE added solutions are found to change with inhibitor concentration, which clearly indicates that the inhibitors controlled both the anodic and cathodic reactions. The IE of CLE attained a maximum value at 0.0005 % concentration of inhibitor. The values of IE increased with increasing concentration of inhibitor, indicating that a higher surface coverage was obtained in solution with optimum concentration of inhibitor. The

effect of the anodic polarization behavior of brass (Figure 4) suggests that protective films formed on the metal surface can alter anodic dissolution in solution shows that CLE formed a film that acted as a barrier to protect the metal surface [19-21].

Table -4: Electrochemical parameters and inhibition efficiency (IE) for corrosion of brass in 0.1 N H_3PO_4 containing different concentrations of CLE

Conc. of inhibitor (%)	OCP (mV) *vs.* SCE	E_{corr} (mV) *vs.* SCE	Tafel constants		i_{corr} ($\mu A/cm^2$)	IE (%)
			b_a (mV/dec)	b_c (mV/dec)		
Blank	-193	-190	300	100	310	0
0.0001	-200	-198	300	95	290	6.45
0.0002	-220	-222	280	160	240	22.58
0.0003	-228	-230	160	150	180	41.94
0.0004	-236	-236	90	140	160	48.39
0.0005	-245	-240	50	150	89	71.29

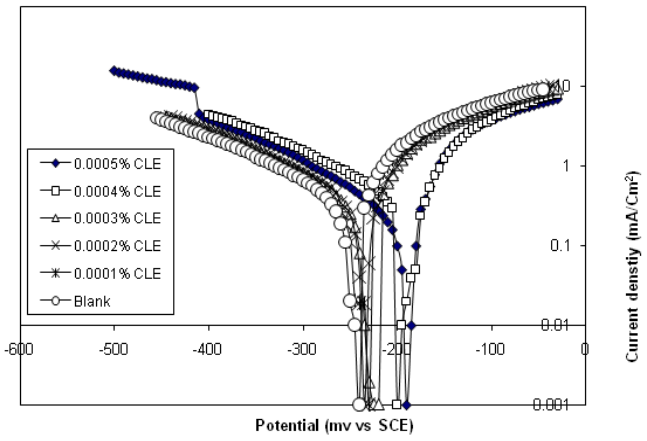

Figure 4: Polarization curves for brass in 0.1 N H_3PO_4 with different concentrations of CLE

3.4 AC IMPEDANCE MEASUREMENTS

AC impedance spectroscopy has been shown to be a powerful tool to study the corrosion process of metals in different environments and to characterize the inhibition ability of a corrosion inhibitor, which is related to the charge transfer resistance (R_{ct}). The double layer capacitance (C_{dl}) can also be used to determine the inhibition ability. The inhibition performance of an organic or natural substance on a metal surface depends not only on the chemical structure of the organic substance and the nature of the metal, but also on the experimental conditions such as the immersion time and concentration of the adsorbent. The corrosion behavior of brass, in acidic solution with and without CLE, is also investigated by AC impedance measurements at 300 K (Figure 5). The impedance parameters and the IE % derived from the investigation are mentioned given in Table-5. As it can be seen from Figure 5:, impedance diagrams show a semi-circular appearance, indicating that a charge transfer process mainly controls the corrosion of brass. From the impedance data, we notice an increase in the charge transfer resistance and decrease of the double layer capacitance with increasing the inhibitor concentration, indicating that PPE inhibits the corrosion rate of brass by an adsorption mechanism. Therefore, the decrease in the C_{dl} value can be attributed to a decrease in the local dielectric constant and/or an increase in the thickness of the electrical double layer, suggesting that the inhibitor molecules act by adsorption at the metal/solution interface as a consequence of the replacement of water molecules by the inhibitor molecules [8].

A comparison may be made between the inhibition efficiency values obtained by different methods (weight loss, potentiostatic polarization and AC impedance methods). We can see that whatever the method used, no significant changes are observed in IE % values. We can then conclude that there is a good agreement with the three methods used in this study at all tested concentrations and that the acid extract of *Chaetomorpha linum* acts as a green inhibitor for acid corrosion of brass.

Table -5: Impedance measurements and inhibition efficiency (IE) for corrosion of brass in 0.1 N H_3PO_4 containing different concentrations of CLE

Conc. of inhibitor (%)	R_{ct} (ohm cm^2)	C_{dl} ($\mu F/cm^2$)	IE (%)
Blank	150.60	5.74	00.00

0.0001	520.18	2.21	71.05
0.0002	685.18	1.80	78.02
0.0003	1300.17	1.01	88.42
0.0004	1910.68	0.73	92.12
0.0005	7370.33	0.19	97.96

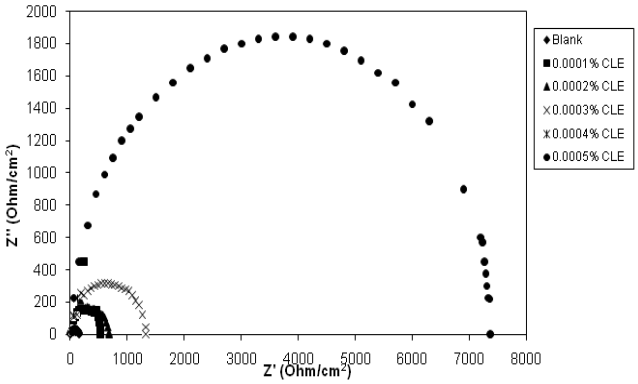

Figure 5: Nyquist plot of brass in 0.1N H_3PO_4 with different concentrations of CLE

3.5 SURFACE EXAMINATIONS

3.5.1 FT-IR SPECTROSCOPY

Figure 6: shows the FT-IR spectrum recorded in the range 400-4000 cm^{-1} to identify the functional groups present in CLE. From FT-IR, It was observed that aromatic molecules with following functional groups, intermolecular hydrogen bonding and O-H stretching (3448.77 cm^{-1}), -C≡N in nitrile (2347.84 cm^{-1}), – C≡C disubstituted alkyne (2099.34 cm^{-1}), -C-H and C=O stretching in aldehyde (1640.73 cm^{-1}), - C=O stretching in ester (1398.92 cm^{-1}), -C-H stretching -C-O-C- (1115.08 cm^{-1}), and -C-H deformation in alkyne (658.02 cm^{-1}) are present in CLE. Further found that CLE inhibits the corrosion of brass specimen with high efficiency due to the presence of N and O in the organic molecules of CLE [22,23].

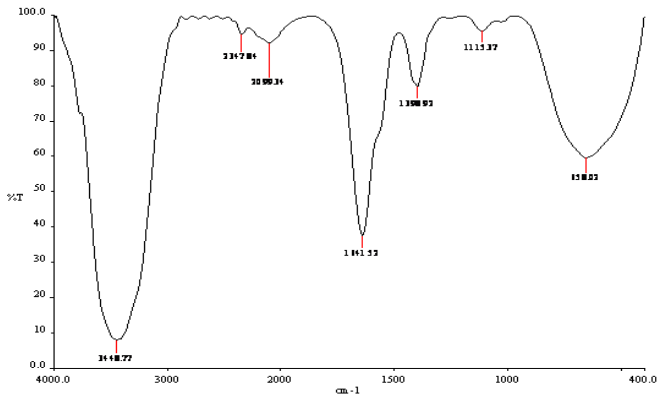

Figure 6: FT-IR spectra of the surface of brass formed by immersing sample in 0.1 N H_3PO_4 with CLE for 6 h

3.5.2 SCANNING ELECTRON MICROSCOPY

SEM micrograms of the polished surface of brass exposed for 6 h in 0.1 N H3PO4 in absence and presence of CLE are shown in Figure 7: (a)-(b) shows the surface morphology of brass formed in 0.1 N H3PO4 without and with CLE for 6 h. In the comparison of the SEM micrograms, there were a rough surface on brass in absence of extract and a smooth surface with deposited extract in presence of the CLE. This confirms that the extract inhibited corrosion of brass through adsorption of the inhibitor molecules on metal surface. After immersing in the inhibitor containing solution, the entire metal surface was covered with a layer formed with inhibitor as a barrier to corrosion, as denoted by rougher over abrasions. The inhibiting layer was possibly consisting of Cu^{2+} and Zn^{2+} complexes formed with the CLE derivatives are mentioned in FT-IR [24,25].

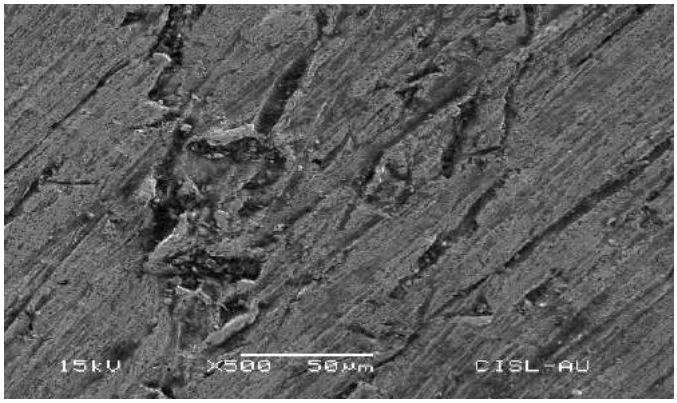

(a)

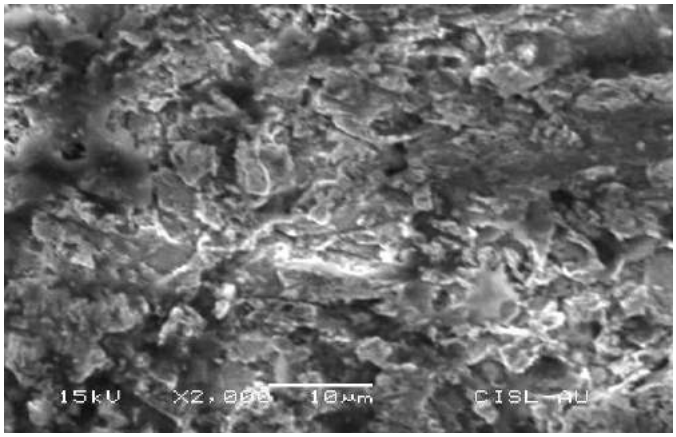

(b)

Figure 7: SEM images of brass surface after 6 h immersion in 0.1N H_3PO_4 in the absence (a) and presence (b) of CLE

4. CONCLUSIONS

The inhibition efficiency of CLE on corrosion of brass in 0.1 N H_3PO_4 increases on increasing of concentration of the extract and decreases with rise in temperature. Adsorption of inhibitor molecules of the extract on brass surface is found to obey Tempkin adsorption isotherm. The increase in the values of activation energies of the corrosion process in the presence of extract indicates that CLE creates a physical barrier to charge and mass transfer, leading to reduction in corrosion rate of brass in 0.1 N H_3PO_4. The negative values of ΔG_{ads} and ΔH highlight that the inhibition of corrosion of brass through adsorption is spontaneous and exothermic. Their values

also reveal that physical adsorption is involved in the adsorption process. Potentiodynamic polarization measurements show that CLE acts as a mixed type inhibitor. Inhibition efficiency values were found to show good trend with weight-loss method, potentiodynamic polarization and electrochemical impedance spectroscopy studies. SEM and FT-IR studies confirm that corrosion inhibition of brass in 0.1 N H3PO4 is due to adsorption of the CLE extract on brass.

REFERENCES

[1]. Chandrasekaran V.; Kannan K.; Natesan M., "Inhibiting properties of some amines on corrosion behaviour of mild steel in phosphoric acid solution at various temperatures". Asian Journal of Chemistry, Vol. 17, No. 3, 2005, p I921-1934.

[2]. Chandrasekaran V.; Kannan K.;Natesan M., "Electrochemical behaviour and inhibiting properties of isopropyl amine on mild steel corrosion in phosphoric acid solution". Oriental Journal of Chemistry, Vol. 21, No. 1, 2005, p 81-88.

[3]. Ranjana; Nandi M. M., "Evaluating two new sulphonamidoimidazolines on the corrosion of brass in 0.6 N aqueous sodium chloride solution". Indian Journal of Chemical Technology, Vol. 18, 2011, p 29-36.

[4]. Ranjana; Ranu Banerjiee; Nandi M. M., "Corrosion inhibition of brass in presence of 1,4,5,6-tetrahydropyridimine derivatives in chloride solution". Indian Journal of Chemical Technology, Vol. 20, p 237-244.

[5]. Ravichandran R.; Rajendran N., "Electrochemical behavior of brass in artificial seawater: effect of organic inhibitors". Applied Surface Science, Vol. 241, 2005, p 449-458.

[6]. Vijayalakshmi P. R.; Rajalakshmi R.; Subhashini S., "Corrosion inhibition of aqueous extract of cocos nucifera-coconut palm-petiole extract from destructive distillation for the corrosion of mild steel in acidic medium". Portugaliae Electrochimica Acta, Vol. 29, No. 1, 2011, p 9-21.

[7]. Ramananda; Mayanglambam S.; Vivek Sharma; Gurmeet Singh, "*Musa Paradisiaca* Extract as a green inhibitor for corrosion of mild steel in 0.5 M sulphuric acid solution". Portugaliae Electrochimica Acta, Vol. 29, No. 6, p 405-417.

[8]. Khadraoui A.; Khelifa A.; Boutoumi H.; Mettai B., Karzazi Y.; Hammouti B., "Corrosion inhibition of carbon steel in hydrochloric acid solution by *Mentha Pulegium* Extract". Portugaliae Electrochimica Acta, Vol. 32, No. 4, 2014, p 271-280.

[9]. Ejikeme P. M.; Umana S. G.; Onukwuli O. D., "Corrosion inhibition of aluminium by *Treculia Africana* leaves extract in acid medium". Portugaliae Electrochimica Acta, Vol. 30, No. 5, 2012, p 317-328.

[10]. Muna K. Irshedat; Eyad M. Nawafleh; Tareq T. Bataineh; Riyadh Muhaidat; Mahmoud A. Al-Qudah; Ahmed A. Alomary, "Investigation of the inhibition of aluminium corrosion in 1 M NaOH solution by *Lupinus varius l.* extract". Portugaliae Electrochimica Acta, Vol. 31, No. 1, 2011, p 1-10.

[11]. Ravichandran R.; Rajendran N., "Electrochemical behavior of brass in artificial seawater: effect of organic inhibitors". Applied Surface Science, Vol. 241, 2014, p 449-458.

[12]. Chandrasekaran V.; Saravanan J., "Effect of S-AITA on mild steel Corrosion in Acidic Medium". Corrosion Science and Technology, Vol. 5, No. 5, 2006, p 160-167.

[13]. Mahmoud S. S., "Corrosion inhibition of Muntz (63% Cu, 37% Zn) alloy in HCl solution by some naturally occurring extracts". Portugaliae Electrochimica Acta, Vol. 24, 2006, p 441-455.

[14]. Elmsellem H.; Basbas N.; Chetouani A.; Aouniti A.; Radi S.; Messali M.; Hammouti B., "Quantum chemical studies and corrosion inhibitive properties of mild steel by some pyridine derivatives in 1 N HCl solution". Portugaliae Electrochimica Acta, Vol. 32, No. 2, 2014, p 77-108.

[15]. Tadeja Kosec; Ingrid Milosev; Boris Pihlar, "Benzotriazole as an inhibitor of brass corrosion in chloride solution". Applied Surface Science, Vol. 253, 2007, p 8863-8873.

[16]. Chandrasekaran V.; Kannan K.; Natesan M., "The Effect of Imidazole and 2-Methyl Imidazole on the Corrosion of Mild Steel in Phosphoric acid solution". Corrosion Science and Technology, Vol. 4, No. 5, 2005, p 191-200.

[17]. Nnaemeka J. N. Nnaji; Nelson O.Obi-Egbedi; Chukwuma O. B. Okoye, "Cashew nut testa tannin: assessing its effects on the corrosion of aluminium in HCl". Portugaliae Electrochimica Acta, Vol. 30, No.2, 2014, p 157-182.

[18]. Megahed H. E., "Ethoxylated fatty esters as corrosion inhibitors for copper in nitric acid solutions". Portugaliae Electrochimica Acta, Vol. 29, No.4, 2011, p 287-294.

[19]. Chandrasekaran V.; Gokulalakshmi K., "Corrosion studies on brass in H_3PO_4 with Benzamide". Bulletin of Electrochemistry, Vol. 22, 2006, p 379-384.

[20]. Chandrasekaran V.; Kannan K.; Natesan M., "Synergistic effect of Isopropyl amine with Cl^- and SO_4^{2+} on inhibition of mild steel corrosion in phosphoric acid". International Journal of Pure and Applied Chemistry, Vol. l, No. 1, 2006, p 101-115.

[21]. Gaikwad A. B.; Patil P. P.; Sudeshna Chaudhari, "Poly (o-anisidine) coatings on brass: synthesis, characterization and corrosion protection". Current Applied Physics, Vol. 9, 2009, p 206-218.

[22]. Ravichandran R.; Nanjudan S.; Rajendran N., "Effect of benzotriazole derivatives on the corrosion of brass in NaCl solutions". Applied surface science, Vol. 236, 2004, p 241-250.

[23]. Du X. S.; Su Y. J.; Li J.X., Qiao L.J.; Chu W.Y., "Inhibitive effects and mechanism of phosphates on the stress corrosion cracking of brass in ammonia solutions". Corrosion science, Vol. 60, 2012, p 69-75.

[24]. Ramananda; Mayanglambam S.; Vivek Sharma and Gurmeet Singh, "*Musa Paradisiaca* Extract as a green inhibitor for corrosion of mild steel in 0.5 M sulphuric acid solution". Portugaliae Electrochimica Acta, Vol. 29, No. 6, 2011, p 405-417.

[25]. Khadraoui A.; Khelifa A.; Boutoumi H.; Mettai B.; Karzazi Y.; Hammouti B., *"Corrosion inhibition of carbon steel in hydrochloric acid solution by Mentha Pulegium Extract".* Portugaliae Electrochimica Acta, Vol. 32, No. 4, 2014, p 271-280.

BIOGRAPHIES

R. SELVA KUMAR, Research Scholar (PT), Department of Chemistry, Bharathiar University, Coimbatore-641 046, Tamil Nadu, India. He is Lecturer in Chemistry, Department of Chemistry, Sree Krishna Polytechnic College, Nagercoil-629 003, Tamil Nadu, India. Email: rselvakumar86@yahoo.com

Dr. V. CHANDRASEKARAN, Assistant Professor in Chemistry, Department of Chemistry, Govt. Arts College (Autonomous), Salem – 636 007, Tamil Nadu, India. Email: chandru_v_m@yahoo.co.in

MULTI-WALLED CARBON NANOTUBE (MWCNT) BASED COMPOSITE MATERIAL: A REVIEW

ABDUL RAHMAN SANAD[1], M.N.M.ANSARI[2], JAMAL O.SAMEER[3], ABDULBASIT ABDULLAH[4], BASSAM ALASEEL[5]

Center for Advance Materials, College of Engineering, Universiti Tenaga Nasional, Malaysia

ABSTRACT

This work discusses multiple applications of multi walled carbon nanotube (MWCNT) based composite materials. Carbon materials are known to possess suitable electrical conductivity, due to its of layered structure and elevated surface area, which results in appliances that have internal electrodes for recharging, such as batteries and components for fuel cell, or devices that work with nano-electronics such as computer chips, storage media for fuel cell for on-board hydrogen supply, and superconductors. This study will shed light on the production, sharing, and storage of energy within these carbon materials (multi-walled carbon tubes). Multi walled carbon nanotubes are regarded as a more useful strengthening factor compared to the shorter multi walled carbon nanotubes. The results agree with the experimental results, which confirms the validity of the model. The current research on carbon materials (multi-walled carbon tubes) focuses on the production, distribution, and storage of energy.

Key Words:*multi walled carbon nanotube; composite material properties; nano structure; matrix and fiber composite.*

1. INTRODUCTION

When carbon nanotubes were discovered in 1991 [1], it became the subject of fascination and research, due to its low density, very high rigidity, flexibility, and strength [2]. Due to these factors, they are regarded as suitable strengthening agent in nano combinations. It was also confirmed that adding 1 wt. % CNTs into a matrix increases the resulting composite's rigidity by 36-42 %, and the tensile strength by 25 % [3]. Both experiments and simulations confirmed the fact that CNTs possess extremely high moduli[4], in the neighborhood of 100 GPa, surpassing carbon fibers. CNTs also possess high geometric fraction, rigidity-to-weight, and strength-to-weight fractions. These properties are transferrable to the matrix via the inclusion of CNTs [5]. Polymer matrices are widely used, but metals and ceramics are currently seeing an upsurge. TEM images of MWCNT–Polystyrene campsite, where nanotubes were dispersed within the polystyrene matrix, is shown in Fig. 1[6]. CNTs are quite easily dispersed into matrices, rendering them suitable structural additions. The properties of the resulting combination relies on workable load shift mechanism between constituents and the matrix. However, any purported advantages from the CNT will be rendered inapplicable if the resulting bonds are negligible. This means that the formation of an interfacial interaction between CNTs and its polymer matrix is vital [7].

Andrews et al. [8] synthesized a PS/MWCNT composite via shear amalgamation, which resulted in a 15% improvement to the tensile strength from 5% volume fraction of MWCNTs in the matrix [9].

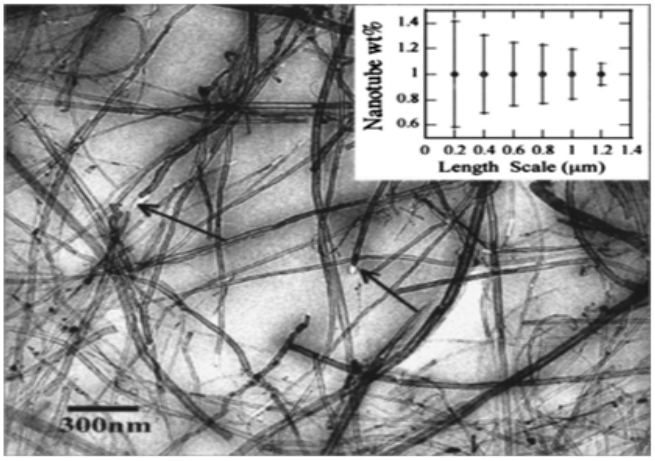

Figure 1: TEM image of MWCNT–Polystyrene film in which the nanotubes are homogeneously distributed in the polystyrene matrix [6].

Among all carbon materials, carbon nanotubes (CNTs) are regarded as the best inclusive assets, as they provide many different benefits, such as strengthening and improvements to the performance cementations compared to traditional fibers. The scientific community has been enamored with CNTs and their corresponding applications to the addition of of new nanocomposites. CNTs possesses hexagonal carbon walls of tubes, which have a graphite-like structure; they are long, have thin fullerenes, and the end caps are madeup of pentagonal rings [10]. These benefits lead to the potential for the utilization for different applications such as strengthening materials[11], or hydrogen containers [12].

MWCNTs were scattered using surfactant-ultrasonic technique with GA, which is a commercially available surfactant. Based on the outcomes of the previous experiment [25], the mass ratio of MWCNTs to dispersant was 1:6, while the pertinent dispersant was first dissolved by four-fifths of the total water in every combination. Later on, the measured MWCNTs were

placed into an aqueous dispersant solutions and scattered adequately in an ultrasound processor (DS-3510DT) for 30 min at room temperature. Finally, 0.13 wt% of deformer was used for the purpose of decreasing the amount of air bubbles within the solution. Matrix materials, such as ceramics and metals, are also included. TEM image of MWCNT–Polystyrene composite, where the nanotubes were homogenously distributed within the polystyrene matrix, were taken.

The current work shows the influence of dispersed MWCNTs on the flexural strength of cement-based composites. Simultaneously, the microstructures of the composites were studied. Field emission scanning electron microscope (FESEM) was used to analyze the morphology and microstructure of cement-composites, while the porosity was analyzed using mercury intrusion porosimetry (MIP).

The two most important types of nanotubes are the single walled nanotubes (SWNT) and the multi-walled nanotubes (MWNT). The SWNTs [13, 14] contain one single sheet of seamlessly rolled grapheme, which forms a diameter of 1 nm, and a length of less than a few centimeters cylinder, while the MWNTs falls within the range of these cylinders, with 0.35 nm separation, organized into a concentric configuration, similar to the graphite's basal plane separation [15]. Its diameter falls within2-100 nm, while its length is tens of microns.

Nowadays, the most widely used synthetic techniques to manufacture SWNTs are the ones based on chemical vapor deposition [17, 18], especially the decomposition of CO [19] and laser ablation [16]. However, certain imperfections of its production in the context of chemical and physical characteristics of the nanotubes can still be improved.

There are many approaches to rolling up a single walled nanotube for the purpose of forming grapheme sheets. When rolling, the symmetry of the planar system is altered, which prompts it to change its directional alignment compared to its hexagonal lattice.

The semi-conducting, metallic, and semi-metallic tube types are distinguished based on the relationship between the unit vectors of the hexagonal lattice and the axial direction. The band gap of the semi-conducting nanotubes varies between 1.8 eV in the case of the tubes with minor diameter, to 0.18 eV for the tubes with major diameter [20].

The conductivity of the pristine carbon nanotubes is particularly high. Owing to their one-dimensional nature, charge carriers can pass through the nanotubes without any scattering, which means that due to the diminished Joule heating, the nanotubes can transport huge current densities of up to 100 MA/cm^2 [21]. With this notable exception, the semi-conducting nanotubes present a carrier mobility of up to 105 cm^2/Vs [22]. SWNTs are predisposed to high conductivity as well, but in order to realize this, a transition temperature of 5 K is required [23].

2. METHOD OF COMPOSITE MWCNT

N. Venkatesan Prabhu &D. Sangetha [24] studied multi partitioned carbon nanotube (MWCNT) in an oxygen cross over, water absorption, and functioning of Chitosan (CHIT) in a single chamber microbial fuel cell (SCMFC). CHI T non-covalently performed MWCNT with CHIT (CHIT–MWCNT), arranged in the shape of membranes, and typified via FTIR,XRD,DRSUV, CD,Raman,SEM, and TEM to rehash the relationship between MWCNT and chitosan. Research outcomes indicated that the MWCNT integrated chitosan composite membrane influenced the assets and functions of CHIT within micro biofuel cellHence, CHIT–MWCNT is regarded as a suitable candidate for micro biofuel cell.

A.K. Singh [25] pointed out that crystallization kinetics are functional restrictions to the material, thus, the study defined the kinetics of Se96Zn2Sb2 (SZS) chalcogenide alloy and its combinations with 0.05% (MWCNT) and 0.05% grapheme (GF). The crystallization of kinetic restrictions was obtained from Differential Scanning Calorimetric (DSC) measurement at 5, 10, 15 and 20 _C/min heating rates from a diversified estimate upon the glass transition, onset crystallization, and peak crystallization temperatures. Afterwards, the Hruby Hr glass shaping capacity parameter, thermal constancy, nucleation and growth order parameter (n), and dimensional parameter (m) of the materials were investigated. The results were indicative of the fact that the objects were within multiple kinetic parameters from the inclusion of MWCNT and GF in SZS. It was also confirmed that MWCNT composite's glass transition activation energy (Eg), onset crystallization temperature (Ec), and peak crystallization (Ep) exceeded the GF composite, while it was less in the case of the parent alloy. However, multiple values for the Hr and thermal constancy were derived for the composites. Generally, two-to-one dimensional nucleation and growth mechanism were approximated for these objects.

P. Jindal et al. [26] experimentally studied the mechanical properties of (MWCNT-PC). The composites of MWCNT-PC were synthesized via a two-step method of solution blending and compression molding. The (MWCNTs) compositions within polycarbonate (PC) were 0.5% to 10% wt%. Mechanical properties such as elastic modulus and hardness were determined using the nanoindentation technique. The improvements to the mechanical properties were in agreement with previous work on Split Hopkinson Pressure Bar (SHPB). The improvements are assumed to be from the enhanced load transfer, increased surface area, and optimized interaction between the reinforcement and its base matrix.

Superior mechanical properties, such as increased strength, stiffness, and aspect ratio of carbon nanotubes render them the perfect support material for nanocomposites [27]. Load transfer in the context of composites were studied under compression and tensile loading conditions in this work. To gauge the material properties using representative volume element (RVE) approach, the continuum mechanics model was used. Numerical analysis was done by Finite Element Modeling (FEM), with the results validated using the rule of mixture. Both results were in agreement. The influence

ofthe width and the length of MWCNTs upon the flexibility of the nanocompositeswas analyzed as well. MWCNT was seen as more effective in strengthening compositescompared to shorter MWCNTs. This is confirmed via FEM analysis. The dispersion of 5% MWCNT-PC within the composite is demonstrated in Fig 2, showing excellent levels of dispersion.

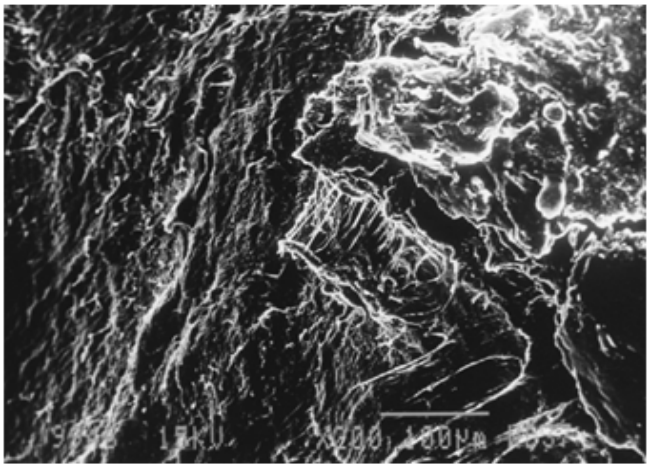

Figure 2: SEM image for 5% MWCNT-PC composite indicating dispersion [27].

Arash Montazeri [28] fabricated MWNT with hydroxyl groups (MWNT-OH), while non-functionalized MWNT were utilized to synthesize MWNT/epoxy composites via sonication. The viscoelastic properties of the composites were determined using the dynamic mechanical, thermal analysis (DMTA) equipment. The outcome indicated that adding nanotubes to epoxy alters the viscoelastic properties. The models of fabricated nanotubes were determined to have a more influential effect upon the Tg compared to the composites, which incidentally possess similar sums of non-functionalized nanotubes. The viscoelastic response was plottedusingthe COLE–COLE diagram from the results gleamed from the DMTA. The outcome of the Perez model and the viscoelastic behaviors of the composite are similar and falls within the range of agreement.

J.-C. Zhao et al. [29] discuss the integration of hyper branched poly (urea-urethane)-grafted multi-walled carbon nanotubes (HPU-MWCNTs) into polyurethane (PU) matrix upon poly (ethylene oxide-tetrahydrofuran) and aliphatic polyisocyanate resin via remedial means. The 9–12 mm thick HPU shell on the MWCNTs were created by dispersing MWCNTs and enhancing the interfacial bond of the PU matrix and MWCNTs, improving the storage modulus and Tg of the composite while enhancing the thermal constancy of PU. It is surmised that MWCNT composites enhanced thermal conductivity while maintaining electrical resistivity, as opposed to neat PU. Fig 3 shows the TEM images of HPU-MWCNT.

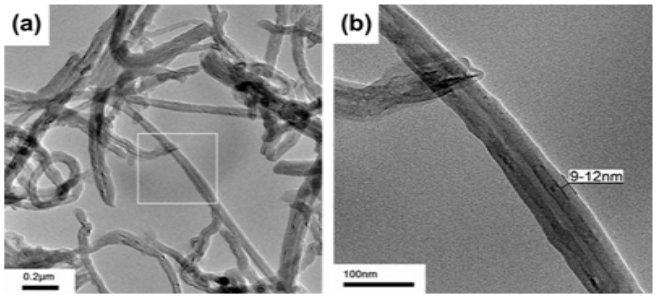

Figure 3: TEM images of (a) HPU-MWCNTs and (b) magnification of white frame in (a) [29].

D. Silambarasan et al. [30] presented experimental work on hydrogen uptake of single-walled carbon nanotubes (SWCNTs-Ti)-titanium metal composite. The composite contains both SWCNTs and Ti powder,fabricated into a tablet via cold pressing. The campsite has been prepared and hydrogenated by evaporating the tablet in a hydrogen-ambient environment on glass substrates using the electron beam (EB) evaporation technique. The obtained hydrogen uptake is due to the cumulative absorption of hydrogen by CNTs and Ti nanostructured materials.

K.K. Awasthi et al. [31] incorporated multi walled carbon nanotubes (MWCNTs) via chemical vapor deposition (CVD). The mice have been autopsied on 7, 14, 21, and 28 days after contact. The liver has been removed, and pieces of it secured in Bouin's solution for histopathological tests. The remaining liver was submerged in cold saline, spotted dry, weighed fast, and homogenized in ice cold buffer. The activity of superoxide dismutase (SOD) and catalase (CAT) has been quickly estimated in the supernatant. The MWCNT in the liver was redirected to medicinal issues, such as damage in the macrophages, cellular abscess, ambiguous infection, death of the cells, and blood coagulation. The evaluation of SOD and CAT is indicative of altered stages within investigated groups, as opposed to the directions. This basically means that MWCNTs derived from ignition within the environment might be disastrous to human health.

J. Zhang & D. Jiang [32] adapted a technique that links MWCNTs, which results in the combination of ethyl chloride and amino sets. SEM shows the formation of hetero-junctions of MWCNTs with diverse morphologies. Afterwards, samples of unspoiled MWCNTs were chemically fabricated and linked, which strengthens the epoxy resin composite produced via cast molding. Malleable properties and the crack in the surfaces of the samples have been looked into as well. The outcomes reflected that comparing unspoiled MWCNTs and chemically fabricated MWCNTs, the chemically linked MWCNTs developed the crack damage, and as a result of this, the harshness of the combinations were considerably developed.

J. Zhang et al. [33] posited that inter-tube bridging of carbon nanotubes (CNTs) enhances inter-tube stress transfer abilities. It was also mentioned that the interfacial interactions provided by a wall-to-wall inter-tube bridging between two single-walled carbon nanotubes (SWCNTs) embedded in a polyethylene (PE)

matrix. Molecular dynamics (MD) models of tube pullout phenomena was represented by the embedding (10, 10)–(10, 10) SWCNT with interconnections into an amorphous PE matrix. The simulations demonstrated that inter-tube bridging improves the pullout energies, mostly due to three micro-mechanics: stress-induced tube deformation with localized auxetic effect, ‘‘cutting through’’ (penetration) between linker and matrix, and the accompanying tube pullout. Moreover, the results also predicted that linkers with long aliphatic chains or aromatic rings provide a further increasein the levels of the nanotube pullout energies. These are of potential importance in guiding the design of CNT/polymer composites through inter-tube linkage.

X. Jiang & L.T. DrzalHigh [34] analyzed High Density Polyethylene (HDPE) composites being strengthened via exfoliated graphene and platelets. Low molecular weight paraffin wax was used to coat both GNP and MWCNT to enhance scattering within HDPE. Wax-covered GNP and MWCNT were produced by combining wax with GNP and MWCNT in hot xylene, followed by solvent evaporation, and vacuum drying. It is assumed that covered GNP and MWCNT are more proficient in the development of electrical conductivity and the flexural properties of HDPE composites. The description of morphology confirmed that the scattering of GNP and MWCNT within the polymer matrix was enhanced via the wax covering technique, which also accounts for the improved electrical and mechanical properties in the nano composites.

M.R. Ayatollahi et al. [35] studied the influence of multi-walled carbon nanotubes (MWCNTs) on the mechanized properties of epoxy/MWCNT nano-combinations, and focused on crack toughness under bending and cut-off loading states. They conducted several finite element (FE) analyses to decide a suitable cut off loading limited states for a single-edge notch, bend sample (SENB), moreover, an equation was derived in order to estimate the cut-off loading crack toughness from the crack load. They saw that the augmentation in crack toughness of nano-composite relies on the style of loading. This outcome indicated that the presence of MWCNTs influenced crack toughness of nano combinations under cut-off loading compared to the usual loading. They scanned several electron microscopy (SEM) pictures from the crack on the surfaces in order to focus on its mechanisms. The outcomes indicated that the link between the distinctiveness of crack surface and the mechanical behaviors are monitored in the crack experiments.

A. Martone et al. [36] analyzed the influence of the bending modulus of dispersed multi-walled carbon nanotube (MWCNT) within epoxy. The enhancement in strength is divided into two restrictive responses; transition regions alongside the development of a percolate network of nanotubes. The introduction of CNTs resulted in maximum strength, which is suggestive of a relationship between percolation and stress transfer theory for large aspect ratio fillers. Fig 4 shows the conductivity of MWCNT/epoxy composites.

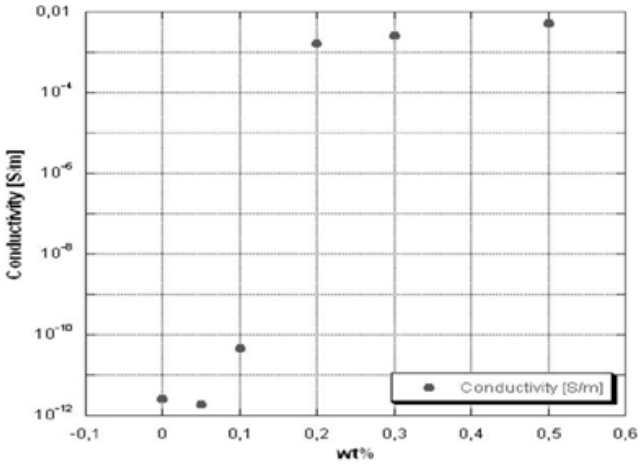

Figure 4: Conductivity of MWCNT/epoxy composites prepared by sonication aided Dispersion at 120 _C vs. MWCNT wt. % content [36].

J. Zhang & D. Jiang [37] obtained linked MWCNTs from the feedback of ethyl chloride and amino sets. SEM indicates that hetero-junctions of MWCNTs with different morphologies were shaped. Afterwards, samples of unspoiled MWCNTs were chemically fabricated and linked to MWCNTs, strengthening the epoxy resin combinations made by cast molding. Tensile properties and crack surfaces of the samples were analyzed as well. Comparing MWCNTs and chemically fabricated MWCNTs, the chemically linked MWCNTs developed crack strains, which increases the toughness of the composites.

M.N. Akhtaret et al. [38] expanded a new aluminum based EM transmitter and NiZn (Ni0.8Zn0.2Fe2O4) ferrite with and without Multiwall carbon nanotubes (MWCNTs) polymer combinations in the form of magnetic feeders within a scaled tank. Nano crystalline NiZn (Ni0.8Zn0.2Fe2O4) ferrite and novel Ni0.8Zn0.2Fe2O4-MWCNTs combinations were synthesized via the solgel method. The models were analyzed using XRD, FESEM, HRTEM, and Raman spectroscopy. FESEM micrographs showed increased grain sizes post-sintering. The results from FESEM and HRTEM demonstrated a coating of Ni0.8Zn0.2Fe2O4 on MWCNTs, showing a better morphology when sintered at 750 C. Due to its superior magnetic property; it was utilized as magnetic feeders for the the EM transmitter. The wave magnitude was enhanced when Ni0.8Zn0.2Fe2O4-MWCNTs polymer composite was utilized.

H. Choi et al. [39] synthesized a counter electrode in dye sensitized solar cells (DSSCs) via the formation of (GMWNTs). They created the grapheme layers by drop throwing on a aSiO2/Si substrate, while (MWNTs) were manufactured in grapheme layers from iron catalyst by chemical vapor deposition (CVD). The GMWNTs sheets were displaced from the substrate via buffered oxide etching, and placed on fluorine-doped oxide glass, with the van der Waals force acting as a counter electrode. Among all electrochemical impedance spectroscopy and energy conversion adaptabilities, the electrochemical properties of GMWNTs are comparable to those of an MWNTs counter electrode. They proposed GMWNTs as an alternative counter electrode for dye-sensitized solar cells.

Sheng-Hao Hsu et al. [40] expanded upon multi-walled carbon nanotube/liquid crystalline epoxy combinations and focused on the influence of incorporating carbon nanotubes (CNTs) on the morphology, thermal, and mechanical properties of the combinations. The CNTs are fabricated by liquid crystalline (LC) 4, 40-bis (2, 3-epoxypropoxy) biphenyl (BP) epoxy resin, as it is easy to disperse to shape for long-range prepared structures. The epoxy fabricated CNT (ef-CNT) were dispersed within the LC BP epoxy resin, and thermally cured using 4, 40-diamino-diphenylsulfone for the purpose of molding the composite. The curing procedure was observed using polarized optical microscopy. The results showed that the LC resin was fabricated to be in parallel with the CNTs possessing dendritic structure firstly to gain micro-sized spherical crystalline along with fibrous crystalline. With consistent scattering and well-built relations between nanotubes and matrix, the combination, including 2.00 wt % ef-CNT, displays excellent thermal and mechanical properties. The outcome indicated that as the quantity of ef-CNT surpasses 2.00 wt %, the confirmation stage of curing has been attained quickly, which decreases the degree of conversion. Compared to neat resin, the composite of 2.00 wt % ef-CNT enhances the glass transition temperature by 70.0 _C, the decomposition temperature by 13.8 ºC, the storage modulus by 40.9%, and the micro hardness by 63.3%.

Niraj Nayan et al. [41] fabricated pure aluminum, strengthened with carbon nanotube (CNT) composite by high-energy attritor milling of up to 48 hrs. The DSC outcomes showed that an exothermic reaction occurred prior to the thawing of aluminum. They focused on the influence of milling time at the start of the exothermic feedback. The climax temperature of the feedback of carbon nanotubes and aluminum is known to be dependent on the heating rate via incessant heating. Noticeable amounts of commencement energy is doubled subsequent to milling for 36 hours, compared to 24 hrs milled models. The method of the feedback kinetics, which relied on feedback order, is immediate nucleation and one dimensional increase for both models. Shaping of Al4C3 has been validated by (XRD) of as-milled powders, and subsequent to acting upon DSC of the milled powders.

P. Joshi & S.H. Upadhyay [42] studied pack removalin multi-walled carbon nanotube (MWCNT) combinations under tension and compression packing states. They utilized the continuum mechanics model to estimate the efficient material properties by means of a representative volume element (RVE) method. Statistical outcomes have been attained by means of Finite Element Modeling (FEM), and these outcomes confirmed the rule of combined outcomes. The study demonstrated that MWNT composite possesses superior Young's modulus in compression as opposed to tension, due to the higher inter-tube load transfer in compression. Proportionally, they also estimated the material properties with single walled carbon nan combination. They observed that multi-walled carbon nanotube combination offer a better resistance against compression compared to single walled carbon nanotubes. The results showed that longer MWNTs strengthen the composite at higher margins compared to its shorter counterpart. The results from FEM agrees with the experimental results, confirming its validity.

Ashori et al. [43] studied the influence of (MWCNTs) as a strengthening agent upon both mechanical and physical properties. In order to enhance the interfacial bonds, maleic anhydride attached polyethylene (MAPE) was inserted as a coupling to all the combinations being studied. In this research, MWCNTs and MAPE were used interchangeably. The morphology of the samples was determined using scanning electron microscopy (SEM). At the highest level of MWCNTs loading (3 or 4 wt %), it enhanced the population of MWCNTs as a result of agglomeration and the blockage to stress transfer. The addition of MWCNTs filler, to a certain extent, decreases the impact of the combinations in terms of mechanical and physical properties of the MAPE. The SEM micrographs also showed the unevenness of the surface was the result of MAPE loading from 0 to 4 wt %. The physical and mechanical properties of the combinations confirmed that MWCNTs resulted inexcellent strengthening, whilethe optimum synergistic outcome of MWCNTs and MAPE were realized at the mixture of 1.5 and 4 wt %, correspondingly.

G.Y. Li et al. [44] adjusted carbon nanotubes using solutions of H2SO4 and HNO3, scattered homogeneously into cement paste via ultrasonic energy. Electrical resistivity and the sensitivity to pressure on the properties under cyclical compressive packing of the combination have been studied and placed side-by-side to that of the untreated - CNT toughened cement paste. The outcomes indicate that the addition of changed or unchanged CNTs towards cement paste resulted in a remarkable reduction in the volume of electrical resistivity and an increase in compressive sensitivity. The small structures of these cement combinations were studied through a scanning electron microscope (SEM). The microscopic observation indicates that not only the changed, but unchanged CNTs were scattered homogeneouslywithin the cement matrix. For unchanged CNT-toughened cement combinations, CNTs with a glossy surface were crisscrossed and stuck to the cement matrix; the bridging of fractures and a well three-dimensional mesh-workwere also examined. For treating-CNT toughened cement combinations, the surface of CNTs was coated by C–S–H, resulting in an advanced automatic power. The contact points of the changed-CNTs in the combinations were lesser than that of the unchanged-CNTs in cement matrix combinations, resulting in a higher compressive sensitivity and lower electrical conductivity.

S. Konsta-Gdoutos et al. [45] proposed that the significant automatic assets of carbon nanotubes (CNT) are perfect candidates for the high presentation cementations composites. However, the most imperative test for the amalgamation of CNTs within cement is its poor dispersion. In this work, the effective dispersion of the diversified length of Multiwall carbon nanotubes (MWCNTs) within water was done using ultrasonic energy andsurfactants combinations. The influence of the methods upon an0.08-wt % MWCNT cement combination were studied. The results confirmed the necessity of

ultrasonic in inducing excellent particle dispersion within the optimal weight ratio of surfactant-to-CNTs. The influence of multiple properties such as length, fracture, and microstructure was analyzed to derive a composed ratio of surfactant-to-MWCNT. It was proven here that the addition of MWCNT enhances both the nano and micromechanical properties of cement paste.

Chewa et al. [46] analyzedimprovements of alternativesto injectable calcium phosphate cement (CPC) composite for orthopedic application. The new CPC composite is made up of β-tri-calcium phosphate (β-TCP) and di-calcium phosphate anhydrous (DCPA), combined with bovine serum albumin (BSA) and multi-walled carbon nanotubes (MWCNTs) or fabricated MWCNTs (MWCNTs–OH and MWCNTs–COOH). Scanning electron microscopy (SEM), compressive power experiments, inject ability experiments, Fourier change infrared spectroscopy, and X-ray diffraction were utilized to analyze the results. Compressive power experiments and SEM micrographs showed that admixture of BSA and MWCNT strengthens CPC combinations. MWCNTs and BSA affects the morphology of the hydroxyapatite (HA) crystals in the CPC matrix. BSA promotes the growth of HA from itssuperficial bonds to the CPC grains. MWCNT–OH and any corresponding combinations showed maximum compressive powers (16.3 MPa) falling within the range of trabecular bone (2–12 MPa).

A. Sobolkina et al. [47] attempted to determine a viable scattering of carbon nanotubes (CNTs) that are beneficial to cement-based composites. Currently, (CNTs) with diversified morphologies are being studied. For a homogenous dispersion of CNTs in cement matrix, the influence ofsanctionson agglomeration of mixed CNTs (anionic/nonionic surfactants) in multiple settings were quantitatively examined, along with the configuration of aqueous scatterings of CNTs for use within cement paste. The relationship between the quality of CNT-scattering, sonication time, and surfactant concentration were determined using UV–vis spectroscopy. After being dispersed, nitrogen-doped CNTs were determined to be individually broken CNTs. Contrarily, and after the treatment of combined single-, double-, and multi walled CNTs, a net-like configuration was found, which is attributed to sonication, making it impossible to differentiate. The replacement of cement paste that are dispersed with CNTs increased the compressive mode by 40%, and in certain select cases, tensile modes at high strain rates were improved as well. However, power development was lacking, and this is especially poignant in the case of quasistatic loading. The results from microscopy analysis showed that the configuration of C–S–H phases vary from one type to another CNTs. This fact, and other supporting data, confirms the influence of the benefits of addition of CNTs.

F. Azhari et al. [48] analyzed electrically conductive combinations of cements by obtaining carbon fibers and nanotubes and their respective capacities in detecting compressive load from resistivity modifications. There are currently two cement-based sensors; carbon fibers, and hybrid fibers/nanotubes. Conventional strain gauges were also directly compared in the context of accumulation of the sensor samples. The results showed that under cyclic loading, resistivity changes will be mirrors in both load and measured material strain under high fidelity for the sensors. Feedbacks are however, rate dependent and nonlinear. In the case of random loadings rates, hybrid sensors, such as combined carbon fibers and nanotubes, gave better outcomes and are more repeatable.

H. Li et al. [49] analyzed a current self-deicing road structure utilizing solar energy. It is made up of a carbon nano-fiber polymer (CNFP) thermal source, an AlN-ceramic insulated encapsulation layer, a Multiwall carbon nanotube (MWCNT)/cement-based thermal conductive layer, and a thermally insulated substrate. The electric and thermo-electric properties of a CNFP, consisting of individual carbon nano-fibers (10–200 NM), were examined as well. The advantage of high thermo-electric effectiveness was confirmed, while of its resistivity proves a piecewise linear temperature-reliant features within (0–280 °C). One way to determine whether or not the CNFP is well organized is to utilize an AlN-ceramic wafer (0.5 mm) in the form of an electro-insulating layer. The resulting structure is utilized in both deicing and field snow-melting, and the effect of ambient temperature, heat flux density, and ice thickness were analyzed in detail. The effectiveness, repeatability, charge, and the possibility of the self-deicing road structure in both deicing and snow melting applications were analyzed as well. Deicing or snow-melting performance of the self-deicing road structure were proposed in the context of its respective indices, with the optimal significances for each parameter beingdemonstrated.

B. Wang et al. [50] modified multi-walled carbon nanotubes (MWCNTs) using anionic Arabic gum, which was mixed into Portland cement pastes to study its effect on flexural roughness. The flexural roughness of the cement combinations was analyzed, and the results showed that the presence of nanotubes significantly enhances both the fracture energy and flexural roughness index of Portland cement pastes. The porosity and pore size of the combinations were determined using mercury intrusion porosimetry. Cement paste with MWCNTs are of lower porosity, however, it possesses a uniform distribution of pore size. The microstructure was viewed using analyzed using FESEM. MWCNT's flexural toughness played the role as a strengthener in the case of cement-based combinations, alongside roughness.

O. Mendoza et al. [51] analyzed the influence of super plasticizer and CA (OH) 2 on the constancy of OHA fabricated multi walled carbon nanotube (MWCNT)/water scatterings manufactured via sonication. The dispersion of MWCNT/water/super plasticizer was quantified using UV–vis spectroscopy. Meanwhile the negative influence of MWCNT was examined with RAMAN spectroscopy, while the influence of CA (OH) 2 steadiness within the dispersion was confirmed using Zeta potential and FTIR spectroscopy. In this case, it was surmised that Ca(OH)2 influences the constancy of MWCNT dispersion from the interactions between the negative alterations from the OHA functional sets, and the delay within electrostatic repulsion between MWCNT and super plasticizer molecules, which will prompt the MWCNT to re-agglomerate.

R. Siddique & A. Mehta [52] are of the opinion that (CNTs) are made up of majority elemental carbon that consist of curved graphene layer, which is asingle layer of carbon atoms in a honeycomb configuration possessing interchangeable metal impurities that are reliant upon its processing parameters. CNT manufacturing is currently experiencing an upheaval of improvement and innovation, translating into massive market presence and decreased costs. CNTs are well known for their strength, determined to be 100 times stronger than the tensile strength of steel at one-sixth its weight, alongside other excellent properties. It was proven that CNTs are applicable in the manufacture of concrete and mortars. This work included some of the reviews pertaining to the utilization of CNTs within concrete and mortars. The influence of CNTs upon compressive strength, tensile strength, modulus of elasticity, flexural strength, porosity, electrical conductivity and autogenesis shrinkage are pointed out here as well.

H.K. Kim et al. [53] used fumes of silica within CNT/cement composites to improve the dispersion of CNTs and its interfacial bondswith hydration products. Their work involves the analysis of the influence of CNTs upon both mechanical and electrical properties cement composites with silica fume inclusion. The SEM was used for qualitative analysis to image surface morphology and microstructure upon multiple loadings of CNTs. Silica fume's influence upon properties such as porosity, compressive power, and electrical resistance of the CNT/cement combinations were studied as well. It is surmised that CNTs dispersion via silica fumes prevents any automated or electrical properties ofCNT/cement combinations, while CNTs within cement combination lacking silica fume failed to develop automatic and electrical benefits of the cement combinations.

3. CONCLUSION

This study analyzed the influence of MWCNTs upon multiple materials in strengthening the physical, mechanical, thermal, and electrical properties, on top of analyzingthe nanostructure of composites. The composites' mechanical and electrical properties were improveddue to the introduction of coupling agents and enhanced interfacial bonding. The adding of MWCNTs as fillers, to some extent,decreased the influence of combinations, not only on the mechanical aspect, but also upon the developed physical properties. The improved mechanical properties are proof that MWCNTs are suitable strengthening agents due to the synergistic affect induced by MWCNT. The results showed that compared to unspoiled MWCNTs and chemically fabricated MWCNTs, chemically linked MWCNTs induce crack damages, and as a result of this, the harshness of the combinations were considerably enhanced. Electrical resistivity and the sensitivity to pressure upon the properties under cyclical compressive packing of the combination were analyzed and comparedto that of the untreated - CNT toughened cement paste. It was pointed out that the addition of altered or unaltered CNTs toward cement paste results in the reduction of volume and electrical resistivity, while it increases compressive sensitivity. The electric and thermo-electric properties of a CNFP, consisting of individual carbon nano-fibers (10–200 nm), showed that the benefits of high thermo-electric effectiveness were suitable, while the resistivity of the CNFP proved the presence of piecewise linear temperature-reliant features within a specific temperature range (0–280 °C). Furthermore, an effective reinforcement is reliant upon shorter MWCNTs are needed, while lower amounts of longer MWCNTs are needed to maintain similar levels of mechanical performance. Models of fabricated nanotubes showed a more profound effect upon thin as opposed to combination models, which have similar values to non-functionalized nanotubes. Malleable properties and surface cracks on the samples were analyzed as well.

REFERENCES

[1] Peigney, A., Laurent, C., Dobigeon, F., & Rousset, A. (1997). Carbon nanotubes grown in situ by a novel catalytic method. Journal of materials research, 12(03), 613-615.

[2] Li, C., & Chou, T. W. (2004). Modeling of elastic buckling of carbon nanotubes by molecular structural mechanics approach. Mechanics of Materials, 36(11), 1047-1055.

[3] Ruoff, R. S., Qian, D., & Liu, W. K. (2003). Mechanical properties of carbon nanotubes: theoretical predictions and experimental measurements. Comptes Rendus Physique, 4(9), 993-1008.

[4] Coleman, J. N., Khan, U., Blau, W. J., & Gun'ko, Y. K. (2006). Small but strong: a review of the mechanical properties of carbon nanotube–polymer composites.Carbon, 44(9), 1624-1652.

[5] Thostenson, E. T., Li, C., & Chou, T. W. (2005). Nanocomposites in context.Composites Science and Technology, 65(3), 491-516.

[6] Qian, D., Dickey, E. C., Andrews, R., & Rantell, T. (2000). Load transfer and deformation mechanisms in carbon nanotube-polystyrene composites. Applied physics letters, 76(20), 2868-2870.

[7] Cadek, M., Coleman, J. N., Barron, V., Hedicke, K., & Blau, W. J. (2002). Morphological and mechanical properties of carbon-nanotube-reinforced semicrystalline and amorphous polymer composites. Applied Physics Letters,81(27), 5123-5125.

[8] Barber, A. H., Cohen, S. R., & Wagner, H. D. (2003). Measurement of carbon nanotube–polymer interfacial strength. Applied Physics Letters, 82(23), 4140-4142.

[9] Andrews, R., Jacques, D., Qian, D., & Rantell, T. (2002). Multiwall carbon nanotubes: synthesis and application. Accounts of Chemical Research, 35(12), 1008-1017.

[10] Iijima, S. (1991). Helical microtubules of graphitic carbon. nature, 354(6348), 56-58.

[11] Yu MF, Lourie O, Dyer MJ, Moloni K, Kelly TF, Ruoff RS. Strength and breakingmechanism of multiwalled carbon nanotubes under tensile load. Science2000;287:637–40

[12] Liu C, Fan YY, Liu M, Cong HT, Cheng HM, Dresselhaus MS. Hydrogen storage insingle-walled carbon nanotubes at room temperature. Science 1999;286:1127

[13] Bethune, D. S., Klang, C. H., De Vries, M. S., Gorman, G., Savoy, R., Vazquez, J., & Beyers, R. (1993). Cobalt-catalysed growth of carbon nanotubes with single-atomic-layer walls.

[14] Iijima, S., & Ichihashi, T. (1993). Single-shell carbon nanotubes of 1-nm diameter.

[15] Iijima, S. (1991). Helical microtubules of graphitic carbon. nature, 354(6348), 56-58.

[16] Puretzky, A. A., Geohegan, D. B., Fan, X., & Pennycook, S. J. (2000). In situ imaging and spectroscopy of single-wall carbon nanotube synthesis by laser vaporization. Applied Physics Letters, 76(2), 182-184.

[17] Fonseca, A., Hernadi, K., Piedigrosso, P., Colomer, J. F., Mukhopadhyay, K., Doome, R., ... & Nagy, J. B. (1998). Synthesis of single-and multi-wall carbon nanotubes over supported catalysts. Applied Physics A, 67(1), 11-22.

[18] Che, G., Lakshmi, B. B., Fisher, E. R., & Martin, C. R. (1998). Carbon nanotubule membranes for electrochemical energy storage and production.Nature, 393(6683), 346-349.

[19] Zhou, W., Ooi, Y. H., Russo, R. A. A., Papanek, P., Luzzi, D. E., Fischer, J. E., ... & Smalley, R. E. (2001). Structural characterization and diameter-dependent oxidative stability of single wall carbon nanotubes synthesized by the catalytic decomposition of CO. Chemical Physics Letters, 350(1), 6-14.

[20] Elliott, J. A., Sandler, J. K., Windle, A. H., Young, R. J., & Shaffer, M. S. (2004). Collapse of single-wall carbon nanotubes is diameter dependent. Physical review letters, 92(9), 095501.

[21] Wei, B. Q., Vajtai, R., & Ajayan, P. M. (2001). Reliability and current carrying capacity of carbon nanotubes. Applied Physics Letters, 79(8), 1172-1174.

[22] Kim BM, Fuhrer AMS. Properties and applications of high-mobility semiconducting nanotubes. J Phys: Condens Matter 2004;16(18): R553–80.

[23] Yao, B., Fleming, D., Morris, M. A., & Lawrence, S. E. (2004). Structural control of mesoporous silica nanowire arrays in porous alumina membranes. Chemistry of materials, 16(24), 4851-4855.

[24] Prabhu Narayanaswamy Venkatesan, Sangeetha Dharmalingam, Characterization and performance study on chitosan-functionalized multi walled carbon nano tube as separator in microbial fuel cell. Journal of Membrane Science 435 (2013) 92– 98

[25] A.K. Singh, Crystallization kinetics of Se–Zn–Sb nano composites chalcogenide alloys. Journal of Alloys and Compounds552 (2013) 166–172.

[26] Prashant Jindal , Meenakshi Goyal , Navin Kumar , Mechanical characterization of multiwalled carbon nanotubes-polycarbonate composites. Materials and Design54 (2014) 864–868.

[27] Preeti Joshi, S.H. Upadhyay, Evaluation of elastic properties of multi walled carbon nanotube reinforced composite. Computational Materials Science xxx (2013) xxx–xxx. .

[28] Arash Montazeri , The effect of functionalization on the viscoelastic behavior of multi-wall carbon nanotube/epoxy composites . Materials and Design45 (2013) 510–517.

[29] Jin-Chao Zhao , Fei-Peng Du, Xing-Ping Zhou , Wei Cui , Xiao-Mei Wang , Hong Zhu , Xiao-Lin Xie ,Yiu-Wing Mai , Thermal conductive and electrical properties of polyurethane/hyperbranched poly(urea-urethane)-grafted multi-walled carbon nanotube composites. Composites: Part B42 (2011) 2111–2116.

[30] D. Silambarasan , V.J. Surya , V. Vasu , K. Iyakutti , Investigation of single-walled carbon nanotubes titanium metal composite as a possible hydrogen storage medium, international journal of hydrogen energy 38 (2 0 1 3) 1 4 6 5 4-1 4 6 6 0.

[31] Kumud Kant Awasthi, P.J. John, Anjali Awasthi, Kamlendra Awasthi. Multi walled carbon nano tubes induced hepatotoxicity in Swiss albino mice. Micron 71 (2011) 466–470.

[32] Jianwei Zhang, Dazhi Jiang, Interconnected multi-walled carbon nanotubes reinforced polymer-matrix composites. Composites Science and Technology 55 (2013) 188– 194 .

[33] Jianwei Zhang, Dazhi Jiang, Fabrizio Scarpa, Hua-Xin Peng. Enhancement of pullout energy in a single - walled carbon nano tube -polyethylene composite system via auxetic effect. Composites Part A (2013) 188-194.

[34] X. Jiang, L.T. DrzalHigh 2011. Improving electrical conductivity and mechanical properties of high density polyethylene through incorporation of paraffin wax coated exfoliated grapheme nan platelets and multi-wall carbon nano-tubes. Composites: Part A 42 (2011) 1840–1849.

[35] M.R. Ayatollahi ,S. Shadlou, M.M. Shokrieh 2010. Fracture toughness of epoxy/multi-walled carbon nanotube nano-composites under bending and shear loading conditions. Materials and Design 32 (2011) 2115–2124 .

[36] A. Martone, C. Formicola, M. Giordano, M. Zarrelli 2010. Reinforcement efficiency of multi-walled

carbon nanotube/epoxy nano composites. Composites Science and Technology70 (2010) 1154–1160.

[37] Jianwei Zhang, Dazhi Jiang 2010. Interconnected multi-walled carbon nanotubes reinforced polymer-matrix Composites. Composites Science and Technology71 (2011) 466–470.

[38] Majid Niaz Akhtar , Noorhana Yahya, Krzysztof Koziol, Nadeem Nasir.2011. Synthesis and characterizations of Ni0.8Zn0.2Fe2O4-MWCNTs composites for their application in sea bed logging. Ceramics International 37 (2011) 3237–3245.

[39] Hyonkwang Choi, HyunkookKim, SookhyunHwang, WonbongChoi, MinhyonJeon 2010.Dye-sensitized solar cells using graphene-based carbon nano composite as counter electrode. Solar Energy Materials & Solar Cells (2011) 323-325.

[40] Sheng-Hao Hsu, Ming-Chung Wu, Sharon Chen, Chih-Min Chuang, Shih-Hsiang Lin, Wei-Fang Su 2011. Synthesis, morphology and physical properties of multi-walled carbon nanotube/biphenyl liquid crystalline epoxy composites. Carbon 50 (2012) 896 - 905.

[41] Niraj Nayan, S.V.S.N. Murty, S.C. Sharma, K. Sree Kumar, P.P. Sinha 2011. Calorimetric study on mechanically milled aluminum and multiwall carbon nanotube composites. Sciverse (2011) 1087-1093.

[42] Preeti Joshi, S.H. Upadhyay 2013. Evaluation of elastic properties of multi walled carbon nanotube reinforced composite. Computational Materials Science xxx (2013) xxx–xxx.

[43] Alireza Ashori, Shabnam Sheshmani,Foad Farhanic 2012.Preparation and characterization of bagasse/HDPE composites using multi-walled carbon nanotubes. Carbohydrate Polymers(2013) 865-871.

[44] G.Y. Li et al (2007) Pressure-sensitive properties and microstructure of Carbon nanotube reinforced cement composites. Cement & Concrete Composites 29 (2007) 377–382.

[45] M.S.Konsta-Gdoutos (2010). Highly dispersed carbon nanotube reinforced cement based materials. Cement and Concrete Research 40 (2010) 1052–1059.

[46] Kean-Khoon Chewa et al (2011). Reinforcement of calcium phosphate cement with multi-walled carbon nanotubes and bovine serum albumin for injectable bone substitute applications Journal of the mechanical behavior of biomedical materials 4 (2 0 1 1) 3 3 1 – 3 3 9.

[47] A. Sobolkina et al (2012). Dispersion of carbon nanotubes and its influence on the mechanical properties of the cement matrix. Cement & Concrete Composites 34 (2012) 1104–1113.

[48] F. Azhari, N. Banthia (2012). Cement-based sensors with carbon fibers and carbon nanotubes for piezoresistive sensing . Cement & Concrete Composites 34 (2012) 866–873.

[49] H. Li et al. (2013) Self-deicing road system with a CNFP high-efficiency thermal source and MWCNT/cement-based high-thermal conductive composites / Cold Regions Science and Technology 86 (2013) 22– 35.

[50] B. Wang et al (2013). Effect of highly dispersed carbon nanotubes on the flexural toughness of cement-based composites.Construction and Building Materials 46 (2013) 8–12.

[51] O. Mendoza et al (2013). Influence of super plasticizer and Ca(OH)2 on the stability of functionalized multi-walled carbon nanotubes dispersions for cement composites application.Construction and Building Materials 47 (2013) 771–778.

[52] R. Siddique, A. Mehta (2013). Effect of carbon nanotubes on properties of cement mortar / Construction and Building Materials 50 (2014) 116 – 129s .

[53] H.K. Kim et al (2013).Enhanced effect of carbon nanotube on mechanical and electrical properties of cement composites by incorporation of silica fume / Composite Structures 107 (2014) 60–69.

BIOGRAPHIES

Abdul Rahman Sanadwas born in Iraq. He obtained his bachelors in General of Mechanical Engineering from Iraq.Officerinthe Ministry of Electricity/Iraq. He is currently pursuing his Master in the field of applied mechanics at Universiti Tenaga Nasional, Kajang, Selangor, Malaysia

Email:engrahman2013@yahoo.com

Mohamed Ansari M. Nainar PhD* department of Mechanical Engineering, Center for Advance Materials, Universiti Tenaga Nasional, Kajang, Selangor, Malaysia

Jamal O. Sameer was born in Iraq. He obtained his bachelors in General of Mechanical Engineering from Iraq. He is currently pursuing his Master in the field of applied mechanics at Universiti Tenaga Nasional, Kajang, Selangor, Malaysia.

Email:eng_jamal79@yahoo.com

www.ijset.in
ISSN (O): 2348-4098
ISSN (P): 2395-4752

Abdulbasit Abdullah was born in Iraq. He obtained his bachelors in General of Mechanical Engineering from Iraq. Officerinthe Ministry of Electricity/Iraq .He is currently pursuing his Master in the field of applied mechanics at Universiti Tenaga Nasional, Kajang, Selangor, Malaysia

Bassam Alaseelwas born in Iraq. He obtained his bachelors in General of Mechanical Engineering from Iraq. He is currently pursuing his Master in the field of applied mechanics at Universiti Tenaga Nasional, Kajang, Selangor, Malaysia

A METHODOLOGY OF OPTIMAL SIZING FOR WIND SOLAR HYBRID SYSTEM

[1]AVINASH NATH TIWARI, [2]NAVNIT DUBEY

[1, 2] Department of Mechanical Engineering, Jagannath University, Jaipur, India

ABSTRACT

This paper proposes a methodology to perform the optimal sizingof a wind solar hybrid system. Themethodology focus at finding the configuration, between a set of systems components to satisfy the desired system reliability requirements, with the lowest possible cost. Due to large number of design setting and the sporadique nature of solar and wind energy sources it become very challenging. In the first step modelling a wind solar hybrid system is considered in the procedure of optimal sizing methodology. While in second step optimum sizing of a system is done according to the loss of power supply probability (LPSP).

KEYWORDS: *optimum system sizing; loss of power supply probability; wind; solar; hybrid system*

1. INTRODUCTION

The rapid depletion and high capital cost of fossil fuel resources attracted much attention towards urgent search for alternative energy source. Alternative energy source as wind and solar energy are the most favourable option. A comman drawback of wind and solar energy is their wind speed characteristic and intermittent solar radiation. The problem is partially overcome by using these systems together with a storage component. These kind of system are known as hybrid system.

In order to efficiently and economically utilize the renewable energy source, an optimum mixture and selection of each component of a wind solar hybrid system is important. The sizing optimization method can help to guarantee the lowest investment and full use of a PV system, WG system and battery bank, so that the hybrid system can work at optimum condition with selected configuration.

Various optimization technique such as probabilistic approach, graphical construction and iteration technique have been recommended by researchers.

Yang el at (2003, 2007) have proposed an iterative optimization technique for the loss of power supply probability model for the wind solar hybrid system. The number selected of the PV modules, wind turbine, and batteries ensures the load demand according to the power reliability requirement and the system cost is minimised.

Genetic algorithm is introduced by Xu, Kang, Chang, Cao for selecting type and number of PV, WG and battery to satisfy a constant load demand.

In this context, the present study presents a methodology for the optimal sizing of wind solar hybrid system with storage batteries. The methodology adopted, taken as the ideal approach to suggest, between a set of system components, the type of units and optimal number in terms of economic and technical concepts; the loss of power supply probability (LPSP) .

2. MODELLING OF THE WIND SOLAR HYBRID SYSTEM COMPONENTS

A wind solar hybrid system consists of PV array, Wind turbine, battery bank, inverter, controller and other devices and cable. To satisfy the load demand PV array and wind turbine works togther. The maximum available power can be extracted from the PV and Wind power sources depending on battery charger technology. In case of low wind speed or irradiation condition battery bank is use to store the energy surplus and to supply. .For a wind solar hybrid system, as shown in Fig.1, three principal subsystems are included, the PV generator, the wind turbine and the battery storage.

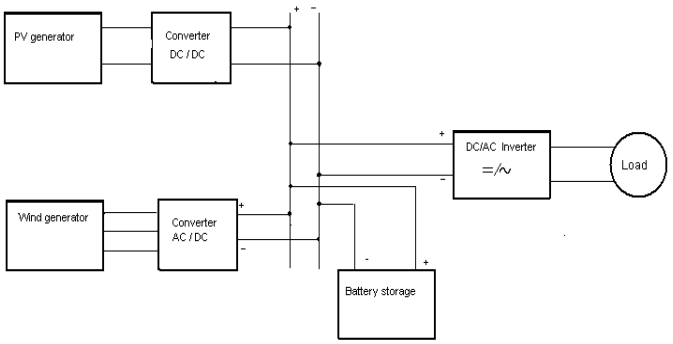

Figure 1: Schematic diagram of hybrid PV/wind system with battery storage

2.1 MODELLING OF PV GENERATOR

Weather data play as important role in PV module performance, especially solar radiation and PV module temperature. The models describing the PV module's maximum power output behaviours are more practical for PV system assessment, as the operation and the performance of PV generator is interested to its maximum power. In this paper, a mathematical model for estimating the power output of PV modules is used.

Using the solar radiation available on the tilted surfaces, the ambient temperature and the data from manufacturers for the PV modules as model inputs, the power output of

the PV generator, P_{PV}, can be calculated with the following equations (Markvard, 2000):

$$P_{PV} = \eta_g \, N \, A_m \, G_t$$

Where, η_g - Instantaneous PV generator efficiency, A_m - Area of a single module used in a system (m^2), G_t - Global irradiance incident on the titled plane (W/m^2) , N - Number of modules.

All the energy losses in a PV generator, including connection losses, wiring losses and other losses, are assumed to be zero.

The instantaneous PV generator efficiency is expressed by the following equation (Habib et al., 1999)

$$\eta_g = \eta_r \, \eta_{pt}[1-\beta_t(T_c - T_r)].$$

Where, η_r - PV generator reference efficiency, η_{pt} - Efficiency of power tracking equipment which is equal to 1 if a perfect maximum power point tracker is used, T_c - Temperature of PV cell (°C),

T_r - PV cell reference temperature, β_t - Temperature coefficient of efficiency, ranging from 0.004 to 0.006 per °C for silicon cells.

Based on the energy balance proposed by (Duffie et al.., 1991), the PV cell temperature can be represented as follows:

$$T_c = T_a + G_t\left(\frac{NOCT - 20}{800}\right)$$

Where, T_a - ambient temperature (°C), (Chedid et al., 1996; Duffie et al., 1991)

Consequently, the instantaneous PV generator efficiency can be expressed as follows:

$$\eta_g = \eta_r \, \eta_{pt}\left\{1-\beta_t(T_a - T_r) - \beta_t \, G_t\left(\frac{NOCT-20}{800}\right)(1-\eta_r\eta_{pt})\right\}.$$

η_{pt}, β_t, $NOCT$, A_m are parameters that depend on the type of module, and given by the manufacturer of the modules.

2.2 MODELLING OF WIND GENERATOR

It is very important for wind solar hybrid system to choose a suitable wind turbine. There are three main factors that determine the power output of a wind turbine, ie, the power output curve (determined by aerodynamics power efficiency, mechanical transmission and converting electricity efficiency) of a chosen WG, the wind speed distribution of a selected site where the wind turbine is installed, and the tower height.(H. Yang et al. 2008). (Yang et al., 2002; Chedid et al., 1998; Eftichios et al., 2006; Lysen, 1983) taken on that the turbine power curve has a linear, quadratic or cubic form. (Troen et al., 1989; Bueno, 2005) approximate the power curve with a piecewise linear function with a few nodes.

As the installation height of the wind turbine has a large effect on the energy available from the system, the process of adopting of the wind profile for height can be taken into account by using an equation of height adjustment. In this study, the power law is applied for the vertical wind speed profile, as shown in equation below (Ilinka et al., 2003).

$$\frac{V}{Vr} = V_r\left(\frac{H}{Hr}\right)^{\alpha_1}$$

Where, V - Wind speed at hub height H, Vr - Wind speed measured at the reference height Hr and α_1 - Wind speed power law exponent.

Wind speed power law expansion which varies from (> 0.10) for very flat land, water or ice to more than 0.25 for heavily forested landscape. The one-seventh power law(0.14) is a good reference number for relatively flat surfaces such as open terrain of grasslands away from tall trees or building (Gipe, 1995).

2.3 MODELLING OF BATTERY STORAGE

To regulate system voltage and to supply power to load in case of low wind speed or low solar radiation, a battery bank is used which is usually made of the lead-acid type to store surplus electrical energy. During the charging process, when the total output of PV and wind generators is greater than the load demand, ie when power generation cannot satisfy load demand requirement, the available battery bank capacity at hour t can be described by (Bogdan et al., 1996:, Bin et al., 2003):

$$C_{bat}(t) = C_{bat}(t-1).(1-\sigma) + \left(E_{PV}(t) + E_{WG}(t) - \frac{E_L(t)}{\eta_{inv}}\right)\eta_{bat}$$

On the other hand, when the load demand is greater than the available energy generated, the battery bank is in discharging state. Therefore, the available battery bank capacity at hour t can be expressed as:

$$C_{bat}(t) = C_{bat}(t-1).(1-\sigma) - \left(\frac{E_L(t)}{\eta_{inv}} - \left(E_{PV}(t) + E_{WG}(t)\right)\right)$$

Where, $C_{bat}(t)$ and $C_{bat}(t-1)$ are the available battery bank capacity (Wh) at hour t and t-1, respectively; η_{bat} = the battery efficiency (during discharging process, the battery discharging efficiency was set equal to 1 and while charging, the efficiency is 0.65 to 0.85 depending on the charging current) (Bin et al., 2003), σ = self-discharge rate of the battery bank.

The manufacturer documentation gives a self-discharge of 25 % over six months for a storage temperature of 20 °C, that is to say 0.14 % per day (Markvart et al., 2003).

$E_{PV}(t)$ and $E_{WG}(t)$ are the energy generated by PV and wind generators, respectively; $E_L(t)$ = the load demand at hour t and η_{inv} = the inverter efficiency (in this study it is considered as constant, 92%).

At any hour, the storage capacity is subject to the following constraints:

$$C_{bat\,min} \le C_{bat}(t) \le C_{bat\,max}.$$

Where $C_{bat\,max}$ and $C_{bat\,min}$ are the maximum and minimum allowable storage capacity.

Using for $C_{bat\,max}$ the storage nominal capacity C_{batn}, then

$$C_{bat\,min} = DOD.C_{batn}$$

Where DOD (%) represents the maximum permissible depth of battery discharge.

3. MODELLING OF SYSTEM RELIABILITY

Power reliability analysis has been considered as an important step in system design process, because of the intermittent solar radiation and wind speed characteristics. Several approaches are used to achieve the optimal configurations of hybrid systems in term of technical analysis. Between these methods, we find the least square method applied by (Kellogg et al., 1996; Borowy et al., 1994), the trade-off method (Elhadidy et al., 1999; Gavanidou et al., 1993) and the technical approach also called loss of power supply probability (LPSP) (Abouzahr et al., 1990, 1991; Hongxing et al., 2002; Yang et al., 2002;).

LPSP is defined as the probability that an insufficient power supply results when the hybrid system (PV module, wind turbine and battery storage) is unable to satisfy the load demand (Yang et al., 2003).A LPSP of 0 means the load will always be satisfied, and LPSP of 1 means that the load will never satisfied(H. Yang al et. 2008).Loss of power supply probability (LPSP) is a statistical parameter to measure of the system performance for an assumed or known load distribution.

In this paper the probabilistic approach is used to calculate the LPSP in order to avoid computational burden thus PLSP is defined as follows: (Mr. Sandeep V Karemore, Mr Shubhash Y Kamdi).

$$LPSP = \frac{\sum_{t=0}^{T} Powerfailuretime}{T}$$

$$LPSP = \frac{\sum_{t=0}^{T} Poweravailble - Powerneeded}{T}$$

Where

T = No. of hours in the study with hourly weather data input. The power failure time is defined as that time the load is not satisfied when the power generated by both the wind turbine and PV array is insufficient and battery storage is depleted.

3.1 SYSTEM SIZE OPTIMIZATION

The required number of WGs, PV module and batteries for a given load demand are calculated as follows:

Calculate the hourly energy output from individual wind generator and PV module for a typical year using wind speed and solar insolation of the site

In order to match the generation with the given hourly load of a year, different combination of wind generator and PV module is used. There will be energy deficit during several consecutive hours in between the hours of excess energy generation for each of the combination. This cluster of energy deficit cannot be supplies by renewable sources.

The combination of wind generator and PV module is selected which minimizes the maximum deficit. The amount of maximum deficit is used to determine the storage size ie. the size of the battery.

Loss of power supply probability (LPSP) and 10-years total cost of the hybrid renewable power system are calculated for each of these combination.

Optimal combination is selected based on desired LPSP and minimum total cost of the system.

3.2 SPECIFICATION OF PV MODULE

Type	Monocrystaline silicon
Short circuit voltage	37.8 V
Short circuit current	8.89 A
Maximum power voltage	31.2 V
Maximum power current	8.18 A
Maximum power rating	255 W
NOCT	45.7 C

3.3 SPECIFICATION OF WIND TURBINE

Power	1000 W
Cut in wind speed	2.5 m/s
Rated wind speed	10 m/s
Maximum wind velocity	40 m/s
H_{low}	11 m
H_{high}	35 m

3.4 SPECIFICATION OF BATTERY

Battery model	Fullriver AGM
Voltage	12 V
Capacity	415 Ah
Price	1032 ($)

3.5 HOURLY LOAD OF A DAY

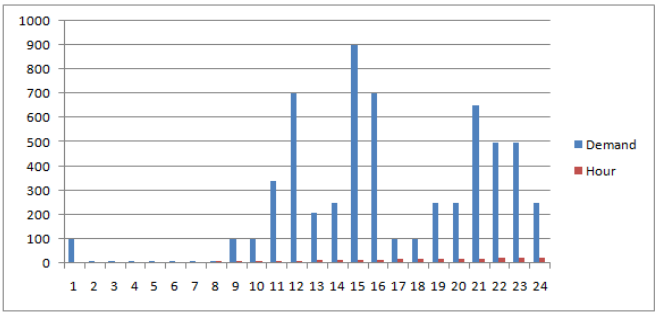

4. RESULTS AND DISCUSSION

A combination of different wind generator and PV module was used to match the energy generation with the load. There was energy deficit in each group of consecutive hours of excess generation, for each of these combinations. Maximum amount of deficit in a cluster among these was determined by calculating the total amount of energy deficit in each of these clusters throughout the year. A simple table was created for this calculation. The first column shows the energy generation of PV module, second column shows the energy generation of WG and third column shows the demand. In the next column total energy generation by WG and PV module is shown. In the next column difference between generation and demand is found negative sign before the energy difference indicates the deficit. In the last column total energy deficit in this group is calculated. It is impossible for renewable energy to meet these deficit directly, for this purpose we need a storage system ie.. Batteries. The excess energy generated by this system could store by charging the battery.

4.1 CALCULATION OF TOTAL ENERGY DEFICIT

PV Gen. (V)	WG Gen.(W)	Demand (W)	Total Gen.	Difference between Gen. & Demand	Deficit	Total deficit
61.26	1.2	200	206	6.76	0	
38.99	1.5	200	209.13	9.23	0	
61.67	2.63	700	72.45	-627.54	-627.54	
61.63	2.5	500	0	-461.56	-461.56	
59.77	2.8	500	0	-500	-500	
43.38	2.85	300	0	-300	-300	
73.192	1.15	200	0	-200	-200	
69.14	1.23	10	0	-10	-10	
57.14	1.58	10	0	-10	-10	
59.166	1.46	10	59.35	49.35	0	
						2109.1

4.2 COMBINATION OF WG, PV AND BATTERY BANK

WG No.	PV No.	Battery No.	Total cost(US$)	LPSP
1	20	4	11936	0.113
1	21	4	12206	0.1091
1	25	4	13286	0.0463
1	28	4	14096	0.0218
1	30	4	14636	0.0009
1	33	4	15446	0
1	34	4	15716	0
1	35	4	15986	0
2	20	4	14336	0.217
2	25	5	16720	0.1347
2	33	6	19914	0.152

Total cost (including capital cost and maintenance cost, replacement cost and operation cost) and LPSP were calculated for each of these combinations. Total lifetime of the system is calculated to be 20 years. The system was sized for loss of power supply probability of zero ie. the load will always satisfy the demand. The number of WG, PV, and battery were found 1, 33 and 4 that satisfy LPSP of zero value with minimum cost.

5. CONCLUSION

The optimal sizing of wind solar hybrid system with battery storage, using an optimization model has been presented in this work. Loss of power supply probability LPSP concept is used to configure the system reliability. The combination of components with the lowest levelised cost of energy is considered as the economical optimal configuration.

REFERENCE

1. Abouzahr, I., Ramakumar. R. 1990. Loss of power supply probability of standalone electric conversion systems: a closed form solution approach. IEEE Transaction on Energy Conv. 5(3), 445-452.
2. Abouzahr, I., Ramakumar. R. 1991. Loss of power supply probability of standalone photovoltaic systems: a closed form solution approach. IEEE Transaction on Energy Conv. 6(1), 1-11.
3. Akai TJ. 1994. Applied numerical methods for engineers, second ed, John Wiley and Sons, New York.
4. Athanasia A. Lazou, Anastassios D. Papatsoris. 2000. The economics of PV stand-alone residential households: A case study for various European and Mediterranean locations; Solar Energy Materials and Solar Cells. 62 411-427.
5. Bagul AD, Salameh ZM, Borowy B. 1996. Sizing of stand-alone hybrid PV/wind system using a three-event probabilistic density approximation. Solar Energy 56(4), 323-335.
6. Beyer HG, Langer C. 1996. A method for the identification of configurations of PV/wind hybrid systems for the reliable supply of small loads. Solar Energy 57(5), 381-391.
7. Bin, A., Hongxing, Y., Shen, H., Xianbo, L.2003. Computer aided design for PV/Wind hybrid system. Renewable Energy 28,1491-1512.

8. Bogdan, S. B. and Salameh, Z. M. 1996. Methodology for optimally sizing the combination of a battery bank and PV array in a wind/PV hybrid system. IEEE Transactions on Energy Conv. 11(2), 367-375.
9. Borowy, B. S., Salameh., Z. M. 1994. Optimum photovoltaic array size for a hybrid wind/PV system. IEEE Transactions on Energy Conv. 9(3), 482-488.
10. Bueno C, Carta JA. 2005. Technical-economic analysis of wind-powered pumped hydrostorage systems. Part I: Model development. Solar Energy 78,382-395.
11. Chedid R, Saliba Y. 1996. Optimization and control of autonomous renewable energy systems. Int J Energy Res. 20, 609-624.
12. Chedid, R ., Rahman, S. 1998. A decision support technique for the design of hybrid solar wind power systems. IEEE Transactions on Energy Conv. 13(1), 76-83.
13. Duffie J. A. and Beckman W. A. 1991. Solar engineering of thermal of thermal process, the second ed., John Wiley and Sons, Inc., New York.
14. Eftichios K., Dionissia K., Antonis P., Kostas K. 2006. Methodology for optimal sizing of stand alone photovoltaic/wind generator systems using genetic algorithms. Solar Energy 80, 1072-1088.
15. Elhadidy, M.A., Shaahid, S. M., 1999. Optimal sizing of battery storage for hybrid (wind + diesel) power systems. Renewable Energy 18, 77-86.
16. Gavanidou, E. S., Bakirtzis A. G. 1993. Design of a stand alone system with renewable energy sources using trade off methods. IEEE Transactions on Energy Conv. 7(1), 42-48.
17. Gipe, Paul, 1995. Wind energy comes of Age. John Wiley & sons,p.536.
18. Gomma, S., Seoud, A. K. A., Kheiralla., H. N., 1995; Design and analysis of photovoltaic and wind energy hybrid systems in Alexandria, Egypt. Renewable Energy 6(5-6), 643-647.
19. Habib MA, Said S.1999. El-Hadidy MA, Al-Zaharna I. Optimization procedure of a hybrid photovoltaic wind energy system. Energy 24, 919-29.
20. Hongxing, Y ; Lu, L., Burnett. L. J. 2002. Probability and reliability analysis of hybrid PV/wind power conversion system in Hong Kong. WREC. cologne Germany.
21. H. Yung el at. 2008. Optimal sizing method fro stand-alone hybrid solar-wind system with LPSP technology by using genetic algorithm.
22. Ilinka, A., McCarthy, E., Chaumel, JL., Retiveau, JL. 2003. Wind potential assessment of Quebec Province. Renewable Energy 28(12),1881-1897.
23. Johnson GL. 1985. Wind energy systems. Englewood Cliffs, NJ,: Prentice-Hall. USA.
24. Karaki, SH., Chedid RB., Ramadan R. 1999. Probabilistic performance assessment of autonomous solar-wind energy conversion systems. IEEE Trans Energy Conv. 14(3), 766-772.
25. Kellogg, W., Nehrir, M.H., Venkataramanan, G., Gerez., V. 1996. Optimal unit sizing for a hybrid PV/wind generating system. Electric power system research 39, 35-38.
26. Lysen, E. H. 1983. Introduction to Wind Energy, second ed., SWD 82–1 Holland.
27. Markvard T. 2000. Solar electricity, the second ed, USA. Willey.
28. Markvart, T., Castaner., L. 2003. Practical hand book of Photovoltaic Fundamentals and applications.
29. M. Shafiqur RAhman Tito, Tek Tjing Lie, Timothy Andersen. A simple optimization method for wind-photovoltaic-battery hybrid renewable energy systems.
30. Mr. Sandeep V Karemore, Mr. Shubhash Y Kamdi. Optimal sizing of autonomous Wind-PV hybrid system by genetic algorithm with LPSP technology.
31. Musgrove ARD. 1988. The optimization of hybrid energy conversion system using the dynamic programming model – RAPSODY. Int. J Energy Res. 12, 447-457.
32. Nelson, D.B, Nehrir, M. H., Wang. C. 2005. Unit Sizing of Stand Alone Hybrid Wind /PV/Fuel Cell Power Generation Systems.IEEE Power Engineering Society General Meeting (3), 2116-2122.
33. Protogeropoulos C, Brinkworth BJ, Marshall RH. 1997. Sizing and techno-economical optimization for hybrid solar PV/wind power systems with battery storage. Int J. Energy Res. 21, 465-479.
34. Ramakumar, Nicholas, R., Butler, G., Alonso, Rodriguez, P., Mani, S. 1993. Economic Aspects of Advanced Energy Technologies. Proceedings of the IEEE. 81 (3).317-333.
35. Troen, I, Petersen, EL. 1989. European wind atlas. First ed., Roskilde: Riso National Laboratory.
36. Yang, H.X., J. Burnett. L. Lu, 2003. Weather data and probability analysis of hybrid photovoltaic wind power generation systems in Hong Kong. Renewable Energy 28, 1813-1824.
37. Yokoyama R, Ito K, Yuasa Y. 1994. Multi-objective optimal unit sizing of hybrid power generation systems utilizing PV and wind energy. J Solar Energy Eng. 116,167-173.
38. Yang Lu, L., Burnett, J. H.X. 2002. Investigation on wind power potential on Hong Kong islands-an analysis of wind power and wind turbine characteristics. Renewable Energy 27, 1-12.

FISHING TRAILS WITH MODIFIED TWO–SEAM OVERHANG TRAWL- *INTRA-SPECIFIC SELECTIVITY STUDIES*

[1, *]N.A.TALWAR, [2]B.HANUMANTHAPPA, [1]M.T.LAXMIPATHI

[1]Associate Professor, Dept. of Fishery Engineering, Faculty of Fishery Sciences, W.B.U.A.F.S. Kol-94

[2] Professor, Dept. of Fishery Engineering, College of Fisheries (KVAFSU), Mangalore-575002.

*Correspondence author: - natalwar@gmail.com

ABSTRACT

A two–seam overhang trawl is modified by incorporating the square mesh panels of 45mm mesh size in forward part of upper belly and 28mm mesh size in codend and fishing trails were carried out during day time, off Karwar coast to study the intra-specific selectivity of some important finfishes and shellfishes. The fishing ground was chosen at random, based on the operation of the other commercial trawlers in the vicinity. The retention lengths ($L_{50\%}$) of some important different finfishes such as Mackerels, Pomfrets, Soles and Ribbon fishes (Trichiurus spp.), clupeids (Sardinella spp.) and Silver bellies (Leiognathus spp.) and some shell fishes such as Metapenaens sp.and Parapenopsis sp. were estimated and compared those with their size at sexual maturity for intra-specific selectivity .

Key words: *Two–seam over hang trawl; Square mesh; Finfishes, shellfishes 50% of retention length (i.e.$L_{50\%}$).and sexual maturity*

1. INTRODUCTION

Selective fishing refers to a fishing method's ability to target and capture organisms by size and species during the fishing operation allowing non-targets to be released unharmed. The mesh size and shape of codend meshes are selected so as to exploit the desired size groups and avoid capture of smaller ones in order to conserve the fishery resources. Chun Chun et al. (1991) observed that the diamond mesh becomes narrow at the middle of the codend causing the mesh lumen to be almost closed during trawling and hence the probability of escapement of undersized and juveniles are in remote. Similar Robertson & Stewart (1988) observed that the codend when filed assumes bulbous shape and the fish escape through a small area of open meshes in front of the bulb, while forward of this point most of the meshes are stretched and closed. Pope (1966) stated that the shape of mesh affects the selectivity of codend. Further; the flow of water also depends on the shape of mesh. Hence for improving the filtering efficiency of mesh, the mesh has to remain open, facilitating more water flow and easy escape of young ones of fish. This can be achieved by using square mesh codends as this will remain open while in operation. The superiority of square mesh over diamond mesh in facilitating escapement of smaller ones has been proven by many workers (Robertson, 1982; 1983; 1986a, & b; Robertson et.al., 1986; Robertson & Stewart, 1988; Kunjipalu & Varhese, 1989; Kunjipalu et.al., 1994; Talwar & Sheshappa, 1996 and Talwar.et al., 2006)

The present fishing trials were carried out to study the intra-specific selectivity of some important finfishes and shellfishes by estimating their 50% of retention lengths (i.e.$L_{50\%}$) caught in modified two–seam over hang trawl and compared those with their size at sexual maturity.

2. MATERIALS AND METHODS

A two-seam over hang trawl of size 25.26m/35.76m (headline/fishing line) was modified by rigging with square mesh panels of 45mm mesh size in forward part of upper belly and 28mm at codend. The specifications of this modified trawl were represented in data sheet and the dimensions and construction characteristics of net was shown in figure.1

The 13.36m OAL wooden stern trawler, fitted with Ruston engine developing 102 BHP at 1800r.p.m.was used for fishing trials. Flat rectangular otter doors measuring 1500mm x 750mm and weighing 65kg each made up of wood and iron were used. A set of nine spherical aluminum floats each of 18.2cm diameter and 2.62kgf buoyancy force and equal number of sinkers weighing 50kgs each were used for the trawl to get the adequate buoyancy force and sufficient sinking force respectively.

Fishing cruises were conducted randomly off Karwar between 24 and 34 isobaths. The towing duration of one and half hour, towing speed of 2knots and scope ratio of 5: 1 was maintained throughout the course of study for all samples.

Total twelve hauls were made throughout season. The catch composition as well as lengths of individuals of different dominant finfishes and shellfishes obtained during each haul and their co-efficient of variations were recorded.

In order to determine the 50% of retention lengths (i.e.$L_{50\%}$) of dominant fin fishes and caught, the length frequency distribution were calculated, where the median lengths of the dominant finfishes and shellfishes were considered instead of mean lengths because any chances of occurrence of few large size fishes in the catch will not affect the medial length.

The total catch was recorded during different hauls and efficiency was judged by Mann Whitney 'U' test (Weber, 1973, Daniel 1977).

DATA SHEET: Specifications of modified Two-Seam overhang trawl

Details of the Gear							
	TOP WING1	SQAURE-1	BUNT-1	BELLY-1	SQ. MESH PANEL	BELLY-2	SQ. MESH CODEND
MESH TOP	60	450	50	450	200	200	110
MESH BASE	150	450	150	150	200	100	110
MESH DEEP	270	130	400	300	100	100	350
MESH SIZE(MM)	48.0	45.0	45.0	45.0	45.0	28.0	28.0
TWINE NOTATION	0.75	0.75	0.75	0.75	0.75	0.75	0.75double
CUTTING RATE	1N.4Bx90	All N	1N.5Bx100	1N.2Bx150	All B	1N.2Bx50	AllB
BATING RATE	-	-	-	1in 3x50	1in 10x10	-	-

LINES AND ROPES

	Details		
	HEAD LINE	FISHING LINE	WING LINE
MATERIALS	Polypropylene(PP)	Polypropylene(PP)	Polypropylene(PP)
DIAMETER	12mm	12mm	12mm
LAY	Regular	Regular	Regular
LENGTH	25.26m	35.76m	3.822m
EXTENSION	1.00m	1.00m	1.00m

PARTICULAR OF OTHERACCESSORIES

	FLOATS	SINKERS	OTTER DOORS
MATERIAL	Aluminum	Galvanised iron	Iron and wooden
NUMBER	9	-	One pair
SHAPE	Spherical	Link chain	Rectangular Flat
SIZE	18.2cm dia	Cross-sect.l area is $11.4x10^{-4}m^2$	1500mmx750mm
WEIGHT IN AIR	-	55Kg	65Kg
OTHER PROPERTIES	Total Buoyancy is 23.48 kgf	Weight in sea water is 46.2 Kg	-

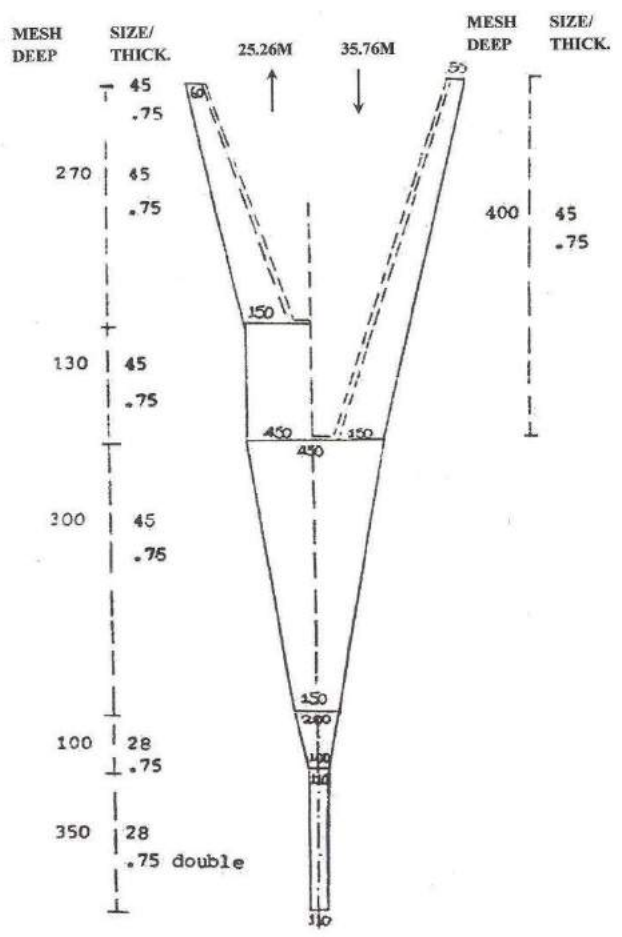

Figure 1: The Dimensions and Construction Characteristics of modified Two-seam overhang Trawl.

3. RESULTS AND DISCUSSION

Result of Mann Whitney 'U' test for total catch during different hauls in modified two-seam overhang trawl shown that there was no significant difference between the average catches obtained during different hauls at 5% level.

Table 1 shows the length ranges with their co-efficient variation of some finfishes and shellfishes caught in modified two-seam trawl with square mesh panels of 45mm mesh size in forward part of upper belly and 28mm at codend. Figure 2a,b,c and 3 gives the percentage cumulative frequency curves for the some important finfishes and shellfishes respectively from which the median lengths ($L_{50\%}$) are measured. All these curves are of sigmoid or S-shape indicating the normal distribution of finfishes and shellfishes in the length range.

3.1 FINFISHES

Mackerels (*Rastrelliger kanagurtha*)**:**

The length range of mackerel caught in modified two seam over hang trawl codend was from 12 to 26cm (Table 2).The ogive curve indicates the median length of mackerels ($L_{50\%}$) caught in square mesh codend was 15.8cm (Fig.2a).Bal and Rao (1990) have reported that, the size of Indian mackerel *(R. kanagurtha*) at first sexual maturity in 22.4 cm and all fish below size are to regarded as juvenils.The mackerel fishery is mostly supported by juveniles. However, from its median lengths ($L_{50\%}$) , it is evident that the modified two seam trawl is not regarded as suitable for caching mackerel and cannot be judged as index of size selectivity for this species. In other words it can be concluded that the square mesh openings of45mm at forward part of upper belly and of 28mm at codend are not enough to escape the juveniles of mackerels.

Clupeids (*Sardinella spp*.)**:**

The length range of clupeids (*i.e.Sarinella spp.*) caught in two- seam trawl with square mesh panels of 45mm mesh size in forward part of upper belly and 28mm at codend ranging from 10 cm to 18 cm .It can be seen from the table 2 that the 50% retention of fishes caught in codend was around 10.5 cm (Fig.2a).

Mature and spawning individual of clupeids are of the size range of 10-10.9 cm in length (Nair, 1951). Attainment of sexual maturity at even smaller length of 8 cm or 9 cm has been reported (Chidambaram and Venkataraman, 1946). The length ranges as well as the median lengths ($L_{50\%}$) caught in the gear indicates that, the modified two-seam overhang trawl catches matured clupeids only which shown better selectivity of this species.

Pomfrets (*Pampus spp*.)**:**

Good numbers of pomfrets (Pampus spp.) were caught in two-seam over hang trawl with square mesh panels of 45mm mesh size in forward part of upper belly and 28mm at codend. The length ranges recorded were i.e.10-26 cm and their co-efficient variation is 27.2% (Table 2). The medial lengths ($L_{50\%}$) of fishes are found to be 16.4cm. (Fig.2b). Kuthalingum (1963) has reported that size at maturity of *Pampus argentus* ranges from 16 to 18 cm and matured specimens have a length range of 10-21 cm .Thus, the trawl with square mesh panels of 45mm mesh size in forward part of upper belly and 28mm at codend is not selective on these species because body shape is oval and escapement through this mesh size is difficult.

Silver bellies (*Leiognathus spp*.):

The length ranges of silver bellies (*Leiognathus spp)* were caught in this trawl with square mesh panels of 45mm mesh size in forward part of upper belly and 28mm at codend are i.e.8-16cm. (Table 1 and 2).and median lengths ($L_{50\%}$) are around 9.2cm (Fig.2b).

Balan (1967) has reported that the minimum size at first sexual maturity for Silver bellies (*L.bindus)* is 8.7 cm.Form the present investigation, it is clear that the gear with square mesh panels of 45mm mesh size in forward part of upper belly and 28mm at codend catch matured size of Silver bellies (*Leiognathus spp*.).In other words it could interpret that there will be enough openings of square meshes of 45mm size at forward part of upper belly and at codend of 28mm size to escape the juveniles.

Soles (*Cynoglossus.spp*)**:**

The length ranges of soles caught in the trawl with square mesh panels of 45mm mesh size in forward part of upper belly and 28mm at codend are 10-24cm (Table 1). But the 50% retention lengths (median lengths) of these species are 11 cm (Fig.2c).Sheshappa and Bhichachar (1954) reported that the minimum size at first maturity of Malabar sole is12cm.Hence, it is evident that this gear has tendency to catch immature ones and it may be concluded that modified two seam overhang trawl with its openings of 45mm square meshes at forward part of upper belly and 28mm at codend are not ideal for selectivity of this species.

Ribbon fishes (*Trichiurus.spp*)**:**

The maximum size of *Trichiurus.spp.*caught in modified two-seam overhang trawl. The median length ($L_{50\%}$) of fishes caught in this gear with square mesh panels in forward part of upper belly and codend is 28.6cm (Table 1 and Fig2c).Bal and Rao (1990) have reported that the minimum size at maturity is 47-48 cm for *Trichiurus lepturus.*This tends to show that ribbon fishes caught in this gear are not of matured size. Hence 45mm square meshes at forward part of upper belly and 28mm at codend is not selective of *Trichiurus.spp.*

3.2 SHELL FISHES

Metapenaeus sp.:

The length of *Metapenaeus sp.* caught in two-seam overhang trawl with square mesh panels of 45mm mesh size in forward part of upper belly and 28mm at codend ranges from 70mm to 140mm and its median length ($L_{50\%}$) is 9.8cm (Fig. 3). Bal and Rao (1990) have reported that the minimum size of sexual maturity of *Metapenaeus sp*. is 8.86 cm. Hence it is evident that in modified trawl by incorporating the square mesh panels of 45mm mesh size in forward part of upper belly and 28mm at codend catches mature species of *Metapenaeus sp.*So it may be concluded that this gear with square mesh openings at forward part of upper belly and codend could be selective for this species of peneaids

Parapenopsis sp:

The length of *Parapenopsis sp*. caught in modified two-seam overhang trawl ranges from 70mm to 150mm and its median length ($L_{50\%}$) is 10.0cm (Fig. 3).Bal and Rao (1990) have reported that the minimum size of sexual maturity of *Parapenopsis sp.* is 6.5cm in males and 7.0cm for females and their maximum growth rate is 9-10 cm in the first year. Hence it clear that this trawl with square mesh panels of 45mm mesh size in forward part of upper belly and 28mm at codend catches matured and maximum sized shrimp of *Parapenopsis sp*. Therefore this gear has well selective for *Parapenopsis sp*.

However, further studies covering all commercially important species of finfishes and shellfishes are required for optimisation of square mesh size with respect to their size at first sexual maturity as well as fishing areas, in order to provide recommendations and informations to the users like fishermen, scientific community, policy makers etc that use the square meshes in different parts of trawl and in codend as management measure.

Table 1: Length Ranges (in cms) of few important fin fishes and shell fishes caught in Modified Two-Seam overhang Trawl.

Name of the fishes	Length Ranges (in cms) Caught	Co-efficient of Variation (%)
Finfishes:		
Mackerel *(R. kanagurtha)*	12 -26	27.2
Clupeids (*Sardinella spp.*)	10-18	18.4
Pomfrets (*Pampus spp.*)	10-26	27.2
Silver Bellies (*Leiognathus spp*)	8-16	21.7
Soles (*Cynoglossus.spp*)	10-24	25.4
Ribbon fishes (*Trichiurus spp.*)	14-40	28.9
Shell Fishes:		
Metapeneaus spp.	2-16	28.7
Parapeneopsis spp.	2-16	28.7

Table 2: Length frequency distribution of few imp. finfishes and shell fishes caught in Modified Two-Seam overhang Trawl.

Mid Class interval	Percentage Cumulative Frequency							
	Finfishes						Shell fishes	
	Mackerel *(R. kanagurtha)*	**Clupeids** (*Sardinella spp.*)	**Pomfrets** (*Pampus spp.*)	**Silver Bellies** (*Leiognathus spp*)	**Soles** (*Cynoglossus. spp*)	**Ribbon fishes** (*Trichiurus spp.*)	***Metapeneaus spp***	***Parapeneopsis spp***
7							0.6	1.8
9	-	-	-	22.9	0.0	0.0	35.4	25.5
11	0.0	22.9	0.0	77.1	10.6	4.90	87.3	73.3
13	7.3	61.4	14.0	97.9	47.0	11.0	98.9	97.6
15	40.0	94.0	33.3	100.0	66.7	15.9	100.0	100.0
17	80.0	100.0	52.6	22.9	78.8	20.7	-	-
19	96.4	-	66.7	-	84.8	23.2	-	-
21	98.2	-	77.2	-	97.00	39.0	-	-
23	98.2	-	92.1	-	100.0	42.7	-	-
25	100.0	-	98.2	-	-	60.0	-	-
27	-	-	100.0	-	-	70.7	-	-
31	-	-	-	-	-	82.3	-	-
33	-	-	-	-	-	92.7	-	-
35	-	-	-	-	-	96.3	-	-
37	-	-	-	-	-	100.0	-	-

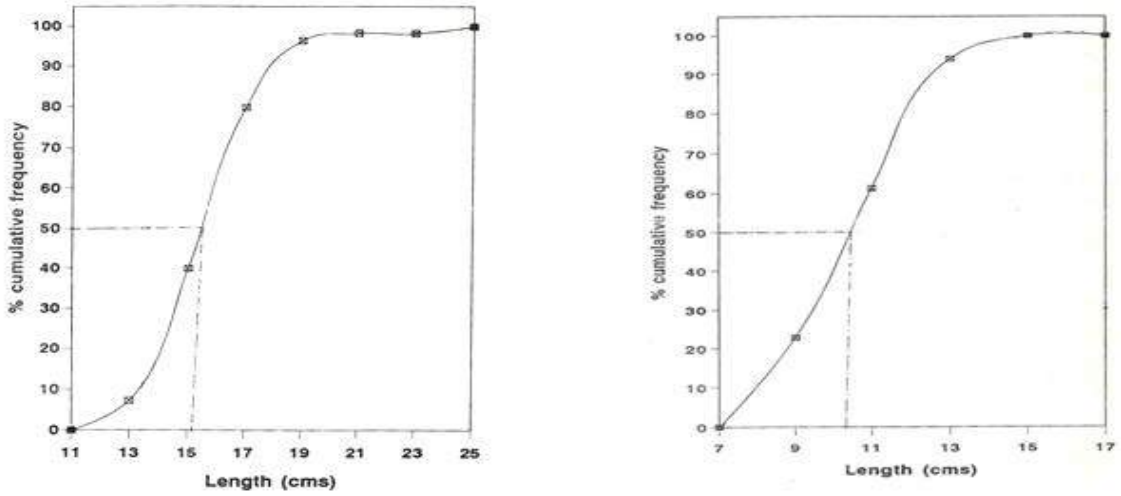

Mackerels (*Rastrelliger kanagurtha)* **Clupeids** (*Sardinella spp*.)**:**

Figure 2a: Percentage cumulative frequency curves for some important fin fishes caught in modified two-seam overhang trawl.

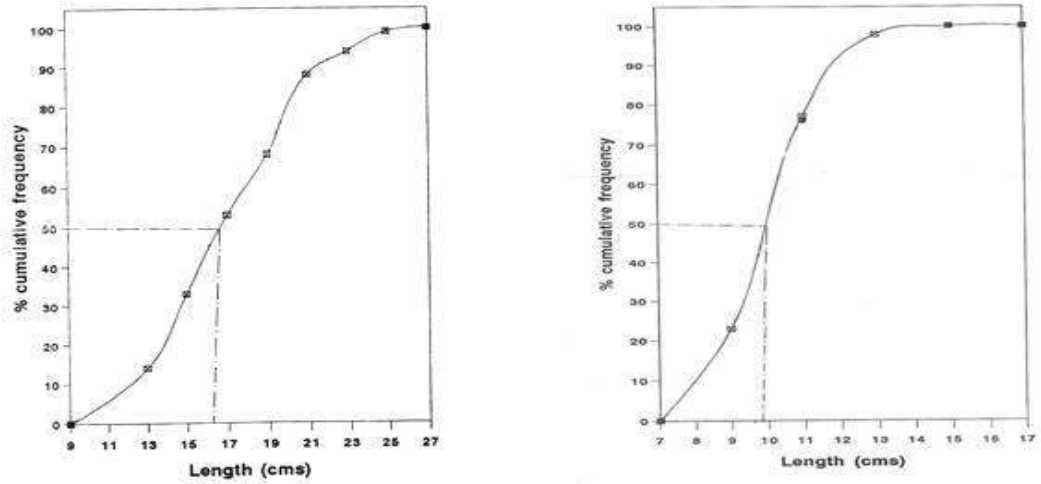

Pomfrets (*Pampus spp*.) **Silver bellies** (*Leiognathus spp*.)

Figure 2b: Percentage cumulative frequency curves for some important fin fishes caught modified in two-seam overhang trawl.

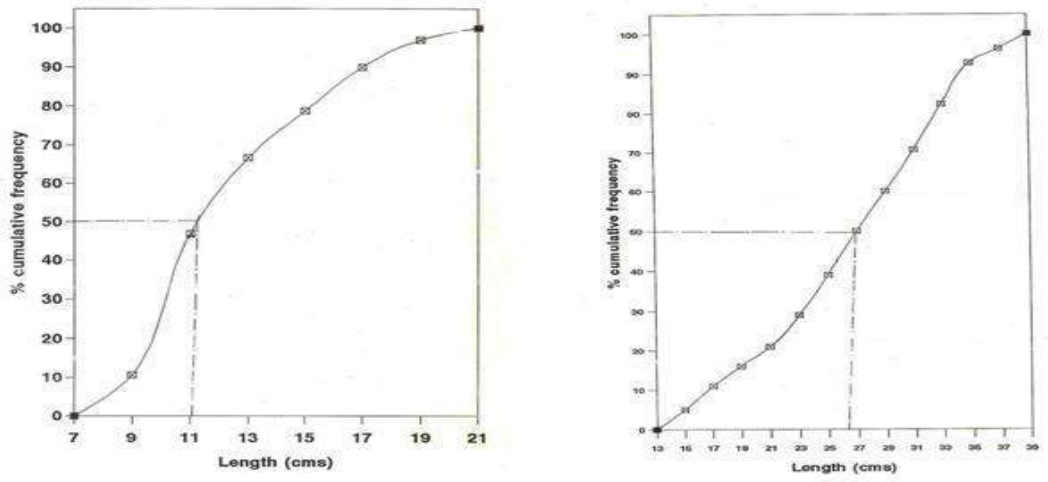

Soles (*Cynoglossus.spp*) **Ribbon fishes** (*Trichiurus.spp*

Figure 2c: Percentage cumulative frequency curves for some important fin fishes caught modified in two-seam overhang trawl.

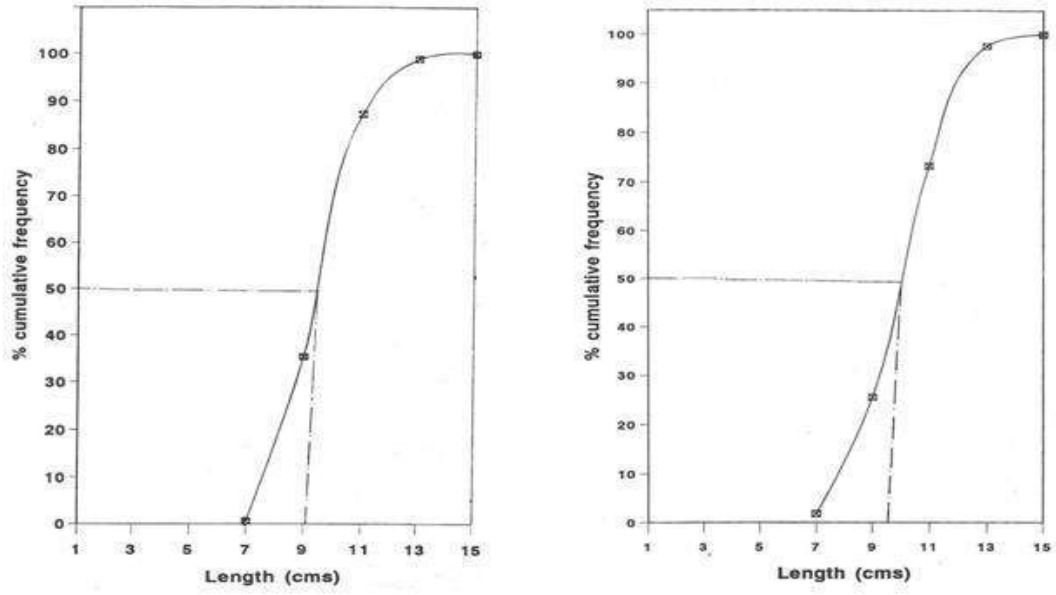

Metapeneaus spp ***Parapenopsis sp***

Figure 3: Percentage cumulative frequency curves for some important shellfishes caught in modified two-seam overhang trawl

REFERENCE

Bal, D.V. and Rao, K.N., 1990. Marine Fisheries Tata *McGraw Hill publishing company (Books) Ltd, New Delhi 20 (4th edition)*: 459pp.

Balan, V., 1967.Biology of silver belly *Leiognathus bindus* (val) of Calicut Coast: *Indian J.Fish*.**10** (1):118-134.

***Chidambaram.K and Venkataraman,R.S.** 1946.Tabular Statements on the fishery of certain marine food fishes of the Madras Presidency-West Coast.*Govt.Press.*:1-26.

***Chun-Chun-Te, Matuda, K and Honda, M.**1991.*Bull.Jap.Soc.Fish*.**57** (7):1313pp.

Daniel.W.W.1977. Introductory statistics with Application. *Houghton Miffon Company London*: pp 473.

***Kuthalingum, M.D.K.,** 1963.Observations on the fishery and Biology of the Silver Pomfret *Pampus argentus* (Euphrasen) from the Bay of Bengal: *Indian J.Fish*.**10** (1):59-73.

Kunjipalu, K.K and Varghese, M.D.1989. Paper presented at the *First Kerala Science Congress, 26-28February, 1989.Cochin, India.*

Kunjipalu, K.K., Varghese, M.D and Nair, A.K.K. 1994. Studies on square mesh codend in trawls-I. Studies with 30mm mesh size .*Fish Technol.Kochi*.**31** (2): 112-117p.

***Nair, R.V.**1951.*Proc.Indo.Pacif.Fish.Coun., Sec.2*.p.103

Pope, J.A.1966.Manual of Methods for Fish Stock Assessment-Part III. Selectivity of Fishing Gear. FAO, *Fisheries Technical Pape*r.*No.41.*

Robertson, J.H.B.1982**.** Square mesh codends *Scottish Fisheries Working Paper*, **3**:11p

Robertson, J.H.B. 1983 Square net help young fish escape.*Fish.News*, (3652):10-11p

Robertson, J.H.B.1986a Design and construction of square mesh cod ends. *Scott.Fish.*

Information.Pam. (12):10pp.

Robertson, J.H.B.1986b. Square mesh codends *Scott. Fish. Bull*., (49):15-16

Robertson, J.H.B., Emslie, D.C., Ballantyne, K.A.and Chapman, C.J. 1986. Square and diamond mesh trawl codend selection trials on *Nephrops norvegiucus Copenhagen-Denmark-ICES-1986/B:* **12** (12):14pp

Robertson, J.H.B. and Stewart P.A.M.1988 .A comparison of size selection of haddock and whiting by square and diamond mesh codends. *J.Counc.CIEM* **44** (2):148-161.

***Sheshappa.G and Bhichachar.B.S.**1954.*Indian.J.Fish*. I: 145-62.

Talwar.N.A and Sheshappa.D.S. 1996 .Effect of square mesh panels in trawls on shrimp fishery off Mangalore. **In**: *The Fourth Indian Fisheries Forum Proceed. 24-26.November, 1996, Kochi*: 445-447 p.

Talwar.N.A ., Sheshappa. D.S. and Hanumanthappa. B. 2006. Reduction of by-catch in two–seam over hang trawl using a square mesh panels in forward part of upper belly and codend. *J.Environ. & Sociobiol.*: **3**(2): p 143-146.

Weber.R.1973. Non-parametric methods, **In**: Bio-statistics in Pharmacology: *Vol-2, Dehaunois, A.L. (Ed) and Pergamum .press (New York)*: 675-716.

** Not refer to original*

EXPERIMENTAL STUDY OF LOCAL SCOUR AROUND CIRCULAR COMPOUND BRIDGE PIER

[1]PROF. P.T. NIMBALKAR, [2]S.S. THORAT

[1]Professor, Department of Civil Engineering, Bharati Vidyapeeth Deemed University, College of Engineering, Pune, INDIA

[2]M. Tech. Scholar, Hydraulic Engineering, Bharati Vidyapeeth Deemed University, College of Engineering, Pune, INDIA

ABSTRACT

Local scour around the circular bridge pier in alluvial channel is main factor for failure of hydraulics structures such as bridge pier, abutment etc. It is a complex phenomenon. Local scour around bridge pier is depends upon the depth of flow, Discharge, Geometry of Pier, Types of sediment particles. Many researchers have studies on scour around uniform cross section of pier without considering the effect of footing of bridge pier. But the study on scour under steady condition for compound bridge piers is limited. In present study, the experimental work was carried out on different geometry of compound bridge pier under clear water scour condition with uniform and non uniform sediments. The compound bridge pier was placed at a various location with respect to initial bed level. i.e. the top level of foundation at bed level, top level of foundation below bed level and top level of foundation above bed level. It is observed that the maximum scour occurs when the foundation top above initial bed level and it is reduce at bed level and below bed level. It is also observed that there is reduction scour in non uniform sediment as compare uniform sediment.

KEYWORDs: - *Bridge pier, Sediment, Scour, Compound pier, Foundation etc.*

1. INTRODUCTION

The process around the bridge pier in which reduces elevation of initial bed level of stream due to degradation of bed soil due to flowing water. It is main factor for failure of hydraulics structures i.e. bridge pier, abutment etc. Local scour is a three dimensional process caused by various agents like changes the flow condition of channel due to construction of bridge pier, flood , human interferences etc. Out of 500 bridges collapsing in the united state since 1951, it was reported that 60% of bridge collapsing due to bridge pier scour. Therefore the study of phenomenon of local scour around the bridge pier has become the important topic in hydraulic engineering.

To determine the maximum depth of scour around bridge pier is important from point of view by design of bridge pier foundation. Local scour is complicated phenomenon due to three dimensional flow separation on upstream side of bride pier and sediment load transport. Lots of research work has been done on this topic for basically to deriving the relationship for maximum depth of scour, to understanding the mechanism of local scour and its control. Therefore the large amount of research work is available on the topic of bridge scour and its protection However, only a few studies are available so far on the flow field around the bridge elements. The flow pattern within the scour hole around circular uniform bridge piers have been studied through laboratory experimentation by following investigator by Melvilleand Raudkivi(1977), Deyetal.(1995), Ahmedand Rajaratnam (1998), Grafand Istiarto (2002),Muzzammil and Gangadhariah (2003) and Deyand Raikar (2007). These investigations have mainly study on scour around such piers which have uniform cross section(orgeometry) along their height but without considering the effect of footing of bridge pier. But actual site (in field work) bridge piers are constructed in different types of shape and sizes and many of them can have varying uniform cross sections along their heights, then such types of pier are known as compound piers (ornon-uniform piers). Kumar and Kothari (2012) conducted experimental work on the flow pattern and turbulence characteristics around the circular uniform and non uniform piers in the presence of scour hole using an ADV. Lu et al (2011) have recently proposed a semi empirical model to estimate the temporal variation of local scour around compound bridge pier without exposed foundation.

The local scour around the bridge pier is time dependent process. It is always show in the graphical form by plotting the maximum scour depth versus the time. It is very difficult to calculate the correct maximum scour depth in the given time due to the complex three dimensional phenomenon. Therefore many methods have been used to developing the relationship between maximum equilibrium scour depth and time. Many attempt to describe phenomenon of the temporal variation of local scour around bridge pier have been made by many authors in the last 50 years. And they show that the temporal variation around the bridge pier is dependent on the flow condition, types of sediment, shape of bridge pier etc.

The circular compound bridge pier defined as the circular bridge pier is placed on the bigger diameter of circular foundation and such geometry piers foundation are mostly used in bridge sub structures in India.

2. EXPERIMENTAL SETUP

The experimental work were carried in a glass both sides rectangular titling flume having 10m long, and cross section of 0.30m in width and 0.50m depth in the hydraulics laboratory at the department of civil

engineering, Bharati Vidyapeeth Deemed University Pune, Maharashtra, India. The titling flume is consists of two controlling gates, one gate upstream side of flume is known as inlet gate and other gate at downstream of flume is known as outlet gate. Water supplied into tilting flume from a underground water tank constructed below the floor of the hydraulics laboratory by using centrifugal pump. For calculating discharge sharp crested weir was fitted at downstream of re-circulating channel. The rehbock weir equation was used to determine the discharge for the experimental work. The flow rate is adjusted by inlet valve. The required water depth is adjusted by using the outlet gate. The depth of water level, initial bed level and depth of scour is measured by using point gauge. The working section 0.70m long, 0.3m in width and 0.1m in thickness located from 4.5m from the upstream side of titling flume. The working section filled with sediment particles. The compound piers of different sizes were used in this experimental work. The compound pier were placed at the vertically at the middle portion of the working section of the titling flume (Sediment area). The bed was levelled before the starting of flow of the titling flume. The initial level of bed was measured by using the point a gauge. The clear water scour condition was maintained during the experiment i.e. $\frac{V}{V_c}$ ratio is less than one,where V= approach flow velocity and V_c = Critical velocity calculated by using the d_{50} and shields method (Garde and Ranga Raju 2006).

2.1 PIER MODEL

The two different types compound piers was made up of PVC pipes, are given below,

1. The diameter of pier was taken as 3cm and diameter of foundation was taken as 6cm
2. The diameter of pier was taken as3cm and diameter of foundation was taken as 7.40cm

The top level of foundation of compound bridge pier was placed at different location Y with respect to initial bed level. In this work, the following three cases are considered,

Case:-A Top level of foundation is taken as 1cm above the initial bed level.

Case:-B Top of foundation is taken as at initial bed level.

Case:- C Top of foundation is taken as 1cm below initial bed level.

2.2 TYPES OF SEDIMENT MATERIALS USED

The bed material was a mixture of river sand with different particle sizes varying range from the sediment filled in the working section up to thickness of 10cm. Mechanical sieve analysis was used to determine the relative proportion of different particle size in a given sediment sampleThree samples of sediments are prepared as given below,

Sample No:- 1 d_{50} = 1mm and standard deviation =1.14

Sample no:- 2 d_{50} = 1mm and standard deviation = 1.68

Sample no:- 3 d_{50} =1mm and standard deviation =2

3. RESULT AND DISCUSSION

Table No. 1. Experimental Data for uniform sediment

Sr. No.	Pier diameter b mm	Foundation Diameter b* mm	Footing elevation w.r.t. Bed levelY mm	Flow depth D in mm	Approach velocity of flow V m/s	Critical velocity of sediment motion Vc m/s	Median grain size d_{50} mm	Geometric standard deviation σ_g
1	30	60	-10	84	0.32	0.378	1	1.14
2	30	60	0	84	0.32	0.378	1	1.14
3	30	60	10	84	0.32	0.378	1	1.14

In this V is the approach velocity of flow calculated from the know discharge and depth of flow for a single discharge value. During the experimental work discharge is adjusted by inlet valve and outlet gate. The discharge can be calculated from the Rehbock equation.Depth of flow is measured in the titling flume for particular discharge values and the approach velocity of flow is calculated by using the continuity equation.

Using Shields chart for threshold condition of uniform sediments in water (Melville and Sutherland 1988) the shear velocity u_{*c} corresponding to d_{50} is obtained .The shear velocity u_{*c} is converted to mean shear velocity V_c by the logarithmic form of velocity profile given in equation 1

$$\frac{V_c}{u_{*c}} = 5.75 \log\left(5.53 \frac{D}{d_{50}}\right) \qquad (1)$$

Similarly required data is obtained for non uniform sediments and given below in table 2

Table 2 Experimental Data for Non Uniform sediments.

Sr.No.	Pier diameter b mm	Footing diameter b_* mm	Footing elevation w.r.t. Bed level .Y mm	Flow depth D mm	Velocity of approach flow V m/s	Critical velocity for sediment motion Va m/s	Median grain size d_{50} mm	Geometric standard deviation σ_g
1	30	60	-10	78	0.36	0.397	1	1.68
2	30	60	0	78	0.36	0.397	1	1.68
3	30	60	10	78	0.36	0.397	1	1.68
4	30	60	-10	90	0.253	0.418	1	2
5	30	60	0	90	0.253	0.418	1	2
6	30	60	10	90	0.253	0.418	1	2
7	30	74	-10	90	0.253	0.418	1	2
8	30	74	0	90	0.253	0.418	1	2
9	30	74	10	90	0.253	0.418	1	2

The method to determine V_a is given in Melville (1997) .Thus Va =0.8 V_{ca}

V_{ca} can be determined from logarithmic form of velocity profile

$$\frac{V_{ca}}{u_{*ca}} = 5.75 \log\left(5.53 \frac{D}{d_{50a}}\right) \qquad (2)$$

In this u_{*ca} is critical shear velocity for d_{50a} size and d_{50a} is median armour size. Shear velocity is determined from Shields diagram for respective sizes.

The particle size d_{50a} is found using the Expression as given by Chin (1985)

$$d_{50a} = \frac{d_{max}}{1.8} \qquad (3)$$

d_{max} is the maximum particle size determined from particle size distribution.

The experimental results are shown in graphical form to observed scour depth versus time as given below,

Case:- I pier Diameter =3cm and footing diameter =6cm with uniform sediment (d_{50} =1 and $\sigma_g = 1.16$

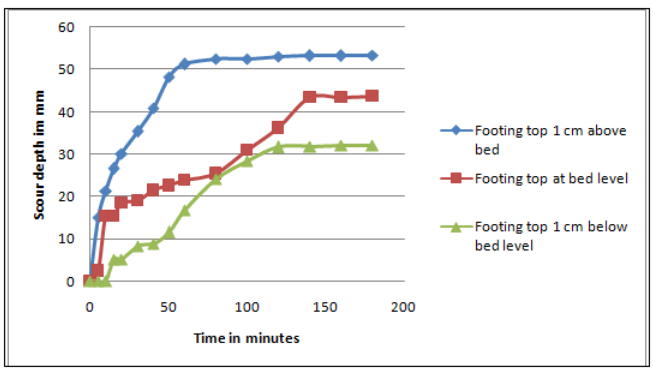

Figure 1: Temporal variation of scour depth in uniform sediments

Case:- II pier Diameter =3cm and footing diameter =6cm with uniform sediment (d_{50} =1mm and $\sigma_g = 1.68$

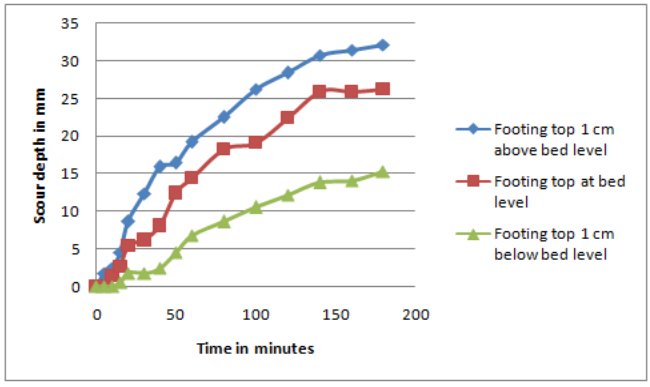

Figure 2: Temporal variation of scour depth in Non uniform sediments

Case:- III Pier Diameter =3cm and footing diameter =6cm with uniform sediment (d_{50} =1mm and $\sigma_g = 2$

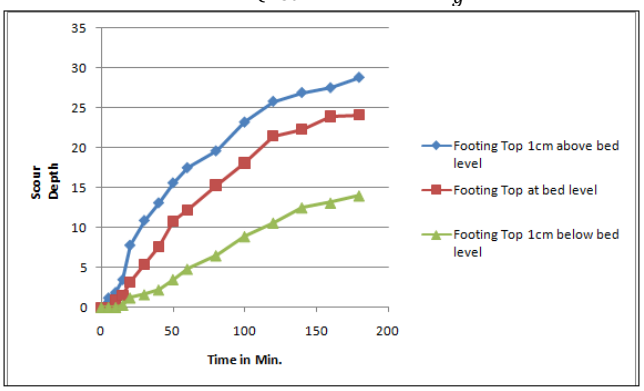

Figure 3: Temporal variation of scour depth in Non uniform sediments

Case:- IV Pier Diameter =3cm and footing diameter =7.4cm with uniform sediment (d_{50} =1mm and $\sigma_g = 2$)

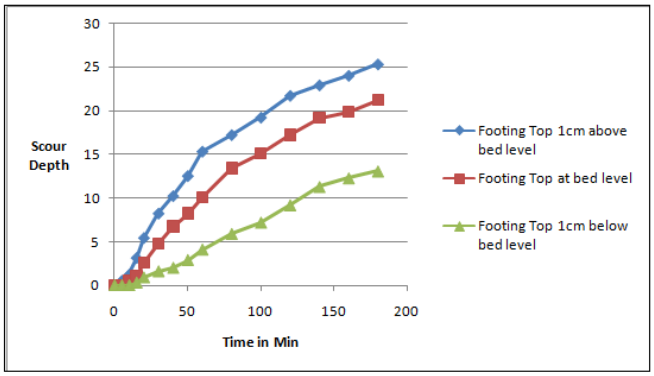

Figure 4: Temporal variation of scour depth in Non uniform sediments

4. CONCLUSION

The following conclusions are based on the experimental work on the scour development process around the compound bridge pier with varying the foundation depth with respect to initial bed level of channel.

1. In the uniform sediment particles the top level of foundation was placed above the initial bed level the maximum scour depth occurs due to more area of foundation was exposed to the flowing water.
2. When the top level of foundation was placed at the at initial bed level with uniform sediment, then scour depth reduces as compare to above condition.
3. When the top level of foundation placed below the initial bed level further reduction was observed in the scour depth.
4. Same pattern of scour was observed in non uniform sediment for the three cases as mentioned above only overall reduction of scour depth was observed as compared to uniform sediment as there is armouring action in non uniform sediment.
5. When the standard geometric deviations increases, then scour depth decreases and for higher value armouring effect occurs on the upstream side of bridge pier.

REFERENCES

1) Ahmed, F., Rajaratnam, N., 1998. Flow around bridge piers. J. Hydrol. Eng. ASCE 124 (3), 288 -300.
2) Beheshti, A. A., Ashtiani,A.B.,2010. Experimental study of three dimensional flow fields around a complex bridge pier. J. Hydrol. Eng. ASCE136(2),143-154
3) Breusers, H.N.C., Nicollet,G.,Shen, H.W.,1977. Local scour around cylindrica l piers. J. Hydrol. Res. IAHR 15 (3), 211-252.
4) Chang, W. Y., Lai, J. S., Yen, C. L., 2004. Evolution of scour depth at circular bridge piers. J. Hydrol. Eng. ASCE130 (9), 905-913.
5) Dey,S.,Bose,S.K.,Sastry,G.L.N.,1995.Clear water scour at circular piers: amodel. J. Hydrol. Eng. ASCE 121 (12), 869-876.
6) Dey, S., Raikar, R.V., 2007. Characteristics of horseshoe vortex in developing scour holes at piers. J. Hydrol. Eng. ASCE 133 (4), 399-413.
7) Graf, W.H., Istiarto, I., 2002. Flow pattern in the scour hole around a cylinder. J.Hydrol. Res. IAHR 40 (1), 13-20.
8) Imamoto,H.,Ohtoshi,K.,1987.Local Scour Around a Non-uniform Pier. In: Proc., IAHR Congr, pp. 304-309.
9) Jain S.C .Maximum clear water scour around circular piers, JHD, ASCE,Vol. 107,No. HY-5,1981
10) Jones,J.S.,Kilgore,R.T.,Mistichelli,M.P.,1992.Effects off ooting location on bridge pier scour. J. Hydrol. Eng. ASCE 118 (2), 280-290.
11) Junke Guo (2012) ,Pier scour in clear water for sediment mixtures. Journal of Hydraulic research 50 (1) ,18-27.
12) Kothyari, U. C., Garde, R. J., Ranga Raju, K. G., 1992. Temporal variation of scour around circular bridge piers. J. Hydrol. Eng. ASCE 118 (8),1091-1106.
13) Kothyari, U. C., Hagar, W. H., Oliveto, G., 2007. Generalized approach for clear-waters courat bridge foundation elements. J. Hydrol. Eng. ASCE133(11),1229-1239.
14) Kumar, A., Kothyari,U.C.,2012.Three dimensional flow characteristics within the scour hole around circular uniform and compound piers. J. Hydrol. Eng. ASCE 138(5), 420-429.
15) Kumar, A., Kothyari, U. C., Ranga raju K.G.2012, Flow structure and scour around circular compound bridge piers –A review. J. of Hydro-environmental research,6 ,251-265
16) Lu, Jau-Yau., Shi, Zhong-Zhi, Hong, Jian-Hao, Lee, jun-ji, Raikar, V.K., 2011.Temporal variation of scour depth at non-uniform cylindrical piers. J. Hydrol. Eng. ASCE 137 (1), 45-56.
17) Melville, B.W. 1975, Local Scour at Bridge Sites. Report No. 117, Univ. of Auckland, School of Engg., Auckland, New Zealand,
18) Melville, B.W., 1997. Pier and abutment scour: integrated approach. J. Hydrol.Eng. ASCE 125 (1), 59-65
19) Melville, B.W., Raudkivi, A.J., 1977. Flow characteristics in local scour at bridge sites. J. Hydrol. Res. IAHR 15 (4), 373-380.
20) Melville, B.W., Raudkivi, A.J., 1996. Effects of foundation geometry on bridge pier scour. J. Hydrol. Eng. ASCE 122 (4), 203-209.
21) Melville, B.W., Sutherland, A.J., 1988. Design method for local scour at bridge piers. J. Hydrol. Eng. ASCE 114 (10), 1210-1226.
22) Muzzammil, M., Gangadhariah, T., 2003. The mean characteristics of horseshoe vortex at a cylinder pier. J. Hydrol. Res. IAHR 41 (3), 285-297.

DESIGN AND DEVELOPMENT OF VERIFICATION ENVIRONMENT TO VERIFY SPI MASTER CORE USING UVM

[1]RAJESH C, [2]SHIVANANDA, [3]MRS. SHANTHI V A

M.Tech, Dept. of ECE, B.N.M Institute of Technology, Bengaluru, India, E-mail: rajesh.cgowda@gmail.com

Assoc. Professor, Dept. of ECE, B.N.M Institute of Technology, Bengaluru, India, E-mail: cshivananda@gmail.com

Senior Technical Staff, Maven Silicon Softech Pvt Ltd, Bengaluru, India, Email: shanthi@maven-silicon.com

ABSTRACT

The main objective of the work is to design an SPI Master Core using Verilog HDL and Verify the designed SPI Master Core using Universal Verification Methodology. SPI (Serial Peripheral Interface) facilitates the transfer of synchronous serial data, which is now a day's engineer's favorite choice for its convenience and saving system resource. SPI (Serial Peripheral Interface) operates in full duplex mode. It communicates in master/slave mode where the master device initiates the data frame. Multiple slave devices are allowed with individual slave select line .Serial Peripheral Interface of symmetrical structure can be designed using Verilog HDL and Synthesized using Xilinx 13.2, and then can be simulated using Questasim 10.0b. SPI is a very popular interface used for connecting peripherals to each other and to microprocessors.

Key Words: *SPI, WISHBONE, QUESTASIM, XILINX ISE, Verilog, UVM, Coverage*

1. INTRODUCTION

In these days almost every system includes some intelligent control, commonly a Microcontroller Core. General-purpose circuits like remote I/O ports, data converters, LCD drivers, EEPROM or RAM. Application oriented circuits for data communication interfaces and/or intensive computation task. So the communications between these modules are important.

In many applications the interface between these modules is still a bottleneck of system performance. In such prospect the reuse of IP (intellectual property) macro cells is becoming the centre of gravity for design productivity and the key for being able to produce chips that work efficiently. Every integrated components should be connected each other and every SoC should be linked with each other in an efficient manner that allows an error-free and fast communication. Communication among SoC is the key to yield higher performances: the most widely used solution used for interconnecting SoC is a serial bus, as it gives a great advantage in terms of cost. With the development of the IC manufacturing, the communication between hardware devices became very important. Presently widely used protocols such as I2C bus protocol, ARM bus protocol, WISHBONE bus protocol, etc., allows the hardware devices to communicate through the appointment of the rules and match the timing for achieving the purpose of data communication. Compared to other protocols, SPI has is simple to use, has higher transmission speed, and little pins advantages. SPI standard protocol requires at least four interfaces. Normally, the devices which are based on SPI protocol are divided into slave-device and master-device for transmitting the data. The clock signal and slave select signal have to be generated by the master-device during the data exchange processing. Therefore, the master device should have multiple slave select interfaces for slave devices as it controls multiple slave devices. That will not meet the standard SPI protocol. The standard SPI communication is a single-master communication, which is all the communications have only one master device. Thus the devices which are based on SPI protocol are limited by both the aspects. The design is fully composed with the four interfaces of standard SPI protocol.

2. SPI DESIGN PRINCIPLES

SPI is a synchronous serial bus protocol developed by Motorola and integrated in many of their microcontrollers. Normally SPI is used for short distance communication,

2.1 ARCHITECTURE OF SPI

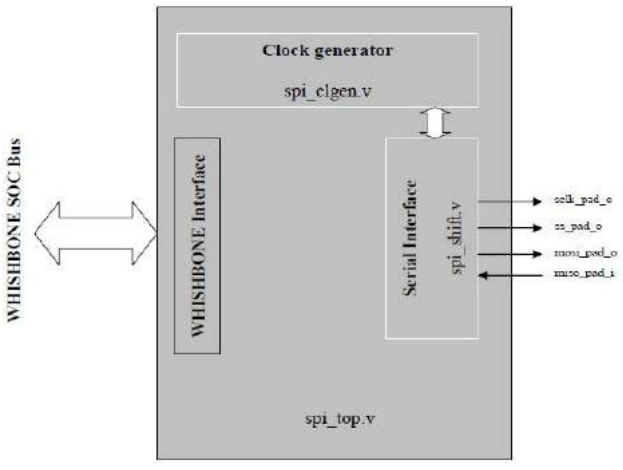

Fig.1: Architecture of SPI

SPI Master Core consists of three main building blocks:

- Clock generator

• Serial interface

• WISHBONE Interface

SPI bus consists of four signals: serial clock (SCK), master in slave out (MISO), master out slave in (MOSI), master in slave out (MISO), and active-low chip select (SS). As a multi-master/slave protocol, communication between the selected slave and master uses the unidirectional MOSI and MISO lines, to achieve higher data rates in full duplex mode. SPI requires separate Slave select lines for each slave. With SPI we can connect as many devices as many pins we have on the main microcontroller. The communication speed between ICs is much faster due to the Full Duplex communication.

2.2 MODULE DESIGN

1) Clock Generator design

The clock signal spi_clgen is root from the external clock wb_clk, the module produces the output signal s_clk according to the different frequency factor of the clock register. Divider is the basic and efficient part of the digital circuits and FPGA design; It is also a very important component of the communication system. The frequency of the serial clock s_clk of the master core system is changed by changing the value of the DIVIDER value in the Divider register. Relation between DIVIDER value, s_clk and wb_clk is given by the following equation:

$$f_{sclk} = \frac{f_{wb\_clk}}{(DIVIDER+1)*2}$$

Clock generation module is synthesized by ISE. Module synthesized shown below shown in Fig 2.

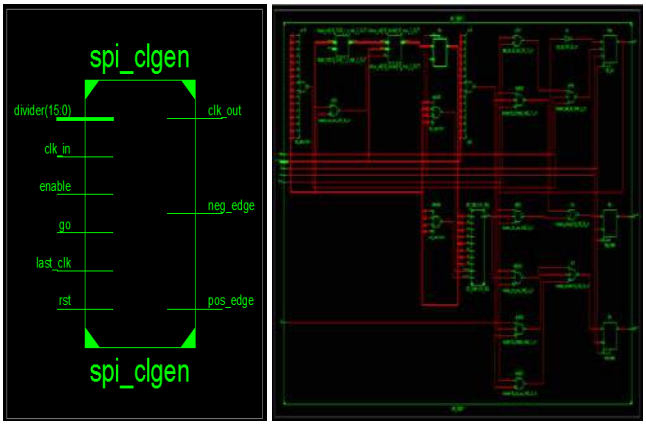

Fig.2 Clock Generator Circuit Module

2) Serial Interface module design-- spi-shift

Serial interface module is the core module of the SPI. Serial interface module is responsible for serial data into parallel out and data parallel into serial out. In this work the design of serial interface is different from the usual serial interface; It increases the overall data transmission rate. SPI Master at the host side acts as a slave device to receive data and acts as the master device to send data. Serial interface module is synthesized by ISE. Verilog code for this module is synthesised module shown in Fig. 3.

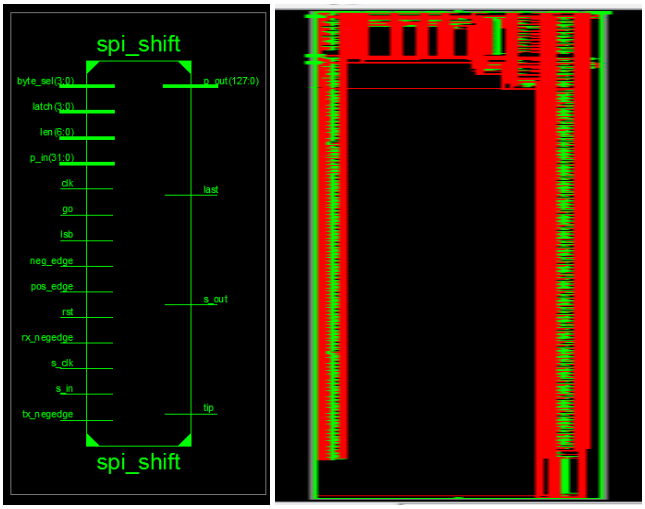

Fig.3 Serial Interface Circuit Module

3) Top-level module –TOP

Based on the specifications of the SPI protocol, we get the basic structure SPI bus by including the clock generation module and serial interface module. An important aspect of the top-level module is to ensure that the sub-modules work smoothly. The SPI top module needs the control word, the efficient operation of sub-modules: clock generation module and serial interface module. SPI top module is synthesized by ISE. Synthesized module is shown in Fig. 4.

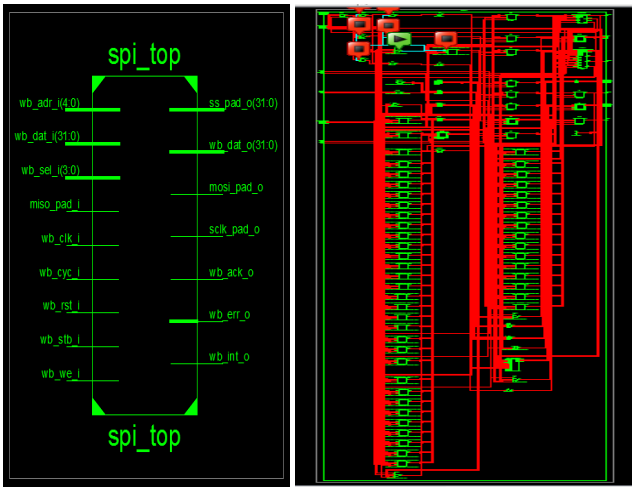

Fig.4 Top Level Circuit Module

3. SIMULATION AND VERIFICATION

Verilog HDL is one of the hardware description languages. Verilog can be used for different levels of logic design, it can be used for digital system logic simulation, timing analysis and logic synthesis. In this work, a SPI Master core Interface Module is designed using Verilog HDL. According to the standard SPI bus principle, we can achieve the bidirectional data transmission between the slave devices and microcontroller. Using Verilog HDL we had designed the SPI Master Core interface circuit, synthesised with ISE, and then used Questasim to simulate. In order to establish the test platform, first setup the master module to simulate the Wishbone protocol, and then setup the slave module to simulate SPI protocol at the same time. Then to compare and check the

receive/send data and addresses. The test bench is designed using universal verification methodology. Verification is also the major part of this work as many modules are designed and having many inputs univrsal verification methodology helps to makes easy to stimulate according to our wish, constraint the unwanted stimulus. Here the SPI Master Core Design is considered as design under test (DUT). Components of Verification Environment are as follows : RTL module, Master and Slave agent tops which consists of master and slave agents which contains sequencer, driver and monitor, virtual sequencer, Scoreboard, TOP level module which encapsulates the above all with RTL and Test Cases.

UVM testbench architecture is as shown in Fig. 5.

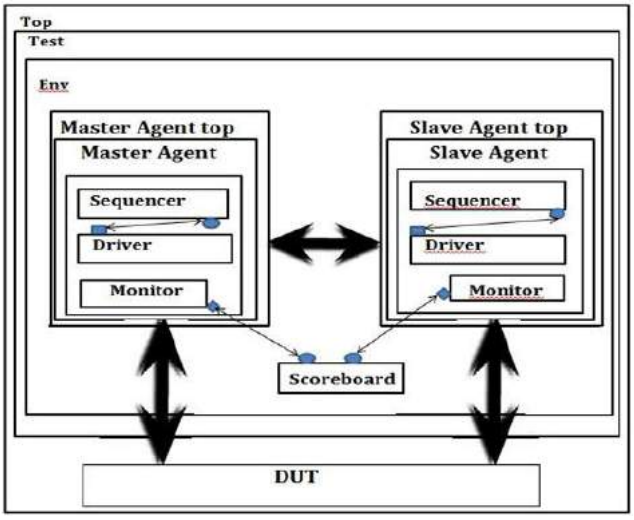

Fig.5: UVM testbench Architecture

The simulation results are as shown below in Fig. 6

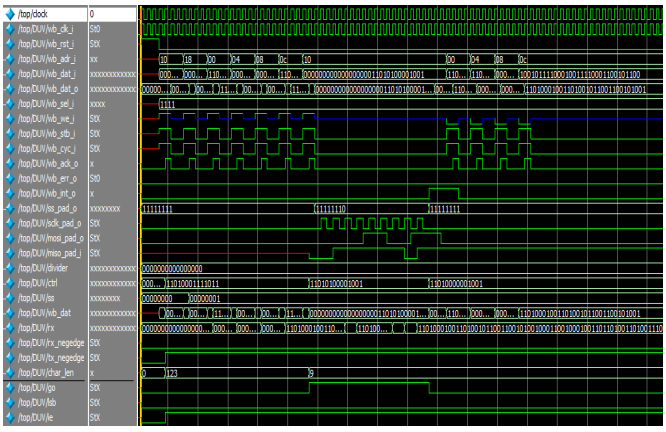

Fig.6: Simulation results

Coverage Report is shown below in Fig. 7

Number of tests run:	4
Passed:	4
Failed:	0

List of tests included in report...

Design Coverage Summary:		Coverage Summary by Type:			
Weighted Average:	100.0%	Weighted Average:			100.0%
Design Scope	Coverage (%)	Coverage Type	Bins	Hits	Coverage (%)
spi_pkg	100.0%	Covergroup	12	12	100.0%
spi_coverage	100.0%				

Fig.7: Coverage report

4. CONCLUSION

In this work, we have designed the SPI Master core Using Verilog HDL language based upon design-reuse methodology. SPI Transmission timing is very strict, so this paper designs a reliable and stable clock generation module, considering both the odd-even frequency cases. Data transmission module is very simple and the transfer speed is faster. We have verified the data in slave device same as the data in the master device. Further, we have also done functional verification. The code coverage is obtained for the RTL design and 100% code coverage and functional coverage is extracted. The complete function of the registers is verified in this paper. The innovation of this article: Universal verification methodology is used in order to cover all the functions of the code and to reuse the class instead of writing the code again. The advantage of using universal methodology is making the things easy by calling the inbuilt classes.

REFERENCES

[1] www.opencore.org Simon Srot.SPIMasterCore Specification, Rev.0.6. May 16, 2007.

[2] Prophet, Graham. Communications IP adds SPI interface to FP-GA. EDN, v 48, n 27, Dec 11, 2003.

[3] Motorola, "MC68HC II manual".

[4] Smart Computing Dictionary, Serial Peripheral Interface (SPI) (online)http://www.smartcomputing.com/editorial/dictionary/detail.asp?guid=&searchtype=1&DicID=12820&RefType=Dictionary (access date 28May 2006)

[5] Frédéric Leens, An Introduction to I2C and SPI Protocols,IEEE Xplore.

[6] Zhang Yan-wei, Verilog HDL detailed design procedure, Posts & Telecom Press.

[7] Wikipedia, the free encyclopedia, “Serial Peripheral Interface Bus”,

Available http://en.wikipedia.org/wiki/Serial_Peripheral_Interface_Bus.

ESTIMATION OF DOMESTIC, CROP WATER REQUIREMENTS AND ESTIMATION OF GROUNDWATER, SURFACE WATER RESOURCES OF RENIA CITY - IRAQ

[1]AHMED TALIB ABDULJALEEL AL-ALIKHAN, [2]PROF. P.T.NIMBALKAR

[1]Research scholar, Department of Civil Engineering Bharati Vidyapeeth Deemed University College of Engineering Pune

[2]Professor, Department of Civil Engineering Bharati Vidyapeeth Deemed University College of Engineering Pune

ABSTRACT

The area understudy is located in the northeastern of Iraq between lat. (36° 10- 42, 46° 31- 00) and long. (47° 21- 00, 4460-41) approx. Area of 980 km^2.The study area is chosen for the hydro--geological study it has high groundwater resources useful for irrigation of medium and large scale projects. The main sources in the studied area are wells, springs and streams. It is reported that drinkable water in Renia district is existing for 91 % of the population

Renia city has an urban population about 65,110. Over the planning period through 2025, its population is projected to increase to approximately 117,540.The water demand for the year 2005 is approximately 28,100m^3/d , and it is projected to increase around 50800 m^3/d by the year 2025. The combined water demand for these sub district Renia city (Batwata, Hejiawa and Chwerqurna) is projected to increase from approximately (34,470m^3/d) to around (62,250 m^3/d), by the year 2025.Well tests for (11) wells that penetrate the Quaternary aquifer indicated specific yield with median value of 0.08m/day, a hydraulic conductivity with median value of 2.10 and transmissivity with median value of 170m^{2}/d.

1. INTRODUCTION

1.1 LOCATION

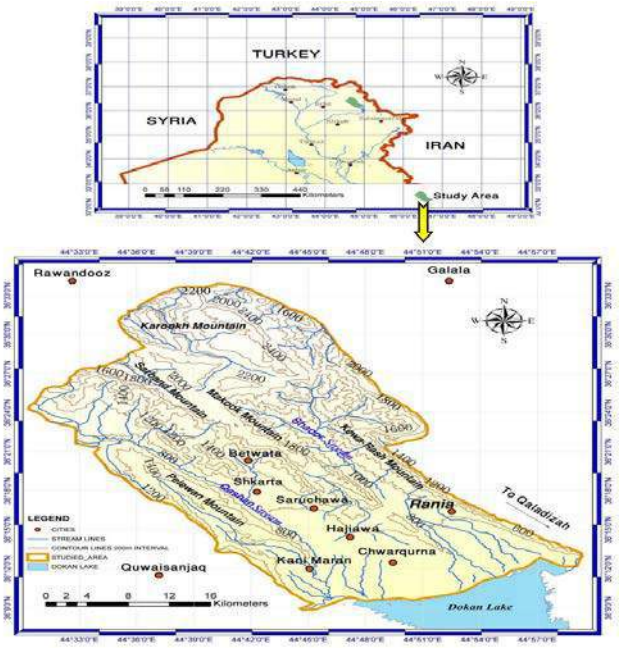

Fig (1) Location of Studied Area

1.2 POPULATION

Estimation of population in 2005, see table (1)

Subdistrict	Urban	Rural	Total
Municipal center(Renia)	65,010	0	65,000
Batwata	13,250	7,400	20,652
Hejiawa	36,000	4,440	39,441
Chwerqurna	41,000	27,060	67,061
Total	**155,260**	**38,900**	**192,154**

Reef Table No.(1), Population of the Renia in 2005

1.3 CHWERQURNA, HEJIAWA, AND BATWATA

The characteristics of the water system are shown in the table

	Renia	Batwata	Hejiawa	Chwerqurna
Population (estimated)	65,010	13,250	36,000	41,000
Area (km2)	10	8	5.5	6
Density (persons/km2)	6,501	1,656	6,545	6,833
Water source	Qula Spring& deep wells(25) 10,601 m3/d	spring 7,001 m3 /d	Wells (23) -3,010 m3/d	Wells (22) - 2,600 m3/d
Projected demand	28,000	4,770	13,860	15,841
Projected demand - 2025 (m3/d)	50,717	8,614	25,034	28,610
Water supply cap - 2005	10,629	7,001	3,010	2,510

Reef Table No (2), Water Systems in the study

1.4 MAIN PROBLEMS

Main problems in water supply system

- Distribution network coverage system is old and inadequate
- Less availability of maintenance equipment
- Less availability of electricity
- Lack of storage facilities

2. PROJECTED NEEDS

2.1 DEMAND PROJECTION

Urban population of Renia city is about approximately 65,010 persons . By its population is projected to increase to around 2025 , its population is projected to increase to around 117,500 in 2005 water demand was around 28,100 m^3/d, it is projected by the year 2025 that water demand will increase around 50800 m^3/d

2.2 EXISTING CAPACITY

Design and existing capacity of Renia water supply system, see Reef Table No. (3) Below

Source	Renia water sources m^3/d	• Design capacity of the existing system * m^3/d
Springs	7,501	7,501
Wells	3,129	10,537
Total	**10,630**	**18,038**

*This design capacity of the existing system based on a 24-hours operation.

2.3 AIM OF THE STUDY

The aims of the study are:

1. An assessment of the available water resources.
2. To determine domestic water requirement for project population
3. To determine crop water requirement by using software program (CROPWAT 8.0) .

2.4 METHODOLOGY

1-For preparing fieldwork the available basic data from different sources are collected topographic and geological maps with relevant scale are selected and images from satellite for background map were made available..

2- Relevant data from another respective offices are calculated from site on use of land groundwater and drilled wells

2.5 FOR THE DISTRICT CENTRE'S PROJECTED NEEDS

According to year 2005, 2015 and 2025, estimated water demand and the supply capacities is presented in table below

Parameter	Quantity m^3/d
Existing operational water production capacity	10,630
Design capacity of the existing system	18,038
Projected demand 2005	28,081
Projected demand 2015	37,738
Projected demand 2025	50,717
Projected production capacity deficit 2005	17,451
Additional production needed in 2015	27,108
Additional production needed in 2025	40,087

Reef Table No.(4),Projected Water Demand and Supply Capacity of Renia City

2.6 FOR DISTRICT CITY

Estimation water demands and the supply capacities for the years 2005, 2015 and 2025 are presented in table for (Batwata, Hejiawa and Chwerqurna).

Batwata	**2005**	**2015**	**2025**
Existing water supply capacity	7,001 m3/d	---	---
Projected water demand	4,769 m3/d	6,410 m3/d	8,614 m3/d
Additional capacity	None	None	1,613 m3/d
Hejiawa	**2005**	**2015**	**2025**
Existing water supply capacity	3,010m3/d	---	---
Projected water demand	13,860 m3/d	18,627 m3/d	25,033 m3/d
Additional capacity	10,850 m3/d	15,617 m3/d	22,023 m3/d
Chwerqurna	**2005**	**2015**	**2025**
Existing water supply capacity	2,600 m3/d	---	---
Projected water demand	15,840 m3/d	21,288 m3/d	28,609 m3/d
Additional capacity	13,240 m3/d	18,688 m3/d	26,009 m3/d
Total of the Subdistricts	**2005**	**2015**	**2025**
Existing water supply capacity	12,500 m3/d	---	---
Projected water demand	34,469 m3/d	46,324 m3/d	62,255 m3/d
Additional capacity required	21,969 m3/d	33824 m3/d	49,755 m3/d

Reef Table No. (5), Projected Water Demand and Supply Capacity

2.6 ANNUAL EFFECTIVE RAINFALL AND EVAPOTRANSPIRATION

	Oct	Nov.	Dec.	Jan.	Feb.	Mar.	Apr.	May	Jun.	July	Aug.	Sep
Peff (mm)	29.7	70.1	113.5	127.4	97.5	96.6	63.9	21.4	1.31	0	0	0
Eto (mm/period)	152.3	92.8	66.8	67.7	66.8	98.1	116.1	162.1	224	239.3	230.4	195.7

Reef Table No.(6). Annual Effective Rainfall and Evapotranspiration for the Studied Area

3. OBTAINED RESULTS FOR THE STUDIED AREA

Reef Table No.((7).Showing output of program (CROPWAT 8.0) for Crops in the Renia Area

	Barley	Wheat	Sunflower	Tobacco	Chickpeas	Sweet melon	Maize
ETo(mm/period)	754	897	724	783	551	849	842
CWR (ETm)(mm/period)	540	605	535	605	405	608	568
Actual crop Evapotranspiration(ETc) (mm/period)	707	711	629	697	477	715	669
Total Rainfall(mm/period)	621	621	145	3.7	57	57	50.4
Effective Rainfall(mm/period)	496	496	126	3.6	52	52	47
Field water supply(FWS) (l/s/ha)	0.24	0.24	0.57	0.9	0.65	0.71	0.64
Net irrigation requirementNIWRi (mm/period)	241	241	516	650	401	658	564
Net irrigation requirementNIWRi (m3/ha)	2410	2410	5160	6500	4010	6580	5640
Cultivated Area (ha)	6394	9040.5	2786	57.6	1432	26	115
Volume of water required M.m^3	15.40954	21.78761	14.37576	0.3744	5.74232	0.17108	0.6486

3.1 WATER RESOURCES USED FOR IRRIGATION

3.1.1 Surface water

Dimane and Qoshan are main water surface used for irrigation in Renia city. Reef Table No. (8) Showing average discharge recorded in one month for one year .The mean discharge for Dimane and Qoshan are (0.7834) m^3/s and (2) m^3/s respectively.

MonthFactor	Oct.	Nov.	Dec.	Jan.	Feb.	Mar	Apr.	May	Jun.	Jul.	Aug.	Sep.	Mean
Qashan (m^3/s)	1.2	1.35	2.2	2.5	3	4.5	3.5	1.8	1.15	1	0.95	0.9	2
Dimana (m^3/s)	0.608	0.635	0.7	0.745	1	1.1	1.15	0.95	0.639	0.63	0.625	0.615	0.783

Table Reef Table No. (8). Average discharge for Dimane and Qoshan

3.1.2 Groundwater

- Wells and major springs are used for irrigation The springs which are used for irrigation are (QolaiRenia , QolaiKanimaren, and Sarochawa) , Reef Table No. (9) showing springs mean discharge

Major spring	discharge m3/sec	discharges used for irrigation	volume of water m.c.m
Qulai Rania	0.5	50%	7.776
Qulai Kanimaran	0.4	100%	12.4416
Saruchawa	6.5	80%	161.7408
Total			181.9584

- Is estimated that the number of wells are nearly (50)wells which operate about 5 hr/d within discharge of water about (6 l/sec/well).

3.1.3 Quaternary Aquifer -Hydraulic Properties

According to Renia groundwater intergranular. The available data for wells (10) drilled with in intergranularaquifer in the study area is based on process

The researcher monitors in an observation well {Transmissivity (T),Hydraulic Conductivity (K) ,Specific Capacity (Sc),and Storativity (S)},Reef Table No. (10)

Well	Q (m^3/d)	s (m)	T.D (m)	SWL (m)	b (m)	Sc(Q/s) (m^2/d)	T (m^2/d)	K (T/b) (cm/sec)
Well 1	907.3	1.2	95.2	13.85	81.2	756.08333	600.81	0.007304
Well 2	1200	10.5	100.1	13.2	87	114.28571	44.61	0.000516
Well 3	1297	4.5	120.5	20.2	100	288.22222	124.52	0.001196
Well 4	1900.5	4.5	100.8	16.8	84	422.33333	199.33	0.002289
Well 5	950.5	2.95	126.6	43.2	81	322.20339	169.65	0.001551
Well 6	1167	6.5	122.4	36.1	86	179.53846	82.142	0.000777
Well 7	583.3	1.14	123.1	65.5	58	511.66667	245.31	0.002306
Well 8	1167	2.35	113.1	37.3	78	496.59574	235.74	0.002412
Well 9	1167	2.83	135.8	43.2	92	412.36749	152.81	0.001302
Well 10	655	3.172	120.3	36.1	84	206.49433	154.73	0.001489
Well 11	1090	0.12	79.4	6.54	72.5	9083.3333	42601	0.620991

Reef Table No. (10), well test data and Pumping Test for Reniea area.

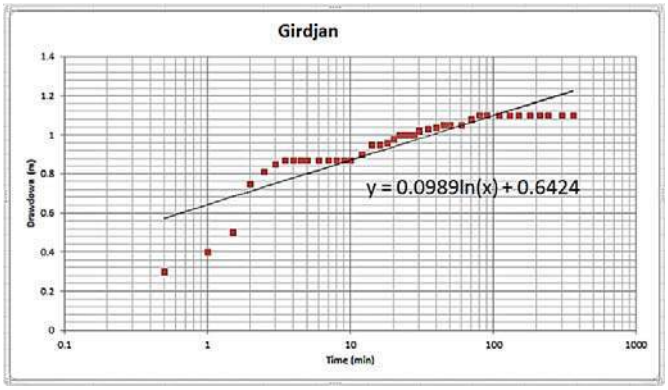

Fig (2).Time-Drawdown Graph for Well 1

4. CONCLUSION

- Renia town has an urban population about 65,010 and it is estimated to increase approximately 117,500, based on water demand criteria .The water demand in the year 2005 was 28,100 m^3/d is projected to increase 50800 m^3/d by the year 2005.

- For sub district centers (Batwata, Hejiawa and Chwerqurna) ,The water demand in the year 2005 was 34,470m^3/d is projected to increase 62,250 $m^3/d$by the year 2025

- Total amount of water for (Renia,Batwata, Hejiawa and Chwerqurna)in the year 2005 was 22.5252$M.m^3$, total amount of water for center and district city is projected to increase 40.698 $M.m^3$ by the year 2025v

- Net Irrigation Water Requirements for the crops will be approximately 58.5 $M.m^3$. The volume of water from (Dimane and Qoshan) will be 86.5 $M.m^3$. The volume of water from springs (QolaiRenia , QolaiKanimaren, and Sarochawa) will be 182 $M.m^3$,see Reef Table No. (9) and the water available of (50) wells will be approximately 2 $M.m^3$. the total amount of water from surface and ground water will be 270.5 $M.m^3$.

REFERENCES

- Parson, R. M. , 1957. Groundwater Resources of Iraq, Vol. XII: SulaimaniaLiwa and area North of Khanaquin. R.M. Parson Co., Ministry of Development, Development Board, Gov. of Iraq, 93p.

- Parsons,C.,2006. Mini Master Plan for the Public Water Supplies for the Governorate of Sulaymaniyah- Iraq .Public Works/Water Sector, Contract No. W914NS-04-C-0003, 358 P.

- Al-Kubaisi, Q.Y. , 2004. Annual Aridity Index of TYPE.1 and TYPE.2 Mode Options for Climate Classification. Iraqi journal of Science. Vol. 45 C, No.1. pp. 32-41.

- Bear: Dynamics of fluids in porous media (1972)(Classic mathematical treatment of fluid flow in soil and rock; difficult)TA357 B38

- Adams, S., Titus, R., Pietersen, K., Tredoux, G. and Harris, C., 2001. Hydrochemical Characteristics of Aquifers near Sutherland in the Western Karoo, South Africa. Journal of Hydrology 24: pp 91-103.

- American Society for Testing and Materials, 1964 Manual on industrial water and industrial waste (2nd.ed.) Philadelphia, 856 p.

EFFECT OF FILLER CONCENTRATION ON PROPERTIES OF GRAPHITE COMPOSITE BIPOLAR PLATE

[1]MOHAMMED A. M., [1]EL-NAFATY U. A., [2]BUGAJE I. M. [3]MUKTHAR B.

[1]Department of Chemical Engineering, Abubakar Tafawa Balewa University, P.M.B 0248 Bauchi, Bauchi State, Nigeria., Email: ammohd.chep@gmail.com

[1] Department of Chemical Engineering, Abubakar Tafawa Balewa University, P.M.B 0248 Bauchi, Bauchi State, Nigeria., Email: elnafaty@gmail.com

[2]National Research Institute for Chemical Technology (NARICT), P. M. B. 1052 Basawa, Zaria, Kaduna State Nigeria, Email: imbugaje@gmail.com

[3]Department of Chemical Engineering, Ahmadu Bello University, Zaria, Kaduna State, Email: belloonline@yahoo.co.uk

ABSTRACT

Fuel Cell as an alternative energy device is expensive due to high cost of production of its components. In this research, a bipolar plate, which is a component of a fuel cell, is fabricated using indigenous raw material (graphite). The plate was produced using epoxy resin as the material matrix and graphite as the filler. In order to produce bipolar plate with best characteristics, eight different formulations (55%, 60%, 65%, 70%, 75%, 80%, 85% and 90% filler concentration) were tested and the plates were produced using compression moulding at 150^{0}C and 100kN. The plates were characterized for electrical conductivity, tensile strength, and flexural strength. ASTM D3039 and D790 were used for tensile and flexural strength test respectively. Electrical conductivity was determined using Van der Pauw technique and the values were found to be 104.35 S/cm and 107.78 S/cm *in 85% and 90% filler concentration plates, which is above US-DOE target. Tensile strength and flexural strength shows varying results due to either increase in elasticity or brittleness with respect to increasing filler concentration. However, the values for tensile and flexural strength were found to be* 15.64 and 54.70MPa *respectively at 70% filler concentration's plate. This is also above the target set by US-DOE in 2012. Therefore, 70/30 wt% graphite/epoxy resin formulation was recommended as the appropriate since its plate has all the mechanical properties above the US-DOE target.*

Index Terms: *Bipolar Plate, Binder, Composite, Epoxy resin, Filler, Fuel cell, Graphite,*

1. INTRODUCTION

Bipolar plate is an important component of a fuel cell, It account for 40-50% of the cost and 60-80% of the weight of a fuel cell stack (Hermann *et al*., 2005). The bipolar plate's main functions include carrying current away from each cell, distributing gas fuels within the cell and providing support for the Membrane Electrode Assembly (Nannan *et al*., 2012). In order to perform these functions, bipolar plates must have high mechanical stiffness and strength, low electrical resistance, low density, and low thickness.

Since the performance of the fuel cell is highly dependent on the performance of the bipolar plates, the properties of the materials selected is highly critical. The United State Department of Energy proposed a technical target of bipolar plates for the year 2010 in which the main requirements are electrical conductivity >100 S/cm and flexural strength >25 MPa. There are a range of materials that have been researched and are currently being evaluated for suitability as bipolar plates (Alayavalli, 2011). This includes metals, alloys and composites. However, the most commonly used material for bipolar plates is currently graphite. Compared with metals, graphite is an excellent material for bipolar plates due to its excellent chemical resistance and low density. However, its brittle nature makes it difficult to manufacture (Nannan *et al*., 2012).

In this direction a lot of effort is going on worldwide to make light-weight and cost-effective bipolar plate for fuel cell application. In the present investigation effort was made to develop graphite-composites bipolar plate by compression moulding technique to achieve the requisite goal. The composites plates were prepared by using different reinforcing fillers such as natural graphite, synthetic graphite, carbon black, carbon fibers with phenolic resin as polymer matrix precursor in its liquid and powder form. The composition of different filler constituent adjusted in between 5 and 40 vol%. The composite plates prepared with appropriate proportion of filler components were characterized for physical and mechanical properties. It was found that no single reinforcing filler constituent composites plate has the requisite properties for being used as bipolar plate in the PEM fuel cell

2. MATERIALS AND METHOD

2.1 MATERIALS

For this research, graphite of 95.42% purity was used as the filler and epoxy-resin (EPON 828) as the material matrix. This purity falls within the acceptable range for

bipolar plate production (Mohammed, *et al*, 2014). TK-330/332 compression moulding machine was used.

2.2 COMPRESSION MOULDING

In compression moulding, graphite mixture composed of crystalline graphite powder and binders such as thermosetting vinyl resin and reinforcing fibers like carbon, glass cotton, etc. are molded at temperatures ranging from 10 ^{0}C to 150 ^{0}C with compression forces varying from 5 to 100 kN.

Compression moulding press was used to produce 21.6 cm long, 17.8 cm wide, and 3 mm thick prototype bipolar plates by Rebecca (2011). In this research, Liquid epoxy resin and graphite powder were used as matrix and filler respectively. Test specimens of dimension 10cm long, 10cm wide and 3mm thick were produced using the following procedure:

i. Graphite powder of 50μm and 95.42% purity was used as filler.

ii. Liquid epoxy resin (EPON 828) with a hardener was used as the material matrix.

iii. The graphite powder and the resins were mixed in the ratio 90% graphite and 10% resin by weight. The formulation was repeated for 85-15%, 80-20%, 75-25%, 70-30%, 65-35%, 60-40%, and 55-45% graphite-epoxy resin weight percent.

iv. A biodegradable mold release was used to coat the molds and a piece of foil paper was placed to cover the bottom of the mold.

v. The press platen temperature was set at 150^{0}C.

vi. Another piece of Foil Paper release liner was placed on the top of the composite material and the mold cover was placed on top to seal in the material.

vii. The mould was then placed between the platens in the press and the pressure button was pressed.

viii. A force of 50kN was applied and allowed to stay for 15min to pre-heat at 150^{0}C.

ix. The force was then increased to 100kN for 5mins at 150^{0}C

x. The mould was cooled using air and water only until the platen temperature reaches 25°C at 100kN.

xi. The mould was removed from the press and the moulded plate is removed from the mould.

2.3 CHARACTERIZATION OF THE PLATE

After successful fabrication of the bipolar plate, the sample was characterized in order to measure some parameters. The following parameters were considered:

i. Electrical conductivity

The electrical conductivity of the composite plate is measured using Van der Pauw Four Point Probe technique. The Van der Pauw technique, due to its convenience, is widely used in the semiconductor industry to determine the resistivity of uniform samples. As originally devised by Van der Pauw, one uses an arbitrarily shape, thin-plate sample containing four very small ohmic contacts placed on the periphery, preferably in the corners, of the plate. A schematic of a rectangular Van der Pauw configuration is shown in Figure 1. The resistance RA and RB are related to the sheet resistance RS through the Van der Pauw equation (equation 1).

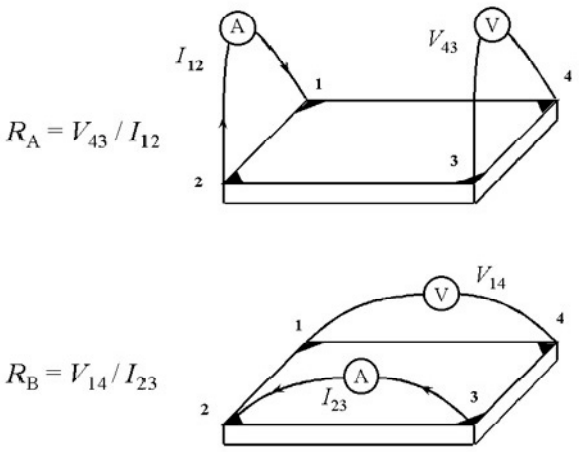

Figure 1: Schematic of a Van der Pauw configuration used in the determination of the two characteristic resistances R_A and R_B (Parker *et al*,, 2012).

The conductivity was then measured through resistivity measurement. The resistivity measurement is done via the follows steps:

1. Four point probe technique.
2. Solving Vander Pauw equation (equation 1) for surface resistance
3. The resistivity is then calculated using Ohms law: (Büchi et al., 2000)

$$exp\left(-\frac{\pi RA}{RS}\right) + exp\left(-\frac{\pi RB}{RS}\right) = 1 \qquad \ldots 1$$

$$\rho = R_S(A/d) \qquad \ldots 2$$

Where,

$\rho = Resistivity\ (ohms * cm)$

$R_S = Surface\ Resistance\ (ohms)$

$A = Sample\ Area\ (cm^2)$

$d = sample\ diametyer\ (cm)$

ii. Tensile strength

Mechanical testing, like tensile strength, plays an important role in evaluating fundamental properties of engineering materials as well as in developing new

materials and in controlling the quality of materials for use in design and construction. If a material is to be used under tension, it is important to know that the material is strong enough and rigid enough to withstand the loads that it will experience in service.

ASTM D3039 was selected to test the bipolar plate. The test specimens were machined to a dumbbell shape, as represented in figure 8, for the tensile test where they are griped in a Hounsfield Tensometer and a load is applied to extent the material. At the point of failure the load was recorded as the maximum load the material can withstand.

Hounsfield Tensometer was used to determine the tensile strength. The equipment set up is as shown in Figure 9. The Tensile strength is calculated using the formula:

$$\delta_T = \frac{F}{bd} \quad ..3$$

Where;

$$\delta_T = Tensile\ strength\ (N|mm^2)$$
$$F = Load\ (force) at\ fracture\ point\ (N)$$
$$b = with\ of\ the\ test\ specimen\ (mm)$$
$$d = Thickness\ of\ the\ test\ specimen\ (mm)$$
$$\delta_{av} = Average\ Tensile\ strength\ (N|mm^2)$$

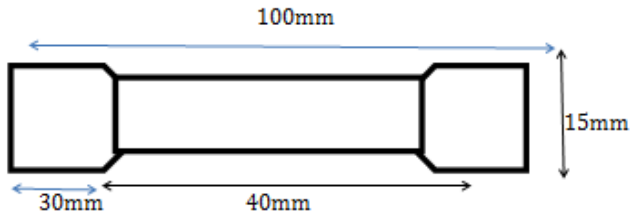

Figure -2: Dumbbell shape for measuring tensile strength

iii. Flexural strength

Flexural strength, also known as modulus of rupture, bend strength, or fracture strength, a mechanical parameter for brittle material, is defined as a material's ability to resist deformation under load. The transverse bending test is most frequently employed, in which a specimen having either a circular or rectangular cross-section is bent until fracture or yielding using a three point flexural test technique. The flexural strength represents the highest stress experienced within the material at its moment of rupture. It is measured in terms of stress, here given the symbol **δ**.

Test specimens were cut into rectangular shape of dimension 100mmx20mm. Each formulation has three specimens, for this test, making a total of 24 test specimens. Three point loading technique was used to determine the flexural strength of each specimen. ASTM D790, which is often used for composite was selected to test the bipolar plate. The resulting stress for a rectangular sample under a load in a three-point bending setup is given by equation 4 and the set up is as shown in Figure 3.

$$\delta_f = \frac{3FL}{2bd^2} \quad ... 4$$

Where;

$$\delta_f = Flexural\ Strength\ (N|mm^2)$$
$$F = Load\ (force) at\ the\ fracture\ poin(N)$$
$$L = Length\ of\ the\ support\ span\ (mm)$$
$$b = width\ of\ the\ test\ speciment\ (mm)$$
$$d = Thickness\ of\ the\ test\ speciment\ (mm)$$
$$\delta_{av} = Average\ Flexural\ Strength\ (N|mm^2)$$

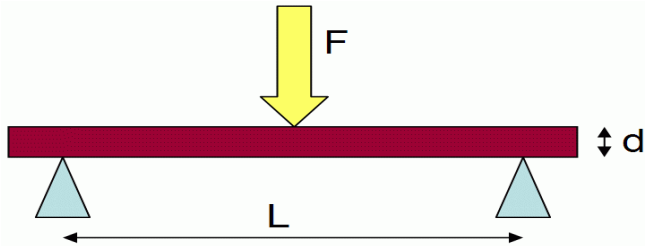

Figure -3: Three Point Loading Technique for Flexural Strength test

3. RESULTS AND DISCUSSION

3.1 ELECTRICAL CONDUCTIVITY

After measuring the resistance R_A and R_B, results were obtained for all the 8 graphite-Epoxy formulation as shown in Table 1. Resistance Rs was calculated by solving equation 1 numerically using Excel spread sheet for the iteration. The values for Rs, resistivity (ρ), and conductivity (δ), for 90% filler loading, are shown in Table 2. Other results are shown in the appendix. Plot of conductivity versus filler concentration of the plates was also represented in Figure 4. The calculation was done using Microsoft Excel spread sheet and the results obtained show that the conductivity increases with the increasing filler concentration. Plates of 85% and 90% filler concentration have a conductivity of 104.35 S/cm and 107.78 S/cm respectively. These results were above the US-DOE target of 100 S/cm. Shane and his co-workers in 2005 (Mercuri, 2005) said that the conductivity can be improve to meet the target when graphite used is greater than 60%. Thus, to improve the conductivity of graphite based composite plate, highly conducting multi-wall nanotubes (MWNTs) in different vol.% are incorporated. Dhakate and co-workers discovered that initially, in-plane conductivity without MWNTs of bipolar plate is 80 S/cm. On addition of 0.5 vol. % MWNTs in composite, the electrical conductivity of nanocomposite suddenly increases from 80 to 165 S/cm. With increasing MWNTs content up to 1.0 vol.%, conductivity increases up to 178 S/cm. But, on further increasing the MWNTs content up to 2 vol.%, the electrical conductivity decreases up to 145 S/cm,

although the value is much higher than that of the graphite-polymer composite (Dhakate *et al,* 2010).

Table 1: Vander Pauw surface resistance

	55%	*60%*	*65%*	*70%*	*75%*	*80%*	*85%*	*90%*
R_A (Ω)	*0.01125*	*0.008438*	*0.008519*	*0.00944*	*0.01969*	*0.00612*	*0.00603*	*0.00553*
R_B (Ω)	*0.0112*	*0.013226*	*0.010323*	*0.008378*	*0.006538*	*0.0075*	*0.007222*	*0.007368*
R_S (Ω)	*0.050812*	*0.048265*	*0.042525*	*0.040346*	*0.039004*	*0.03084*	*0.029948*	*0.028994*
ρ (Ω.cm)	0.020833	0.018341	0.013608	0.012507	0.013261	0.010795	0.009583	0.009278
δ (S/cm)	48.00072	54.52379	73.48561	79.95273	75.40632	92.63507	104.3487	107.7813

Table 2: Conductivity parameters for 90% filler concentration plate

90% , d = 3.3mm

Va (mΩ)	Ia (A)	Vb (mΩ)	Ib (A)	Ra (Ω)	Rb (Ω)	Rs (Ω)	F_R	ρ (Ω.cm)	δ (S/cm)
4.2	0.76	5.6	0.76	0.0055263	0.007368421	0.028994	0.00048	0.009278	107.7813

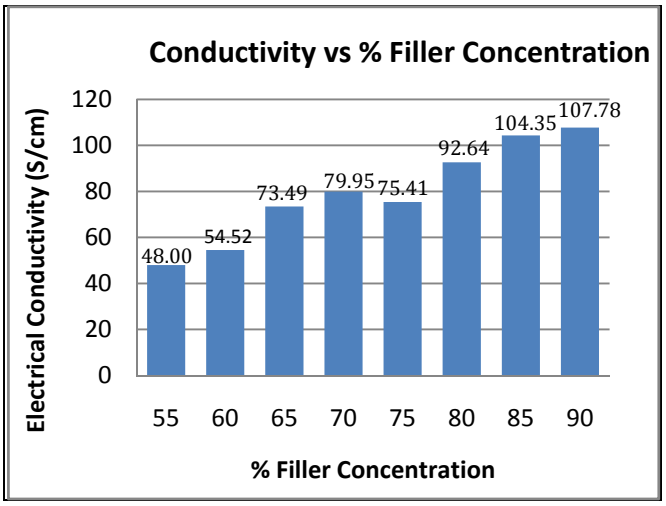

Figure 4: Electrical Conductivity Vs Filler concentration

3.2 TENSILE STRENGTH TEST

The dumbbell shaped test specimen was subjected to a load until it breaks and the results were recorded at that point. Table 4 shows one of the tensile test results and the rest are in appendix E. The Tensile strength is calculated using equation 3 and the results are represented by the chat in Figure 5.

Hounsfield Tensometer was used to determine the tensile strength of the plates. The results obtained shows that the plates with 65% 70% and 75% filler concentration have better tensile strength of 15.23, 15.64 and 14.35MPa respectively. These values are also above the US-DOE target of 15MPa. The strength decreases as the percentage filler concentration increases as shown in Figure 5. This is because the plate becomes more brittle with increasing graphite concentrations.

However, the 55% and 60% plates also show a decreasing Tensile strength. This is because the plates became more elastic as the percentage of epoxy resin increases; therefore, the plates experienced higher elongations before failing at lower loads. Table 3 shows the tensile strength results for a filler formulation containing 70 wt% graphite and 30 wt% epoxy resin. The same was done for the remaining seven formulations and was represented in appendix B. The tensile results shown are of the three samples from each formulation. The average value and standard deviation were calculated as displayed in Table 3.

Table 3: Tensile strength parameters for 65% and 70% plates

65% graphite filler			70% graphite filler		
	spec5	spec6		spec9	spec10
b (mm)	9.1	9.1	b (mm)	9.2	9.5
d (mm)	3.2	3.3	d (mm)	3.1	3.2
F (N)	480	420	F (N)	425	498
e (mm)	2.6	2.6	e (mm)	2.6	2.9
δ	16.4835	13.9860	δ	14.9018	16.3816
δav	15.23		δav	15.64	

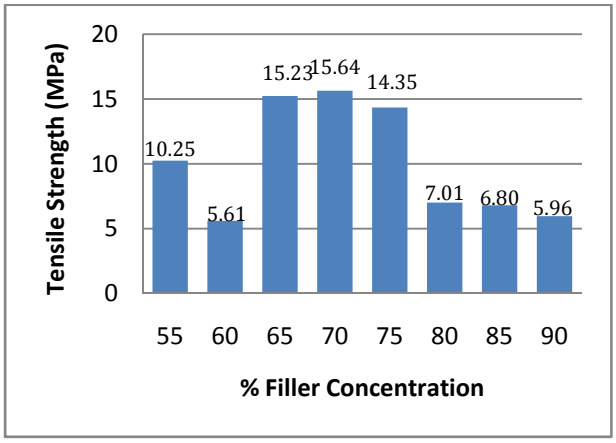

Figure 5: Tensile Strength vs % Filler concentration

3.3 FLEXURAL STRENGTH

The average of the three results was used for each formulation. Standard deviation of the three results was as shown in the appendix. The resulting stress for a rectangular sample under a load in a three-point bending setup gives the results presented in Table 4. Other results of the tensile test are shown in appendix F.

Equation 4 was used to calculate the resulting flexural strength and the results are displayed in Figure 6. The flexural strength was evaluated using three points loading techniques and the results obtained shows that the 65% and 70% plates has values (49.89 and 54.70MPa) equivalent and above US DOE respectively as represented in Table 4. This is because of the same reason as, in tensile strength, above. The flexural strength is decreasing with increasing graphite concentration (Mathur *et al* 2008) with some deviation in the 55% and 60% plates which have low flexural strength but with higher bending elongations because of their elastic properties as shown in Table 5. This is because as the filler concentration increases the material become more brittle and hence experience decrease in mechanical strength. The values obtained, however, are greater than 45MPa obtained by Mathur and co-workers in 2008 and less than 60MPa by Dhakate and co-workers in 2007 which is obtained from three fillers. Therefore, it is obvious that the flexural strength can go higher than the target if more than one filler is used.

Table 4: Flexural Strength Parameters for 70% Filler Concentration

70% graphite filler			
	spec13	spec14	spec15
b (mm)	19	21.5	20
d (mm)	3.1	3.2	3.1
F (N)	107	101	97
e (mm)	2.9	3	3.6
δf (Mpa)	62.0587	48.5824	53.4459
δav (Mpa)		54.6957	
std dev		6.8245	

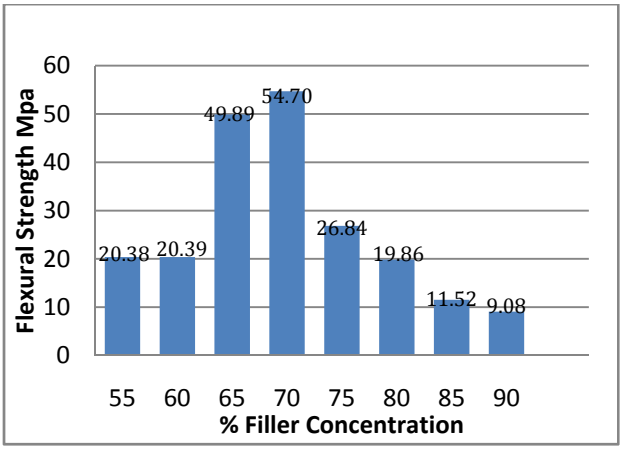

Figure 6: Flexural strength result

4. CONCLUSIONS

Graphite bipolar plates were successfully fabricated and tested to ascertain different performance characteristics. The process of compression moulding simplifies the difficulties of bipolar plate development and manufacturing. The difference in filler concentration shows varying properties and characteristics within the plates. Electrical conductivity keeps on increasing as the percentage filler increases. This is because graphite is a conductor of electricity and the higher the percentage of graphite in the plate the more conductive the plate becomes. The plate has low tensile strength but high elasticity, due to high resin content in 55% and 60% graphite concentration. This improves at 65% and 70% but start decreasing from 75% to 90% due to high graphite content which made the material more brittle. Similar pattern, as in tensile strength, was exhibited for flexural strength. From the results obtained it was recommended that 70/30 wt% graphite/epoxy resin formulation was appropriate since it has both mechanical properties (Tensile and Flexural) above the US-DOE target. Moreover, the flow field inscription on the mould makes the production of the plate easier without any further machining.

REFERENCES

[1]. Alayavalli K. C. (2011): Design, Fabrication and Testing of graphite bipolar plates for Direct Methanol Fuel Cells by Inderect Laser Sintering, PhD Dissertation. University of Texas, Austin USA.

[2]. Büchi, F. N., Marmy, C. A., Panozzo, R., Scherer, G. G., Haas, O., (2000). *PSI Scientific Report 1999,* pp. 92-93.

[3]. Dhakate S.R., Mathur R.B., Kakati B. K., and Dhami T.L (2007). Properties of graphite-composite bipolar plate prepared by compression molding technique for PEM fuel cell. *International Journal of Hydrogen Energy; 32(17),* pp. 4537-4543

[4]. Dhakate S.R., Sharma S., Chauhan N., Seith R. K. Mathur R.B.(2010). CNTs nanostructuring effect on the properties of graphite composite bipolar plate**.** *International Journal of Hydrogen Energy; 35(9),* pp. 4195-4200.

[5]. Hermann A., Chaudhuri T., Spagno P., (2005): "Bipolar plate for PEM fuel cell". *Journal of Hydrogen Energy. Vol. 30,* pp. 1297

[6]. Marthur R. B., Dhakate S. R., Gupta D. K., Dhalmi T. L., Aggarwal R. K. (2008):Effect of different carbon fillers on the properties of graphite composite bipolar plate; *Journal material processing technology, vol. 203,* pp. 184-192

[7]. Mercuri, R. A. (2005). Assembling bipolar plates, Google Patents.

[8]. Mohammed A. M., El-Nafaty U. A., and Bugaje I. M. (2014) Characterization of Graphite from Sama-Borkono Area of Bauchi State – Nigeria. *International Journal of Recent Development in Engineering and Technology. Vol 3 (2); pp 157-162*

[9]. Nannan G., Ming C. L. (2012): Experimental study of PEMFC using graphite composite bipolar plate fabricated by selective laser sintering. Missouri University of science and technology, Rolla, MO 65409, USA

[10]. Parker, M., Pokalativ, A., Raba, K., and Kübarsepp, T. (2012). Accurate measurements of electrical conductivity of metals. 8th international DAAM Baltic conference, Tallinn, Estonia.

[11] Rebecca, A. H. (2008). "Synergistic Effects and Modeling of Thermally Conductive Resins for Fuel Cell Bipolar Plate Applications". Ph.D. dissertation, Chemical Engineering Department, Michigan Technological University, USA**.**

APPENDIX A: Electrical Conductivity Parameters and Calculations

Electrical Conductivity Calculations:

$$F_R = exp\left(-\frac{\pi RA}{RS}\right) + exp\left(-\frac{\pi RB}{RS}\right) - 1 = 0$$

Table A1: Conductivity parameters for 55% filler Concentration Plate

55%, d = 4.1mm

Va (mΩ)	Ia (A)	Vb (mΩ)	Ib (A)	Ra (Ω)	Rb (Ω)	Rs (Ω)	F_R	ρ (Ω.cm)	δ (S/cm)
3.6	0.32	2.8	0.25	0.01125	0.0112	0.050812	0.00086	0.020833	48.00072

Table A2: Conductivity parameters for 60% filler Concentration Plate

60%, d = 3.8mm

Va (mΩ)	Ia (A)	Vb (mΩ)	Ib (A)	Ra (Ω)	Rb (Ω)	Rs (Ω)	F_R	ρ (Ω.cm)	δ (S/cm)
2.7	0.32	4.1	0.31	0.008438	0.013226	0.048265	0.0002	0.018341	54.52379

Table A3: Conductivity parameters for 65% filler Concentration Plate

65% , d = 3.2mm

Va (mΩ)	Ia (A)	Vb (mΩ)	Ib (A)	Ra (Ω)	Rb (Ω)	Rs (Ω)	F_R	ρ (Ω.cm)	δ (S/cm)
4.6	0.54	6.4	0.62	0.008519	0.010323	0.042525	0.00058	0.013608	73.48561

Table A4: Conductivity parameters for 70% filler Concentration Plate

70%, d = 3.1mm

Va (mΩ)	Ia (A)	Vb (mΩ)	Ib (A)	Ra (Ω)	Rb (Ω)	Rs (Ω)	F_R	ρ (Ω.cm)	δ (S/cm)
6.7	0.71	6.2	0.74	0.009437	0.008378	0.040346	0.000409	0.012507	79.95273

Table A5: Conductivity parameters for 75% filler Concentration Plate

75% , d = 3.1mm

Va (mΩ)	Ia (A)	Vb (mΩ)	Ib (A)	Ra (Ω)	Rb (Ω)	Rs (Ω)	F_R	ρ (Ω.cm)	δ (S/cm)
6.3	0.32	3.4	0.52	0.0196875	0.006538462	0.039004	0.20461	0.013261	75.40632

Table A6: Conductivity parameters for 80% filler Concentration Plate

				80% , **d =3.5mm**					
Va (mΩ)	Ia (A)	Vb (mΩ)	Ib (A)	Ra (Ω)	Rb (Ω)	Rs (Ω)	F_R	ρ (Ω.cm)	δ (S/cm)
4.1	0.67	4.6	6.1	0.0061194	0.0075	0.03084	5.87E-05	0.010795	92.63507

Table A7: Conductivity parameters for 85% filler Concentration Plate

				85%, d = 3.2mm					
Va (mΩ)	Ia (A)	Vb (mΩ)	Ib (A)	Ra (Ω)	Rb (Ω)	Rs (Ω)	F_R	ρ (Ω.cm)	δ (S/cm)
4.1	0.68	5.2	0.72	0.0060294	0.007222222	0.029948	3.65E-05	0.009583	104.3487

APPENDIX B: Tensile Strength Parameters and Calculations

Tensile Strength Calculations:

$$\delta_T = \frac{F}{bd} \qquad ..3$$

Table B1: Tensile Strength Parameters for 55% and 60% Filler Concentration Plate

55% graphite filler			**60% graphite filler**		
	spec 1	spec2		spec 3	spec4
b (mm)	9.8	9.5	b (mm)	9.3	9.2
d (mm)	4.2	4.5	d (mm)	3.8	3.7
F (N)	312	552	F (N)	132	255
e (mm)	2	4.2	e (mm)	1.6	2.7
δ	7.580175	12.91228	δ	3.735144	7.491187
δav	10.25		δav	5.61	

Table B2: Tensile Strength Parameters for 75% and 80% Filler Concentration Plate

75% graphite filler			**80% graphite filler**		
	spec7	spec8		spec11	spec12
b (mm)	9.2	9.2	b (mm)	9.5	9.6
d (mm)	3.4	3.5	d (mm)	3.3	3.5
F (N)	420	492	F (N)	220	235
e (mm)	2.6	2.9	e (mm)	2	1.7
δ	13.42711	15.2795	δ	7.017544	6.994048
δav	14.35		δav	7.01	

Table B3: Tensile Strength Parameters for 85% and 90% Filler Concentration Plate

85% graphite filler			**90% graphite filler**		
	spec7	spec8		spec11	spec12
b (mm)	9	9	b (mm)	9	9.2
d (mm)	3.5	3.1	d (mm)	3	3.2
F (N)	198	204	F (N)	175	160
e (mm)	3.7	4.8	e (mm)	2	1.7
δ	6.285714286	7.311828	δ	6.481481	5.434783

δav	6.80	δav	5.958132045

APPENDIX C: Flexural Strength Parameters and calculations

Flexural Strength Calculations:

$$\delta_f = \frac{3FL}{2bd^2} \qquad ..4$$

Table C1: Tensile Strength Parameters for 85% and 90% Filler Concentration Plate

55% graphite filler			
	spec1	spec2	spec3
b (mm)	19	21	19
d (mm)	4.2	4.5	3.8
F (N)	87	84	33
e (mm)	2	2.2	1.4
δf (Mpa)	27.4893	20.9185	12.7376
δav (Mpa)		20.38180712	
std dev		7.390438405	

Table C2: Flexural Strength Parameters for 60% Filler Concentration

60% graphite filler			
	spec4	spec5	spec6
b (mm)	18.8	19	21.2
d (mm)	3.8	3.7	4
F (N)	65	45	56
e (mm)	2.2	4.2	5.4
δf (Mpa)	25.3562	18.3211	17.4835
δav (Mpa)		20.3869	
std dev.		4.32384	

Table C3: Flexural Strength Parameters for 65% Filler Concentration

65% graphite filler			
	spec7	spec8	spec9
b (mm)	20	19.4	22.8
d (mm)	3	3.2	3.3
F (N)	96	102	91
e (mm)	1.3	1.5	1.4
δf (Mpa)	56.48	54.3744	38.81277
δav (Mpa)		49.88905493	
std dev		9.649947008	

Table C4: Flexural Strength Parameters for 75% Filler Concentration

75% graphite filler			
	spec10	spec11	spec12
b (mm)	23	20	18.7
d (mm)	3.5	3.3	3.3
F (N)	65	48	63
e (mm)	2.4	3.6	3.2
δf (Mpa)	24.43123	23.33884	32.76174
δav (Mpa)		26.84394039	
std dev		5.153992255	

Table C5: Flexural Strength Parameters for 80% Filler Concentration

80% graphite filler			
	spec16	spec17	spec18
b (mm)	18.2	21.4	20
d (mm)	3.3	3.2	3.5

F (N)	42.5	45	35
e (mm)	3.6	1.9	2
δf (Mpa)	22.70835	21.74677	15.12857
δav (Mpa)		19.86123094	
std dev		4.126706925	

Table C6: Flexural Strength Parameters for 85% Filler Concentration

85% graphite filler			
	spec19	spec20	spec21
b (mm)	21	19	18.5
d (mm)	3.5	3.1	3
F (N)	25	21	19
e (mm)	7.2	6	6.6
δf (Mpa)	10.29155	12.17975	12.08468
δav (Mpa)		11.51865895	
std dev		1.063774104	

Table C7: Flexural Strength Parameters for 90% Filler Concentration

90% graphite filler			
	spec13	spec14	spec15
b (mm)	19	21.5	20
d (mm)	3.3	3.2	3.1
F (N)	20	17	16
e (mm)	2.9	3	3.6
δf (Mpa)	10.23633	8.177235	8.815817

δav (Mpa)	9.076462078
std dev	1.054004292

SEISMIC PERFORMANCE EVALUATION OF RC BUILDINGS WITH VERTICAL IRREGULARITIES SUBJECTED TO BIAXIAL EXCITATION

DR.MOHD.HAMRAJ[1], MOHAMMED MOIZ KHAN[2]

[1]Professor, Civil Engineering Department, Muffakham Jah College of Engineering and Technology, Telangana, India, hamraj567@gmail.com

[2]Post Graduate Student, Civil Engineering Department, Muffakham Jah College of Engineering and Technology, Telangana, India, moiz9229@gmail.com

ABSTRACT

Reinforced concrete multi-storied buildings are very complex to model as structural systems for analysis. The current version of the IS: 1893-2002 requires that practically all multistoried buildings be analyzed as three-dimensional systems. This is due to the fact that the buildings have generally irregularities in plan or elevation or in both and later that may have a detrimental influence and effectiveness on seismic performance itself. Seismic analysis is generally performed by creating a structural model which is excited with forces in two orthogonal directions separately i.e. they are subjected to uniaxial excitation. But an actual earthquake will have its effect in both the directions simultaneously (Biaxial excitation). Limited research has been carried out on effect, of such biaxial excitation on vertical irregular buildings. The study as a whole makes an effort to evaluate the effect of vertical irregularities on RC buildings subjected to biaxial excitation. The objective of this work is to carry out Nonlinear Time history Analysis (THA) of vertically irregular RC building frames.For the purpose of the work, comparative study has been done with regular shear wall to analyze the effect of vertical irregularities (irregular shear wall and soft first storey) on low-rise and high-rise symmetric buildings. The symmetry is imposed to avoid the torsional effects and enhance the irregularities in elevation.The analysis engine used for the analysis and design is ETABS version 13. In the study, base shear, story displacement and story drifts of the three structures were studied; one with irregular shear wall in elevation (Building B), the other with irregular shear wall in core of the building (Building C) and the third with soft first storey (Building D). The results obtained were compared with those obtained from the structure with regular shear wall (Building A).The earthquake demand was obtained from a time response dynamic analysis using acceleration record from the Bhuj Earthquake of January 26, 2001. The analytical results show that there is a reduction in base shear by 39% and 46% of buildings B and C respectively and the story displacement is increased by 14% and 29% respectively when they are compared with the building A. There is a lot of increase in story drift by 66% and 84% in both building B and C respectively when it is compared with building A.The Building D with soft first storey has 19% reduction in base shear when it is compared with the Building A. Also, there is large increase in story displacement and story drifts of the building by 75% and 67% respectively when compared with Building A. The results illustrated that significant effect of the vertical irregularities was observed on the storey drift, base shear, storey displacement of low rise and high rise symmetric buildings.

Index Terms: *Vertical Geometric Irregularity; Stiffness Irregularity; Biaxial Base excitation; Nonlinear Time history analysis.*

1. INTRODUCTION

During an earthquake, failure of structure starts at points of weakness. This weakness arises due to discontinuity in mass, stiffness and geometry of structure. The structures having this discontinuity are termed as Irregular structures. Irregular structures contribute a large portion of urban infrastructure.

Vertical irregularities are one of the major reasons of failures of structures during earthquakes. For example structures with soft storey were the most notable structures which collapsed. So, the effect of vertically irregularities in the seismic performance of structures becomes really important. Height-wise changes in stiffness render the dynamic characteristics of these buildings different from the regular building.

IS 1893 definition of Vertically Irregular structures: The irregularity in the building structures may be due to irregular distributions in their mass, strength and stiffness along the height of building. When such buildings are constructed in high seismic zones, the analysis and design becomes more complicated. There are two types of irregularities-

1. Plan Irregularities.

2. Vertical Irregularities.

Vertical Irregularities are mainly of five types-
a) Stiffness Irregularity — Soft Storey-A soft storey is one in which the lateral stiffness is less than 70 percent of the storey above or less than 80 percent of the average lateral stiffness of the three storeys above.

b) Stiffness Irregularity — Extreme Soft Storey-An extreme soft storey is one in which the lateral stiffness is less than 60 percent of that in the storey above or less than 70 percent of the average stiffness of the three storeys above.

ii) Mass Irregularity-Mass irregularity shall be considered to exist where the seismic weight of any storey is more than 200 percent of that of its adjacent

storeys. In case of roofs irregularity need not be considered.

iii) Vertical Geometric Irregularity- A structure is considered to be Vertical geometric irregular when the horizontal dimension of the lateral force resisting system in any storey is more than 150 percent of that in its adjacent storey.

iv) In-Plane Discontinuity in Vertical Elements Resisting Lateral Force-An in-plane offset of the lateral force resisting elements greater than the length of those elements.

v)Discontinuity in Capacity —Weak Storey-A weak storey is one in which the storey lateral strength is less than 80 percent of that in the storey above.

As per IS 1893, Part 1 Linear static analysis of structures can be used for regular structures of limited height as in this process lateral forces are calculated as per code based fundamental time period of the structure. Linear dynamic analysis are an improvement over linear static analysis, as this analysis produces the effect of the higher modes of vibration and the actual distribution of forces in the elastic range in a better way.

1.1 IMPORTANCE OF SEISMIC ANALYSIS

The prediction of the response of a structure to a particular type of loading is of utmost importance for the design of structure. Basically the codes and previous experiences provide us with a lot of information regarding the type of loads and their intensities for different types of structures and the site conditions. The analysis procedure to be adopted purely depends upon the engineers choice as per the accuracy of the work required. The nonlinear time history analysis can be regarded as the most accurate method of seismic demand prediction and performance evaluation of structures. Although, this method requires the selection of an appropriate set of ground motion, detailed site conditions and also a numerical tool to handle the analysis of the data, which is in many cases computationally expensive still it is regarded as the most detailed analysis and highly accurate analysis method.

2. OBJECTIVE AND SCOPE OF THE STUDY

The present work aims at the evaluation ofdesign lateral forces on buildings with two irregularities namely vertical geometric irregularity (irregular shear wall) and stiffness irregularity (soft first storey) subjected to biaxial excitation and to compare the results of different structures. The buildings analyzed in this work are:

1) Building A: Regular Shear Wall (Shear Wall up to top storey both in core and elevation of the building)

2) Building B: Irregular Shear Wall (Shear wall interrupted at mid story in elevation of the Building A).

3) Building C: Irregular Shear Wall (Shear Wall interrupted at mid story in core of the Building A)

4) Building D: Building having Soft First Storey.

These four types of buildings were generated in 4, 8, 12 story reinforced concrete symmetrical buildings. The structures are analyzed in accordance with seismic code IS 1893:2002 and using time history analysis in E-tabs package.

3. METHODOLOGY

The purpose of the NLTHA is to evaluate the expected performance of a structural system by estimating its strength and deformation demands in design earthquakes by means of a dynamic inelastic analysis, and comparing these demands to available structures with irregular shear wall so as to observe the increase in the response of structures of interest. The evaluation is based on an assessment of performance parameters like storey displacements, storey drift, torsional moment, base shear.The NLTHA is perhaps the only procedure which captures the realistic response of the structures when subjected to real earthquake loading.Following are the general sequence of steps involved in performing NLTHA using ETABS V13 in the present study:

1. A two or three dimensional model that represents the overall structural behavior created.
2. For reinforced concrete elements the appropriate reinforcement is provided for the cross sections.
3. Gravity loads composed of dead loads and a specified proportion of live load is assigned as seismic weight to the structure.
4. Free vibration un-damped modal analysis is performed to make note of the frequencies and time periods of the structure.
5. The time history function from a file is selected and the time history function is defined.
6. The non-linear direct integration time history load cases are defined by assigning the ground acceleration time history function as loading in X &Y direction and by assigning proportional damping NLTHA is set to run.
7. After the analysis is completed the displacement pattern of the structure is studied and drifts are calculated.
8. The other responses such as base shear and displacements are noted.

4. PARTICULARS OF BUILDINGS

The aim of the present work is to evaluate the seismic response of the structure subjected to biaxial excitation having vertical irregularities in elevation using ETABS. The layout of plan having symmetric 3X3 bays of equal length of 4m. The plan is kept same for all buildings by varying floor levels of 4, 8 and 12.The structures are subjected to seismic excitations in both X and Y directions and observed the seismic response. The BHUJ earthquake data is used as ground motion data for performing non-linear time history analysis.

Assumed preliminary data required for the analysis of the frame

1. Type of Structure: Moment Resisting Frame

2. Floor height : 3m

3. Live load : 5 kN/m²

4. Dead load : 10 kN/m²

5. Materials : M30, Fe500

6. Size of column : 450x450mm(G+4,G+8)

750x750mm (G+12)

7. Size of beams : 300 x 300 mm (G+4,G+8)

450 x 450 mm (G+12)

8. Specific weight of RCC: 25 KN/m³

9. Zone : V

10. Importance factor : 1

11. Response reduction factor : 5

12. Type of soil : Medium.

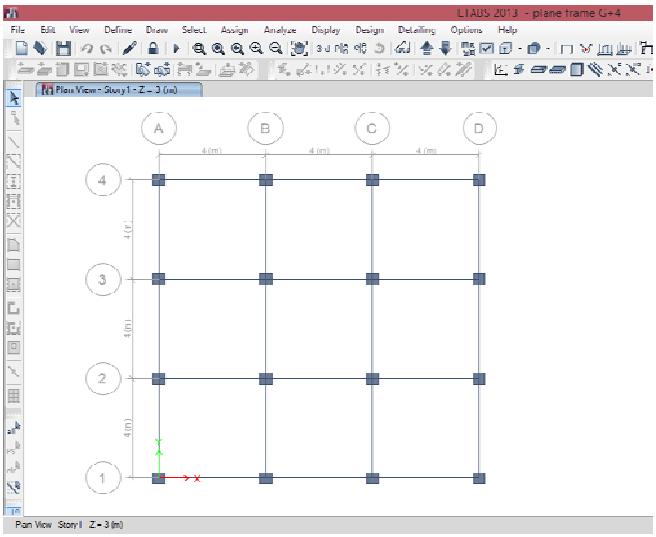

Fig 4.1 Plan view of Buildings without shear wall

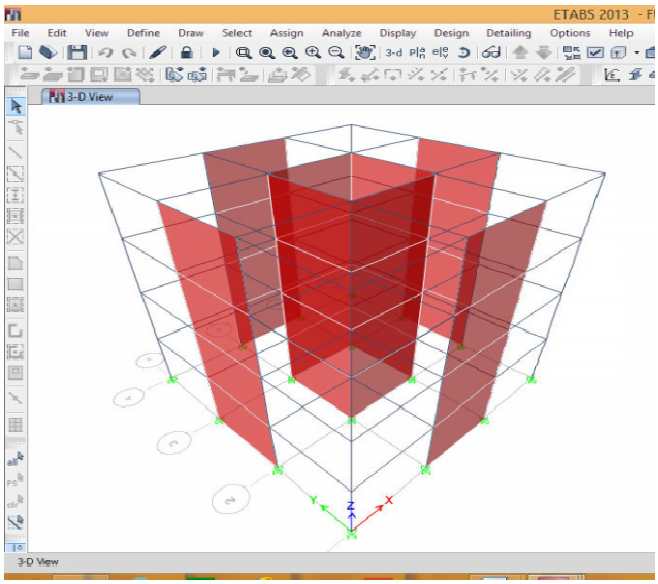

Fig 4.1.13D view of Building A

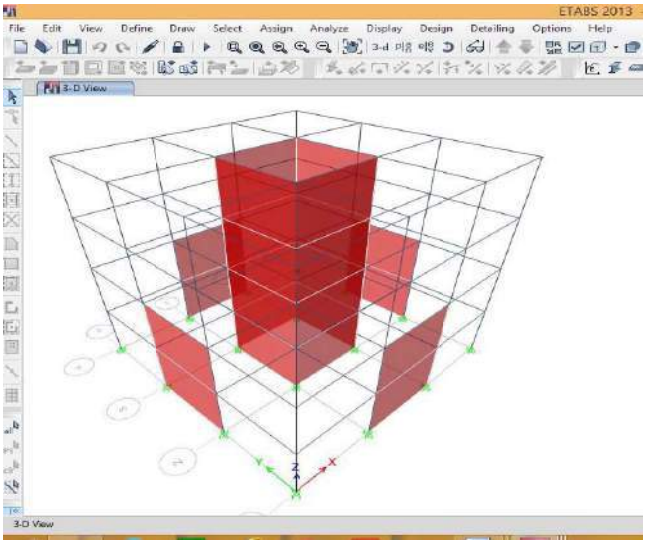

Fig 4.1.2 3D view of Building B

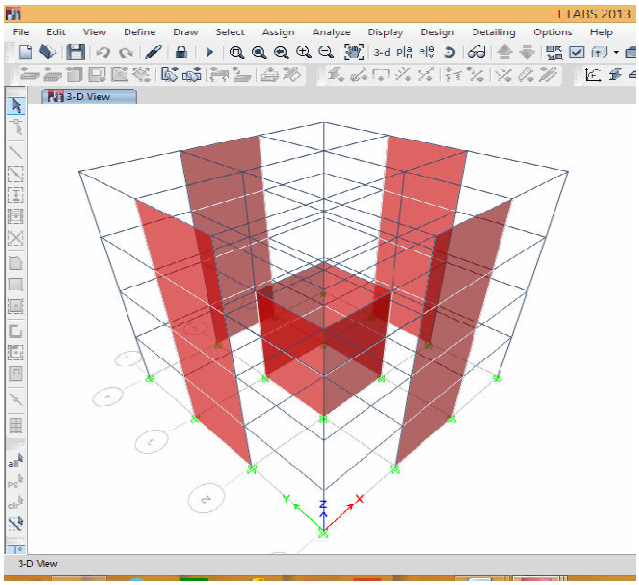

Fig 4.1.3 3D view of Building C

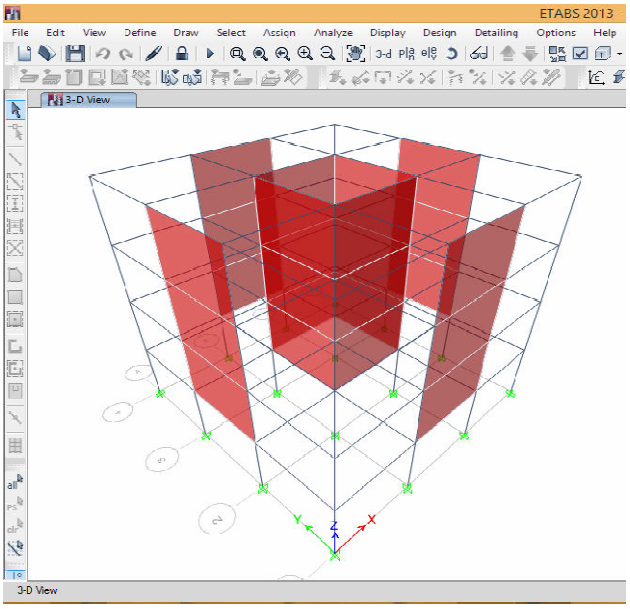

Fig 4.1.4 3D view of Building D

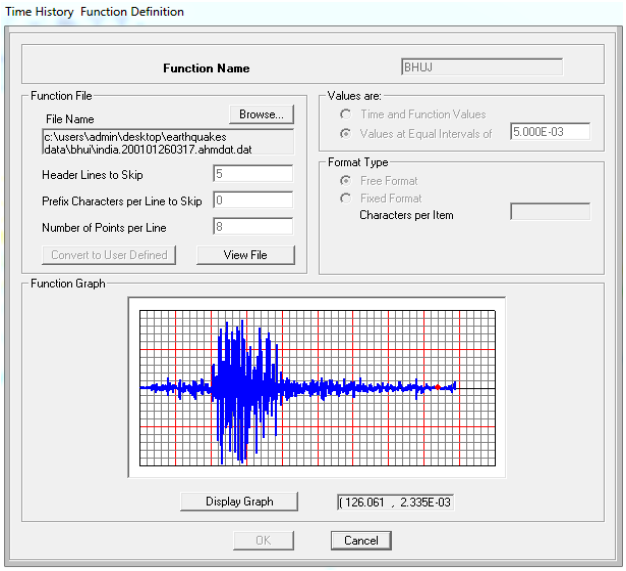

Fig 4.1.5BHUJ N-W component earthquake ground acceleration record

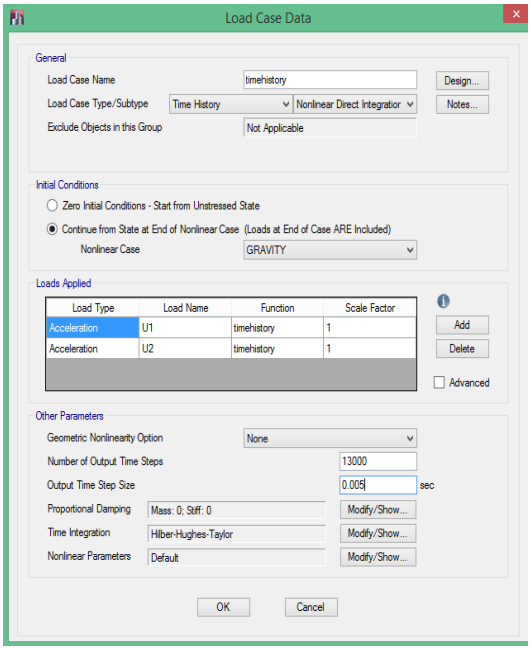

Fig 4.1.6 Illustrates the non-linear direct integration time history load case using BHUJ N-W time history function.

4.1 COMPARISON OF RESULTS OF BUILDINGS WITH VERTICAL GEOMETRIC IRREGULARITY

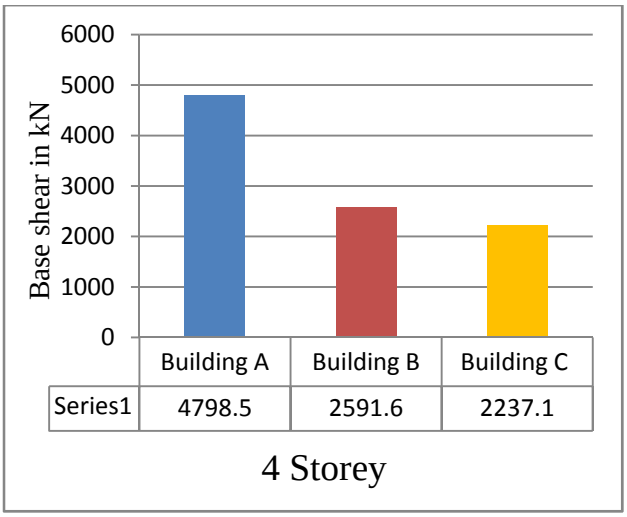

Fig 4.2 Base shear comparison of four storey symmetric buildings

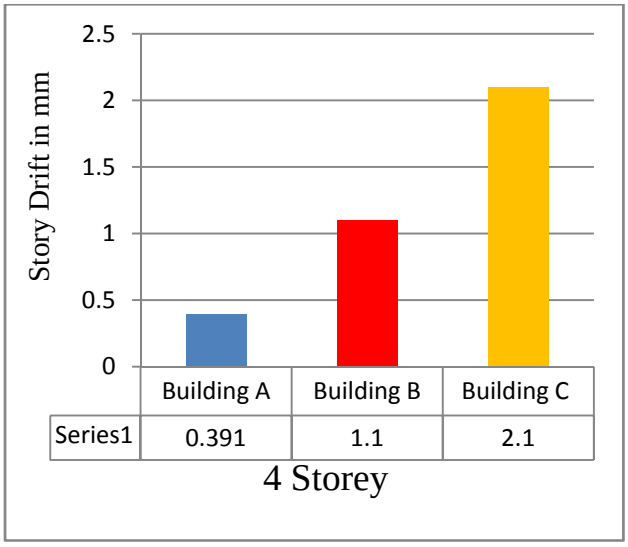

Fig 4.2.1 Story Drift comparison of four storey symmetric buildings

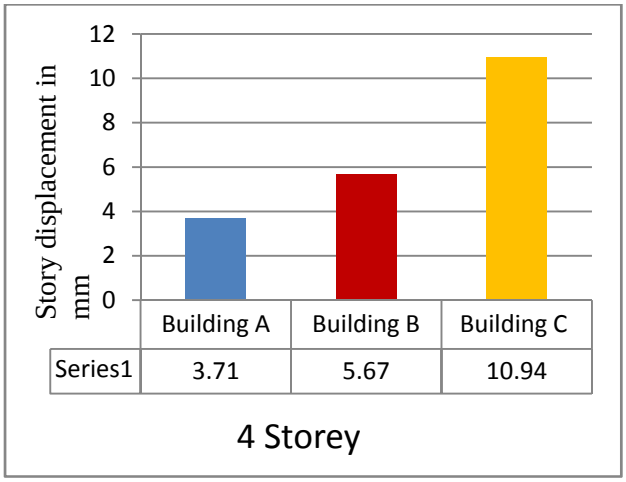

Fig 4.2.2 Story displacement comparison of four storey symmetric buildings

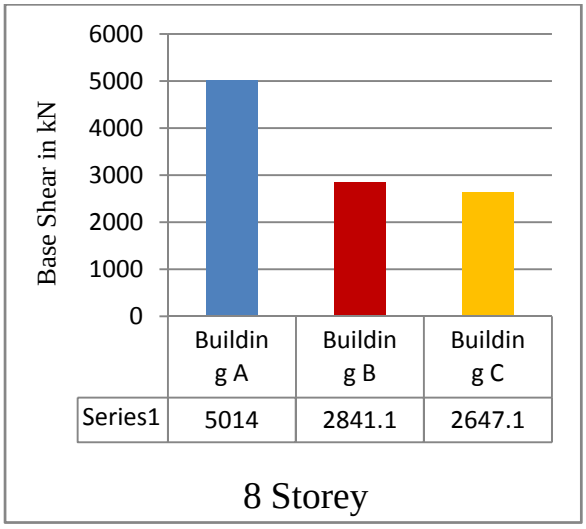

Fig 4.2.3 Base shear comparison of eight storey symmetric buildings

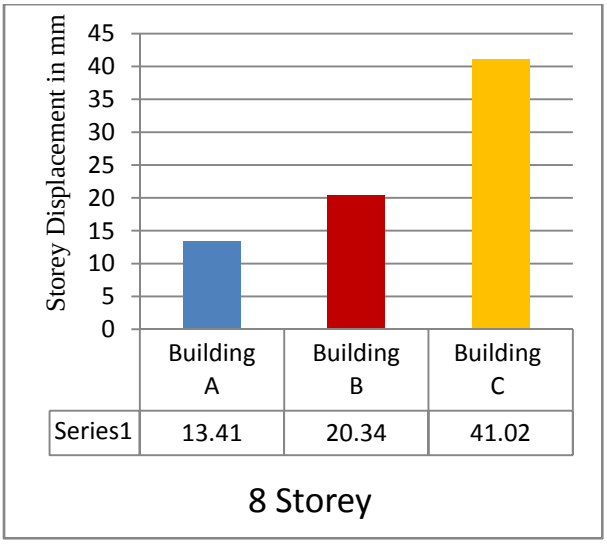

Fig 4.2.4 Story displacement comparison of eight storey symmetric buildings

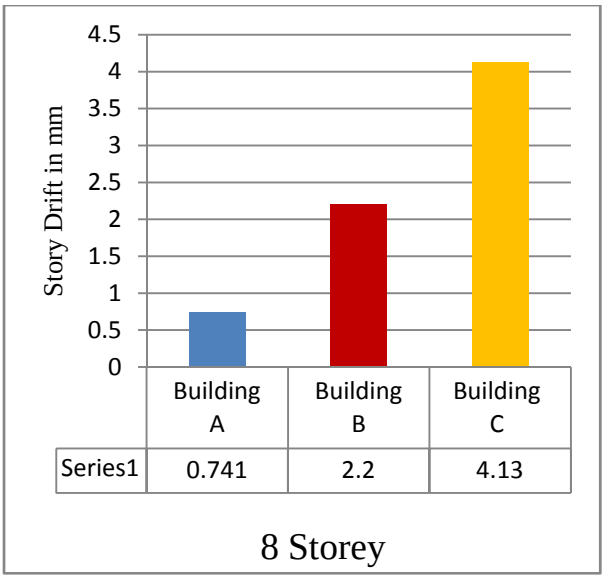

Fig 4.2.5 Story drift comparison of eight storey symmetric buildings

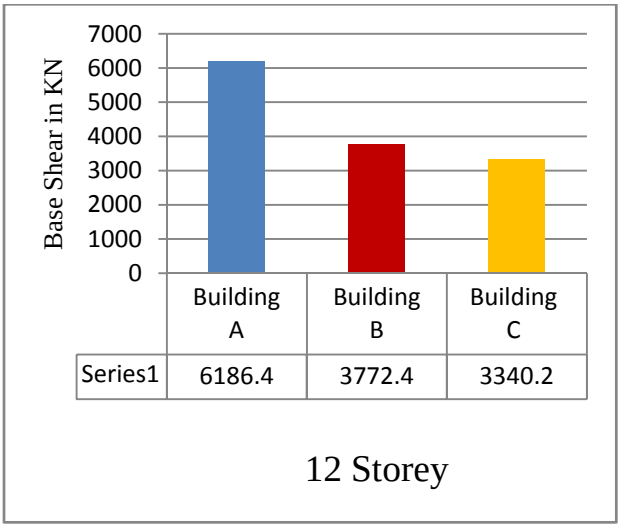

Fig 4.2.6 Base shear comparison of twelve storey symmetric buildings

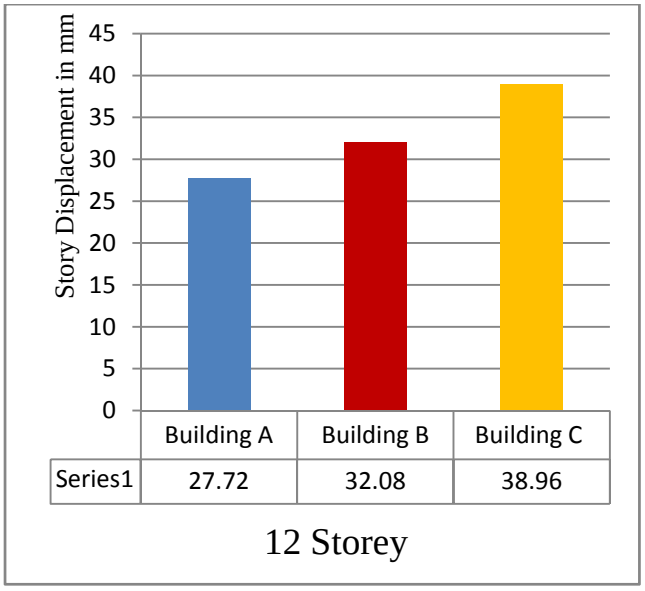

Fig 4.2.7 Story displacement comparison of twelve storey symmetric buildings

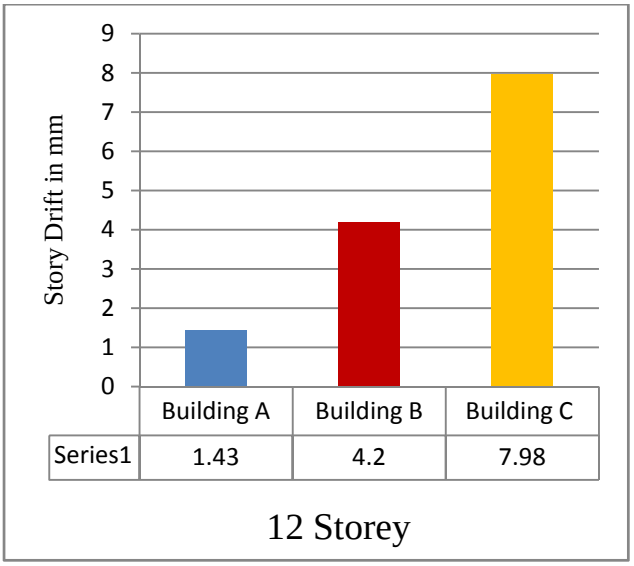

Fig 4.2.8 Story driftcomparison of twelve storey symmetric buildings

4.2 COMPARISONOF RESULTS OF BUILDINGS WITH STIFFNESS IRREGULARITY

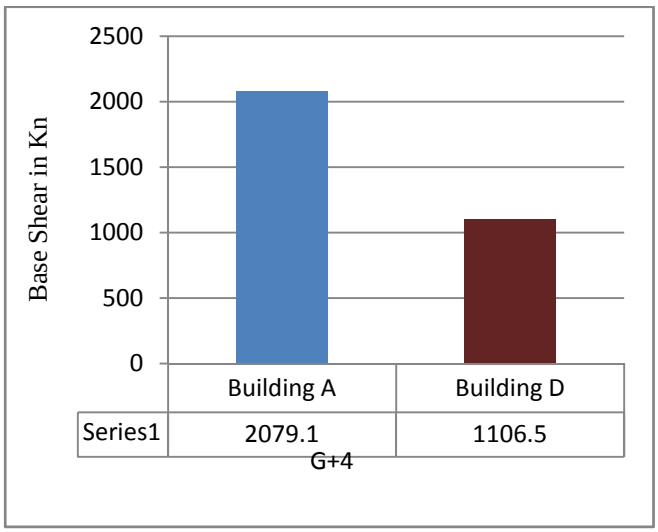

Fig 4.3 Base shear comparison of four storey symmetric buildings

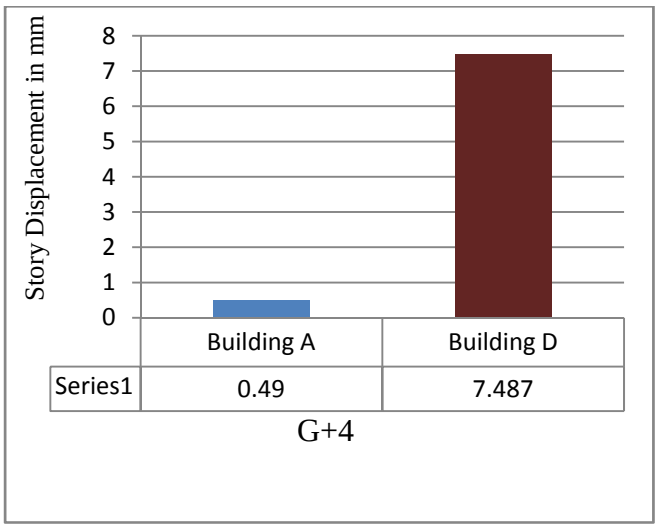

Fig 4.3.1 Story Displacement comparison of four storey symmetric buildings

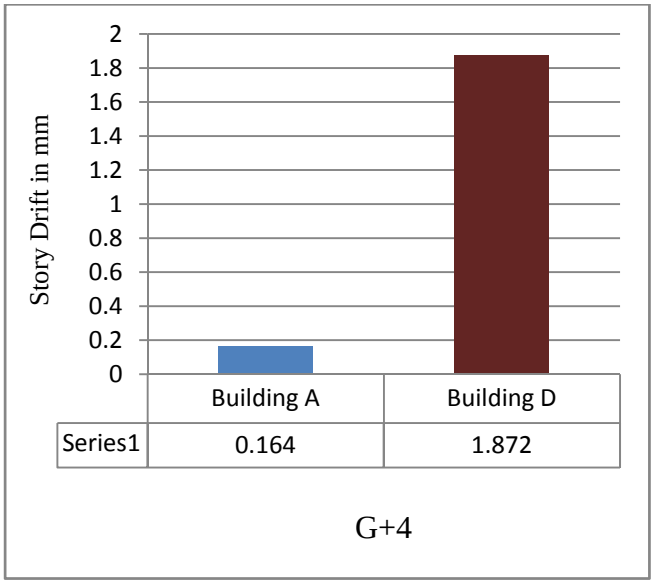

Fig 4.3.2 Story Drift comparison of four storey symmetric buildings

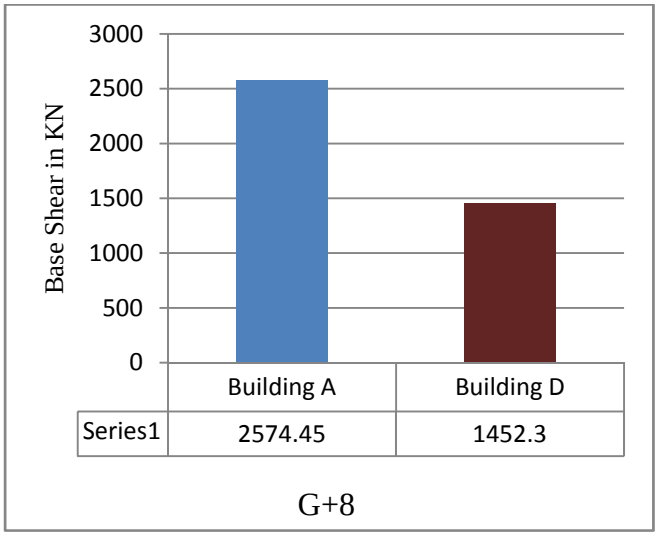

Fig 4.3.3 Base shear comparison of eight storey symmetric buildings

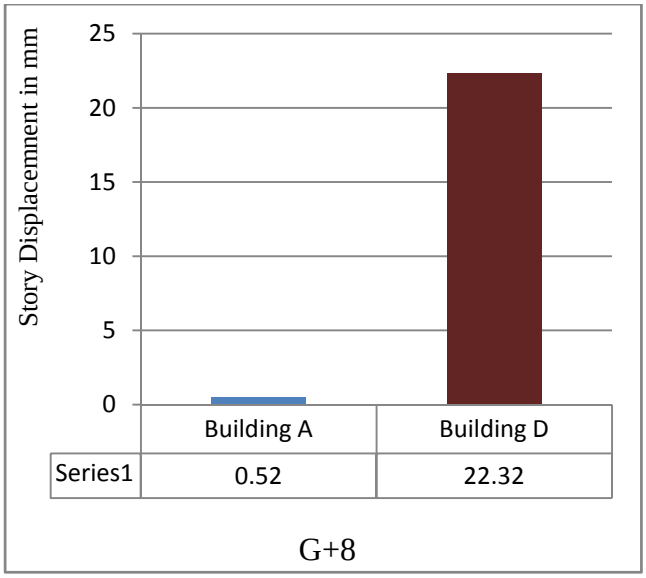

Fig 4.3.4 Story displacement comparison of eight storey symmetric buildings

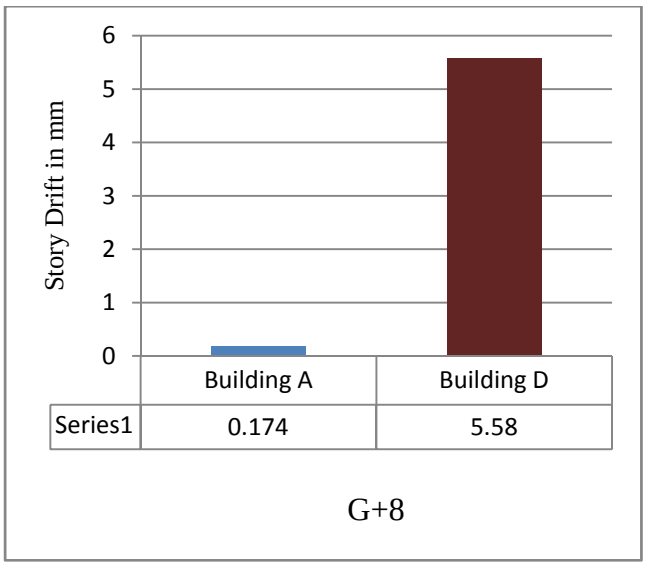

Fig 4.3.5 Story drift comparison of eight storey symmetric buildings

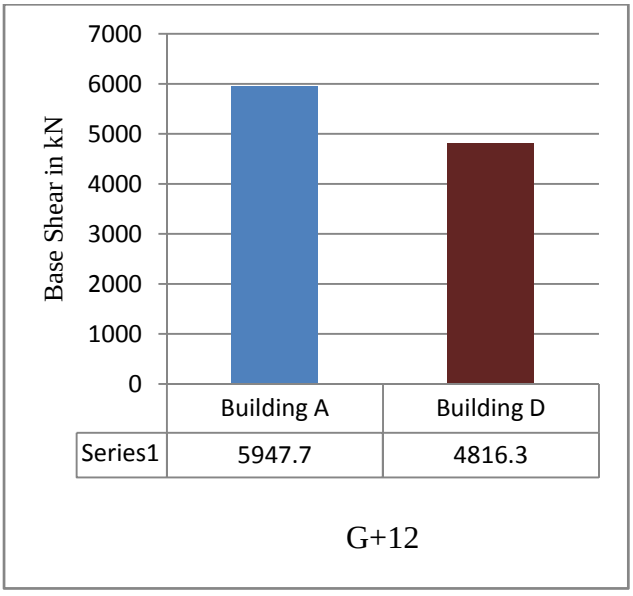

Fig 4.3.6 Base shear comparison of twelve storey symmetric buildings

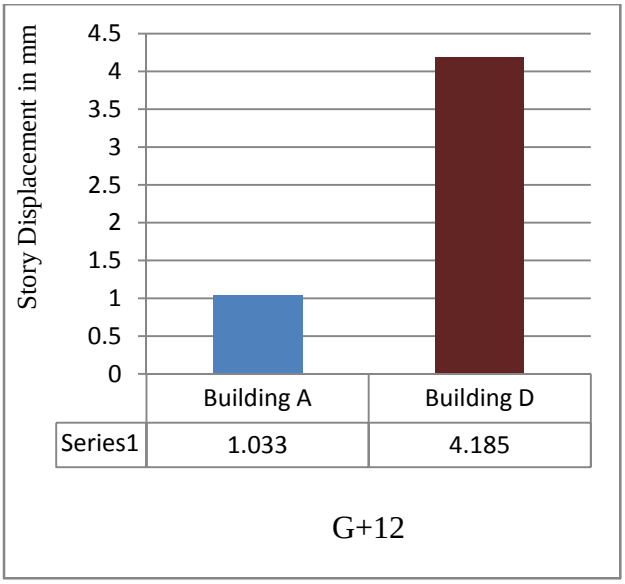

Fig 4.3.7 Story displacement comparison of twelve storey symmetric buildings

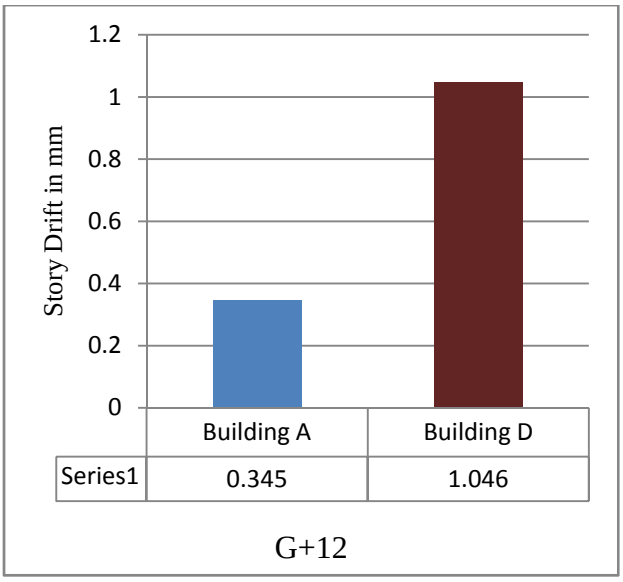

Fig 4.3.8 Story drift comparison of twelve storey symmetric buildings

5. CONCLUSIONS

In this work, the preliminary results of a large parametric study, whose aim is the performance evaluation of irregularity in elevation for frame buildings, are shown. After the numerical investigation, following conclusions can be made:

1. The Building B reduces the base shear by 46%, 43% and 39% for 4, 8 and 12 stories respectively when compared with the Building A. Whereas, the Building C reduces the base shear by 53%, 47% and 46% as storey level increases when compared with the Building A.

2. The increase in Story displacement of Building B is 35%, 34% and 14% for 4, 8 and 12 stories respectively when compared with the Building A. Whereas in case of Building C, there is an significant increase in story displacement by 66%, 67% and 29% when compared with Building A.

3. The increase in Story drift of Building B is 64%, 66% and 66% for 4, 8 and 12 stories respectively when compared with the Building A. Whereas in case of Building C, there is an significant increase in story displacement by 81%, 82% and 84% when compared with Building A.

4. Maximum story drift and story displacement will increaseas the vertical irregularities increase in models. The structural and architectural configurations should be observed keenly to attain the optimum performance of the building in terms of its seismic response.

5. When time history analysis was done for regular as well as stiffness irregular building (soft storey), it was found that displacements of upper stories did not vary much from each other but as we moved down to lower stories the absolute displacement in case of soft storey were higher compared to respective stories in regular building.

6. The Building D with soft first storey reduces the bases hearby 47%, 44% and 19% for 4 , 8 and 12 stories respectively when compared with the building A.

7. There is a large amount of increase in Story displacements at first storey of the building D by 93%, 97% and 75% for 4, 8 and 12 stories respectively when compared with the building A.

8. Also there is much increase in the story drifts of the Building D at first storey by 91%, 96% and 67% as storey level increases when compared with the Building A.

5.1 SCOPE OF FURTHER STUDY

1. Soil structure interaction has always attracted many researchers as an interesting topic for static procedures; the same can also be done for non- linear time history analysis using soil structure interaction.

2. Non-linear time history analysis could also be performed to study the effect of other types of irregularities on the structures by varying seismic zones and subjecting to biaxial excitation.

REFERENCES

1. Influence of Vertical Irregularities in the Response of Earthquake Resistant Structures by J. H. Cassis and E. Cornejo, Eleventh World Conference on Earthquake Engineering, (1996), Paper No. 1102.

2. Study of Response of Structural Irregular Building Frames to Seismic Excitations by Anil and Gupta Ashok ISSN 2249-6866 Vol.2, Issue 2 (2012) 25-31.

3. Inelastic Effects of Biaxial Excitation on Geometrically Asymmetric Plan Building with Biaxial Eccentricity by Nishant Kumar K., Rajul K. Gajjar

(2013)International Journal of Engineering and Advanced Technology (IJEAT).

4. CemalettinDonmez, "The lateral Drift of Simple Structural Systems Subjected to Biaxial Excitation"13thWorld Conference on Earthquake Engineering.

5. C. M. Ravi Kumar and et al., Seismic Performance Evaluation of RC Buildings with Vertical Irregularity. Indian Society of Earthquake Technology. 2012., Paper No. E012.

6. K. Güler, M. G. Güler, B. Taskin and M. Altan., ―Performance Evaluation of a Vertically Irregular RC Building‖. 14th World Conference on Earthquake Engineering, (2008), Beijing., China.

7. Dolce, M. and S. Simoninin (1986) the influence of structural regularity on the seismic behavior of buildings. Proc. 8th European Conference on Engineering, Portugal.
8. "Soft Story" and "Weak Story" in Earthquake Resistant Design: A Multidisciplinary Approach by L.Teresa Guevara-Perez, 15th World Conference on Earthquake Engineering, Lisboa 2012.

9. IS 1893(Part1) 2002 - Indian Standard criteria for earthquake resistant design of structures (5th revision), 2002.

BIOGRAPHIES

	**Dr.Md.Hamraj,** Professor & Coordinator (ME Structural Engg.), Civil Engineering Dept., Muffakham Jah College of Engg. & Technology, Email:hamraj567@gmail.com
	**Mohd. Moiz Khan,** Post Graduate Student, M.E. (Structures), Civil Engineering Dept., Muffakham Jah College of Engineering & Technology, Email:moiz9229@gmail.com

STUDY OF THE IODINATION OF INDOLE-3-BUTYRIC ACID BY AQUEOUS IODINE USING HYDRODYNAMIC VOLTAMMETRY

[1] RAJENDRA P.YADAV, [2] BHARAT B. BAHULE, [3] VITTHAL T. BORKAR, [4,*] VIJAY T. DANGAT, [5] KANCHAN G. SHINDE

[1,2,3,4]Department of Chemistry, Nowrosjee Wadia College, Pune 411 001, India

Email: [1]rajendra11yadav@gmail.com ; [2]bharatbahule@gmail.com ; [3]vt.borkar@gmail.com 4*vijaydangat@gmail.com; [5]shinde.kanchan20@gmail.com

ABSTRACT

The fast kinetics of the iodination of indole-3- butyric acid (3-IBA) in aqueous medium by molecular iodine at 7 pH has been studied using hydrodynamic voltammetry in the present study. The reaction is very rapid and this special technique has been employed in these investigations. The reaction is found to be of the second order and the specific reaction rate has been evaluated as 590 M^{-1} s^{-1} at 22.0 ^{0}C. The frequency factor, energy of activation and entropy change in the reaction are evaluated as 3.48 x 10 ^{9} $M^{-1}s^{-1}$, 38.3 kJ $mole^{-1}$ and –243.1 J mol^{-1} K^{-1}respectively. These thermodynamic data are used to elucidate the reactivity of the heterocycle under study on a quantitative scaffold in terms of the steric compulsions in the reaction dynamics. The heterocycle chosen for this study has pharmacodynamic significance as it is a component of the precursors of several biologically important drug molecules.

Keywords: *Hydrodynamic voltammetry, Indole-3- butyric acid, Molecular iodine.*

1. INTRODUCTION

Iodinations of aromatic substrates are known to be electrophilic substitution reactions [1]. These are rapid reactions in aqueous medium devoid of iodide ions, due to the lack of formation of the nucleophile I_3^- in these reactions [2]. Iodo derivatives of aromatic substrates are known to have several pharmaceutical applications, hence the rates and mechanisms of the formation of these derivatives is of significance [3]. In aqueous medium, halogenations of aromatic substrates follow rapid kinetics necessitating special techniques like temperature jump, pressure jump, competition technique, stopped flow method and pulse radiolysis [4].

We have herein adopted a relatively simple yet efficient technique, hydrodynamic voltammetry to monitor the rate of the fast iodination of the indole derivative; 3-indole butyric acid in aqueous medium[5].

The indole subunit is a ubiquitous component of many bioactive molecules in natural products. Its study has attracted the attention of researchers because of its ability to bind multiply to receptors. The resulting privileged structures have immense pharmacodynamic significance as precursors of drugs that are inhibitors of carcinogenesis [6].

The reaction under study is as follows,

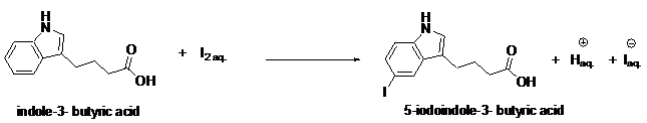

Iodine being the only species in the reaction that is electro-active at a micro-electrode, its decay during the reaction may be tracked by measuring the diffusion limited current at a rotating platinum microelectrode [RPE] that rotates at 600 rpm. The reference electrode is the saturated calomel electrode [SCE].The following are the two half-cell reactions at the two electrodes in the galvanic cell used in this hydrodynamic voltammetry technique:

$I_2 + 2e^- \rightarrow 2\,I^-$ ……. The positive electrode, RPE

$2Hg + 2Cl^- \rightarrow Hg_2Cl_2 + 2e^-$ ……. The negative electrode, SCE

$I_2 + 2Hg + 2Cl^- \rightarrow Hg_2Cl_2 + 2I^-$ ……. Overall Reaction

The use of a large concentration of the supporting electrolyte KNO_3 ensures linear proportionality of the diffusion limited current at the RPE due to the iodine concentration in the reaction.

2. MATERIALS AND METHOD

2.1 EXPERIMENTAL

2.1.1 Chemicals

Iodine : A stock solution of iodine is prepared in double distilled water devoid of iodide ions. The strength of this solution is determined iodimetrically.

Indole-3-Butyric Acid: The required weight of A. R. grade 3-IBA (CAS NO is 133-32-4) is used to prepare the stock solution in double distilled water.

Potassium Nitrate: A. R. grade potassium nitrate is used as the supporting electrolyte.

2.1.2 Electrodes

RPE – The cathode is a bent platinum electrode (RPE) rotated at a speed of 600 rpm in the reaction vessel causing stirring action in the solution as it senses the concentration of the electro-reducible entity in the reaction in terms of the diffusion current.

SCE - A saturated calomel electrode is the reference electrode (SCE). A constant potential of + 0.2 V versus the RPE is applied between the two electrodes using a potentiometer.

A galvanometer with a sensitivity of 0.10 nA cm^{-1} provided with a lamp and scale arrangement is used for the measurement of the diffusion current due to iodine in terms of the deflection of the galvanometer light spot. The current passing through the galvanometer is controlled by using a shunt so that the deflection of the light spot is within scale limits.

2.2 CALIBRATION

The RPE and SCE are dipped in 50.0 cm^3 of 5×10^{-3} M potassium nitrate which is the supporting electrolyte. The galvanometer light spot is adjusted to zero deflection on the scale. Potassium nitrate solution is then replaced by 5×10^{-5} M iodine solution containing 5×10^{-3} M potassium nitrate. The shunt is adjusted for the deflection of the galvanometer light spot to be around 40 cm. The shunt value is kept constant throughout the experiment. The diffusion current values in terms of deflection of the light spot on the scale are recorded for various concentrations of iodine in the range of 1×10^{-6} M to 5×10^{-6}M. The plot of deflection observed in cm versus concentration of iodine is found to be linear.

The calibration readings are carried out at five different temperatures and the readings are recorded only after the solutions have attained the thermostat temperatures at which the kinetic reading are to be observed subsequently.

TABLE-1: CALIBRATION OF THE DIFFUSION CURRENT OF AT VARIOUS TEMPERATURES FOR THE IODINATION OF INDOLE-3- BUTYRIC ACID AT pH 7

$[I_2]/10^{-5}$ M	Diffusion Current/nA				
	12.2^0 C	17.4^0 C	22.0^0 C	27.2^0 C	32.40^0 C
0.25	6.0	6.2	6.5	6.7	7.0
0.50	12.1	12.5	13.0	13.4	13.9
0.75	18.2	18.7	19.4	20.2	20.9
1.00	24.0	25.0	25.9	26.9	27.8
1.25	30.0	31.2	32.4	33.6	34.8

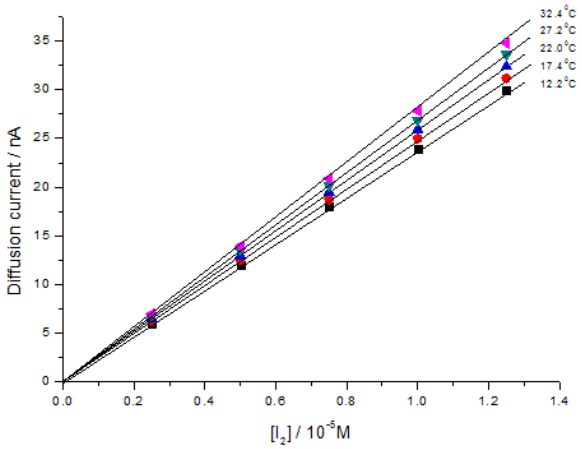

Fig. – 1 : Calibration of the diffusion current of I_2 at various temperatures of 3-IBA in aqueous medium.

TABLE-2: KINETICS OF IODIATION OF 3-IBA AT 22. 0^0C BY I_2 IN AQUEOUS MEDIUM AT 7 pH

Time/s	**Diffusion current /nA**	**$[I_2]/10^{-5}$M**	**$[I_2]^{-1}/10^4M^{-1}$**
0	32.4	1.25	8.0
30	25.9	1.02	9.8
60	22.5	0.86	11.6
90	19.5	0.74	13.4
120	17.1	0.65	15.2
150	15.0	0.59	16.8
180	13.5	0.53	18.6

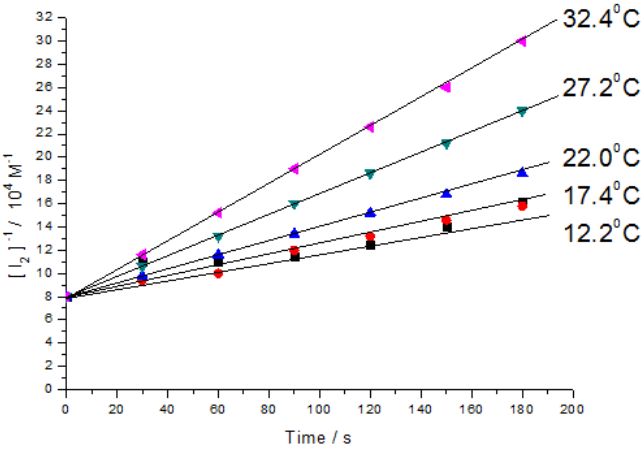

FIG.2 : KINETICS OF 3-IBA BY I_2 AT 7 pH AT DIFFERENT TEMPERATURES

TABLE-3: VARIATION OF SPECIFIC REACTION RATE OF IODINATION OF 3-IBA WITH TEMPERATURE AT 7 pH

T/K	$[T]^{-1}/10^{-4}$ $[K^{-1}]$	$k/M^{-1}s^{-1}$	log k
285.2	35.0	297	2.472
290.4	34.4	438	2.641
295.3	33.8	590	2.770
300.2	33.3	897	2.952
305.4	32.7	1212	3.082

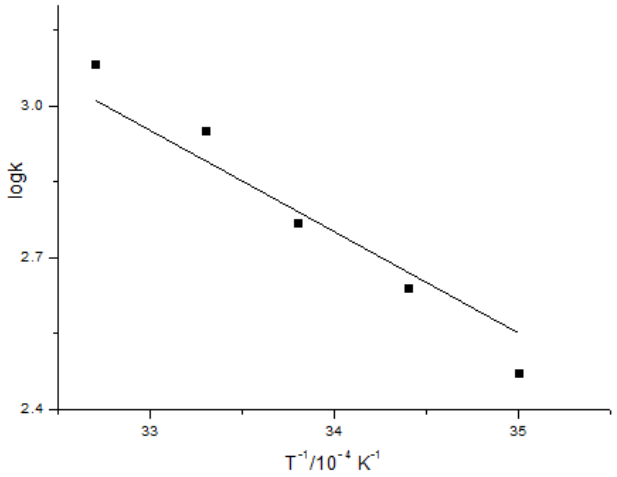

FIG. 3 ; ARRHENIUS PLOT FOR THE IODINATION OF 3-IBA BY I_2 AT 7 pH

2.3 KINETIC MEASUREMENTS

50 cm^3 each of 2.5×10^{-5} M 3-indole butyric acid and iodine containing hundred fold potassium nitrate and the buffer components required for 7 pH are kept in a thermostat in different containers in a thermostat. After attaining the desired temperature they are mixed in the reaction vessel kept in the thermostat in which the SCE is dipped and the RPE is rotating. At the time of mixing a stop-clock is started. As the reaction proceeds, the galvanometer deflection decreases steadily and the deflections are recorded at every 10 seconds for about 80 seconds.

The above procedure of calibration and kinetic measurement is repeated thrice for checking the reproducibility of the galvanometer readings. These are found to be within the limits of ± 0.2 cm which corresponds to ± 0.20 nA current.

From the observed deflections during the kinetic study, the concentrations of the unreacted iodine at various instant are obtained using the calibration curve (Fig.-1).

A plot of $[I_2]^{-1}$ versus time is found to be linear and hence the reaction is inferred to be of the second order. The slope of this plot gives the specific reaction rate k shown typically for 22.0^0C (Fig.-2).

These studies are carried out at various temperatures in range 10–30^0C, from which the energy of activation, 'Ea' for the reaction is evaluated [Fig.3]. Further, the frequency factors A and the entropy change ΔS# for the reaction are also evaluated.

3. CALCULATIONS

From Fig. 3,

Slope of the graph of log k Vs 1/T = $-2000\ M^{-1}\ s^{-1}$

Energy of activation (Ea): $= -2.303 \times 8.314 \times -2000$

$= 38.3$ kJ mole $^{-1}$

Frequency factor (A):

$$k = Ae^{(Ea/RT)}$$

$$A = 3.48 \times 10^9\ M^{-1}s^{-1}$$

Entropy of activation (ΔS)

$$A = (ekTe^{\Delta s\#}/R)/h$$

$$\Delta S = -243.12\ J\ mol^{-1}K^{-1}$$

TABLE 4: KINETIC PARAMETERS EVALUATED FOR THE IODINATION OF 3-IBA AT 7 pH AT 22.0^0C

No.	Parameters	Values
1	Specific reaction rate/$M^{-1}s^{-1}$	590
2	Energy of activation/kJ mol^{-1}	38.3
3	Frequency factor/$10^9M^{-1}\ s^{-1}$	3.48
4	Entropy of activation/$JK^{-1}\ mol^{-1}$	−243.1

4. RESULTS AND DISCUSSION

The sole halogenating agent in the reaction is the halogen atom in the aqueous equilibria, considering the equilibrium constant values.

The reaction are found to follow second order kinetics since the plot of $1/[I_2]$ versus time straight line. The gradient of this line is the specific reaction rates for the iodination reaction..

The product in the reaction is 5-iodoindole-3-butyric acid considering the confirmation from NMR data and from stoichiometry.

5. CONCLUSION

The potential of nitrogen having a lone pair to donate electrons is accentuated in Indole-3-butyric acid because of conjugation of the benzene ring and hence a lone pair of electrons is involved in conjugation. This increases the nucleophilicity of the benzene ring and activates position 5.

In Indole-3-butyric acid, the third position is blocked by the substituent and hence the iodination occurs at the fifth position of the ring. This is confirmed using ^{13}C and ^{1}H NMR spectra.

It is noteworthy that the present study is in total accord of green chemistry principles. The reactions are fast and microgram chemicals are used. The solutions are extremely dilute and are non- hazardous.

The rapidity of the reaction ensures low power consumption for the equipment which is needed to be operated only for a few seconds for the completion of the study of a single set of observations.

REFERENCES

[1] Berliner E.[1966] The Current State of Positive Halogenating Agents, *J.Chem. Edu.,* 43(3): 124-133

[2] Bonde,S.L., Dangat,V.T., Borkar,V.T. and Yadav,R.P. [2012] Rapid Iodinations of Xylidines in Aqueous Medium: Kinetic Verification of Speculated Reactivities *Res.J.Chem.Sci.*2(6);1-5

[3] Langen, K.J., Dirk, P. and Coenen, H.H. [2002] 3-[^{123}I]Iodo-α-methyl-L-tyrosine: uptake mechanisms and clinical applications. *Nuclear Medicine and Biology.*29 (6); 625-631

[4] Hart,E.J. and Boag,J.W.[1962] Absorption Spectrum for the Hydrated Electron in Water and Aqueous Solutions.*J.Amer.Chem.Soc.*84,4090

[5] Borkar, V.T., Dangat, V.T., Bonde, S.L. [2013] A Quantitative Structure-Reactivity Assessment of Phenols by Investigation of Rapid Kinetics using Hydrodynamic Voltammetry: Application of the Hammett Equation in Aqueous Medium. *International Journal of Chemical Kinetics (Wiley Pub).*9.(46),693-702.

DE-EMBEDDING OF TEST FIXTURE: A NECESSARY STEP IN POST SILICON VALIDATION FOR ACCURATE CHARACTERIZATION OF HIGH SPEED DEVICES

[1]SURENDRA KUMAR DADORE, [2]LALITA GUPTA, [3]SIYARAM SAHU

[1]National Institute of Technology, Bhopal, Email : Surendra1210@gmail.com

[2]Assistant Professor, National Institute of Technology Bhopal, Email : Gupta.lalita@gmail.com

[3]National Institute of Technology, Calicut (India), Email : Siyaram.sahu709@gmail.com

ABSTRACT

High speed interconnects on a PCB can alter the performance of the device when the data rate is in the order of Gbps range. These interconnects are necessary parts on a PCB since direct measurement of frequency characteristics of a device under test (DUT) at microwave frequencies is often difficult due to some intervening fixture used for feeding theDUT.These test fixtures or interconnect need to be characterized first andthen de-embedded. This paper focuses on measurement techniques used to characterize high speed devices and describesan algorithm used to de-embed a test fixture (interconnects on PCB) with the help of measured S-parameters. Effects of De-embedding operation on various time domain parameters i.e. Eye width, Peak to peak amplitude level, Rise time etc. are analyzed.

1. INTRODUCTION

The advancement of semiconductor process technology to sub-micron dimension has led to the development of broad spectrum of integrated circuit (IC) system components. These complex system components are being further integrated on silicon to form larger System-on-a-Chip (SOC) [7]. This leads towards the integrated circuits to work at higher speeds. Post silicon validation and characterizations is the last step in development of any electronics product.Ensuring the integrity of signals and correct operation of products for these high data rates has become challenging and has been a major focus of research and development since it is the vital stage of product life cycle. These efforts led to remarkable advances in the theory of signal integrity and practice of validation of systems over several decades. Validation is a very crucial phase of today's design and manufacturing process which takes more time as the products moving towards leading edge technologies and high frequencies because of signal integrity effects .

As the data rate of systems is moving to gigabits range, platform designers now face the challenge of Creating interconnects between various components of a PCB in High speed communication to maintain the signal as well as power integrity of a signal [6]. For example MPHY, which transfers data at a rate of 6 Gb/s and at 10^{-10} BER. Size, weight and cost constraints along with higher operating frequencies and advances in the technology are driving the use of smaller and more integrated packaged parts at the assembly level. A test fixture or cable is usually inserted between the compliance point and the instrument to facilitate a more convenient measurement. A few inches of PCB routing and/or cable can distort the signal hence it is very necessary to remove all the effects of a test fixture from the measured results [1]. At higher speeds, board traces, various interconnect and package signal nets behave like transmission line that may cause distortion in signal quality [2]. In order to meet these high speed requirements the design engineer must consider and minimize all the factors that affect the integrity of the signal in order to ensure the correct system functioning.

2. SILICON VALIDATION FLOW

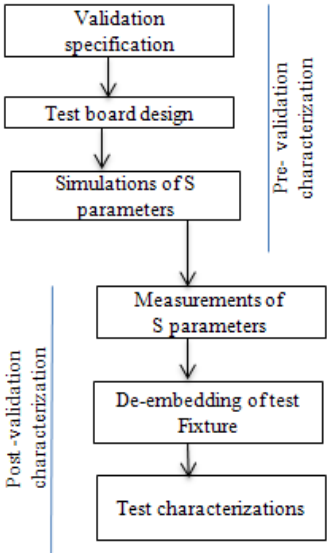

Figure1: Silicon validation flow

The silicon validation flow begins with the design of a high speed board satisfying the required validation specifications. Later, it needs to perform different analyses on various objects that are used in the board design. Figure 1 shows Silicon validation flow of high speed devices.

According to the protocols mentioned in the specification, Printed circuit board is designed, once the layout of the board iscompleted. It requires analysing the board transmission lines in a virtual environment in terms of S parameters. Agilent ADS tool is used to simulate S-parameters and this step comes under the pre-test characterization. In practical environment a test

engineer cannot rely with simulated results so is the actual measurements required. VNA is a suit for S parameter measurements that measures S-parameters. The measured S-parameters are used later in de-embedding operation. Once the de-embedding has been performed then only setup is ready for test characterizations.

3. DE-EMBEDDING OF TEST FIXTURE

De-embedding of a test fixture begins with the measurement of S-Parameters. Figure shows a cascaded system that comprises of test fixtures on both sides of a DUT [4]. The goal of de-embedding is to get S parameter of the DUT, while the measurement is done with fixture L and fixture R.

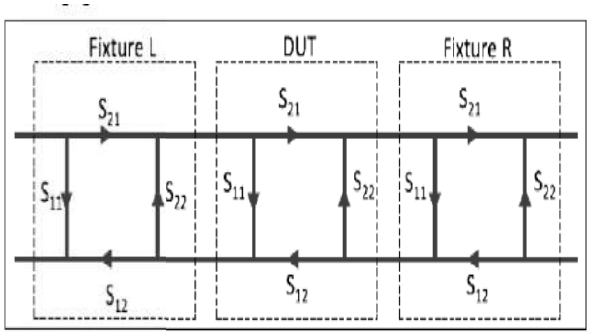

Figure 2

The S-parameter networks are translated into T parameter networks first, so that we can easily multiply them for the three cascaded networks above. The combined network can be viewed as a two port network [4].

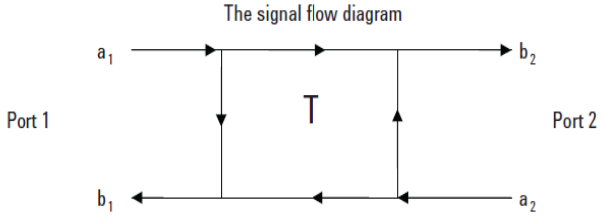

Figure 3

The general equations for reflection and transmission waves as a function of the T-parameters is shown below [4]

$b_1 = a_1T_{11} + a_2T_{12}$ (1)

$b_2 = a_1T_{21} + a_2T_{22}$(2)

For each of the three networks of the cascaded system, the translation between T parameter and S parameter is:

$$[T] = \begin{bmatrix} \frac{S21 \cdot S12 - S22 \cdot S11}{S12} & \frac{S22}{S12} \\ -\frac{S11}{S12} & \frac{1}{S21} \end{bmatrix} (3)$$

$$[S] = \begin{bmatrix} -\frac{T21}{T22} & \frac{1}{T22} \\ \frac{T11 \cdot T22 - T12 \cdot T21}{T22} & \frac{T12}{T22} \end{bmatrix} (4)$$

The measured T-matrix for the combined setup with test fixture is [4]

$[T_{Measured}] = [T_R]\ [T_{DUT}]\ [T_L]$(5)

Where $[T_R]$ and $[T_L]$ are known

T-matrix of DUT can be calculated as [4]

$[T_{DUT}] = [T_R]^{-1}\ [T_{Measured}][T_L]^{-1}$(6)

4. DE-EMBEDDING OF TEST FIXTURE BY OSCILLOSCOPE

After calculating S-parameter matrix for a test fixture using vector network analyser (VNA), its de-embedding is performed on a digital signal oscilloscope (DSO). DSO internally performs the mathematical operations which are explained above in Equations 3, 4, 5 and 6 to eliminate the effect of a text fixture. The figure shown below is a schematic of the test environment in which measurement/De-embedding has been performed.

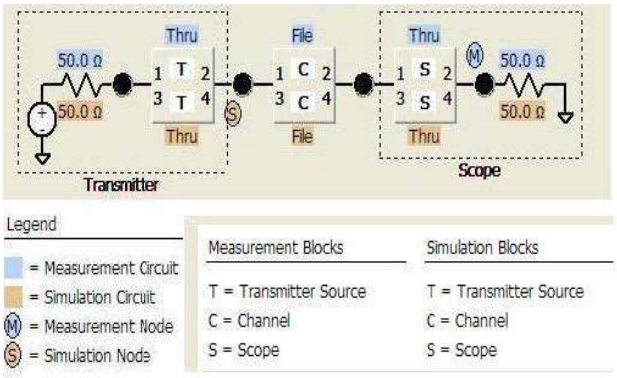

Figure 4 User Interface on a DSO

There are three blocks in the above figure namely transmitter, scope and test fixture which lies between simulation node and measurement node. Ideally measurement should be performed at the Simulation node but it is performed at the measurement node in practical condition due to test probing limitation of the PCB board. The measurements performed at the measurement node also include the effects of text fixture which is undesirable and need to be eliminated. VNA generates S-parameter data in terms of two port data (S2P) which can be used further to de-embed the effects of the text fixture.

5. RESULTS

Effects of De-embedding depends on the measurement of S-parameters from VNA i.e any inaccuracy in the measured S-parameters will degrade the De-embed output hence the process of De-embedding will be effective only if accurateS-parameters measurements are made. For validating purpose, a comparison is done

between simulated S-parameters and actual S-parameters generated from VNA. Figure shows the comparison between simulated and actual S-parameters of a PCB track. Simulated graphs are obtained from Agilent ADS tool.

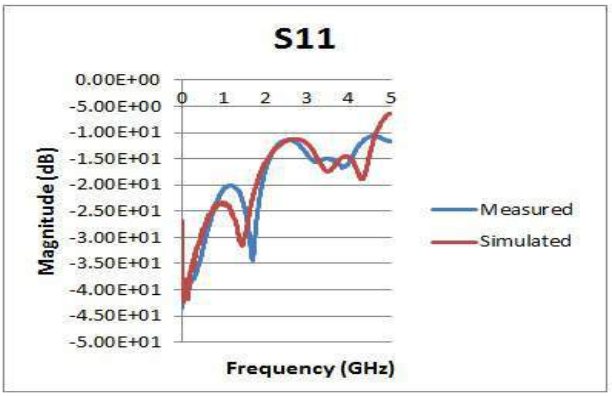

Figure 5

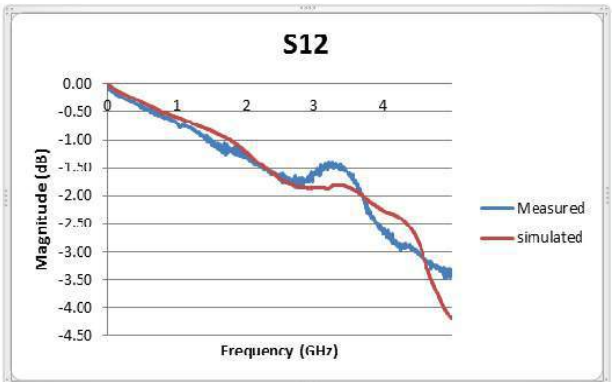

Figure 6

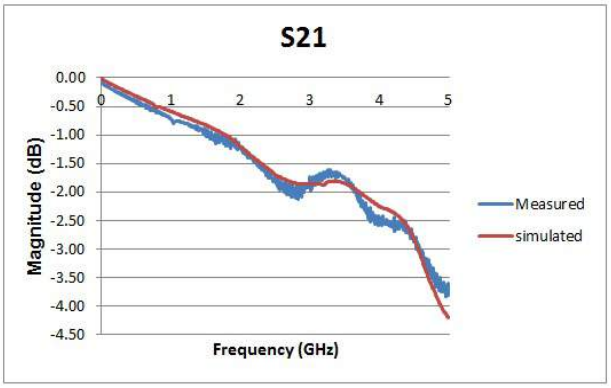

Figure 7

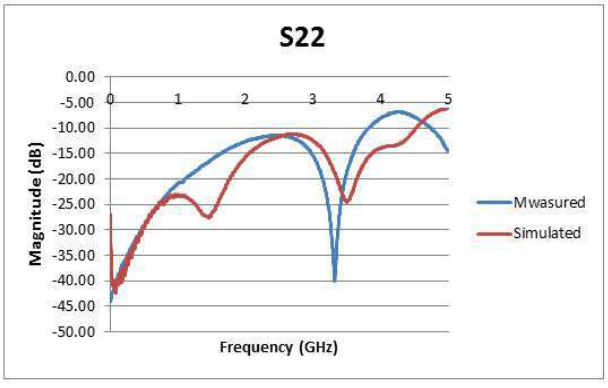

Figure 8

The figure depicts three different eye diagram plots which are plotted for different conditions.Figure 9 shows eye diagram plot for ideal case i.e. without any test fixture in between the simulation and measurement node. Figure 10 shows the plot with the effects of the test fixture and figure 11 shows eye diagram plot after de-embedding the effects of the test fixture. Based upon these plots, a quantitative analysis of various time domain parameters i.e rise time, fall time etc. has been performed. Table 1 shows the effects of a test fixture and its de-embedding on these parameters.

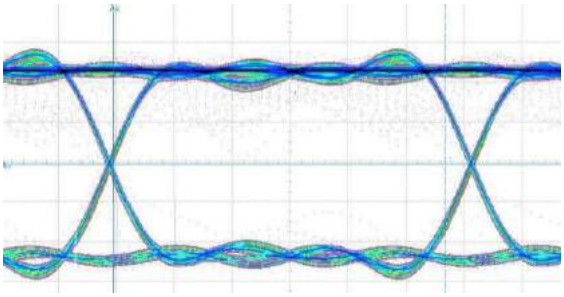

Figure 9 Ideal case (without any Test Fixture)

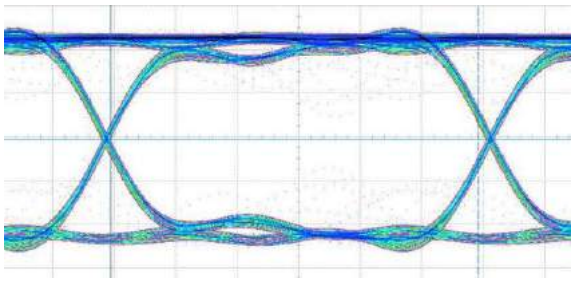

Figure 10 with Test Fixture without De-embedding

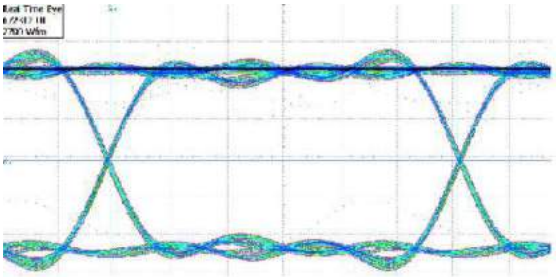

Figure 11 with Test Fixture with De-embedding

Table 1 De-embedding effects on time domain parameters

Oscilloscope Configuration	**Real Time Parameters**			
	Eye-Width	***Peak to peak voltage***	***Rise time***	***Fall time***
Ideal Case(without any test fixture)	982	568	200	196

Oscilloscope Configuration	**Real Time Parameters**			
	Eye-Width	***Peak to peak voltage***	***Rise time***	***Fall time***
With test fixture without De-embedding	975	584	338	258
With test fixture with De-embedding	978	568	196	198
Unit of measurement	pS	mV	pS	pS

6. CONCLUSION

In order to characterize high speed devices accurately, this paper describes de-embedding algorithm which is necessary to eliminate the effects of a test fixture, parasitics of pad and interconnections with a singlemeasurement [5]. This algorithm is very useful in an environment where probing limitations occur [3]. The accuracy of de-embedding algorithm depends on the measurement of S-parameters from VNA. Any inaccuracy in the measured S-parameters will reflect in the de-embedded output. This method is quick, accurate and convenient for high speed devices.

REFERENCES

[1]. Xiaoning Ye, Ben Smith, Per Fornberg, Adam Norman, "*Method and Applications of Oscilloscope Waveform De-embedding*", 978-1-4244-1699-8/08/$25.00 ©2008 IEEE.

[2]. Paul D. Hale, , Jeffrey Jargon, , C. M. Jack Wang, Brett Grossman, Mathew Claudius, José L. Torres, Andrew Dienstfrey, and Dylan F, *"A Statistical Study of De Embedding Applied to Eye Diagram Analysis"* , IEEE TRANSACTIONS ON INSTRUMENTATION AND MEASUREMENT, VOL. 61, NO. 2, FEBRUARY 2012.

[3]. Di Hu, Jaemin Shin, and Timothy Michalka,*"Fixture-free Measurement Technique for PDN Discrete Components",*2013 Electronic Components & Technology Conference, 978-1-4799-0232-3/13/$31.00 ©2013 IEEE.

[4]. Xiaoning Ye Data Centre and Connected Systems Group, Intel Corp,*"De-embedding Errors due to Inaccurate Test Fixture Characterization"*, 2012 IEEE Electromagnetic Compatibility Magazine – Volume 1 – Quarter 4.

[5]. Alexei s. Adalev', japan, Nkolay v. Korovk, Russia, Masashi "*De-embedding microwave fixtures with the genetic algorithm",* 0-7803-9374-0/05/$20.00 2005 IEEE.

[6]. Evan Fledell, Brett Grossman "*PCB Manufacturing Variation Impact on high frequency measurement fixtures"* Manuscript received October 18, 2010.

[7]. Vittorio Ricchiuti, Antonio Orlandi, Guilio Antonini, Siemens CNX, L'Aquila-Italy *"De-embedding Methods for characterizing PCB interconnections"* 0-7803-9054-7/05/$20.00200 05 IEEE.

IMPLEMENTATION OF DOUBLY-FED WIND TURBINE ALONG WITH PID CONTROLLER TO MAINTAIN THE DESIRED OUTPUT LEVELS AND CONTROL THE PITCH ACCORDING TO WIND DIRECTION

[1]AJAY SHUKLA, [2]ANIL GUPTA

[1]M.Tech. Scholar, Department of Electrical and Electronics Engineering, LNCT, Bhopal, India

[2]Assistant Professor, Department of Electrical and Electronics Engineering, LNCT, Bhopal, India

ABSTRACT

In order to increase energy demand, alternative source of energy generation is required. A many hybrid system involve wind system due to availability and easy access of wind resource. The wind generated power fluctuating due to time varying nature and causing stability problems. When Wind turbine system is connected to the power grid to generate power always fluctuating due to environmental conditions. This paper is to modify and simulation for a wind farm with a high voltage transmission network. Here model is designed to control pitch angle by using PID controller and to maintain output level by stabilizing rotor speed. Analytical model of wind turbine has been presented and this was followed by the modelling of the wind farm under Sim Power of simulink. The stimulated turbine system uses a Doubly fed Induction Generator (DFIG) having a capacity of 9 MW wind farm comprising of six 1.5 MW wind turbines linked with 25 kV distribution system transfers power to a 120 kV grid for a 30 km, 25 kV feeder . Initially in this model the wind speed is maintained constant at 15 m/s. PID Controller is introduced to regulate speed of rotor by adjusting pitch which controls speed changes. Result shows due to controlling of pitch angle output level is improved and good quality factor is achieved. We have applied fuzzy controller to establishe maximum power delivery to the grid at trip. This design having full control on the electrical torque, speed and also makeup a reactive power compensation and operation under grid disturbances which improve desired output levels.

Key words--- Modelling simulation, DFIG, PID Controller, Pitch angle, output, Fuzzy logic Control

1. INTRODUCTION

Due to heavy requirement of electricity, renewable energy has been widely developed. Wind power technology is one of the most popular renewable energy that is clean, easy maintenance, low cost and plentiful on the earth. Man well and Rogers (2002), [1] , defines conversion of kinetic energy from the wind into both mechanical energy and electrical power. In the early days, large farms used wind power generated by windmills to do farm works. Recently, advanced technology enables wind turbines to generated large electrical power to full fill the energy demand. Wind turbine technique has been greatly developed in the past few decades.

Doubly - fed electric machines are basically electric machines that are fed ac currents into both the stator and the rotor windings. Mostly doubly fed electric machines in industry are three phase wound - rotor induction machine, and are one of the most common types of generator used to produce electricity in wind turbines.

The primary advantage of doubly - fed induction generators when used in wind turbines is that they allow the amplitude and frequency of their output voltages to be maintained at a constant value, doesn't effects the speed of the wind blowing on the wind turbine rotor. By the, doubly fed induction generators can be directly connected to the ac power network and remain synchronized at all times with the ac power network and includes the ability to control the power factor.[2]

The problems encountered in the electrical network comprising wind energy systems are due to the continuous variations in the wind regime. These variations may inflect undesirable fluctuation in the network and thus has limited the capacity of the wind energy systems which can be integrated with the network to a modest penetration factor. Various techniques have been proposed to cope with the variations in the wind speed to ensure high performance and steady output for the wind energy systems and hence contribute to allow for higher penetration factor.

The effect of the variation in the wind speed may result in:

1- Change in the output voltage

2- Change in the output frequency

3- Change in the output power

4- Shift in the operating point

The maintain change in the output voltage and frequency is is discussed in this paper by adopting the system which employs a doubly fed induction generator connected to the network. The voltage and frequency are govern by the main network, the variation in the output power is

addressed in a companion paper by using a storage battery to smooth the changes in the output power[3].

Initially for the improvement of power quality or reliability of the system FACTS devices like static synchronous compensator (STATCOM), static synchronous series compensator (SSSC), interline power flow controller (IPFC) and unified power flow controller (UPFC) etc. These FACTS devices are created for the transmission system. But now a days more attention is on the distribution system for the improvement of power quality. In these devices variations are introduced and known as custom power devices. The custom power devices which are used in distribution system for power quality improvement are distribution static synchronous compensator (DSTATCOM), dynamic voltage restorer (DVR), active filter (AF), unified power quality conditioner (UPQC) etc.

For renewable source of energy Wind energy are focused, and has become gradually more widespread. Wind turbines use wind-energy capturing systems. Pitch control, which is normally required to attain a stable output power when the wind speed is above thenevaluated wind speed, is accomplished by regulating the pitch angle of the wind turbine blades to limit the output powerand protects wind turbine gearbox and generator. Therefore pitch control designed for variable-speed turbines are increasingly critical which is modified in this paper by fuzzy logic controller.

The proportional-integral-derivative (PID) controller is the common closed-loop control system which improves overall response of system is using to design the pitch control system. In addition to typical PID control systems, studies have suggested different methods for controlling the pitch angle. Modern studies have adopted to determine the stability region of PID control systems. In stable synthesis of a PI-based pitch controller was suggested. A graphical methodology was used to define the stability region and set the parameters of the controller to achieve an arbitrary-order time delay system. An alternate way to regulate the pitch angle in wind turbine generators is setting various operating points for the control system [4].

Fuzzy logic Controller is used with trip to optimize itself according to angle of wind flow. Fuzzy Logic is createdby logical functions. The conception of Fuzzy logic is derived from set theory. There are several controllers which provide effectual control for linear systems. In case of nonlinear systems a Fuzzy Logic Controllers are used. Fuzzification, rule formation, and defuzzification are the steps present in fuzzy logic system to perform operation. The input to the fuzzy controller is in the form of real variables. In the process of fuzzificationthe real variables are converted into fuzzy variable and each fuzzy variable are represented by membership function. In second step we form a fuzzy rules, fuzzy rules are based on definite decision i.e., in the form of IF-THEN. Finally when all the operations of control is completed at the last stage the fuzzy variables are again converted into real variables which is as known defuzzification.[5]

In order to extract maximum power from available wind have to take fuzzy logic control of generator side converter and thus control of generator speed was used. The advantages in using fuzzy logic controller is pointed out in better response to frequently changes in wind speed [6].

2. PREVIOUS WORK

Several techniques have been used in the past years on model of wind systems for power generation. Mostlyexisting models are analytical while others are computer based. Hansen & al. [7], provided a comprehensive report on the modelling of wind turbine at both system and component level using the DIgSILENT software. Their work dealt with the description of DIgSILENT built-in models of electrical components used for wind turbine system comprising: an induction generator, a power converter and other models developed by user in the dynamic simulation language (DSL) of DIgSILENT. Also, models of non-electrical components of wind turbine system such as wind speed model, aerodynamic model and others, were equally made available.

The three phase injected current into the grid from STATCOM will cancel out the distortion caused by the nonlinear load and wind generator. The IGBT based three-phase inverter is connected to grid through the transformer. The generation of switching signals from reference current is simulated within hysteresis band of 0.08. The choice of narrow hysteresis band switching in system improves the current quality and control signal of switching frequency within itsoperating band. [8]

In addition, Bolik (2004), developed a computer model of wind turbine that has been widely used by power-system operators to study load flow, steady state, voltage stability, dynamic and transient behaviour of power system. This system was also simulated with DigSILENT. DigSILENT has the capability to simulate load flow, RMS fluctuations and transient events. It provides models on different levels and can also be used to simulate load flow, RMS fluctuation and transient events in the same environment.

Besides and Fingersh& al. (2006), [9] developed under The National Renewable Energy Laboratory (NREL), an agency of US, a wind turbine model intended to provide reliable cost projections for wind-generated electricity based on different scales (sizes) of turbines. The model was mainly analytical. Petru (2001), has also developed a

similar analytical model of wind turbine as a project work and this was well elaborated on other aspects of wind system such as the aerodynamic modeling, the wind data modeling, the mechanical aspect

Moreover, Sulla (2009), [10] modeled and simulated a doubly fed Induction Generator and the fixe speed Induction generator with MATLAB Sim power system toolbox. The system was made of a graphical model built under Simulink with already existing models for transmission line, loads, wind turbine and others. Several cases of faults have been tested and analysed in order to show the robustness of the system.

Bharanikumar (2010), presents a maximum power point control for variable speed turbine driven permanent magnet generator [11]. In summary, his paper discusses the variable-speed wind energy conversion system using a permanent magnet generator and proposes the optimal control strategy of permanent magnet generator that helps to maximize the power generated.

Furthermore R. Melicio (2009), [12], developed a model of WTGS using a permanent magnet synchronous generator. The work aimed at improving the transient stability of the system by acting on the pitch angle. A new control strategy was proposed and simulated; simulation results show an improvement of system performances and robustness. In addition an analysis was carried out on the Total Harmonic Distortion (THD), which is a measure of system quality. Results show that the total THD was much lower than 5% which is the limit imposed by IEEE-519 standard. In summary, the above review of literature demonstrate that wind turbine modeling mostly goes with the use of doubly fed or squirrel cage induction generator and can be modeled and simulated under various conditions by two reputed software namely, DigSILENT and MATLAB. It was also found that, models of computation and validation of wind data, including Stochastic, Deterministic, Weibull and Exponential models were made available under MATLAB software.

3. METHODOLOGY

Simulation Methods of the Designed and Implemented model. On the basis of the frequency range to be represents, three simulation methods are presently available in Sim Power Systems to model VSC based energy conversion systems connected on power grids. The phasor model (continuous): This model is better adapted to simulate the low frequency electromechanical oscillations over long periods of time (tens of seconds to minutes). In the phasor simulation method, the sinusoidal voltages and currents are substituted by phasor quantities (complex numbers) at the system minimal frequency (50 Hz or 60 Hz).This is the technique which is also used in transient stability softwares. A 9 MW wind farm comprising of six 1.5 MW wind turbines linked to a 25 kV distribution system transfers power to a 120 kV grid through a 30 km, 25 kV feeder. However to enhance its power generation and quality of the generated power PID controller has been implemented over the wind speed block so as to control and regulate the wind speed according to the desired output power, also PID controller works only on the proportional constant and the integral value to attain the maximum output from the wind. Proportional constant can be further termed as the gain constant of the PID Controller. Wind Turbines do not operate at the speed above 55 miles per hour; this can be overcome by the use of PID Controller. As the PID Controller controls the wind speed for the designed model it becomes equally important to regulate the trip of the wind turbine as the amplified wind speed output may damage or block the wind turbine. To control the trip or the blade direction of the wind turbines Fuzzy Logic or Vector control method can be used, however in this model Fuzzy Logic is used as it is more responsive accurate and less complex than the vector control box. To control the pitch of the blades fuzzy logic generate a pulse to maneuver the blade direction or its pitch, so that the blades always remain in parallel to the wind and keep rotating to generate the maximum output. Wind turbines via a doubly-fed induction generator (DFIG) comprise of a wound rotor induction generator and an AC/DC/AC IGBT-based PWM converter. The stator winding is connected straight to the 60 Hz grid whereas the rotor is fed at variable frequency through the AC/DC/AC converter. 120 KV generator is required to synchronize the output power generated by the wind turbine. The DFIG technology permits extracting maximum energy from the wind form low wind speeds by optimizing the turbine speed, while decreasing mechanical stresses on the turbine during gusts of wind. Initially in proposed model the wind speed is maintained constant at 15 m/s. The control system uses a torque controller in order to maintain the speed at 1.2pu. The reactive power generated by the wind turbine is regulated at 0 Mvar at a wind speed of 15 m/s, the turbine output power is 1 pu of its rated power, the pitch angle is 8.7 degree and the generator speed is 1.2 pu. A proportional-integral-derivative controller (PID controller) is a control loop feedback mechanism (controller) widely used in industrial control systems. The PID controller computes an error value as the difference between a measured process variable and a desired set point.

Fuzzy Logic A fuzzy control system is a control system based on fuzzy logic—a mathematical system that analysesanalog input values in terms of logical variables that take on continuous values between 0 and 1, in contrast to classical or digital logic, which operates on discrete values of either 1 or 0 (true or false, respectively).

4. RESULTS

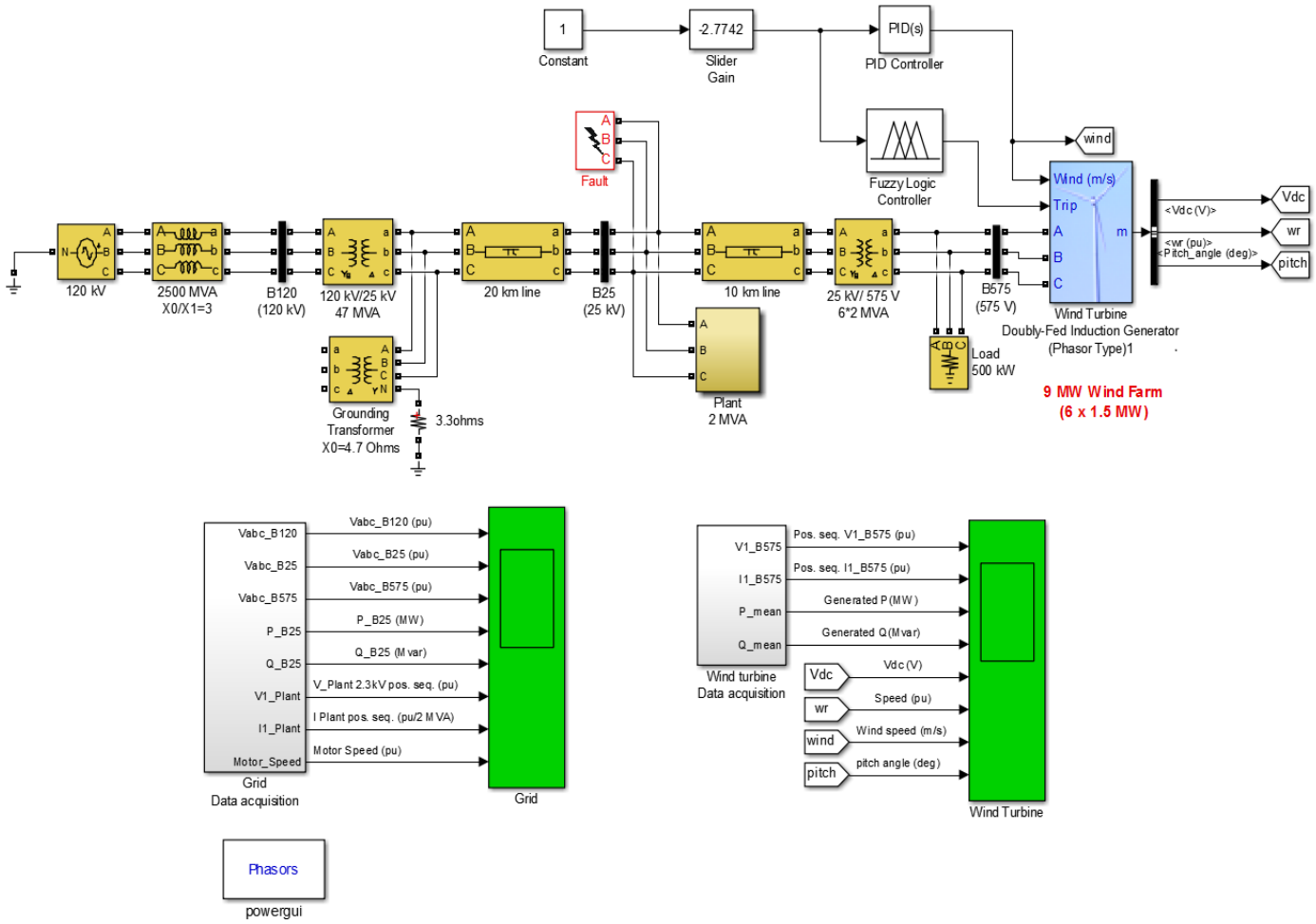

Figure1: Detailed Proposed MATLAB Model

Output Responses

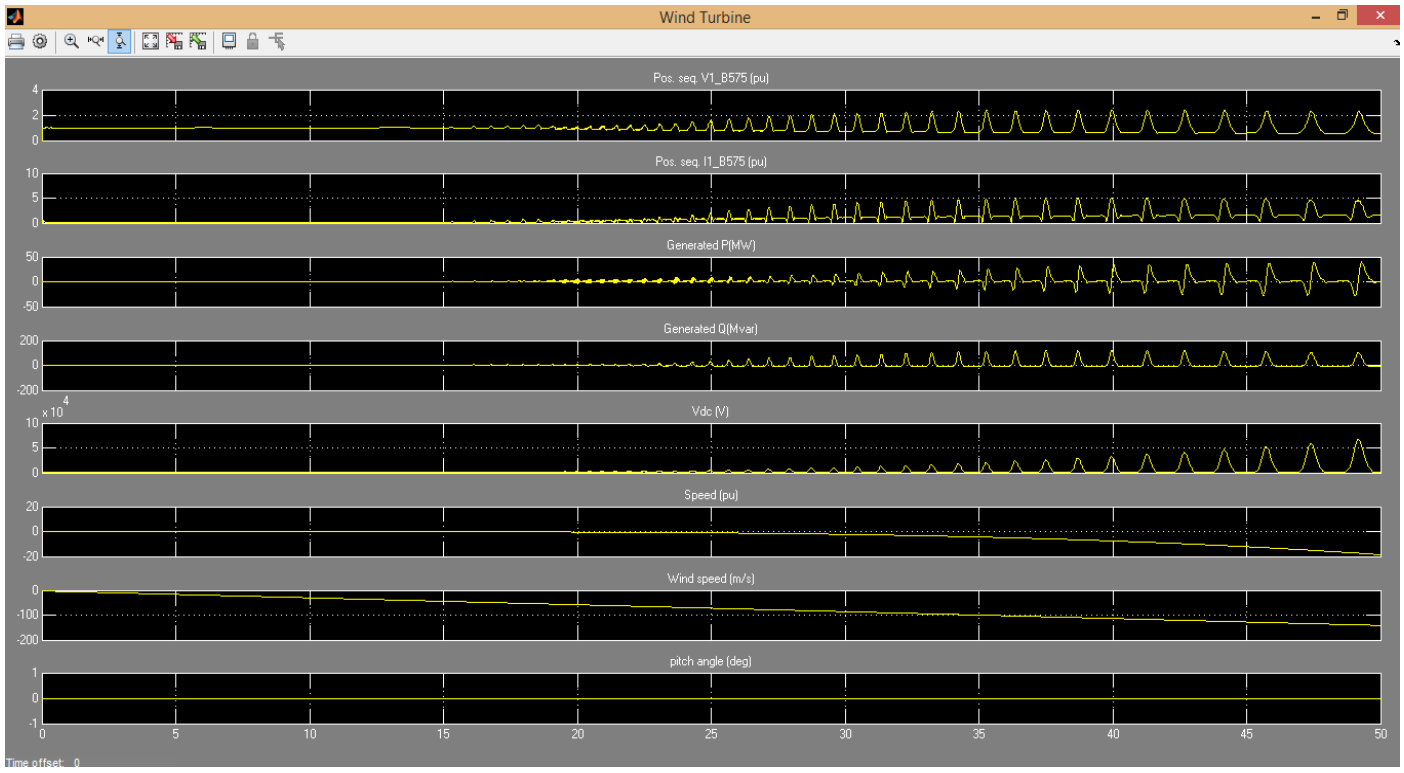

Figure2: Out Put Response of Wind Turbine

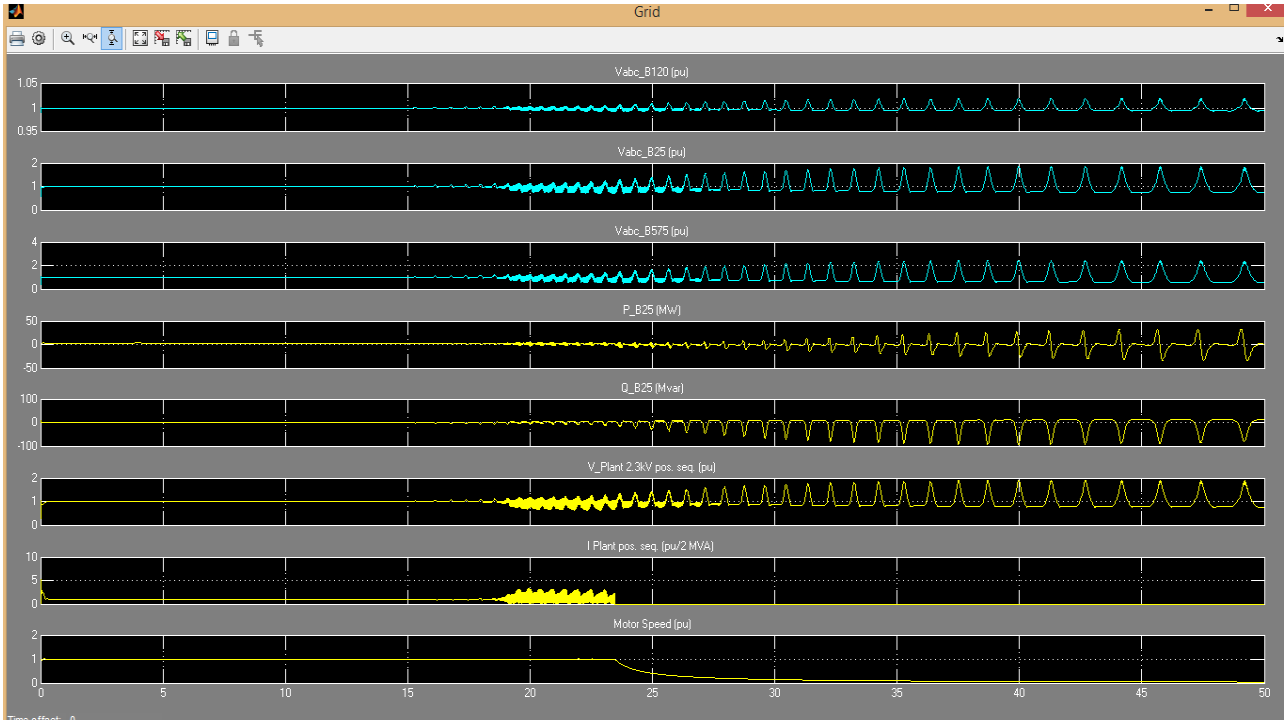

Figure3: OutPut Response of Grid

5. CONCLUSIONS

On implementing PID controller with wind turbine have controlled the desired output level and power quality also improved. This system is previously proposed for capacity of 9 MW but after introducing PID controller, its transient and steady state response is improved so its output power reached upto 30 MW.

In this paper, I also controlled the pitch angle of wind turbine by introducing fuzzy logic controller with trip to control its angle of blades according to wind flow.

REFERENCE

[1] WIND ENERGY EXPLAINED THEORY, DESIGN AND APPLICATION; SECOND EDITION - J.F. MANWELL | J.G. MCGOWAN University of Massachusetts, USA| A.L. ROGERS DNV – Global Energy Concepts, Washington, USA

[2] Principles of Doubly-Fed Induction Generators (DFIG); Courseware Sample 86376-F0 - 01/2015

[3] M. Azouz, A. Shaltout and M. A. L. Elshafei,Cairo University Fuzzy Logic Control of Wind Energy Systems, 14th International Middle East Power Systems Conference, Cairo University, Egypt, December 19-21, 2010

[4] C.EbbieSelva Kumar, V.Jegathesan, R.EvelinePregitha, Modeling and Control of Power Converter for Doubly Fed Induction Generator Wind Turbines using Soft Computing Techniques Journal of Energy Technologies and Policy ISSN 2224-3232 (Paper) Vol.2, No.3, 2012

[5] Jau-WoeiPerng *, Guan-Yan Chen and Shan-Chang Hsieh ; Optimal PID Controller Design Based on PSO-RBFNN for Wind Turbine Systems ISSN 1996-1073 ; 07/2014

[6] EvgenijeAdzic*, ZoranIvanovic*, Milan Adzic**, Vladimir Katic* ; Maximum Power Search in Wind Turbine Based on Fuzzy Logic Control, Vol. 6, No. 1, 2009

[7] Anca D. Hansen, Clemens Jauch, PoulSørensen, Florin Iov, FredeBlaabjerg ; Dynamic wind turbine models in power system simulation tool DIgSILENT, ISBN 87-550-3198-6 - 2004

[8] D. Srinivas , M. Rama Sekhara Reddy, Power Quality Improvement in Grid Connected Wind Energy System Using Facts Device and PID Controller , IOSR Journal of Engineering (IOSRJEN) e-ISSN: 2250-3021, p-ISSN: 2278-8719, Volume 2, Issue 11 (November 2012), PP 19-26

[9] L. Fingersh, M. Hand, and A. Laxson, Wind Turbine Design Cost and Scaling Model, Technical Report NREL/TP-500-40566 December 2006

[10] Francesco Sulla, Simulation of DFIG and FSIG wind farms in M ATLAB SimPowerSystems , Division of Industrial Electrical Engineering and Automation Lund University, CODEN:LUTEDX/(TEIE-7235)/1-007/(2009)

[11] R. Bharanikumar, A.C. Yazhini, A. Nirmal Kumar; Modeling and Simulation of Wind Turbine Driven Permanent Magnet Generator with New MPPT Algorithm, Asian Power Electronics Journal, Vol. 4 No.2 August 2010

[12] R. Melício, V. M. F. Mendes, J. P. S. Catalão ; Computer Simulation of Wind Power Systems: Power Electronics and Transient Stability Analysis , International

Conference on Power Systems Transients (IPST2009) in Kyoto, Japan June 3-6, 2009

DIVERSITY, PREVALENCE AND ROLE OF SUPEROXIDE DISMUTASE IN CYANOBACTERIA

KANU PRIYA[1], NAMITA SINGH*[2], INDERJEET SINGH[3]

[1]Research Scholar, Microbial Biotechnology Laboratory, Department of Bio & Nano Technology, Guru Jambheshwar University of Science & Technology, Hisar, Haryana-125001, India. Email: kanupriya.mohil@gmail.com
[2]Associate Professor, Microbial Biotechnology Laboratory, Department of Bio & Nano Technology, Guru Jambheshwar University of Science & Technology, Hisar, Haryana-125001, India. Email: namitasingh71@gmail.com
[3]Director, Safe Agro Producer Company Ltd., Hisar, Haryana- 125001, India. Email: ispanghal@gmail.com

*Corresponding Author- E-mail: namitasingh71@gmail.com

ABSTRACT

Superoxide dismutase (SOD), the antioxidant enzyme exists in four diverse forms in cyanobacteria i.e. FeSOD, MnSOD, Cu/ZnSOD and NiSOD. FeSOD has an ancestral origin from the GSB ancestor of PSI while MnSOD has protobacterial ancestor to PSII & mitochondria. Cu/ZnSOD shows lateral gene transfer while NiSOD is rarely found. Fe & Mn forms share similarity while Cu/Zn form does not. SOD is prevalent in all subcellular locations where O^{2-} (superoxide) radicals are formed. SOD plays a defensive role at the time of environmental stress like chilling, dessication, light stress, metatoxicity etc and its activity is usually seen higher at the time of stress. Inactivation of SOD gene results in oxidative damage to the cell.

Key words: *SOD, Antioxidant, Isoforms, Localization, Environmental stress.*

1. INTRODUCTION

Superoxide dismutases (SOD, E.C. 1.15.1.1) are ubiquitous metalloenzymes with molecular weight 17 to 85 kDa that catalyze the disproportionation reaction of conversion of superoxide radicals to peroxide and molecular oxygen as shown in fig. 1. The metal ions are alternatively oxidized and reduced. There are four different metalloforms of SOD found in cyanobacteria but these are not equally distributed. The forms are FeSOD, MnSOD, CuZnSOD and NiSOD. A cambialistic form that uses Fe/Mn in its active site also exists.

Though oxygenic Photosynthetic Electron Transport (PET) and aerobic respiration have improved the efficiency of Carbon metabolism but the benefits are partially offset by their tendency to form reactive oxygen species (ROS). ROS can react with lipids, proteins, nucleic acids etc to cause irreversible damage to a cell. This necessitated the co-evolution of antioxidant systems with PET and aerobic respiration.

Cyanobacteria are the oldest oxygen evolving photosynthetic prokaryotes and possess plethora of bioactive compounds (Sudha *et al*, 2011). The name "cyanobacteria" comes from the Greek word kyanos, which means blue- green. These occupy a crucial position between prokaryotes and eukaryotes. They are considered as responsible for the conversion of primitive anaerobic reducing environment into the modern oxidizing one (Lukow *et al.,* 2000). They have adapted to survive in almost every ecological niche including the extreme ones (Schopf, 2000). The protective role of cyanobacterial SOD was first studied in *Anacystis nidulans* (Herbert *et al.*, 1992). Though the photosynthetic apparatus of cyanobacteria is similar to that of algae and plants but the antioxidant system is simpler as compared to plants. Also, it is easier to genetically manipulate it in respect to plants, like genes for antioxidant enzymes can be easily inactivated by insertional mutagenesis (Weixing *et al.*, 2007). SOD possesses high therapeutic value and it was first commissioned in 1985 as a drug in USA for defence of donor organs against oxidative stress during periods of ischemia and reperfusion (Vellard, 2003).

2. THE DIVERSE FORMS OF SOD

Four different isoforms of SOD are found to be known till date in cyanobacteria. Among these Fe and Mn forms are the most prevalent.

***Iron and Manganese SODs*:** According to Fink and Scandalios (2002), Fe and Mn SODs share 50% similarity based on amino acid alignments and suggest that they might have evolved from gene duplication from a common ancestor. The similarity in structure between the two forms is due to similar electrical properties of Fe & Mn. Both are homodimers or tetramers containing one metal atom per 200 to 220 amino acid residue subunit with molecular weight ranging from 14 to 30 kDa. Some Archea also possess cambialistic form of SOD. Inspite of high degree of similarity between these two forms, two specific amino acid residues i.e. 77 (glutamine in FeSOD and glycine in MnSOD) & 146 (alanine in FeSOD and glutamine or histidine in MnSOD) differentiate them (Weatherburn, 2001). However, it is possible to substitute Fe for Mn in the active site of MnSOD or vice versa but little or no catalytic activity is retained. An important difference between these two forms is their intracellular location. The FeSOD is found in the chloroplasts and cytoplasm (Fink and Scandalios, 2002) while MnSOD is mostly localized in mitochondria (Okamoto *et al.,* 2001). An N terminal, hydrophobic, transmembrane helix tail on the MnSOD determines its

localization in cyanobacteria (Atzenhofer *et al.,* 2002; Regelsberger *et al.,* 2002).

***Copper-zinc SODs*:** CuZnSOD exhibit structural as well as evolutionary dissimilarity from Fe and MnSOD because of different electrical properties of Cu/Zn from Fe & Mn. It is a homodimer with molecular weight between 31 to 33 kDa for each subunit and amino acid residues of length 150 to 160 per subunit (Fridovich, 1998). The enzyme is having two active sites one containing Cu and another Zn for each subunit. It is very stable as it can withstand multiple freeze-thaw cycles and prolonged refrigeratin once purified. This may be attributed to high glycine content (13 to 17%) contributing to extensive β-pleated sheet conformation (Chen *et al.,* 2001).

***Nickel SODs*:** it is completely different from the other three forms of SOD. It was first discovered, cloned and characterized in the bacterial genus, *Streptomyces* (Wuerges *et al.,* 2004). A survey of available genomes suggests that this form is also available in cyanobacteria as well (Palenik *et al.,* 2003).

The reason behind the metal substitution during its evolutionary history may be related to the availability of soluble transition metal compounds in the biosphere with respect to the oxygen content of the atmosphere in different geographical eras (Bannister, 1991).

2.1 EVOLUTIONARY ASPECT AND LOCALIZATION OF SOD

The tree of life shows distribution of SOD in archaebacteria, bacteria and eukaryote as shown in fig. 2. The ancestral history reflects origin of FeSOD from the GSB ancestor of PSI while MnSOD from protobacterial ancestor to PSII and mitochondria. The Cu/ZnSOD is believed to be originated by lateral gene transfers. SOD enzymes are compartmentalized in a cell. This may be due to the reason that O^{2-} radicals cannot cross the cytoplasmic membranes and are imperative to be removed (Takahashi and Asada, 1988). All SODs are encoded by the nucleus and appear to have evolved by lateral gene transfer of three distinct genes to the nucleus after the endosymbiotic acquisition of mitochondria and plastids. FeSOD is localized in the chloroplasts and cytoplasm while MnSOD is found in the mitochondria. NiSOD is found to be associated with plastids. Cu-ZnSOD is found in chloroplast, cytoplasm & periplasm as shown in fig. 3.

2.2 PREVALENCE OF SOD FORMS IN DIFFERENT ORDERS OF CYANOBACTERIA

Below given is the prevalence of different forms of SOD in different orders of cyanobacteria based on analysis of Priya *et al,* (2007). It is cleared that the most prevalent forms are Fe and Mn.

Fe-SOD- *Anabaena variabilis, Cyanothece sp., Gloeobacter violaceus, Lyngbya sp., Nostoc sp., Plectonema boryanum, Spirulina platensis, Synechococcus sp., Synechocystis sp., Thermosynechococcus elongatus*

Mn-SOD- *Anabaena variabilis, Crocosphaera watsonii, Gloeobacter violaceus, Leptolyngbya valderiana, Nostoc sp., Plectonema boryanum, Synechococcus sp., Thermosynechococcus elongatus, Trichodesmium erythraeum*

Cu/Zn-SOD- *Lyngbya sp., Synechococcus sp.*

Ni-SOD- *Crocosphaera watsonii, Prochlorococcus marinus, Synechococcus sp., Trichodesmium erythraeum*

2.3 PROTECTIVE ROLE OF SOD IN CYANOBACTERIA

Researchers have demonstrated that SOD plays a protective role against oxidative damage in cyanobacteria during different types of environmental stress. O^{2-} radicals are produced inevitably in respiratory electron transport (Yankovskaya *et al.,* 2003) and also in the chloroplasts by the reduction of oxygen at the site of PSI (Asada, 1999). SOD is found to protect the proton donating system in nitrogen fixation against ROS in heterocysts forming cyanobacterium *Anabaena cylindrical* (Henry *et al.,* 1978). Several studies have been done using mutant strains of cyanobacteria with altered levels of SOD activity. A photooxidation resistant mutant strain of *Plectonema boryanum* with increased levels of MnSOD activity was isolated by Steinitz *et al.,* (1979). The protective role of SOD during different environmental tress conditions is described below.

Chilling stress: Chilling stress is propounded to decrease membrane fluidity which is a primary symptom (Nishida and Murata, 1996). Chilling in presence of light increases production of ROS by creating reducing atmosphere which is further worsen by production of H_2O_2 and O_2 which inhibits enzymes of Calvin cycle (Kaiser, 1979). The activity of the Calvin Cycle and soluble enzymes has been found to decrease with low temperature without causing any significant decrease in light harvesting and electron transfer system. Recent studies offer that chilling suppress nitrate uptake in *Synechococcus* sp. PCC7002 (Sakamoto and Bryant, 1999) which resulted in chlorosis. Role of SODs in safeguarding chilling ravage in cyanobacterium *Synechococcus* sp. PCC79421 was done by David *et al*, 1999. Kwang *et al*, (2005) reported differential expression of MnSOD in near isogenic lines of wheat during cold acclimation. Punia and co-workers *(*2011) reported the role of SOD in combating chilling stress in *Arthrospira* isolates. SOD activity was 5 times higher in tolerant strain and 2.5 times higher in sensitive strain at the time of chilling stress as compared to optimum temperature on native gel.

Desiccation: The role of SOD has been well studied in *Nostoc commune* after many years of desiccation to find out its function in detoxifying ROS and reducing stress (Shirkey *et al.,* 2000). The study unveiled that FeSOD was the third most abundant soluble protein in *Nostoc commune* even after storage in desiccated state for long period. The FeSOD purified from *Nostoc commune* was purposed to be a 21kDa polypeptide. N-terminus of sodF was sequenced which was encoded by 200 codons. Upon rehydration, FeSOD was released in the cells and extra cellular fluid and suggested that this process helps in reducing oxidative stress offered by multiple cycles of desiccation. The retained activity of SodF after years of dessication in *Nostoc commune* suggested that the enzyme might have structural features which allow it to

remain in the native state despite of the removal of water from the cells or it might be sequestered in cell microenvironment (Shirkey *et al.,* 2000). Similarly, considerable activity of SOD found in cell free extracts of dessication tolerant cyanobacteria *Lyngbya arboricola* (Tripathi & Srivastava, 2001). Marked tolerance against high solar radiation along with dessication stress is reported in the cyanobacterium, *Tolypothrix byssoidea*, occurring on the exposed rock surfaces of temples and monuments in various regions of India (Adhikary *et al.,* 2000). The FeSOD gene was amplified and sequenced which was a 292 bp polypeptide encoding for 96 amino acids. The resulting gene found to be 49.2% similar with FeSOD of *Anabaena* sp. PCC7120. Another sequence of 358 bp was also sequenced and was supposed to be similar to sodF encoding for soluble FeSOD protein found in *Nostoc commune.* Efforts for transferring gene of desiccation tolerance in cyanobacterium *Chroococcidiopsis* have been made Daniela *et al.,* 2001. *Chroococcidiopsis* is dominating community found in deserts. Plasmids from *Nostoc sp.* PCC7524 were transferred to various isolates of *Chroococcidiopsis* via conjugation and electroporation methods and offered as a suitable experimental strain for genetic studies.

Visible light stress: Light plays an important limiting factor for growth of photosynthetic organisms. Quail (1994) propounded that signal transduction and expression of protein is controlled by light. The impact of high irradiance on algae is drawing special attention (Cullen and Lewis, 1995). ROS are produced in a heavy amount by photochemical processes involved in photosynthesis. High light intensity reduces the rate of photosynthesis by harming photosynthetic apparatus (Critchley, 1994). Studies of photosystem expose that FeSOD is related with the protection of PSI (Thomas *et al.,* 1998). SOD found to be selectively protective to heterocysts which can fix nitrogen and posses only PSI (Canini *et al.,* 1998). Oxygen is reduced using light by PSI in cyanobacteria (Slain, 1991). SODs play crucial role in defending against ROS and its detoxification (Touati, 1997) and provide best tolerance to oxidative stress (Bhattacharya et al., 2004). MnSOD which is membrane associated in cyanobacteria are found to be protective to the photosynthetic apparatus in *Anabaena* sp. PCC7120 when exposed to high light intensity (Weixieng *et al.,* 2007). The study confered that lipid peroxidation occurd at a highr rate in absence of MnSOD under high light intensity. MnSOD was found to be critical in preserving both PSI and PSII in test sample. Earlier researches purposed that superoxide ions are produced by PSII when light intensity is high (Navari-Izzo *et al*., 1999). So it was hypothesized that the major role of SOD is in shielding of PSII against photoinhibition. An intense study on *Synechocystis* sp. PCC6803 to understand light dependent expression of SOD was done by Jae and Kyong (2005). Results revealed that FeSOD was more active in cultures maintained in continuous light. Respiratory reaction largely contributes in activation of FeSOD as electron transfer system is a major site of O_2 generation (Imlay and Fridovich, 1991). *Microcystis aeruginosa* which is a bloom producing cyanobacteria when exposed to heavy irradiation for longer time, accounted for decrease in rate of photosynthesis (Abeliovich and Shilo, 1972). FeSOD is inactivated if *Microcystis aeruginosa* is exposed to light stress for longer duration due to the production of excess of H_2O_2. There are records of about eightfold increase in amount of FeSOD when *Nodularia* collected at the depth of 10 m from Baltic sea was exposed to high irradiation (Canini *et al.,* 1998).

Ultraviolet radiation stress: Ultraviolet radiation can cause oxidative damage depending upon its wavelength. UV-B (280-320 nm) can cause photosynthetic damage (Sinha and Hader, 2002). Another study stated that inactivation of cyanobacterial nitrogenase after exposure to UV-B (Kumar *et al.,* 2003). UV-A also exhibits ravaging effect on the cell. UV-A stimulates genes in bold in negative phototactic responses in cyanobacteria when exposed for long time and high intensity. Photosensors such as cryptochrome Cry-DASH are involved in UV-A dependent signaling at low fluence rate. UirS-UirR and PCD are the important signalling component which have important role under oxidative stress condition in cyanobacteria. Study of SODs confirms its crucial role in maintaining UV-B level in algae (Rijstenbil, 2002) but there is no significant increase in SODs level when exposed to UV-A. Various nonenzymatic systems and SODs are suggested to have different target sites for UV-A and UV-B sabotage (Rijstenbil, 2003).

Nutrient stress*:* The rate of metabolism starts declining under nutrient stress condition which is a result of impairment caused to the cellular scaffolding. Due to lack of nutrients, catabolism of cellular protein starts in order to maintain photo synthetic activities (Falkowski and Raven, 1997). These conditions of respiratory degradation leads to the production of ROS. Punia and co-workers (2011) reported decreased activity of SOD in Pi starved strains of *Arthrospira*. Studies on role of SODs under nutrient limitation in cyanobacteria are getting more attention which will hopefully open up new perspectives in future.

Metaltoxicity: Presence of excess metal ions induces Fenton reactions. Cyanobacteria has been studied intensively and found to produce metal chelators and antioxidant buffers in order to absorb trace metals and different metals are found to be important for regulation of various metabolic processes (Mc Kay *et al.,* 2001). Micronutrients settle the output of metabolic processes based on macronutrients uptake (Sunda 2000) and prevent Fenton reaction by acting as an antioxidant buffer (Martinez *et al.,* 2000). *Synechocystis aquatilis* manifest decline of growth rate when concentration of copper is increased (Shavyrina *et al.,* 2001). *Asparagopsis armata* also suffered reduction in growth in presence of metal (Segot *et al.,* 1983). Copper is found to produce hydroxyl radical whereas zinc and lead disturb metabolic machinery via freezing antioxidant pool which results to increase load of ROS (Briat, 2002). Cu is mostly studied for understanding various SODs responses under presence of excess metal (Okamoto *et al.,* 2001). A study on effect of heavy metal in *Anabaena variabilis* was done by Padmapriya and Anand (2010) to determine their effect on SODs. Copper was found to inhibit growth of *A. variabilis* to maximum amount. Production of peroxide was found to be less in Fe and Mn varied cultures whereas highest in Cu and Zn amended cultures. Increase in SOD activity was observed when amendments in micronutrients were done. Increase in

copper concentration in *A. doliolum* lead to 63% increase in SOD activity which also resulted in increase in lipid perooxidation (Mallick and Rai, 1999). A mutant strain of *Synechococcus* sp. PCC7942 has been constructed lacking detectable FeSOD activity and its photosynthetic electron transport was found to be more sensitive in the presence of methyl viologen and elevated O^2 concentrations (Herbert *et al.,* 1992; Thomas *et al.,* 1998) but is not sensitive to oxidative stress induced with Norflurazon (David *et al.,* 1999). The sodB$^-$ strain had increased MnSOD activity as demonstrated by Herbert *et al., (*1992). It might be possible that the increased MnSOD activity was to compensate for the FeSOD and thus resists the effects of NF. SOD plays a significant role in combating heavy metal stress in the cyanobacterium *Spirulina platensis*-S5 (Meenakshi *et al.,* 2006).

Other stress: Some filamentous cyanobacteria posseses specialized cells known as heterocysts which are specialized chambers with thick lining involved in protection of nitrogenase enzyme from the poisonous effect of oxygen and hyterocysts are formed under nitrogen deprived conditions (Zhang *et al.,* 2006). SOD from heterocysts of *A. Cylindrica* have been isolated so far which gives a strong evidence that SOD is necessary for scavenging ROS in N_2 fixing cells (Henry *et al.,* 1978). *Anabaena* sp. PCC7120 heterocysts posses two SOD genes encoding for FeSOD (Liu *et al.,* 2000; Kaneko *et al.,* 2001) and MnSOD (Regelsberger *et al.,* 2002; Li *et al*., 2002; Kaneko *et al.* 2001) where FeSOD level increases when cell from nitrogen abundant conditions are transferred to nitrogen deprived conditions but MnSOD doesn't show any up regulation. Nitrate uptake at low temperature slowdowns because at low temperature all three enzymes involved in nitrate assimilation are protected by membrane lipid unstauration which reduces rate of nutrient uptake. Hence low temperature and nutrient stress both are involved in condition called nitrogen starvation.

3. CONCLUSION

SOD has gone under different metallic substitutions during its evolutionary history. This was due to the availability of different metals in context to oxygen in the biosphere in different geographical eras. Four different metalloforms exist in cyanobacteria with Fe & Mn as the most prevalent. Owing to its presence in all subcellular locations where superoxide radicals are produced it offers an effective defense system to the cell. Its gene inactivation results in oxidative damage to the cell. Cyanobacteria photosystem resembles to that of plants and thus can be extensively studied for stress mechanisms. Mass cultivation of cyanobacteria for SOD extraction can be promoted for use in therapeutics and clinical research.

ACKNOWLEDGEMENT

The authors acknowledge DBT(Department of Biotechnology) sponsored HRD & BIF(Bioinformatics) Program and UGC-SAP (University Grants Commission-Special Assistance Programme), New Delhi, India for providing financial and infrastructure support.

REFERENCES

1. Abeliovich, A. and Shilo, M. 1972 "Photooxidative death in blue-green algae". *Journal of Bacteriology,* 111: 682-689.
2. Adhikary, S.P. 2000 "Chlorophyll stability of epilithic cyanobacteria from temples of India." *Arch Hydrobiol Suppl*, 98:119-131.
3. Asada, K. 1999 "The water-water cycle as alternative photon and electron sinks". Philos. Trans. R. Soc. Lond. *B Biol. Sci*., 355:1419–31.
4. Atzenhofer, W., Regelsberger, G., Jacob, U., Peschek, G., Furtmuller, P., Huber, R. & Obinger, C. 2002 "The 2.0A ° resolution structure of the catalytic portion of a cyanobacterial membrane-bound manganese superoxide dismutase". *J. Mol. Biol*., 321:479–89.
5. Priya, B., Premanandh, J., Dhanalakshmi, R.T., Seethalakshmi, T., Uma1, L., Prabaharan, D and Subramanian, G. 2007 ''Comparative analysis of cyanobacterial superoxide dismutases to discriminate canonical forms''. *BMC Genomics*, 8:435.
6. Baldauf, S. L., Bhattacharya, D., Cockrill, P., Hugenholtz, P., Pawlowski, J. & Simpson, A. G. B. 2004 ''The origin and radiation of life on earth. In Cracraft, J. & Donoghue, M. J. [Eds.] Assembling the Tree of Life''. Oxford University Press, New York.
7. Bannister, W.H., Bannister, J.V., Barra, D., Bond, J. and Bossa, F. 1991 ''Evolutionary aspects of superoxide dismutase; the copper/zinc enzyme''*. Free Radical Research Communications*, 12-13, 349-361.
8. Bhattacharya, J., Ghosh, D.K., Chatterjee, A., Majee, M. and Majumder, A.L. 2004 "*Synechocystis* Fe superoxide dismutase gene confers oxidative stress tolerance to *Escherichia coli*". *Biochem Biophys Res Commun,* 316:540–544.
9. Shirkey, B., Kovarcik, D.P., Wright, D.J., Wilmoth, G., Prickett, T.F., Helm, R., Eugene, F., Gregory, M. and Potts, M. 2000 "Years of Desiccation *Nostoc commune*(Cyanobacteria) after Dismutase and Abundant *sodF* mRNA in Active Fe-Containing Superoxide" *J. Bacteriol.*, 182(1):189.
10. Briat, J.F. 2002. "Metal ion activated oxidative stress and its control. In: Inze, D., Montagu, M.V. (Eds.), Oxidative Stress in Plants". *Taylor and Francis*, New York, pp. 171–189.
11. Canini, A., Leonardi, D. and Caiola, M.G. 2012 ''Superoxide dismutase activity in the Cyanobacterium Microcystis aeruginosa after surface bloom formation''. *New Phytologist,* 152:107-116.
12. Canini, A., Albertano, P. & Caiola, M. G. 1998 "Localization of Fe containing superoxide dismutase in cyanobacteria from the Baltic Sea: depth and light dependency". *New Phytol*. 139:247–54.
13. Chen, J., Liao, C., Mao, S. J., Chen, T. & Weng, C. 2001 "A simple technique for the simultaneous determination of molecular weight and activity of superoxide dismutase using SDS-PAGE". *J. Biochem. Biophys. Methods,* 47:233–7.
14. Critchley, C. 1994 "D1 protein turnover: response to photodamage or mechanism? In Baker, N. & Bowyer, J. R. [Eds.] Photoinhibition of Photosynthesis from Molecular Mechanisms to the Field". *BIOS Scientific Publ,* Oxford, pp. 195–201.
15. Cullen, J. J. & Lewis, M. R. 1995 "Biological processes and optical measurements near the sea-surface:

some issues relevant to remote sensing". *J. Geophys. Res*. 100:13255–66.
16. Daniela, B., Friedmann, E.I., Helm, R.F. and Potts, M. 2001 "Gene Transfer to the Desiccation-Tolerant Cyanobacterium *Chroococcidiopsis" Journal Of Bacteriology,* April 2298–2305.
17. David, J. T., Jannette, B.T., Shane, D.P., Nicole, E.N. and Stephen, K.H. 1999 "Iron Superoxide Dismutase Protects against Chilling Damage in the Cyanobacterium *Synechococcus* species PCC79421." *Plant Physiology*, 120, pp. 275–282.
18. Falkowski, P. G. & Raven, J. A. 1997. "Aquatic Photosynthesis". *Blackwell Science, Ltd.,* Malden, 374 pp.
19. Felisa, W.S., Daniel, G., Oscar, S. and Paul, G.F. 2006 ''The role and evolution of Superoxide dismutases in Algae''. *Plant Physiol*., 142(4), 1701-1709.
20. Fink, R. C. & Scandalios, J. G. 2002. "Molecular evolution and structure-function relationships of the superoxide dismutase gene families in angiosperms and their relationship to other eukaryotic and prokaryotic superoxide dismutases". *Arch. Biochem. Biophys*. 399:19–36.
21. Gallon, J. R. 1992. ''Reconciling the incompatible: N2 fixation and Oxygen''. *New Phytologist, 122:* 571–609.
22. Henry, L.E., Gogotov, I.N. and Hall, D.O. 1978 "Superoxide dismutase and catalase in the protection of the proton-donating systems of nitrogen fixation in the blue-green alga *Anabaena cylindrical". J. Biochem.,* 174: 373–377.
23. Herbert, S. K., Samson, G., Fork, D. C. & Laudenbach, D. E. 1992 "Characterization of damage to photosystems I and II in a cyanobacterium lacking detectable iron superoxide dismutase Activity". *Proc. Natl. Acad. Sci*. USA 89:8716–20.
24. Imlay J.A. and Fridovich, I. 1991 "Assay of metabolic superoxide production in *Escherichia coli*". *J Biol Chem,* 266:6957–6965.
25. Jae-Hyun, K. & Kyong, H.S. 2005 "Light-dependent expression of superoxide dismutase from cyanobacterium *Synechocystis* sp. strain PCC 6803" *Arch Microbiol,* 183: 218–223.
26. Kaiser, W.M. 1979. ''Reversible inhibition of the Calvin-cycle and activation of oxidative pentose phosphate cycle in isolated intact chloroplasts by hydrogen peroxide''. *Planta., 145*:377-382.
27. Kaneko, T., Nakamura, Y., Wolk, C.P., Kuritz, T., Sasamoto, S., Watanabe, A., Iriguchi, M., Ishikawa, A., Kawashima, K., Kimura, T., Kishida, Y., Kohara, M., Matsumoto, M., Matsuno, A., Muraki, A., Nakazaki, N., Shimpo, S., Sugimoto, M., Takazawa, M., Yamada, M., Yasuda, M. and Tabata, S. 2001 "Complete genomic sequence of the filamentous nitrogen-fixing cyanobacterium *Anabaena* sp. strain PCC 7120". *DNA Res*., 8: 205-213.
28. Kumar, A., Tyagi, M.B., Jha, P.N., Srinivas, G. and Sinha, A. 2003. ''Inactivation of cyanobacterial nitrogenase after exposure to ultraviolet-B radiation''. Curr. *Microbiol*. 46, 380-384.
29. Kwang, H.B. and Daniel, Z.S. 2005 ''Differential expression of manganese superoxide dismutase sequence variants in near isogenic lines of wheat during cold acclimation''. Plant cell Rep. DOI 10.1007/s00299-005-0073-6.
30. Li, T., Huang, X., Zhou, R., Liu, Y., Li, B., Nomura, C. & Zhao, J. 2002 "Differential expression and localization of Mn and Fe superoxide dismutases in the heterocystous cyanobacterium Anabaena sp. strain PCC 7120". *J. Bacteriol*., 184:5096–103.
31. Liu, Y., Zhou, R. and Zhao, J. 2000 "Molecular cloning and sequencing of the sodB gene from a heterocystous cyanobacterium *Anabaena* 7120". *Biochim. Biophys.* Acta, 1491: 248–252.
32. Lukow, T., Dunfiel, P.F. and Liesack, W. 2000 ''Use of the T-RFLP technique to assess spatialand temporal changes in the bacterial community structure within an agricultural soil planted with transgenic and non-transgenic potato plants''. *FEMS Microbiol. Ecol.,* 32:241-247.
33. Mallick, N. and Rai, L.C. 1999 "Response of the antioxidant systems of the nitrogen fixing cyanobacterium *Anabaena doliolum* to copper". *Journal of Plant Physiology*, 155: 146-149.
34. Martinez, J. S., Zhang, G. P., Holt, P. D., Jung, H.-T., Carrano, C. J., Haygood, M. G. & Butler, A. 2000 "Self-assembling amphiphilic siderophores from marine bacteria". *Science,* 287:1245–7.
35. Mc Kay, R.M.L., Twiss, M.R. and Nalewajko, C. 2001 "Trace metal constraints on carbon, nitrogen and phosphorus acquisition and assimilation by phytoplankton. In: Algal adaptation to Environmental Stresses: Physiological, Biochemical and Molecular mechanisms". (Eds) *Rai, L.C and J. P. Gaur. Springer* -Verlag, berlin. pp. 21-43.
36. Meenakshi, C., Umesh, K.J., Mohammed, A.K., Sunaina, Z. and Tasneem, F. 2006 ''Effect of heavy metal stress on proline, malondialdehyde, and superoxide dismutase activity in the cyanobacterium *Spirulina platensis*-S5''. *Ecotoxicology and Environmental Safety.* 66(2), 204-209.
37. Navari-Izzo, F., Pinzino, C., Qaurtacci, M.F. and Sgherri, C.L. 1999 "Superoxide and hydroxyl radical generation, and superoxide dismutase in PSII membrane fragments from wheat". *Free Radical Res*., 30: 3–9.
38. Nishida, I. and Murata, N. 1996 ''Chilling sensitivity in plants and cyanobacteria: The crucial contribution of membrane lipids*. Annu. Rev. Plant Physiology Plant Mol. Biology, 47:*541-568.
39. Noctor, G. and Foyer, C.H. 1998 ''Ascorbate and glutathione: keeping active oxygen under control''. *Annual Review of Plant Physiology Plant Molecular Biology, 49:* 249-279.
40. Ogawa, K., Kanematsu, S., Takabe, K. and Asada, K. 1995 ''Attachment of CuZn-superoxidedismutase to thylakoid membranes at the site of superoxide generation (PSI) in spinach chloroplasts: detection by immuno-gold labeling after rapid freezing and substitution method''. *Plant Cell Physiology*, 36: 565-573.
41. Okamoto, O. K., Pinto, E., Latorre, L. R., Bechara, E. J. H. & Colepicolo, P. 2001 "Antioxidant modulation in response to metal-induced oxidative stress in algal chloroplasts". *Arch. Environ. Contam. Toxicol*. 40:18–24.
42. Padmapriya, V. and Anand, N. 2010 " The Influence Of Metals On The Antioxidant Enzyme, Superoxide Dismutase, Present In The Cyanobacterium, *Anabaena variabilis*" KÜTZ Asian Research

Publishing Network *Journal of Agricultural and Biological Science Vol*. 5, *No*. 2.

43. Palenik, B., Brahamsha, B., Larimer, F. W., Land, M., Hauser, L., Chain, P., Lamerdin, J., Regala, W., Allen, E. E., Mccarren, J., Paulsen, I., Dufresne, A., Partensky, F., Webb, E. A. & Waterbury, J. 2003 "The genome of a motile marine *Synechococcus*". *Nature,* 424:1037–42.
44. Punia, S., Singh, N. and **Kanupriya** 2011 ''Expression of SOD under chilling and phosphate stress in cyanobacterium Spirulina''. *Annals of Biology, 27(1): 17-22.*
45. Quail, P.H. 1994 "Photosensory perception and signal transduction in plants". *Curr Opin Genet Dev,* 4:652–661.
46. Regelsberger, G., Atzenhofer, W., Ruker, F., Peschek, G.A., Jakopitsch, C., Paumann, P.G. & Obinger, C. 2002 "Biochemical characterization of a membrane-bound manganese-containing superoxide dismutase from the cyanobacterium *Anabaena* PCC 7120". *J Biol Chem*, 277:43615-43622.
47. Rijstenbil, J. W. 2002 "Assessment of oxidative stress in the planktonic diatom *Thalassiosira pseudonana* in response to UVA and UVB radiation". *J. Plankton Res*., 24:1277–88.
48. Rijstenbil, J. W. 2003 "Effects of UVB radiation and salt stress on growth, pigments and antioxidative defense of the marine diatom *Cylindrotheca closterium*". *Mar. Ecol. Prog. Ser*., 254:37–47.
49. Sakamoto, T. and Bryant, D.A. 1999 ''Nitrate transport and not photoinhibition limits growth of the freshwater cyanobacterium Synechococcus species PCC 6301 at low temperature''. *Plant Physiol., 119:*785-794.
50. Schopf, J.W. 2000 ''The Fossil Record: Tracing the roots of the cyanobacterial lineage. In the Ecology of Cyanobacteria''. Whitton BA.
51. Segot, M., Codomier, L., Combaut, G., 1983 "Action de quatre metaur e lourds (cadmium, cuivre, mercure, Plombs) sur la croissance de Asparagopsis armata en culture". *J. Exp. Mar. Biol. Ecol.,* 66, 41–48.
52. Shavyrina, O.B., Gapochka, L.D., Azovskii, A.I., 2001 "Development of tolerance for copper in cyanobacteria repeatedly exposed to its toxic effect". *Biol. Bull.* 28 (2), 183–187.
53. Sinha, R.P. and Hader, D.P. 2002 ''Life under solar UV radiation in aquatic organisms''. *Adv. Space Res.,* 30, 1547-1556.
54. Slain, M.L. 1991 "Chloroplast and mitochondrial mechanisms for protection against oxygen toxicity". *Free Radical Res Commun,* 12–13:851–858.
55. Steinitz, Y., Mazor, Z. and Shilo, M. 1979 ''A mutant of the cyanobacterium *Plectonema boryanum* resistant to photooxidation''. *Plant Sci. Lett.,* 16:327–335.
56. Sudha, S.S. Karthic, R., Francis, M., Soumya, T.S., RengaRamanujam, J. 2011 ''Isolation and preliminary characterization of associated microoorganisms from spirulina products and their silver mediated nanoparticle synthesis''. *J. Algal Biomass Utln., 2 (3):* 1– 8.
57. Sunda, W.G. 2000 "Trace metal/ phytoplankton interactions in aquatic systems. In: Environmental microbe-metal interactions". *Ed. Lovely DR. ASM press*, Washington. pp. 79-107.
58. Takahashi, M. and Asada, K. 1988 ''Superoxide production in aprotic interior of chloroplast thylakoids''. *Arch. Biochem. Biophys*., 267:714–722.
59. Thomas, D.J., Avenson, T.J., Thomas, J.B. & Herbert, S.K. 1998 "A cyanobacterium lacking iron superoxide dismutase is sensitized to oxidative stress induced with methyl viologen but not sensitized to oxidative stress induced with norflurazon". *Plant Physiology*, 116:1593-1602.
60. Touati, D. 1997 "Iron and oxidative stress in bacteria". *Arch Biochem Biophys,* 373:1–6.
61. Tripathi, S.N. and Srivastava, P. 2001. ''Presence of stable active oxygen scavenging enzymes superoxide dismutase, ascorbate peroxidase and catalase in a desiccation-tolerant cyanobacterium *Lyngbya arboricola* under dry state''. Current Science, 81:197-200.
62. Vellard, M. 2003 ''The enzyme as drug: Application of enzymes as pharmaceuticals''. *Curr Opinion in Biotech.,* 14: 1-7.
63. Weatherburn, D. C. 2001 "Manganese-containing enzymes and proteins". In Bertini, I., Sigel, A. & Sigel, H. [Eds.] "Handbook on Metalloproteins". *Marcel Dekker, Inc*., New York, pp. 193–268.
64. Weixing, Z. Qinxi, G. and Jindong, Z. 2007 ''A Membrane-Associated Mn-Superoxide Dismutase Protects the Photosynthetic Apparatus and Nitrogenase from Oxidative Damage in the Cyanobacterium Anabaena sp. PCC 7120''. *Plant Cell Physiol.,* 48(4): 563–572.
65. Wuerges, J., Lee, J.-W., Yim, Y.-I., Yim, H.-S., Kang, S.-O. & Carugo, K. D. 2004. "Crystal structure of nickel-containing superoxide dismutase reveals another type of active site". *Proc. Natl. Acad. Sci*., USA 101:8569–74.
66. Yankovskaya, V., Horsefield, R., Tornroth, S., Luna-Chavez, C., Miyoshi, H., Leger, C., Byrne, B., Cecchini, G. and Iwata, S. 2003 ''Architecture of succinate dehydrogenase and reactive oxygen species generation''. *Science*, 299: 700–704.
67. Zhang, C.C., Laurent, S., Sakr, S., Peng, L. and Bedu, S. 2006 "Heterocyst differentiation and pattern formation in cyanobacteria: a chorus of signals". *Mol. Microbiol*., 59: 367–375.

FIGURES

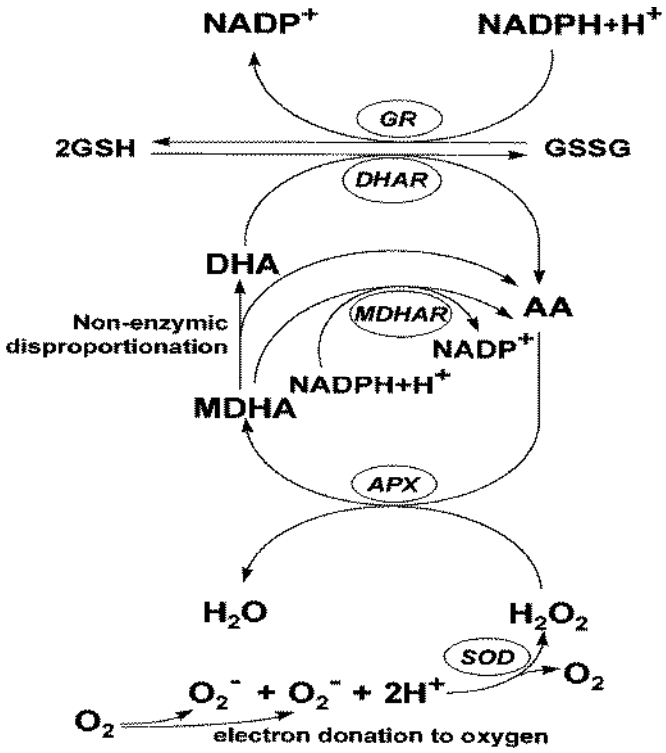

Figure 1: The Ascorbate-Glutathione cycle representing SOD as first line of defense to act (Source; Noctor and Foyer, 1998).

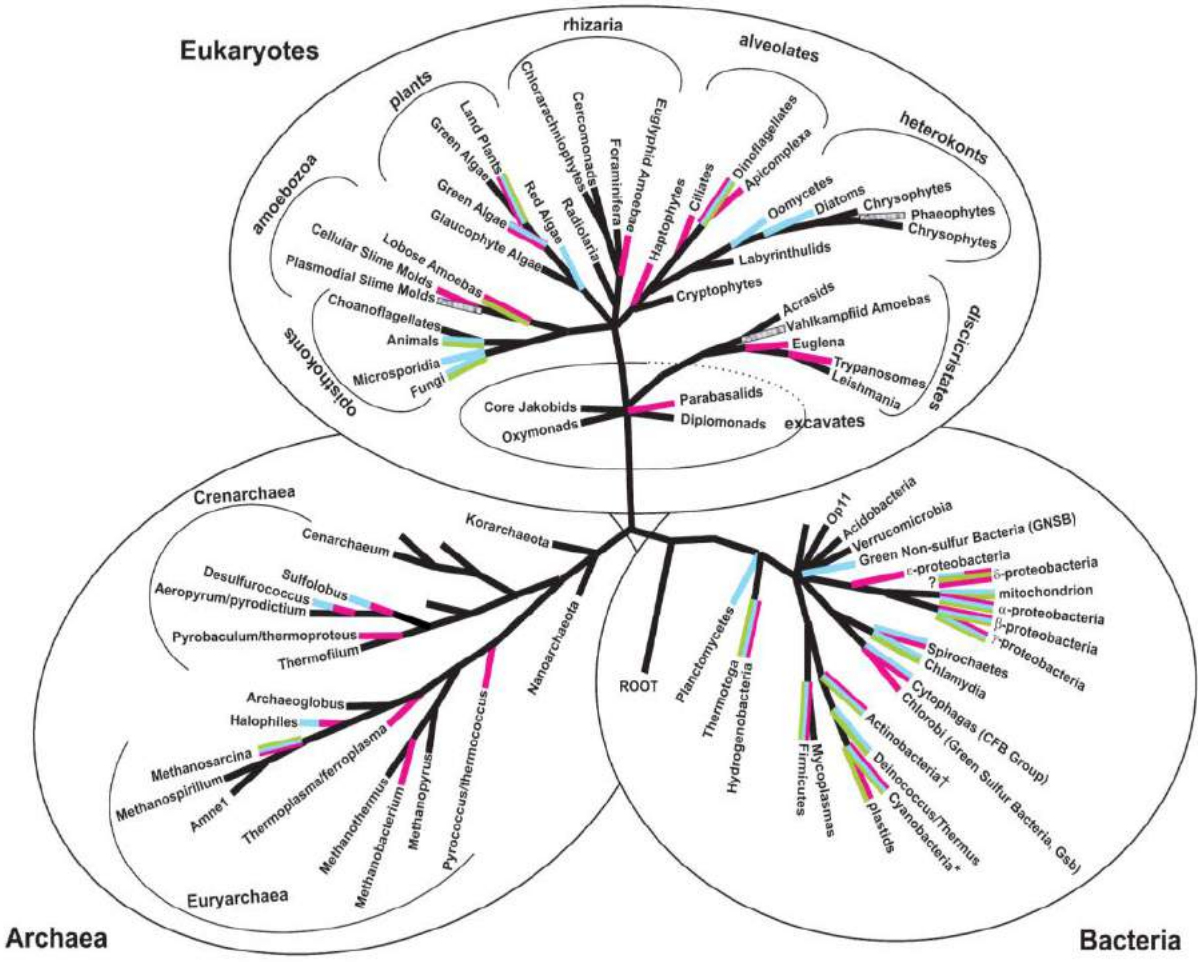

Figure 2: Synthetic distribution based on known evidence from biochemical and genetic data of the various SODs over the tree of life (figure modified after Baldauf *et al* 2004). Fe and MnSOD both having contrasting evolutionary histories, The

FeSOD is prevalent in all the major clades while MnSOD more in bacteria and Eukaryota. In cyanobacteria, FeSOD may have ancestral origin from the GSB ancestor of PSI while MnSOD may have the protobacterial ancestor to PSII and mitochondria. The CuZnSOD shows multiple lateral gene transfers and organisms often possess multiple copies of it in their genomes which are significantly phylogenetically distant. The NiSOD genes are found in genomes of four cyanobacteria. Branches are colored according to known SODs: magenta, FeSOD; cyan, MnSOD; cyan/magenta, Fe/MnSOD cambialistic); green, CuZnSOD; and gray, unknown form of SOD **(**Felisa *et al,* 2006).

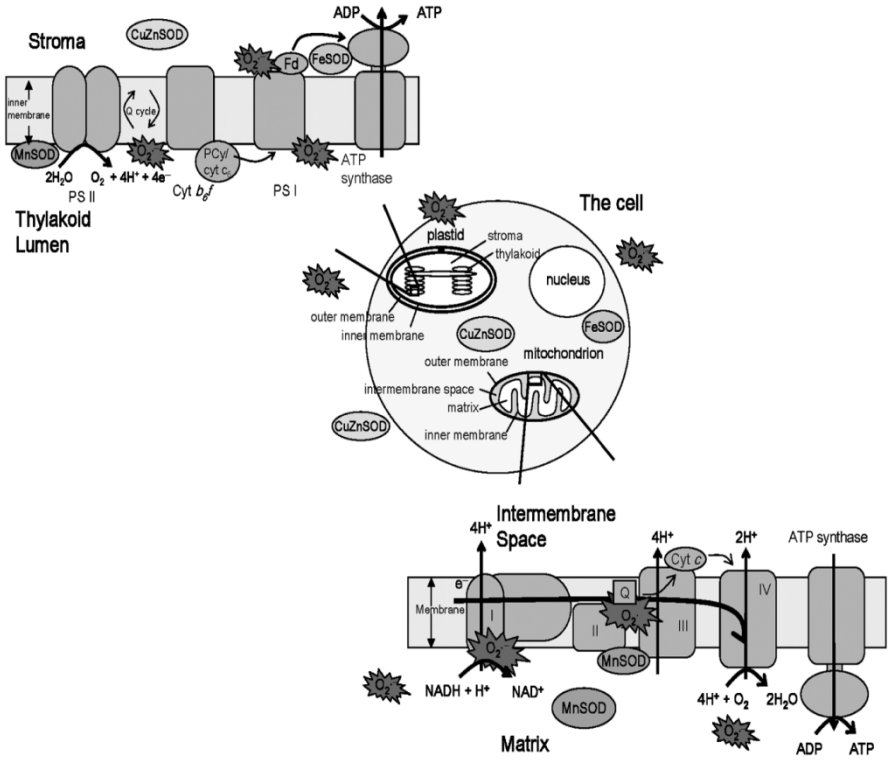

Figure 3: Subcellular localization of SODs. This conceptual scheme represent all the possible locations of SODs in a eukaryotic cell (Felisa *et al,* 2006).

SYNTHESIS, CHARACTERIZATION AND ANTIMICROBIAL EFFICACY OF CYANOBACTERIAL (POLYMER) SILVER NANO PARTICLE CONJUGATES

[1]RITIKA CHANAN, [2]MINAKSHI LALIT, [3]NAVEEN, [4,*]NAMITA SINGH

[1]Research Scholar, Microbial Biotechnology Laboratory, Department of Bio and Nano Technology, Guru Jambheshwar University of Science and Technology, Hisar-125 001, Haryana, India, Email: chananriti16@gmail.com

[2]Research Scholar, Microbial Biotechnology Laboratory, Department of Bio and Nano Technology, Guru Jambheshwar University of Science and Technology, Hisar-125 001, Haryana, India, Email: pr.minal@gmail.com

[3]M. Tech. Student, Microbial Biotechnology Laboratory, Department of Bio and Nano Technology, Guru Jambheshwar University of Science and Technology, Hisar-125 001, Haryana, India

[4]Associate Professor, Microbial Biotechnology Laboratory, Department of Bio and Nano Technology, Guru Jambheshwar University of Science and Technology, Hisar-125 001, Haryana, India, Email: namitasingh71@gmail.com

*corresponding address: Email: namitasingh71@gmail.com

ABSTRACT

Emergence of microbial resistance is the one of the major problem nowadays; thus there have been tremendous efforts towards finding new metabolites for the development of new antimicrobial drugs. Cyanobacteria have been identified as one of the most promising group of micro-organisms from which novel and biochemically active natural products can be isolated. Synthesis of nanoparticles using plant extracts has gained utmost importance in research world but biosynthesis of nanoparticles using microbes is still unexplored and underexploited. In the case of micro-algal species, Cyanobacteria have been studied in great detail for in-vitro silver nano-particle generation and stabilization. Treatment of Cyanobacterial cell extracts with silver nitrate solution in proper concentration and conditions may cap the microbial metabolic proteins and may cause the reduction of silver ions leading to synthesis of silver nanoparticles. In the present study, chemically synthesized silver nanoparticles (particle size – 85nm) were stabilized using different Cyanobacterial polymeric particles (biological) and were evaluated in terms of antibacterial activity and characterized using UV-Visible Spectroscopy, Fourier Transform Infrared Spectroscopy (FTIR) techniques. The particle size of nanoparticles was determined using particle size analyzer. With this study, these nanoparticles bearing antimicrobial activity thus, can be used as a novel source for commercial applications in the different fields: pharmaceutical, cosmetics, industrial, Environmental, food, Agricultural, chemical, medical sector etc.

EY WORDS: *Silver nanoparticles, Cyanobacterial polymeric particles, Antimicrobial activity*.

1. INTRODUCTION

Due to unique electronic, mechanical, magnetic and chemical properties of metal nanoparticles that are significantly different from those of bulk materials [1] attributed to their small sizes and large specific surface area, scientists found that silver nanoparticles exhibit interesting antibacterial activities [2, 3]. Antibacterial activity of the silver-containing materials can be used, for example, in commercial sectors- medical, pharmaceutical, agricultural, textile etc [4-10]. Different methods to synthesize metal nanoparticles include: electrochemical method, thermal decomposition, laser ablation, microwave irradiation and sono-chemical synthesis [11-17]. The simplest and the most commonly used synthetic method for metal nanoparticles is the chemical reduction of metal salts [18, 19]. This chemical method involves reduction of an ionic salt in an appropriate medium in the presence of surfactant using various reducing agents [20, 21].Stability and toxicity of nanoparticles is the main problem that affects the commercial use of silver nanoparticles [22]. In this study, we have tried using biological (Cyanobacterial) polymer to minimize toxicity and stability problem. Long term stability of the silver nanoparticles is not desirable, due to this reason; we have used cyanobacteria to stabilize the silver nanoparticles by their secreted proteins [23]. Stress tolerance during adverse conditions by Cyanobacterial nanoparticles is because they possess highly heterogeneous polymers containing a number of distinct polysaccharides and non-carbohydrate constituents including proteins, phospholipids and nucleic acids. Studies have shown that polysaccharides play a crucial role in bio-sorption and binding of toxic heavy metals (silver particles).These properties of bio-nanoparticles find special applications in bioremediation, food, and pharmaceutical industries [24]. Our study signifies on the usage of cyanobacteria as a stable carrier for silver nanoparticles and calcium alginate as a cross linker between silver nanoparticles and cyanobacteria**.** Alginate and its composites have been used in many biomedical applications including drug delivery and wound dressings. It can also be effectively used for the immobilization of silver nanoparticles [25]. Cyanobacterial silver nano-particle conjugates were bio-evaluated against *E.coli* and *S.aureus*.

2. MATERIALS AND METHODS

2.1 CHEMICAL SYNTHESIS OF SILVER NANOPARTICLES

8.5 mg of silver nitrate was dissolved in 50 ml distilled water (1m M). Tri-sodium citrate was used as a reducing agent. 5ml of 1% tri-sodium citrate was added drop-wise in the silver nitrate solution at 85^{0}C on continuous stirring at 50-70 rpm [26]. The samples were analysed with visual inspection and UV-Vis spectroscopy. Pale yellowish colour was observed. The time scale of visual evolution depends on the silver nitrate solution. In general, nano-particle formation is visually appreciable after 4min of the beginning of the reaction.

2.2 CULTIVATION OF CYANOBACTERIA

The cultivation of cyanobacteria was carried out using BG-11 media at 27±2^{0}C, under continuous illumination of 2000lux maintained by white fluorescence lamps. The cultures were regularly sub-cultured and maintained under continuous shaking conditions for few weeks. The cells were separated from the medium by centrifugation (4000rpm/10min) followed by filtration with Whatman filter paper. Finally, the Cyanobacterial pellets were lyophilized and stored at – 20 ^{0}C. Three Cyanobacterial samples depicting high amounts of protein/lipo peptides/pigments in the extraction medium were used in different concentration and dissolved in PBS (Phosphate buffer saline) buffer. The chlorophyll concentrations of the cyanobacteria at 665nm absorbance: *Microcystis aeruginosa*, *Frischerella* and *B6* strain (Personal culture collection of Dr. Namita Singh's, Microbial Biotechnology Laboratory, and Department of Bio And Nano Technology) were 35µg/ml, 28µg/ml and 21µg/ml respectively. The cultures were dissolved in PBS buffer as follows: *Microcystis aeruginosa* (0.2g of the lyophilized biomass was dissolved in 10ml PBS buffer), *Frischerella* (0.16g of the lyophilized biomass was dissolved in 5ml PBS buffer) and *B6* isolate (0.1g of the lyophilized biomass was dissolved in 5ml PBS buffer), keeping in view that all the three samples had same protein concentration, determined by Bradford's method.

2.3 PREPARATION OF LINKERS WITH CYANOBACTERIAL SAMPLES (CYANOBACTERIA-LINKER SOLUTION)

70mg of Sodium alginate was dissolved in 20ml distilled water (3mM) and calcium chloride solution (45mg in 10ml, 0.03M) was added drop wise on continuous stirring to sodium alginate solution. To the above mixture, after 10 minutes, PBS dissolved three different Cyanobacterial samples were added drop wise in three different beakers. These solutions were used in 5:1:4 respectively.

2.4 CONJUGATION OF SILVER NANOPARTICLES WITH CYANOBACTERIAL - LINKER SOLUTION

Mix 5ml of each cyanobacteria-linker sample to 5ml of silver nano-particle solution on continuous stirring for 3 to 4 hours. The samples were further subjected for UV-visible spectroscopic analysis.

2.5 TEST MICRO-ORGANISMS

The micro organisms including gram positive and gram negative bacteria were used in this study. *Staphylococcus aureus* NCIM 5021 (gram positive), *E.coli* MTCC-723 (gram negative) were provided from NCIM (National Collection of Industrial Microorganisms) culture collection, Pune and Institute of Microbial Technology, Chandigarh, India respectively. The bacterial strains were maintained on nutrient agar slants and incubated at 30^{0}C.

2.6 ANTIBACTERIAL ASSAY

The antimicrobial susceptibility of Silver Nanoparticles (Ag NPs) was evaluated using well diffusion method. Zones of inhibition were measured after overnight incubation at 30^{0}C. The comparative study was made between cyanobacteria linked silver nanoparticles and silver nanoparticles alone.

3. RESULTS AND DISCUSSION

Silver nanoparticles were synthesized according to the chemical reduction method.

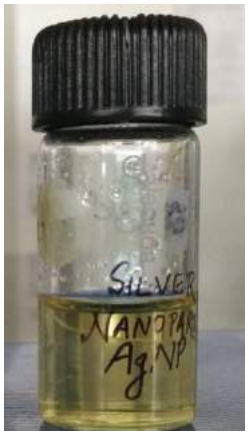

Figure 1: Silver Nanoparticle solution

The transparent colourless solution was converted to the characteristic pale yellow colour, when citrate of sodium (tri-sodium citrate) was used as stabilizing agent. The occurrence of colour indicated the formation of silver nanoparticles. The change in colour is because of the strong absorption of visible light due to excitation of the nano-particle surface Plasmon [27-29].

Analytical Assays:

3.1 UV-Visible Spectral Analysis

UV-Visible spectroscopy is one of the most widely used techniques. Nanoparticles can be structurally characterized using this technique. The change in the color and thus the formation of silver nanoparticles was confirmed by the UV-Vis experiment. The UV-Vis photo spectra of Ag NPs (Silver Nanoparticles) was recorded with respect to the substrate placed in the reference beam using double beam spectrophotometer (Shimadzu, Model: UV-2450) in the range 200–800 nm. Absorption peak of Silver nano-particle synthesized by chemical reduction method using tri-sodium citrate and silver nitrate was recorded. In the figure 1.1(1), UV-Visible spectra of the silver nitrate solution gave a peak around 217nm, as expected for silver ions. It was observed that

surface Plasmon absorption maximum was shifted to lower wavelength with addition of citrate of sodium as reducing agent [30]. UV-Visible Spectroscopy for Cyano bacteria-*Microcystis aeruginosa* showed the absorption maxima at 300-700 nm with the presence of chlorophyll *a,* phycoerythrin and phycocyanine and absorption maxima at 700-800 nm showed the presence of chlorophyll *a* [31]. **Fig 2** describes the UV-Vis photo spectra of the mixture sample of (a) Silver Nano-particles (b) *Microcystis aeruginosa* linked silver nano-particles (c) *Frischerella* linked silver nanoparticles and (d) B6 Cyanobacteria linked silver nanoparticles recorded in the range of 200–800 nm.

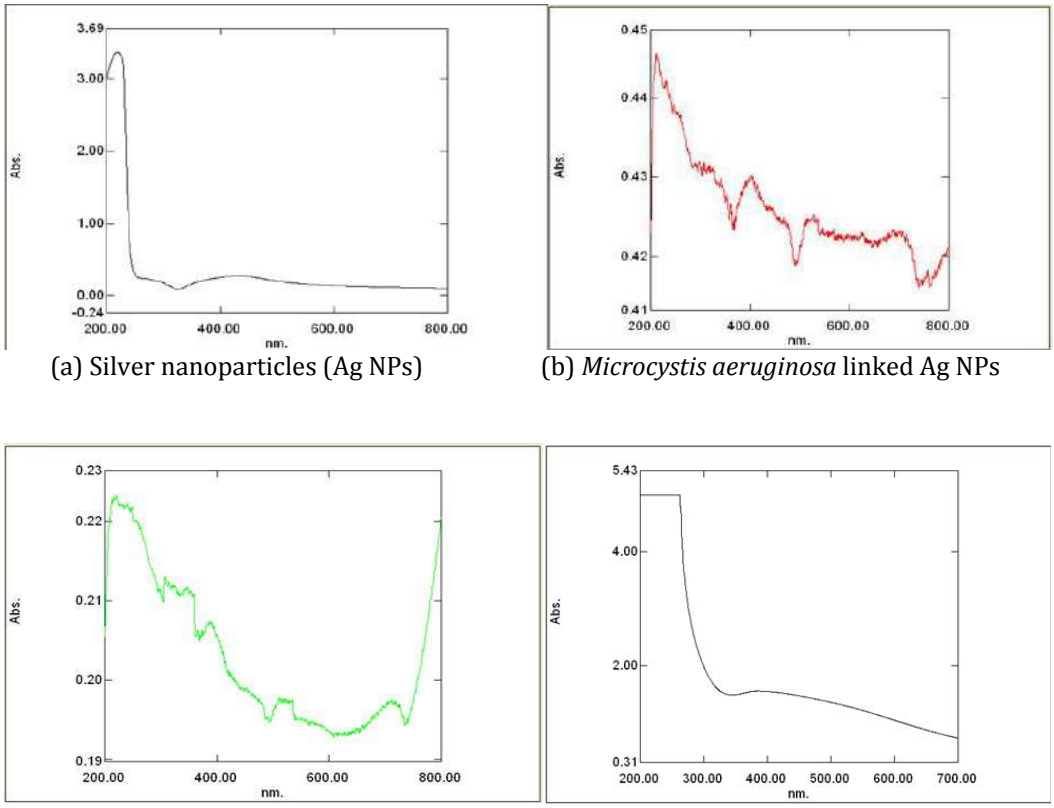

(a) Silver nanoparticles (Ag NPs) (b) *Microcystis aeruginosa* linked Ag NPs

(c) *Frischerella* linked Ag NPs (d) B6 linked Ag NPs

Figure 2: UV-Visible Spectra of Ag NPs and Cyanobacteria linked Ag NPs

3.2 PARTICLE SIZE ANALYSIS

Particle size of Ag NPs formed was 85nm in diameter. Shape of the particles and spherical structure of the particles can be controlled experimentally. The result indicated that the average particle size of the synthesized silver nanoparticles was highly influenced by the reaction. The nano size of material results in specific physicochemical characteristics different than those of their bulk materials or larger particles. This effect is mainly credited to high surface-area-to-volume ratio, which results in increased reactivity; hence, the nano scale materials are more advantageous than their bulk counterparts. Average size of silver nano-particles was recorded to be 85 nm. After conjugation, *Microcystis* linked silver nano particles conjugate showed 144nm size of particles. *Frischerella* linked silver nanoparticles conjugate showed 503nm size of the particle. Cyanobacteria B6 linked silver nanoparticles showed 216nm size of particles. This means these particles, give high-surface-to-volume ratio, which results in increased reactivity.

Table-1: Peak values depicting Average Size (r. nm), Intensity (%), and Width (r. nm) of three different Cyanobacterial samples inked with Ag NPs

SAMPLE	PEAK		
	Average Size (r. nm)	Intensity%	Width (r. nm)
Silver Nano-particles (Ag NPs)	85.0	100.0	46.28
Microcystis aeruginosa linked Ag NPs	144	87	517.8
Frischerella linked Ag NPs	503	100	118.3
Cyano *B6* linked Ag NPs	216	95.7	106.9

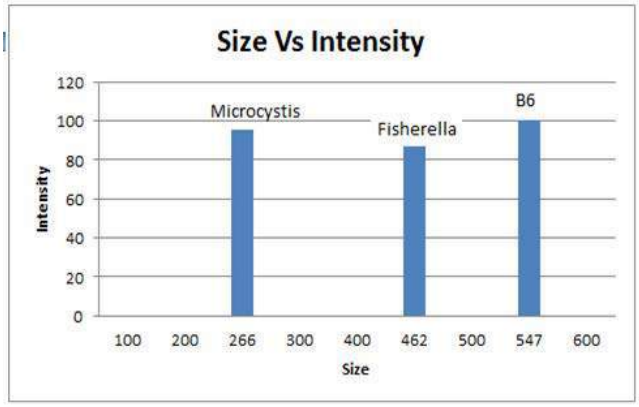

Chart-1: Relationship between intensity and size (r. nm) of silver nanoparticles prepared from different Cyanobacterial samples: *Microcystis, Frischerella, B6* isolate.

The FTIR spectrum indicates various functional groups present at different positions. IR spectroscopy study has confirmed that the carbonyl group of amino acid residues and peptides of proteins has a stronger ability to bind metal, so that the proteins may form a coat, covering the metal nanoparticles (i.e. capping of Ag NPs) to prevent the agglomeration of the particles and to stabilize the nanoparticles in the medium. In the case of *Microcystis aeruginosa, Frischerella , B6 Isolate* linked silver nano particle conjugates, the peaks in the region between 3859.55 to 3422.27 are assigned to O-H stretching of alcohol and phenol compounds and aldehyde–C-H- stretching of alkanes. The peaks in the region 1615.76 to 1407.02 and 1300 to 650 corresponds to N-H(bond) of primary and secondary amides and –C-N- stretching vibration of amines or C-O stretching of alcohols,ether and carboxyic acid.

3.3 FTIR ANALYSIS

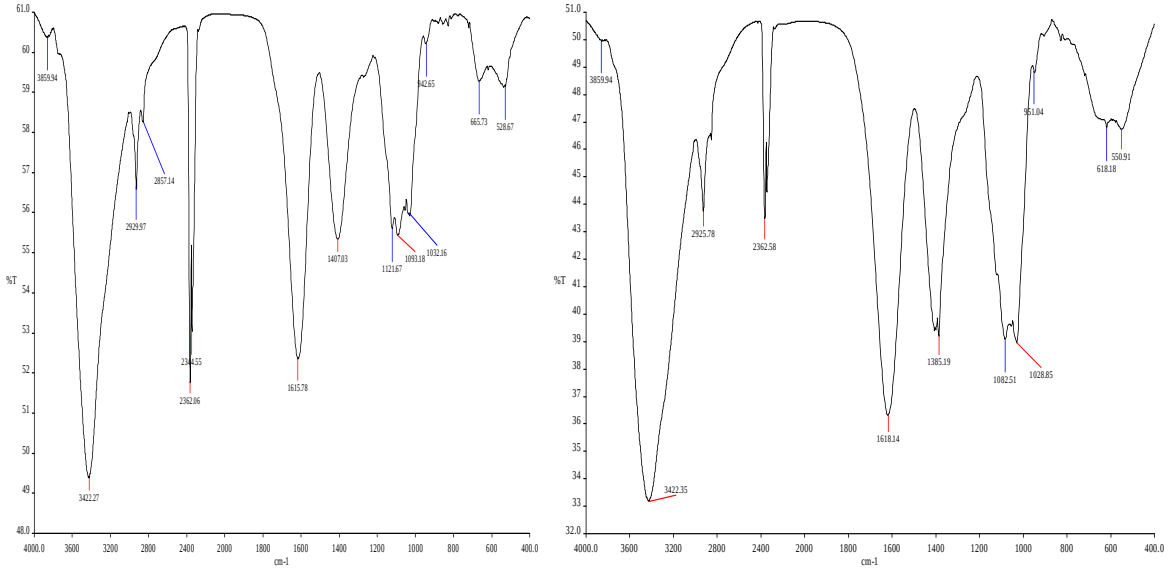

(a) *Microcystis aeruginosa* linked Ag NPs (b) *Frischerella* linked Ag NPs

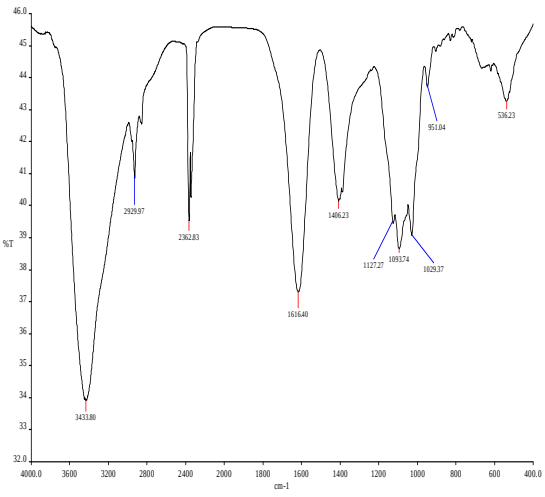

(c) B6 linked silver nanoparticles

Figure 3: FTIR Spectra of Silver Nanoparticles linked with three different Cyanobacteria

The overall peaks from FTIR observation confirm the presence of protein in the samples of silver nanoparticles. It can be assumed that there is the presence of nitrate reducing bacteria to produce nitrate reductase enzyme (protein). This reduces to silver nitrate solution from silver nano particles [32, 33]. The

bands at 1622 cm^{-1} and 1527 cm^{-1} correspond to the stretch molecule vibration. The two bands existing at 1412 cm^{-1} and 1029 cm^{-1} can be assigned to the C-N stretching vibrations of aromatic and aliphatic amines. The corresponding bending vibrations were seen at 1651 cm^{-1} and 1548 cm^{-1}, respectively. The two bands observed at 1379 cm^{-1} and 1033 cm^{-1} can be assigned to the C–N stretching vibrations of aromatic and aliphatic amines, respectively [34]. The silver ions were reduced in the presence of nitrate reductase, leading to the formation of a stable silver hydrosol 10-25 nm in diameter and stabilized by the capping agent [35]. The presence of protein acts as a stabilizing agent and surrounds silver nanoparticles [36]. The clarity of the peak showed the presence of protein in the conjugation. The shifting of some peak at 528, 805, 1127 and 1320 showed the presence of disulphide, S-OR, thio-carbonyl, phosphonate groups also.

Table-2: Stretching and vibration of functional group of Nano formulations

Frequency (cm^{-1})	Functional group
3200-3400	Alcohol/phenol stretching
2800-320`	C-H structure
1615	Alkene stretching
1450	$-CH_3$ (bend)
1000-1300	Alcohol, ether esters, carboxylic acid, anhydrides
650-1000	Alkene (out-of-plane bend)

3.4 ANTIMICROBIAL ACTIVITY

It is well known that silver ion nanoparticles are highly toxic to microorganisms. Silver nanoparticles have been known to have inhibitory and bactericidal effects and thus we extend its application as an antibacterial agent. The biological activity of silver based materials, depending on their structure and physicochemical properties, affects the interaction with the cytoplasmic membrane of bacteria and influences cell metabolism. In our study, the antimicrobial activity of nano-silver-containing Cyanobacterial films was investigated against *E. coli* and *Staphylococcus aureus.* The Antibacterial activity is estimated by the zone of inhibition [37]. The differences in the composition of the cell wall of Gram negative (*E. coli)* and Gram positive (*S. aureus)* bacteria and hydrophilic and hydrophobic character of *E. coli* and *S. aureus* respectively induce different antimicrobial activity. The mechanism of the bactericidal effect of silver and silver nanoparticles remains to be understood. Several studies propose that silver nanoparticles may attach to the surface of the cell membrane disturbing permeability and respiratory function of the cell. It is also possible that silver nanoparticles not only interact with the surface of membrane, but can also penetrate inside the bacteria [38]. It may be observed that silver nanoparticles have comparatively higher anti-bacterial activity against gram negative organism than gram positive, probably due to thinner peptidoglycan layer and presence of porins [39].
Two aspects are to be considered:

- Mean Width of Zone of inhibition (Diameter, cm)
- Microorganism used:

Escherichia coli MTCC 723

Staphylococcus aureus NCIM 5021

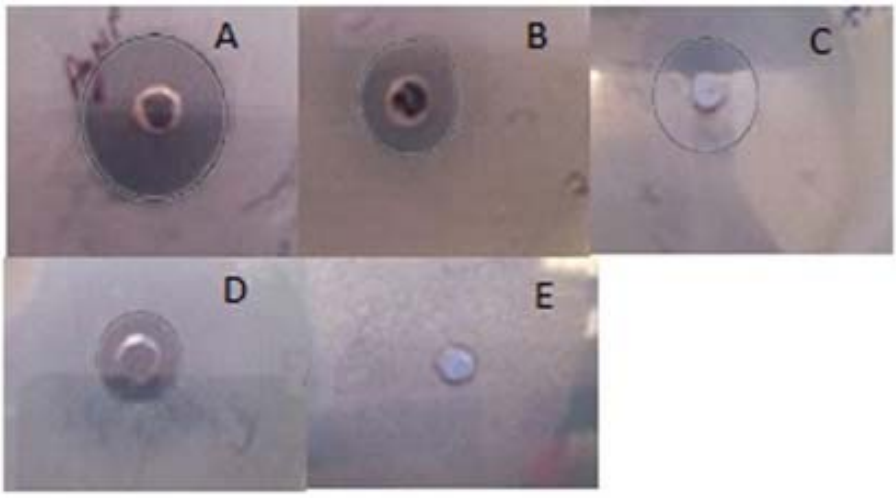

Figure 4: Antimicrobial efficacy of (A)AgNP(Positive Control),(B)*Microcystis* linked AgNP, (C)*Frischerella* linked AgNP, (D)B6 linked AgNP (E) Negative control (Only PBS Buffer instead of the test extract) against *E.coli.*

www.ijset.in
ISSN (O): 2348-4098
ISSN (P): 2395-4752

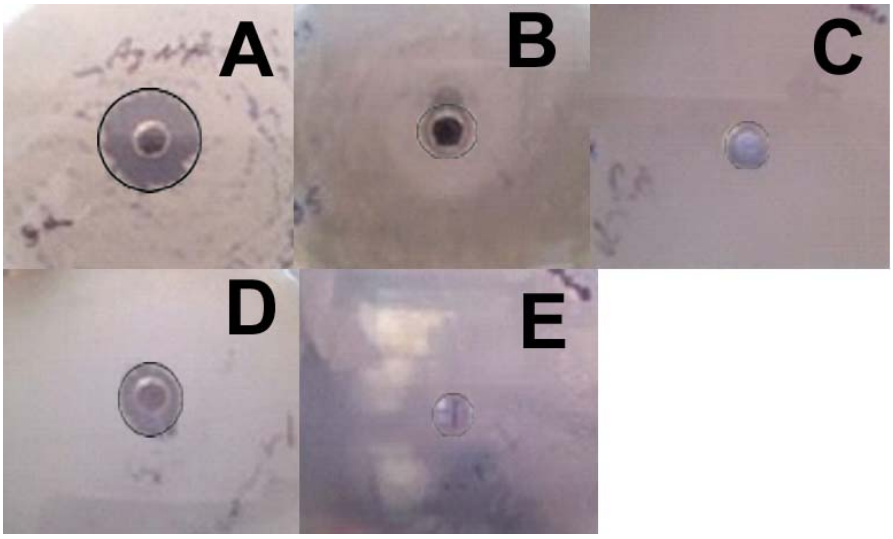

Figure 5: Antimicrobial efficacy of (a) Ag NP (Positive control), (b) *Microcystis aeruginosa* linked Ag NP, (c) *Frischerella* linked Ag NP, (d) B6 linked Ag NP (e) Negative control (PBS Buffer instead of test extract)against *S. aureus*.

Table-3: Zone of Inhibition of silver nanoparticles and Cyanobacteria linked Ag NPs. Parenthesis showing% reduction in zone of inhibition after 30 days storage of silver nanoparticles at 4°C.

Sample	Zone of Inhibition (diameter in cm)	
	E-coli	*S. aureus*
Silver nanoparticles(Positive Control)	2 (76%)	1 (83%)
PBS Buffer(Negative Control)	0 (NIL)	0 (NIL)
Microcystis aeruginosa linked silver nanoparticles	1 (2%)	0.6 (0%)
Frischerella linked silver nanoparticles	0.8 (1%)	0.2 (0%)
B6 linked silver nanoparticles	1.2 (0%)	0.8 (0%)

The antibacterial activity of the test extracts (Cyanobacteria Linked Silver Nanoparticles) and positive control (Silver Nanoparticles alone) maintained at 4^0C, were again measured after one month against test pathogens in terms of zone of inhibition. It was observed that the zone of inhibition in cms for the silver nanoparticles decreased in diameter. The possible reason for this decrease could be due to the agglomeration of the silver nanoparticles with time whereas the zone of inhibition of cyanobacteria linked silver nanoparticles remained same in diameter even after one month. This indicated that the nanoparticles linked with cyanobacteria did not agglomerate and were stabilized for a longer period of time due to the secretion of proteins from cyanobacteria which acted as a capping agent to help these conjugates to not to lose their effective bioactivity whereas non-conjugated silver nanoparticles showed a decrease in size of their zone of inhibition and bioactivity with time.

4. CONCLUSION

In our study, silver nanoparticles with mean diameter of 85nm were synthesized using tri-sodium citrate as a reducing agent. The nanoparticles were characterized by UV/Vis Spectroscopy, FTIR. UV/Vis spectra showed the characteristic Plasmon absorption peak for the silver nanoparticles ranging from 200- 230 nm. Additionally, the antibacterial activity of the nanopartículate dispersion was measured. The results of this study clearly demonstrated that the colloidal silver nanoparticles inhibited the growth and multiplication of the tested bacteria, including highly multi resistant bacteria such as *S. aureus* and *Escherichia coli.* The silver nanoparticles linked cyanobacteria help to reduce the toxicity of the silver nanoparticles and improve the stability of the silver nanoparticles by the secretion of proteins (capping agent) after conjugation with cyanobacteria. The Bio-Nano-formulation of cyanobacteria and silver nano-particles conjugate were more stable than the silver nanoparticles alone against pathogenic bacteria and thus these conjugates find application in commercial fields such as- biomedical, pharmaceutical, cosmetics, health, food and agriculture sectors.

ACKNOWLEDGEMENT

Authors acknowledge UGC-BSR and DST for financial support in the form of fellowship to the student and DBT –HRD Programme , UGC-SAP for infrastructure facilities created in the department.

REFERENCES

[1]. Mazur, M., "*Electrochemically prepared silver nano-flakes and nano-wires*". Electrochemistry Communications, vol. 6, 2004, p 400-403.
[2]. Shahverdi, A.R..; Fakhimi, A., "*Neural Network Modelling For Prediction Size Of Silver*

Nanoparticles In Montmorillonite/Starch Synthesis By Chemical Reduction Method". Digest Journal of Nanomaterials and Biostructures, vol.3, 2007, p 168-171.

[3]. Pal, S., "*A General Strategy for Nano crystal Synthesis*". Applied and Environmental Microbiology, vol. 73, no.6, 2007, p 1712-1720.

[4]. Roldan, M.V.; Frattini, A.L., "*Synthesis, chemical reduction method and their antibacterial activity*". Anales AFA, vol.17, 2005, p 212-217.

[5]. Yin, H.; Amamoto, T.Y.; Wada, Y., "*Microwave-Mediated Rapid Synthesis of Gold Nanoparticles*". Materials Chemistry and Physics, vol.83, 2004, p 66-70.

[6]. Zhu, Z.; Kai, L.; Wang, Y., "*Synthesis and applications of hyper branched polyesters preparation and characterization of crystalline silver nanoparticles".* Materials Chemistry and Physics, vol.96, 2006, p 447-453.

[7]. Edelstein, A.S.; Cammarata, R.C., "*Nanomaterials synthesis, properties and applications*". Institute of Physics Publications, Bristol and Philadelphia Publishers, 1996.

[8]. Mock, J.J.; Barbic, M., "*Shape effects in plasmon resonance of individual colloidal silver nanoparticles*". J. Chem. Phys.,vol. 116, no.15, 2002, p 6755-6759.Duran, N.; Marcato, P.L.; Alves, O.L., J. Nano-biotechnology, vol. 3, no.8, 2005, p 1-7.

[9]. Duran, N.; Marcato, P.L.; Alves, O.L., "*Mechanistic aspects of biosynthesis of silver nanoparticles by several Fusariumoxysporum strains*". J. Nano-biotechnology, vol. 3, no.8, 2005, p 1-7.

[10]. Maillard, M.; Giorgo, S.; Pileni, M.P., "*Silver Nano Disks"*. Adv. Mater, vol. 14, no.15, 2002, p 1084-1086.

[11]. Tang, Z.; Liu, S.; Dong, S.; Wang, E., "*Electrochemical synthesis of Ag nanoparticles on functional carbon surfaces"*. Journal of Electro analytical Chemistry, vol. 502, 2001, p 146-151.

[12]. Mazur, M., "*Electrochemically prepared silver nano-flakes and nano-wires*". Electrochemistry Communications, vol.6, 2004, p 400-403.

[13]. Zhu, J.; Zhu, X.; Wang, Y., "Electrochemical synthesis and fluorescence spectrum properties of silver nanospheres". Microelectronic Engineering,vol.77, 2005, p 58..

[14]. Kim, Y.H.; Lee, D.K.; Kang, Y.S., "*Colloids and Surfaces, Physicochemical and Engineering Aspects*". vol.273, 2005, p 257–258.

[15]. Bae, C.H.; Nam, S.H.; Park, S.M., "*Formation of silver nanoparticles by laser ablation of a silver target in NaCl solution*". Applied Surface Science, vol.197–198, 2002, p 628-634.

[16]. Patel, K.; Kapoor, S.; Dave, D.P.; Mukherjee, T., "*Synthesis of nano-sized silver colloids by microwave dielectric heating*". J. Chem. Sci, vol. 117, no.4, 2007, p 311-315.

[17]. Zhang, J.; Chen, P.; Sun, C.; Hu, X., "*Sonochemical Synthesis of Colloidal Silver Catalysts for Reduction of Complexing Silver in DTR System*". Applied Catalysis A., vol. 266, 2004, p 49.

[18]. Chaudhari, V.R.; Haram, S.K.; Kulshreshtha, S.K., "*Micelle assisted morphological evolution of silver nanoparticles*". Colloids and Surfaces A., vol.301, 2007, p 475-480.

[19]. Pal, A.; Shah, S.; Devi, S., "*Synthesis of Au, Ag and Au–Ag alloy nanoparticles in aqueous polymer solution*". Colloids and Surfaces A., vol. 302, 2007, p 51-57..

[20]. Chen, Z.; Gao, L., "*A facile and novel way for the synthesis of nearly mono disperse silver nanoparticles*". Materials Research Bulletin, vol. 42, 2007, p 1657-1661.

[21]. Kumar, A.; Joshi, H.; Pasricha, R.; Mandale, A.B.; Sastry M., "*Phase transfer of silver nanoparticles from aqueous to organic solutions using fatty amine molecules*".Journal of Colloid and Interface Science, vol. 264, 2003, p396.

[22]. Kittler, S.; Greulich, C.; Diendorf, J.; Epple, M., "*Toxicity of Silver Nanoparticles Increases during Storage Because of Slow Dissolution under Release of Silver Ions*". Chem. Mater, 2010, vol.22, p 4548–4554.

[23]. Mubark Ali D.; Sasikala, M.; Gunasekaran, M., "*Biosynthesis and characterization of silver nanoparticles using marine Cyanobacterium, oscillatoria willei, NTDM01*". Digest Journal of Nanomaterials and Biostructures, vol. 6, no. 2, 2011, p 385-390.

[24]. Chug, R.; Mathur, S., "*Extracellular Polymeric Substances from Cyanobacteria: Characteristics, Isolation and Biotechnological Applications-A Review*". International Journal of Advances in Engineering, Science and Technology (IJAEST) vol. 3, no. 2, 2013, p 49-53.

[25]. Augustine, R.; Rajarathinam, K., (2011) Department of Bioengineering, V H N S N College, Virudhunagar TamilNadu.

[26]. Basavarajudapudi; Naik, P.K., "*Synthesis and Characterization of Silver Nanoparticles*". IJPBS vol. 2, no. 3, 2012 p 10-14.

[27]. Lee, J.; Lee, H.J.; Wark, A.W., "*Nanoparticle enhanced surface Plasmon resonance detection of proteins at attomolar concentrations*". Anal Chem vol. 84, 2012, p 1702-1707.

[28]. Ray, P.C., "*Size and shape dependent second order nonlinear optical properties of nanomaterials and their application in biological and chemical sensing*". Chem Rev, vol.110, 2010, p 5332-5365.

[29]. Hartland, G.V., "*Optical studies of dynamics in noble metal nanostructures*". Chem Rev, vol. 11, 2011, p 3858-3887.

[30]. Guzmán, M.G.; Dille, J.; Godet, S., "*Synthesis of silver nanoparticles by chemical reduction method and their antibacterial activity*". World Academy of Science, Engineering and Technology, vol. 2, 2008.

[31]. Purves et al., Life: The Science of Biology 4th Edition.

[32]. Ahmad, A.; Mukherjee, P.; Senapati, S.; Mandal, D.; Khan, M.I.; Kumar, R.; Sastry, M., "*Extracellular biosynthesis of silver nanoparticles using the fungus Fusarium oxysporum*". Colloids Surfaces B: Biointerfaces , vol. 27, 2003, p 313-318.

[33]. Jayashree J.; Pradhana, N.; Prasad Dashb, B.; Kumar P., "*Biosynthesis and characterization of silver nanoparticles using microalga chlorococcum humicola and its antibacterial activity*". International Journal of Nanomaterials and Biostructures, vol. 3 no.1, 2013, p 1-8.

[34]. Shaligram, S.N.; Bule, M.; Bhambure, R.; Singhal, S.R.; Singh, K.; Szakacs, S.; Pandey, A., "*Biosynthesis of silver nanoparticles using aqueous extract from the compacting producing fungi*". Process Biochem, vol.44, 2003, p 939–943.

[35]. Metuku, R.P.; Pabba, S.; Burra, S.; Gudikandula, K.; "*Biosynthesis of silver nanoparticles from Schizophyllum radiatum HE 863742.1: their characterization and antimicrobial activity*". J. Biotech, vol.4, 2014, p 227–234.

[36]. Metuku, R.P.; Pabba, S.; Burra, S.; Gudikandula, K.; "*Biosynthesis of silver nanoparticles from Schizophyllum radiatum HE 863742.1: their characterization and antimicrobial activity*". J. Biotech, vol.4, 2014, p 227–234.

[37]. Jenaa, J.; Pradhana, N.; Dashb, B.P.; Suklaa, L.B.; Pand, P.K., "*Biosynthesis and characterization of silver nanoparticles using microalga chlorococcum humicola and its antibacterial activity*" International Journal of Nanomaterials and Bio structures vol. 3(1), 2013, p 1-8.

[38]. Prabhu, S.; Poulose, E.K., "*Silver nanoparticles: mechanism of antimicrobial action, synthesis, medical applications, and toxicity effects*". *International Nano Letters, 2012.*

[39]. Metuku, R.P.; Pabba, S.; Burra, S.; Gudikandula, K.; (2014) "*Biosynthesis of silver nanoparticles from Schizophyllum radiatum HE 863742.1: their characterization and antimicrobial activity*". J. Biotech, vol.4, 2014, p 227–234.

Publication Fee :

For Online Version

For Indian Author	For Foreign Author
INR 2500₹	USD 100$

For Print Version

For Indian Author	For Foreign Author
INR 3500₹	USD 160$

Address :
310/A, Ram Nagar Extension, Sodala,
Jaipur-302019, Rajasthan, INDIA
Tel.: +91 992-943-5130, 992-967-8789